



**HAL**  
open science

# Structural Health Monitoring Optimization

Christelle Geara

► **To cite this version:**

Christelle Geara. Structural Health Monitoring Optimization. Civil Engineering. Université Clermont Auvergne; Université Saint-Joseph (Beyrouth), 2021. English. NNT : 2021UCFAC087 . tel-03663965

**HAL Id: tel-03663965**

**<https://theses.hal.science/tel-03663965v1>**

Submitted on 10 May 2022

**HAL** is a multi-disciplinary open access archive for the deposit and dissemination of scientific research documents, whether they are published or not. The documents may come from teaching and research institutions in France or abroad, or from public or private research centers.

L'archive ouverte pluridisciplinaire **HAL**, est destinée au dépôt et à la diffusion de documents scientifiques de niveau recherche, publiés ou non, émanant des établissements d'enseignement et de recherche français ou étrangers, des laboratoires publics ou privés.

**UNIVERSITÉ CLERMONT AUVERGNE**

École Doctorale  
Sciences Pour l'Ingénieur

**UNIVERSITÉ SAINT-JOSEPH DE BEYROUTH**

École Supérieure d'Ingénieurs de Beyrouth

**Thèse**

Présentée par

**Christelle GEARA**

En vue d'obtenir le grade de:

**Docteur d'Université**

**Spécialité : Matériaux**

# **Optimisation de la surveillance de la santé structurale**

Soutenue publiquement le 22 Juillet 2021 devant le jury :

Président :

M. Emilio BASTIDAS-ARTEAGA      La Rochelle Université

Rapporteurs :

M. Franck SCHOEFS      Université de Nantes

M. André ORCESI      Cerema

M. Fadi HAGE CHEHADE      Université Libanaise

Examinatrice :

Mme Farah HOMSI      Université Saint-Joseph de Beyrouth

Directeurs de thèse :

M. Alaa CHATEAUNEUF      Université Clermont Auvergne

M. Wassim RAPHAEL      Université Saint-Joseph de Beyrouth

M. Rafic FADDOUL      Université Saint-Joseph de Beyrouth

This page is intentionally left blank

# **Structural Health Monitoring Optimization**

by

**Christelle GEARA**

*A thesis submitted in partial fulfillment of the  
requirements for the degree of Doctor of Philosophy  
(Structural Engineering)*

**2021**

**Clermont Auvergne University  
Saint-Joseph University**

This page is intentionally left blank

*To my parents Fadi and Feyrouz,  
My brother Patrick,  
And last but not least my husband Adam*

*« When I see a bird that walks like a duck and swims like a duck and quacks  
like a duck, I call that bird a duck »*

**James Whitcomb Riley**

This page is intentionally left blank

## Acknowledgement

This work could not have been accomplished without the presence, both physical and moral, of many people who helped me and contributed to the development of this thesis. So as a preamble to this dissertation, I would like to extend my sincere gratitude to the following persons:

All the jury members for agreeing to participate in my thesis defense and letting it be an enjoyable moment. I would like to thank Prof. Emilio Bastidas-Arteaga for presiding my jury, Prof. Franck Schoefs, Prof. André Orcesi and Prof. Fadi Hage Chehade for their time to report and review my work, their constructive comments and helpful suggestions and Dr. Farah Homsy the quality feedback she offered with regard to my work.

Prof. Alaa Chateaneuf, Prof. Wassim Raphaël and Dr. Rafic Faddoul for the quality of their supervision, their assistance, their sincere and selfless support, their patience and their ample time spent. They were always encouraging and available to give me their invaluable and wise advices during my research.

The National Council for Scientific Research in Lebanon (CNRS-L) and the Research Council at Saint Joseph University for their financial support.

Prof. Fadi Geara and Prof. Fouad Kaddah for their expertise, relevant advices, constructive discussions and particular follow-up which contributed in improving my research.

Finally, I can never thank my family enough for their love and affection. I dedicate this modest work to my parents Fadi and Feyrouz for the trust and unconditional support they have demonstrated throughout the past years, to my brother Patrick for his permanent encouragement and last but not least, my husband Adam who was able to cheer me up regularly during this long period and was my main source of motivation.



This page is intentionally left blank

## Résumé

Suite à l'expansion croissante des infrastructures de génie civil tout au long du vingtième siècle, le problème d'Inspection, Maintenance et Réhabilitation (IM&R) des ouvrages bénéficie actuellement d'une attention toute particulière. L'importance du problème se manifeste dans les pays industrialisés du fait de l'importance de leur patrimoine, sans cesse grandissant, en termes d'ouvrages de génie civil vieillissants. Par ailleurs, on assiste dans les pays en voie de développement à une accumulation des besoins de maintenance à cause du manque de budgets nécessaires pour de tels travaux. Ainsi, la réallocation des dépenses budgétaires pour l'inspection, la maintenance et la réhabilitation des structures existantes se fait au détriment des nouvelles constructions.

Dans ce contexte, la gestion de la durée de vie des structures existantes devient un enjeu majeur de la société. La surveillance des structures au moyen de capteurs permanents (connue sous le terme *Structural Health Monitoring* « SHM »), permet d'identifier et de suivre l'état de dégradation, afin d'en tirer des indicateurs sur la santé structurale et la durée de vie résiduelle. Mais cette instrumentation étant coûteuse, trouver une configuration optimale pour l'installation des capteurs est indispensable. Une autre méthode, plus couramment utilisée, se base sur une surveillance ponctuelle des structures par des inspections visuelles et/ou des techniques de détection non destructives. Or, ces moyens de surveillance ponctuelle permettent difficilement de détecter tout défaut dans la structure lors d'une visite. Dans certains cas, par exemple, un défaut critique pourrait apparaître entre deux inspections successives et ne pas être détecté à temps.

Ce travail de recherche a donc pour objectif d'améliorer les méthodes de détection, de localisation et de caractérisation d'endommagements ainsi que l'optimisation de la configuration des capteurs afin d'aboutir à une détection qui soit, à la fois, efficace et rentable.

Dans un premier temps, une synthèse bibliographique est présentée passant en revue les travaux concernant la surveillance des structures, les méthodes de détection ainsi que les méthodes d'optimisation. Dans un deuxième temps, quatre méthodologies ont été développées :

La première méthodologie, basée sur une mise à jour bayésienne, concerne la détection d'endommagements dans une structure sans avoir à résoudre le problème inverse qui est généralement mal défini. Le grand avantage de cette méthode réside dans sa capacité à prendre en considération, systématiquement et de façon transparente, toutes les incertitudes affectant le système structural ainsi que le système de mesure.

Cette méthodologie est en outre développée pour renforcer les informations sur les éléments et/ou structures moins surveillés (dont l'état de dégradation est défini avec une grande incertitude) en profitant des informations sur des structures/éléments bien surveillés (dont l'état de dégradation est défini avec une faible incertitude).

Une autre méthodologie s'intéresse à la fusion d'informations provenant d'une surveillance continue des structures et d'inspections conventionnelles afin de définir une planification optimale de surveillance et de maintenance des structures.

Ensuite, une nouvelle approche de type proie-prédateur a été proposée pour l'optimisation de la configuration (i.e. nombre et emplacement) des capteurs au sein de la structure. Toutes ces méthodes ont montré leur efficacité à travers des applications numériques sur différents types de structures.

**Mots-clés** : Surveillance de la santé structurale, analyse modale opérationnelle, évaluation des dommages, mise à jour Bayésienne, optimisation de l'instrumentation, algorithme Proie-Prédateur.

## Abstract

Following the growing expansion of civil engineering infrastructure throughout the twentieth century, the problem of Inspection, Maintenance and Rehabilitation (IM&R) of structures is currently given a particular attention. The importance of the problem manifests itself in industrialized countries because of the importance of their ever-growing heritage in terms of aging civil engineering structures. Thus, the reallocation of budgetary expenditure towards the inspection, maintenance and rehabilitation of the structures was made. As for the developing countries, a different pattern is observed. Despite the accumulation of maintenance needs due to the lack of budgets, available budgets are devoted to new constructions.

In this context, managing the lifespan of existing structures is becoming a major challenge for the society. The evaluation of structures' health state customarily relied on intermittent surveillance of structures at specific points in time by visual inspections and / or non-destructive detection techniques. However, these intermittent surveillance techniques make it difficult to detect any defect in the structure during an inspection visit. In some cases, for instance, a critical defect could appear between two successive inspections and not be detected in time. Monitoring structures using permanent sensors (known as Structural Health Monitoring "SHM") overcome this shortcoming and makes it possible to continuously identify and monitor the state of deterioration. The obtained results would be used in order to draw indicators on the structure's health and to assess its residual life. Unavoidable budget and resource limitations lead to the need for an optimal configuration of sensors.

The aim of the thesis is therefore to develop a framework consisting of several algorithms for the detection, localization and characterization of damage as well as the optimization of the sensors configuration.

First, a state-of-the-art review considering works done on structural monitoring, detection methods and optimization methods is presented. Four methodologies are then developed:

The first methodology, based on a hierarchical Approximate Bayesian inference, concerns the detection of structural damage without having to solve the inverse problem which is generally ill-posed. The main advantage of this method lies in its ability to take into account, systematically and transparently, all uncertainties affecting the structural system as well as the measurement system.

This methodology is further developed to amplify the information about less monitored elements and/or structures (whose condition states are defined with high uncertainty) using information collected from well monitored structures and/or elements (whose condition states are defined with low uncertainty).

An approach is then proposed to optimize the planning for the monitoring and maintenance of structures using data fusion of SHM results and conventional inspections outcomes.

Finally, a new predator-prey approach is proposed for optimizing the configuration (i.e. type, number and location) of sensors in a structure. All these methods have shown their effectiveness through numerical applications on different types of structures.

**Keywords:** Structural Health Monitoring, output-only modal identification, damage assessment, Bayesian updating, optimal sensor placement, Predator-Prey optimization, borrowing strength.

## List of notations

$\bar{M}$	Mass matrix
$\bar{C}$	Damping matrix
$\bar{K}$	Stiffness matrix of the undamaged structure
$\bar{K}^d$	Stiffness matrix of the damaged structure
$\overline{\Delta K}_e$	Element stiffness matrix perturbation caused by a damage of element $e$
$\Delta$	Change in a certain parameter
$\bar{u}$	Displacement vector
$\dot{\bar{u}}$	Velocity vector
$\ddot{\bar{u}}$	Acceleration vector
$\bar{p}(t)$	Vector of external forces
$\Psi$	Principal Component
$\omega_J$	Pulsation frequency relative to the mode of vibration J
$\omega_J^2$	Eigenvalue relative to the mode of vibration J
$\omega^{Md}$	Measured eigenvalue
$\omega^d$	Eigenvalue of the damaged structure
$\overline{\omega^2}$	Eigenvalue matrix
$\lambda_j$	Eigenfrequency relative to the mode of vibration J
$\bar{\lambda}$	Eigenfrequency vector of the undamaged structure
$\bar{\lambda}^d$	Eigenfrequency vector of the damaged structure
$\bar{\lambda}^{Md}$	Measured eigenfrequency vector of the damaged structure
$\bar{\lambda}^{SMd}$	Simulated eigenfrequency vector of the damaged structure
$\bar{\Phi}_J$	Eigenvector relative to the mode of vibration J
$\bar{\Phi}^d$	Eigenvector of the damaged structure
$\bar{\Phi}$	Eigenvector matrix of the undamaged structure
$\bar{\Phi}^d$	Eigenvector matrix of the damaged structure
$\bar{\Phi}^{Md}$	Measured eigenvector matrix of the damaged structure
$\bar{\Phi}^{SMd}$	Simulated eigenvector matrix of the damaged structure
$\bar{\alpha}_e$	Vector whose components represent alterations to various properties of element $e$
$\alpha_e$	Damage extent of element $e$
$\bar{\alpha}$	Vector of damage extents
$\bar{S}$	Sensitivity Matrix
$l$	Discrete Laplacian Transform
$\mu$	Mean of a distribution
$\sigma$	Standard deviation of a distribution
$\Phi''$	Curvature mode shape
$\mathcal{M}$	Bending moment
$E$	Modulus of elasticity

$I$	Moment of inertia
$\bar{F}$	Flexibility matrix
$\zeta$	Damping ratio
$M$	Conductance
$P$	Probability
$F_G$	Standard Gaussian cumulative distribution
$\bar{\varepsilon}_{Mo}$	Random vector representing model uncertainty
$\bar{\varepsilon}_{Me}$	Random vector representing measurement uncertainty
$\varepsilon_{Mo}$	Model uncertainty
$\varepsilon_{Me}$	Measurement uncertainty
$\varepsilon$	Tolerance reflecting an accuracy
$\rho$	Distance Measure
$\bar{\theta}$	Vector of the condition states of each element
$\theta^e$	True discretized condition state of the element $e$
$\bar{x}$	Mean of a sample
$\bar{a}$	Vector whose components are the chosen action for each element
$\bar{a}^e$	Maintenance actions applied to element $e$
$\bar{f}^e$	Feature vector of an element
$\beta_e$	Deterioration Rate
$\beta_c$	Class parameter
$\beta_c^e$	Deterioration rate of element $e$ belonging to class $C$
$\alpha_c^e$	Degradation extent of element $e$ belonging to class $C$
$\bar{A}^e$	Square transition matrix
$\alpha_{ij}^e$	Probability that state $\theta^e$ of element $e$ changes from $\theta^e = i$ to a new value $\theta^e = j$ after the application of the action $a^e$
$\bar{i}$	Vector whose components are the chosen inspection for each element
$\bar{i}^e$	Type of the inspection technique applied to element $e$
$r_l$	Result of an inspection for each element state $l$
Pr[ ]	Probability distribution
$C(a, \theta)$	Consequence derived from an action $a$ and a state of nature $\theta$
$ci(i^e)$	Cost due to the application of the inspection method $i^e$ on element $e$ .
$ca(a^e)$	Cost of the action $a^e$ applied on element $e$
$cs(\theta^e)$	Cost suffered by the user of the structure due to element $e$ being in state $\theta^e$
E[]	Expected value
U[]	Utility
$P_{sensors}$	Population of sensors
$Ch_{sensors}$	Chromosome of sensors
$f_s$	Fitness function of $P_{sensors}$
$C_s$	Cost induced by a configuration of sensors
$P_{defects}$	Population of defects

$Ch_{defects}$	Chromosome of defects
$f_d$	Fitness function of $P_{defects}$
$C_d$	Cost induced by a configuration of defects
$n_c$	Number of installed sensors
$c_c$	Unit price of sensors
$\bar{v}$	Vector whose components are the belief states of the individual elements
$\bar{v}_d$	Vector of the belief states of the elements in the damaged structure
$^*\bar{v}$	Vector whose components are the certain belief states of the individual elements
$^*\bar{v}_d$	Vector of the certain belief states of the elements in the damaged structure
$C(^*\bar{v})$	Cost induced by the application of the optimal maintenance actions based on $^*\bar{v}$
$C_{IMP}(^*\bar{v})$	Cost incurred by the application of the optimal maintenance actions, based on the imperfect information $\bar{v}$ , on a structure with a true certain state $^*\bar{v}$
$\alpha_{IMP}^e$	Imposed maintenance action on element $e$
$f_i$	Fitness of the chromosome $Ch_i$
$f_{cum_i}$	Cumulative fitness of the chromosome $Ch_i$
$P_{cum_i}$	Cumulative probability of selection of the chromosome $Ch_i$
$N_G$	Number of genes in a chromosome
$N_C$	Number of chromosomes in a population
$N_{C-acc}$	Number of chromosomes accepted in the new population
$N_{comb}$	Number of combinations
$N_d$	Number of defects chromosomes
$N_s$	Number of sensors chromosomes
$P_i$	Probability of selection of the chromosome $Ch_i$
$p_c$	Crossover probability
$p_m$	Mutation probability
$g_i$	Gene $i$ of a chromosome
$d_{Ch_i-Ch_j}$	Euclidean distance between two chromosomes $Ch_i$ and $Ch_j$
rnd	Random number
$FI_{Sensor}$	Fitness indicator for the sensors chromosomes
$FI_{Defect} = f_d$	Fitness indicator for the defects chromosomes



## List of abbreviations

ABC	Approximate Bayesian Computation
AR	Auto-Regressive
BSSP	Backward Sequential Sensor Placement
BWIM	Bridge Weigh-In-Motion
CC	Cross-Correlation Coefficient
CDF	Curvature Damage Factor
COMAC	Coordinate Modal Assurance Criterion
DLAC	Damage location assurance criterion
DOF	Degree-Of-Freedom
DI	Damage Indicator
DR	Diversity Rate
EMA	Experimental Modal Analysis
EMI	ElectroMechanical Impedance
ERA	Eigensystem Realization Algorithm
EV	Expected Value
EVPI	Expected Value of Perfect Information
EVII	Expected Value of Imperfect Information
FDD	Frequency Domain Decomposition
FEM	Finite Element Model
FGA	Float-Encoded Genetic Algorithm
FSE	Fractional Strain Energy
FSSP	Forward Sequential Sensor Placement
GA	Genetic Algorithm
HS	Harmony Search
IMPSO	Integer-encoding Multi-swarm Particle Swarm Optimization
IM&R	Inspection, Maintenance and Rehabilitation
LFCR	Local Frequency Change Ratio
MAC	Modal Assurance Criterion
MDLAC	Multiple Damage Location Assurance Criterion
MDOF	Multiple Degree-Of-Freedom
<i>mDOF</i>	Measured Degree-Of-Freedom
MR	Member Replacement
MSAD	Maximum Sum of Absolute Differences
N	Action of doing Nothing

OMA	Operational Modal analysis
OMAX	Operational Modal Analysis with eXogenous forces
OSP	Optimal Sensor Placement
PCA	Principle Component Analysis
PDF	Probability Density Function
PMF	Probability Mass Function
PSO	Particle Swarm Optimization
PZT	Piezoelectric Transducer
RMSD	Root-Mean Square Deviation
RMSE	Root-Mean Square Error
RNFC	Relative Natural Frequency Change
RRA	Regression Robust Analysis
SHM	Structural Health Monitoring
SR	Standard Repair
SSI	Stochastic Subspace Identification
SSP	Sequential Sensor Placement
S-PSO	Sequential Particle Swarm Optimization
T.M.	Transition Matrix
VI	Value of Information

# Contents

Résumé .....	i
Abstract .....	iii
List of notations .....	v
List of abbreviations .....	viii
Contents .....	x
Synthèse des travaux .....	1
1. Contexte .....	1
2. Objectifs de la thèse .....	2
3. Mise à jour bayésienne de l'état de dégradation des structures .....	3
4. Informations renforcées pour la surveillance de la santé structurale .....	7
5. Approche hybride inspection-surveillance pour une planification optimale de maintenance des structures .....	12
6. Optimisation de type proie-prédateur pour le placement optimal des capteurs .....	18
7. Conclusions .....	24
8. Perspectives .....	25
General Introduction .....	27
Overview .....	27
Contribution .....	28
Thesis Outline .....	29
Chapter 1: Literature Review .....	30
1.1 Introduction .....	30
1.2 Structural Health Monitoring .....	30
1.2.1 Monitoring Concepts: Inspection and Continuous Monitoring .....	30
1.2.2 Global and Local Monitoring .....	33
1.2.3 Passive and Active Monitoring Approaches .....	35
1.2.4 Data Interpretation Approaches .....	37
1.3 Operational Modal Analysis (OMA) .....	39
1.4 Damage Detection .....	41
1.4.1 Introduction .....	41

1.4.2	Damage Detection Methods.....	42
1.4.2.1	Modal-based methods .....	42
1.4.2.1.1	Natural Frequency.....	42
1.4.2.1.2	Mode Shape and Curvature Mode Shape.....	45
1.4.2.1.3	Modal Strain Energy .....	50
1.4.2.1.4	Modal Flexibility .....	52
1.4.2.1.5	Modal Damping .....	52
1.4.2.2	Electromechanical Impedance-based method.....	53
1.4.3	Damage Detection Approaches.....	55
1.4.3.1	Statistical Pattern Recognition.....	55
1.4.3.2	Bayesian Probabilistic Approach.....	55
1.4.3.2.1	Classical Bayesian Framework.....	55
1.4.3.2.2	Approximate Bayesian Computation.....	58
1.4.3.2.3	Hierarchical Bayesian Framework.....	59
1.4.4	Synthesis .....	60
1.5	Optimal Sensor Placement .....	61
1.5.1	Introduction.....	61
1.5.2	Optimal Sensor Placement Techniques .....	62
1.5.2.1	Particle Swarm Optimization.....	62
1.5.2.2	Sequential Sensor Placement .....	63
1.5.2.3	Simulated Annealing.....	64
1.5.2.4	Harmony Search .....	65
1.5.3	Genetic Algorithm .....	66
1.5.4	Synthesis .....	70
1.6	Conclusion .....	71
Chapter 2: Bayesian updating of the condition state of a structure .....		73
2.1	Overview .....	73
2.2	Modal Analysis of a structure .....	73
2.3	Definition of a damage.....	75
2.4	Model and Measurement Uncertainties .....	76

2.4.1	Model imperfection and simplification.....	76
2.4.2	Intrinsic aleatory uncertainty of some variables .....	77
2.4.3	Numerical errors and approximations.....	77
2.4.4	Measurement uncertainties .....	77
2.4.5	Partial observability of the system.....	77
2.5	Approximate Bayesian Computation for a single structure .....	79
2.6	Evaluation Metric $\rho$ .....	82
2.7	Numerical Applications .....	83
2.7.1	Steel Truss.....	84
2.7.2	Multistory Concrete Frame .....	88
2.7.3	Sensitivity analysis on damage detection .....	92
2.7.3.1	Steel Truss.....	93
2.7.3.2	Multistory Concrete Frame .....	97
2.8	Conclusion .....	101
Chapter 3: Information amplifying by borrowing strength for Structural Health Monitoring .....		102
3.1	Introduction.....	102
3.2	Classification Scheme for Elements .....	103
3.3	Hierarchical Approximate Bayesian Computation for Borrowing Strength.....	105
3.4	Numerical Applications .....	109
3.4.1	Four Steel Truss Structures.....	110
3.4.2	Multistory Concrete Frame .....	117
3.4.3	Sensitivity analysis on damage detection .....	121
3.4.3.1	Four Steel Truss Structures.....	121
3.4.3.2	Multistory Concrete Frame .....	125
3.5	Conclusion .....	128
Chapter 4: Hybrid inspection-monitoring approach for optimal maintenance planning .....		129
4.1	Overview .....	129
4.2	Decision Making under Uncertainty .....	130
4.2.1	M&R Decision-Making Without Inspection .....	130
4.2.2	IM&R Decision Making With Inspection .....	133

4.2.3	Value of Information .....	135
4.3	Dynamic IM&R Optimal maintenance planning .....	136
4.3.1	Methodology .....	136
4.3.2	False Positives and False Negatives .....	140
4.4	Numerical Applications .....	141
4.4.1	Steel Truss.....	141
4.4.2	Multistory Concrete Frame .....	150
4.5	Conclusion .....	158
Chapter 5:	A predator-prey optimization for optimal sensor placement .....	159
5.1	Overview .....	159
5.2	Predator-Prey Relationship .....	160
5.3	Genetic Algorithm steps.....	161
5.3.1	Initialization .....	161
5.3.2	Evaluation (Fitness function calculation) .....	162
5.3.2.1	Sensor configuration fitness.....	163
5.3.2.2	Defect configuration fitness .....	165
5.3.3	Selection.....	165
5.3.4	Crossover .....	166
5.3.5	Mutation.....	167
5.3.6	Termination criterion .....	168
5.4	Predator-Prey optimization with Genetic Algorithm .....	168
5.5	Diversification.....	171
5.6	Numerical Application .....	172
5.6.1	Steel Truss.....	172
5.6.2	Multistory Concrete Frame .....	183
5.7	Conclusion .....	192
General Conclusion.....		194
Perspectives .....		196
References.....		197
Appendix A: Modal analysis results .....		212

Appendix B: Sensitivity Analysis results .....216  
Appendix C: Best configurations of sensors obtained by the numerical applications.....223

# Synthèse des travaux

## 1. Contexte

La surveillance de la santé structurale (SHM) par des capteurs permanents est en forte progression au cours des dernières décennies, grâce aux progrès technologiques dans plusieurs domaines (e.g. la technologie des capteurs, le traitement des données, etc.). La SHM combine diverses technologies pour la détection et la localisation des dommages afin d'évaluer l'état de dégradation d'une structure et de prévoir sa durée de vie résiduelle. Dans le domaine de la SHM, deux approches peuvent être adoptées :

- (i) L'approche locale basée sur une évaluation directe d'un élément ou d'une partie de structure pour déterminer son état de dégradation ;
- (ii) L'approche globale basée sur une modélisation mécanique de la structure où des capteurs (dont le nombre et les emplacements doivent être optimisés) sont implémentés pour surveiller l'ensemble de la structure. Compte tenu des budgets limités pour le suivi, l'entretien et la réhabilitation des ouvrages et infrastructures, l'installation de capteurs en chaque degré de liberté de la structure est impossible dans la pratique. Il est donc préférable de suivre indirectement la structure par le biais d'approches globales qui se caractérisent par leur capacité à prendre en compte, systématiquement, toutes les incertitudes affectant les paramètres structuraux (i.e. dimensions géométriques, module d'Young), les mesures imparfaites, etc. Cette approche permet de placer judicieusement peu de capteurs sur une structure, afin de prédire l'état de dégradation de ses éléments.

Selon Rytter (1993), les techniques de détection de dommages peuvent classées en quatre niveaux : (i) détection de la présence de dommages dans la structure ; (ii) localisation des défauts ; (iii) estimation de l'étendue des dommages et (iv) calcul de la durée de vie résiduelle de la structure et évaluation des risques. Au cours des dernières années, les progrès technologiques dans le domaine du génie civil et des disciplines connexes se sont concentrés sur le développement de méthodologies d'évaluation des dommages qui permettent de satisfaire un ou plusieurs niveaux du classement de Rytter. Une des techniques d'identification les plus adéquates pour les problèmes inverses est la mise à jour bayésienne fournissant un outil rationnel et robuste, capable de trouver toutes les valeurs possibles des paramètres du modèle. Toutefois, dans la plupart des travaux, des hypothèses sont prises en compte afin de construire une fonction de vraisemblance appropriée qui pourrait être difficile à exprimer explicitement.

De plus, la littérature se concentre uniquement sur l'évaluation de l'état d'une seule structure, où les éléments peuvent être moins surveillés que d'autres en raison du nombre limité de capteurs. En tant que tel, des développements sont nécessaires pour surveiller un grand nombre de structures à la fois (e.g. bâtiments identiques dans des complexes d'habitation ou des ponts similaires dans une même ville) et obtenir des informations sur le



plus grand nombre d'éléments (même au sein d'une même structure) en implémentant un nombre réduit de capteurs.

Un autre concept couramment utilisé pour le suivi des structures est l'inspection périodique commençant par une inspection visuelle qui peut être suivie par des techniques destructives et/ou non destructives. Une telle approche connaît de nombreuses limites. Par exemple, l'état de dégradation de la structure n'est connu qu'à des moments discrets, au moment de l'inspection. Ainsi, la dégradation des structures est partiellement surveillée. Tout défaut qui pourrait apparaître entre deux inspections successives et éventuellement nécessiter une action de maintenance urgente, pourrait demeurer non détecté jusqu'à la date d'inspection suivante. De plus, le coût d'une inspection est généralement fonction de sa précision. Il est donc utile de combiner les deux concepts : inspections périodiques et surveillance permanente (SHM).

Enfin, pour optimiser la surveillance de la santé structurale, les capteurs doivent être judicieusement implémentés dans la structure en termes de nombre et d'emplacement. Un nombre optimal de capteurs doit être installé à des emplacements optimaux afin de : (i) minimiser le coût des capteurs, (ii) maximiser la probabilité de détection des dommages, (iii) maximiser la précision de la localisation des dommages et (iv) maximiser la précision de la quantification des dommages. Il s'agit d'un problème d'optimisation avec des objectifs contradictoires à différents niveaux. Par exemple, maximiser la probabilité et la précision de détection entraîne une augmentation du coût des capteurs. Aussi, pour un nombre donné de capteurs, l'augmentation de la précision de surveillance pour certains éléments se traduit généralement par une diminution de précision pour les éléments restants.

## **2. Objectifs de la thèse**

Cette étude a pour objectif de contribuer à surmonter les défis énumérés ci-dessus concernant la détection des dommages, le placement optimal des capteurs et la planification de la maintenance.

Tout d'abord, une approche de Calcul Bayésien Approché (connu sous le terme *Approximate Bayesian Computation* « ABC ») a été proposée afin d'évaluer l'état de dégradation d'une structure sans passer par des solutions analytiques. Cette approche permet de prendre en compte toutes les incertitudes liées à la dégradation des éléments, au modèle mécanique et à la précision des mesures de capteurs. L'ABC est considéré comme le noyau de la thèse, étant donné qu'il est intégré dans toutes les méthodologies développées.

Cette approche est davantage développée pour extraire des informations d'éléments/structures bien surveillées afin de renforcer les informations sur les éléments/structures moins surveillées. Autrement dit, un calcul bayésien hiérarchique approché (HABC) est proposé pour mettre à jour l'état d'un élément et/ou d'une structure en fonction des données générées à partir de la surveillance d'éléments et/ou de structures similaires appartenant à la même classe. Cette technique contribue à renforcer l'évaluation des structures et à réduire le nombre de capteurs nécessaires pour surveiller plusieurs éléments et/ou structures à la fois.

Une autre contribution consiste en la combinaison de données provenant de différentes sources telles que la surveillance permanente et les inspections conventionnelles pour définir une planification optimale d'inspection, de maintenance et de réhabilitation des structures. Cette procédure applique l'approche ABC dans un cadre d'analyse de décision. Elle offre au décideur la possibilité de choisir de manière optimale, à un moment précis, la nécessité d'inspecter un élément particulier ou d'appliquer directement des actions de maintenance (i.e. une réparation ou un remplacement) sur les éléments s'il juge nécessaire. Lorsqu'une inspection est prescrite, ses résultats sont pris en considération et combinés aux résultats de la SHM, ce qui contribue à réduire l'incertitude affectant l'évaluation des dommages.

Une partie du travail a également porté sur l'amélioration des algorithmes génétiques pour un placement optimal des capteurs. Un nouveau concept a été introduit, le concept prédateur-proie appliqué dans un algorithme génétique. Cette méthode repose sur l'approche ABC et permet une coévolution antagoniste de la population de capteurs et de la population de défauts, chacune évoluant en fonction de l'évolution de l'autre. Il en résulte une configuration optimale de capteur capable de détecter autant de configurations de dommages que possible.

### **3. Mise à jour bayésienne de l'état de dégradation des structures**

La détection, la localisation et l'évaluation des anomalies sont les trois principaux piliers de la surveillance de la santé structurale. Ils appartiennent à la catégorie "diagnostic des dommages" qui englobe des techniques d'identification des dommages et des données de capteurs pour évaluer l'état d'endommagement d'une structure. Identifier les paramètres de rigidité des structures saine et endommagée à l'aide des données de vibration collectées est un moyen très courant pour détecter un dommage. Dans de tels cas, un dommage est défini par la réduction de la rigidité (Ching et Beck 2004). Ce sujet représente le centre d'intérêt de nombreux chercheurs qui ont développé différentes techniques pour détecter les dommages dans une structure en comparant sa réponse vibratoire avant et après qu'un dommage se produise (Das et al.2016; Hu et Afzal 2006). Parmi toutes ces techniques, la mise à jour bayésienne, basée sur une approche d'identification inverse du système s'est avérée très efficace pour identifier les dommages dans une structure à l'aide des données vibratoires. La distribution *a priori* postulée d'un paramètre, qui peut être informative ou non, est mise à jour avec chaque nouvelle information obtenue à partir des capteurs. Cependant, dans la plupart des publications, des hypothèses sont prises en compte pour formuler une fonction de vraisemblance appropriée qui est, dans de nombreux cas, difficile à exprimer explicitement.

Dans ce contexte, une nouvelle méthodologie est développée pour mettre à jour l'état d'endommagement d'une structure sans avoir recours à des hypothèses aboutissant à des fonctions de vraisemblance explicites. Le degré d'endommagement des éléments structuraux est évalué à l'aide d'un cadre hiérarchique de calcul bayésien approché (ABC). Il prend explicitement en compte toutes les incertitudes liées à la précision des capteurs, au manque de données dû au fait que tous les degrés de liberté ne sont pas mesurés, au modèle mécanique et à la dégradation des éléments.

Un endommagement dans la structure est caractérisé par une perte dans la matrice de rigidité d'un ou plusieurs éléments de la structure. Ce changement affecte les éléments de la matrice de rigidité de manière inégale en fonction du type d'endommagement, sa source et sa répartition locale (par exemple, perte de section due à la corrosion, fissures dues à la fatigue, etc.). Par conséquent, le vecteur de l'étendue de dégradation  $\bar{\alpha}_e$  d'un élément est défini comme un vecteur dont les composantes représentent des altérations de diverses propriétés de l'élément  $e$  (module d'Young, moment d'inertie, etc.). Adoptant la notation de Shi et al. (2000), un endommagement est représenté par :

$$\bar{K}^d = \bar{K} + \sum_{e=1}^N \bar{\Delta K}_e \quad (1)$$

où  $\bar{K}^d$  et  $\bar{K}$  sont les matrices de rigidité des structures endommagée et saine respectivement,  $N$  le nombre d'éléments et  $\bar{\Delta K}_e$  la perturbation de la matrice de rigidité élémentaire causée par un endommagement de l'élément  $e$  ( $\bar{\Delta K}_e = f(\bar{\alpha}_e)$ ).

Toute information préalable sur l'étendue des dommages peut être exprimée par la distribution de probabilité *a priori* de  $\bar{\alpha}_e$ . En choisissant les bornes zéro et un pour  $\bar{\alpha}_e$ , des connaissances en ingénierie peuvent être introduites dans le modèle (i.e. la rigidité des éléments est une fonction décroissante monotone non négative en termes de dégradation, tant qu'aucune maintenance n'est effectuée).

Le comportement réel d'une structure présente des écarts plus ou moins importants par rapport au comportement mécanique prévu. Les incertitudes du modèle et de mesure sont définies et prises en compte dans la méthodologie proposée. Ces écarts résultent de différentes sources d'incertitude telles que : les erreurs d'observation, l'inadéquation du modèle, l'incertitude des paramètres, les approximations mathématiques, etc.

Pour tenir compte de l'incertitude du modèle, on considère :

- $\bar{\lambda}$  et  $\bar{\lambda}^d$  les vecteurs de fréquences propres de la structure saine et endommagée respectivement.
- $\bar{\Phi}$  et  $\bar{\Phi}^d$  les matrices de vecteurs propres de la structure saine et endommagée respectivement.
- $\bar{\varepsilon}_{Mo}$  un vecteur aléatoire représentant l'incertitude du modèle.
- $\bar{\varepsilon}_{Me}$  un vecteur aléatoire représentant l'incertitude de mesure.

Similairement à l'équation (1), la réponse structurale de la structure est représentée par :

$$\bar{\lambda}^d = \bar{\lambda} + \bar{\Delta \lambda} \quad (2)$$

$$\bar{\Phi}^d = \bar{\Phi} + \bar{\Delta \Phi} \quad (3)$$

Le comportement mécanique de la structure endommagée peut être représenté par :

$$(\bar{\lambda}^d, \bar{\Phi}^d) = g(\bar{K}^d, \bar{\varepsilon}_{Mo}) \quad (4)$$

où  $g()$  est une fonction déterministe dépendant de  $\bar{\varepsilon}_{Mo}$ . Dans l'application numérique,  $g()$  représente un algorithme FEM.

D'autre part, la réponse structurale mesurée  $(\bar{\lambda}^{Md}, \bar{\Phi}^{Md})$  diffère de la vraie réponse structurale  $(\bar{\lambda}^d, \bar{\Phi}^d)$  à cause du bruit et des incertitudes de mesure. Ainsi :

$$(\bar{\lambda}^{Md}, \bar{\Phi}^{Md}) = w(\bar{\lambda}^d, \bar{\Phi}^d, \bar{\varepsilon}_{Me}) = w(g(\bar{K}^d, \bar{\varepsilon}_{Mo}), \bar{\varepsilon}_{Me}) = w(g(\bar{K} + \sum_{e=1}^N \bar{\Delta K}_e, \bar{\varepsilon}_{Mo}), \bar{\varepsilon}_{Me}) \quad (5)$$

où  $w()$  est une fonction déterministe qui dépend de  $\bar{\varepsilon}_{Me}$ .

Lors de l'application de l'algorithme ABC sur la structure, les réponses structurales simulées et observées sont comparées en calculant une distance  $\rho$ , afin de mettre à jour le modèle et d'identifier les dommages. Dans notre cas, nous proposons d'utiliser la somme maximale des différences absolues comme suit :

$$\rho = \max_{mDOF} \sum_{i=1}^M |\bar{\Phi}_{DOF-i}^{Md} - \bar{\Phi}_{DOF-i}^d| \quad (6)$$

où  $M$  représente le nombre de modes de vibration et  $mDOF$  les degrés de liberté mesurés.

La valeur maximale de sommation des différences entre les valeurs des vecteurs propres observés et simulés est acceptée avec une probabilité  $\psi(\rho)$ . La fonction kernel  $\psi(\rho)$  représente la distribution de probabilité (connue sous le terme *Probability Density Function* « PDF ») des erreurs de mesure. Si  $\psi(\rho)$  est une PDF uniforme, alors la probabilité d'acceptation est équivalente à ce qui suit:

$$p = \begin{cases} 1 & \text{if } \rho \leq \varepsilon \\ 0 & \text{if } \rho > \varepsilon \end{cases} \quad (7)$$

où  $\varepsilon$  est définie comme une erreur de mesure sur les données.

Dans notre problème, le but de la mise à jour bayésienne est de calculer la PDF *a posteriori* de l'étendue des dommages  $\alpha_e$  ( $\bar{\alpha}_e$  est réduit à une composante  $\alpha_e$ ) pour chaque élément, après avoir observé la réponse structurale  $(\bar{\lambda}^{Md}, \bar{\Phi}^{Md})$ :

$$f(\bar{\alpha} | \bar{\lambda}^{Md}, \bar{\Phi}^{Md}) = \frac{f(\bar{\lambda}^{Md}, \bar{\Phi}^{Md} | \bar{\alpha}) \times f(\bar{\alpha})}{f(\bar{\lambda}^{Md}, \bar{\Phi}^{Md})} \quad (8)$$

où  $\bar{\alpha}$  est un vecteur dont les composantes sont les étendues d'endommagement  $\alpha_e$  de chaque élément,  $f(\bar{\alpha})$  est la distribution *a priori*,  $f(\bar{\alpha} | \bar{\lambda}^{Md}, \bar{\Phi}^{Md})$  la distribution *a posteriori* pour une observation donnée  $(\bar{\lambda}^{Md}, \bar{\Phi}^{Md})$  et  $f(\bar{\lambda}^{Md}, \bar{\Phi}^{Md} | \bar{\alpha})$  la fonction de vraisemblance.

La mise à jour bayésienne de l'équation (8) peut être conceptuellement partitionnée en une mise à jour bayésienne hiérarchique comme suit:

$$f(\bar{\lambda}^d, \bar{\Phi}^d | \bar{\lambda}^{Md}, \bar{\Phi}^{Md}) = \frac{f(\bar{\lambda}^{Md}, \bar{\Phi}^{Md} | \bar{\lambda}^d, \bar{\Phi}^d) \times f(\bar{\lambda}^d, \bar{\Phi}^d)}{f(\bar{\lambda}^{Md}, \bar{\Phi}^{Md})} \quad (9a)$$

$$f(\bar{K}^d | \bar{\lambda}^d, \bar{\Phi}^d) = \frac{f(\bar{\lambda}^d, \bar{\Phi}^d | \bar{K}^d) \times f(\bar{K}^d)}{f(\bar{\lambda}^d, \bar{\Phi}^d)} \quad (9b)$$

$$f(\bar{\alpha}|\bar{K}^d) = \frac{f(\bar{K}^d|\bar{\alpha}) \times f(\bar{\alpha})}{f(\bar{K}^d)} \quad (9c)$$

Dans notre problématique, la fonction de vraisemblance est implicite, étant donné que la relation entre les paramètres structuraux ( $\bar{K}^d$ ) et la réponse ( $\bar{\lambda}^d, \bar{\Phi}^d$ ) est décrite par un modèle numérique tel que la méthode des éléments finis. Par la suite, nous adoptons le calcul bayésien approché (Approximate Bayesian Computation ABC) qui donne une approximation de la distribution *a posteriori* en générant des échantillons de données à partir d'un modèle précis. Ainsi, afin de calculer la distribution de probabilité *a posteriori*  $f(\bar{\alpha}|\bar{K}^d)$ , nous proposons les étapes de calcul suivantes (Fig. 1) :

- 1- Générer  $\bar{\alpha}$  d'une distribution *a priori* appropriée de l'étendue des dommages ;
- 2- A partir des  $\bar{\alpha}$  générés, simuler  $(\bar{\lambda}^{SMd}, \bar{\Phi}^{SMd})$ . Pour le calcul de  $(\bar{\lambda}^{SMd}, \bar{\Phi}^{SMd})$ , on peut éventuellement ajouter un bruit à n'importe quelle étape du calcul pour tenir compte des incertitudes du modèle, autres que celles prises en compte par le seuil  $\varepsilon$ ;
- 3- Calculer une distance  $\rho$  entre la réponse structurale observée  $\bar{\lambda}^{Md}, \bar{\Phi}^{Md}$  et la réponse simulée  $(\bar{\lambda}^{SMd}, \bar{\Phi}^{SMd})$ ;
- 4- Accepter  $\bar{\alpha}$  avec une probabilité  $\psi(\rho)$ .  $\psi$  est une fonction noyau décroissante monotone de  $\rho$ . Si  $\psi(\rho)$  est une distribution uniforme, alors la règle d'acceptation se réduit à :  
si  $\rho \leq \varepsilon$  où  $\varepsilon$  est un petit seuil d'acceptation choisie ;
- 5- Définir la distribution *a posteriori* de l'étendue des dommages basée sur l'ensemble des valeurs acceptées de  $\bar{\alpha}$ .

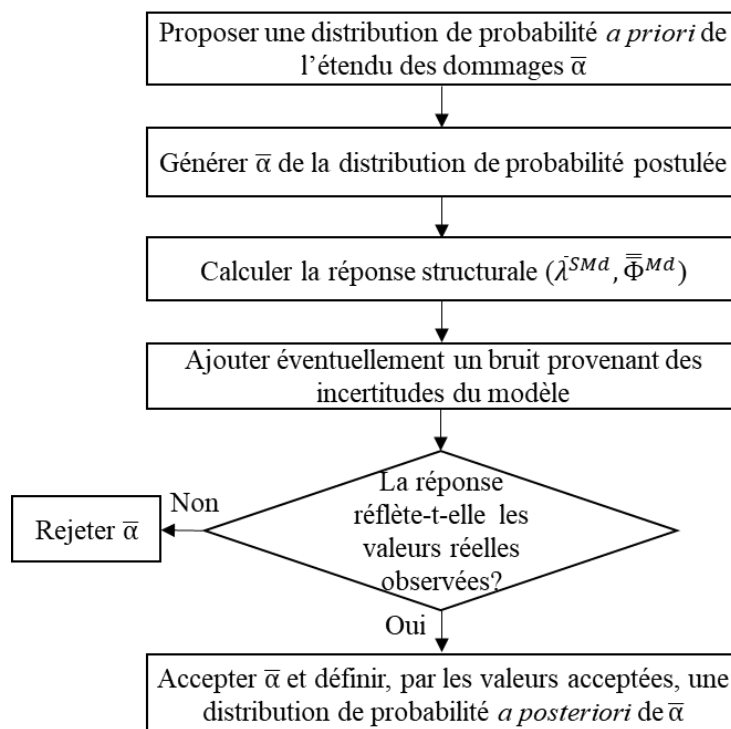


Figure 1: Organigramme de la mise à jour Bayésienne pour une structure singulière.

Dans un cadre général, les valeurs acceptées de  $\bar{a}$  forment une approximation de la vraie fonction *a posteriori* à moins que  $\varepsilon = 0$  ou  $\varepsilon = \infty$ . Cependant, Wilkinson (2013) a montré que si les erreurs de modèle et/ou de mesure sont modélisées comme une variable aléatoire uniformément distribuée sur un intervalle  $[-\varepsilon, \varepsilon]$ , alors la distribution *a posteriori* calculée sera exacte. Il a également présenté une extension de l'ABC d'origine où le modèle et/ou les erreurs de mesure peuvent avoir n'importe quelle distribution de probabilité donnée.

La méthodologie proposée a été validée par deux applications numériques : (i) un treillis métallique composé de 33 éléments et (ii) un portique en béton à quatre étages composé de 20 éléments. Les deux structures planes sont soumises à une excitation ambiante inconnue (provenant du trafic, du vent, des vagues dans le cas d'une structure offshore, etc.). L'erreur de mesure est considérée comme une variable aléatoire uniforme ayant une moyenne nulle dans les limites de  $0.15 \text{ m/s}^2$ . On suppose que les erreurs du modèle sont uniformément réparties dans les limites de 10% de la valeur réelle.

Ces applications ont démontré que l'ABC est capable d'évaluer un dommage modéré et sévère. Cependant, dans certains cas, les dommages légers pourraient ne pas être détectés, en particulier si ces dommages affectent des éléments ayant de faibles effets sur les formes modales d'une structure. La source de cette incertitude provient de la précision de mesure et du placement des capteurs. L'utilisation de capteurs plus précis, à leur emplacement optimal, améliore la capacité de détection. Néanmoins, ces capteurs peuvent ne pas être toujours disponibles ou sont très coûteux. Dans les paragraphes suivants, nous développerons des méthodologies pour améliorer la capacité de détection par : (i) une mise à jour bayésienne avec renforcement des informations, (ii) une analyse de décision prenant en considération les résultats de la mise à jour bayésienne, (iii) le placement optimal des capteurs.

#### **4. Informations renforcées pour la surveillance de la santé structurale**

L'évolution des dommages au cours des dernières décennies s'est principalement articulée autour de trois enjeux principaux, à savoir : (i) accroître l'efficacité des algorithmes d'optimisation ; (ii) accroître la disponibilité des données pertinentes et (iii) développer de nouvelles techniques de maintenance et d'inspection rentables. On peut ainsi noter qu'une part importante de la littérature spécialisée est consacrée aux méthodologies visant à améliorer l'optimalité du processus décisionnel en exploitant au maximum les données disponibles. Viser à maximiser un tel objectif n'est pas une tâche facile à faire. En effet, augmenter la quantité et diversifier les types de données utilisées peut facilement conduire à des problèmes d'optimisation insolubles. En outre, les sources de données utiles peuvent ne pas être immédiatement évidentes pour les chercheurs et les décideurs.

De ce fait, une méthodologie est proposée pour améliorer les informations fournies par les capteurs SHM et /ou l'inspection en appliquant le concept bayésien pour emprunt de force (par emprunt de données) dans des modèles hiérarchiques. En adoptant cette approche, des informations sur des éléments et / ou structures moins surveillées (dont l'état de dégradation est défini avec une grande incertitude) peuvent être extraites d'autres éléments et/ou

structures similaires bien surveillés (dont l'état de dégradation est défini avec une faible incertitude). Les éléments bénéficiant de l'emprunt de force peuvent appartenir à la même structure ou à des structures différentes.

L'application de la méthode de l'emprunt de force sur certains éléments (ou structures) nécessite un certain degré de similitude entre ces éléments (ou structures). Par éléments similaires, nous désignons des éléments partageant une ou plusieurs valeurs caractéristiques, telles qu'un même matériau, une géométrie similaire, des joints mécaniques similaires, des charges de même type et ordre de grandeur, conditions environnementales similaires, etc. Dans ce qui suit, un schéma de classification est proposé afin de catégoriser les éléments en fonction de leur similitude par rapport à un mécanisme de dégradation donné.

Le vecteur caractéristique d'un élément est défini par :

$$\bar{f}^e = [f_1^e, \dots, f_i^e, \dots, f_F^e] \quad (10)$$

où  $F$  est le nombre total d'entités pertinentes et  $f_i$  une mesure de l'entité  $i$ .

$f_i$  peut être pris comme: (i) une variable continue (e.g. porosité d'un matériau); (ii) une variable booléenne binaire (e.g. matériau de l'élément); (iii) une variable entière ordinale (e.g. exposition environnementale de l'élément). Ainsi, chaque élément appartient essentiellement à un espace de caractéristiques dimensionnelles  $F$ . Certaines dimensions de cet espace ne sont pas continues.

Une classe d'éléments est considérée comme le produit cartésien des intervalles de caractéristiques  $F$  (une pour chaque dimension):

$$C = \prod_{i=1}^F [f_{i,L_i}, f_{i,U_i}] \quad (11)$$

où  $f_{i,L_i}$  et  $f_{i,U_i}$  sont respectivement les bornes inférieure et supérieure d'un sous-intervalle d'une caractéristique  $f_i$ .

Les éléments d'une même classe peuvent appartenir à une ou plusieurs structures. En ce qui concerne le nombre de niveaux de hiérarchie, à un extrême, on pourrait attribuer un niveau à chaque caractéristique pertinente. Dans un tel cas, le classement de la hiérarchie dépend de l'importance de la caractéristique. À l'autre extrême, on pourrait opter pour une hiérarchie à deux niveaux uniquement. Dans ce cas, les caractéristiques sont supposées avoir la même importance. Le choix du nombre de niveaux dépend du nombre d'éléments et de la complexité calculatoire. Selon cette définition des classes, le degré de similitude entre les éléments appartenant à la même classe sera : (i) une fonction décroissante monotone de la longueur d'intervalle de chaque dimension ; et (ii) une fonction croissante monotone de la dimensionnalité  $F$  de l'espace des caractéristiques. Dans la méthodologie proposée, l'ensemble des séquences possibles est restreint à celles qui représentent une classification de plus en plus fine en termes de similitude des éléments d'une même classe par rapport à un mécanisme de dégradation donné. Autrement dit, le schéma de classification consiste à classer les éléments en commençant par l'élément le plus pertinent (le niveau de classe le

plus élevé), par rapport à un mécanisme de dégradation donné, jusqu'à l'élément le moins pertinent (le niveau de classe le plus fin / le plus bas).

La présente méthodologie intègre le cadre ABC décrit dans le paragraphe précédent. Par conséquent, nous admettons que la dégradation d'un élément est caractérisée par une modification de son comportement mécanique. Le processus de dégradation lié à une classe d'éléments n'est généralement pas déterministe en raison (i) des incertitudes intrinsèques liées à l'effet du matériau, de l'environnement, du chargement, etc. ; (ii) des différences entre les éléments appartenant à cette classe ; (iii) des incertitudes statistiques dues au fait que l'estimation des paramètres du processus de dégradation est généralement basée sur des estimateurs calculés à partir d'échantillons de taille finie. Ces incertitudes, en plus de celles dues à des erreurs de mesure et des informations incomplètes, sont prises en compte dans notre méthodologie.

L'un des principaux avantages de la mise à jour bayésienne est la possibilité de profiter des connaissances sur un paramètre pour renforcer les informations issues des données observées. Par exemple, des informations utiles concernant le taux de dégradation d'un élément pourraient être: (i) l'état de dégradation des éléments lors des inspections / évaluations précédentes; (ii) le taux de dégradation d'éléments similaires (i.e. appartenant à la même classe); (iii) une estimation experte de l'impact des conditions environnementales sur le taux de dégradation; etc. Dans le paradigme bayésien, cette variété d'informations est prise en compte via deux mécanismes principaux : (i) les PDF *a priori* utilisant les informations disponibles sur un paramètre incertain  $\beta_i$  et (ii) la modélisation hiérarchique permettant d'utiliser des informations sur les paramètres liés  $\beta_{j \neq i}$  pour déduire la distribution de probabilité (PDF) postérieure de  $\beta_i$ . Ce flux d'informations de  $\beta_{j \neq i}$  vers  $\beta_i$  est souvent désigné par le terme « Borrowing Strength » (ou emprunt de force). En considérant que les taux de dégradation des deux éléments sont liés hiérarchiquement via le paramètre de classe parent, on peut déduire du taux de dégradation du premier élément compte tenu des observations liées au deuxième.

Dans ce schéma, nous choisissons une modélisation bayésienne hiérarchique du taux de dégradation  $\beta_c^e$ . Les informations stochastiques liées au taux de dégradation sont divisées en deux niveaux, à savoir le niveau de l'élément et le niveau de la classe. Le taux de dégradation des éléments dépend donc de deux paramètres : l'un est lié à la classe (représentant le point commun entre les éléments de cette classe) et l'autre est lié à l'élément individuel (représentant la variabilité des éléments d'une même classe). On pourrait supposer que plus la classe est élevée dans la hiérarchie, plus le processus de dégradation qui y est lié est incertain. Cette augmentation de l'incertitude est due au fait que les classes élevées dans la hiérarchie ont moins de caractéristiques les définissant et, par conséquent, contiennent des éléments plus dissemblables.

La distribution de probabilité postérieure dans un schéma hiérarchique est définie par:

$$f(\beta_c^e, \beta_c | \bar{\lambda}^{Md}, \bar{\Phi}^{Md}) = \frac{f(\bar{\lambda}^{Md}, \bar{\Phi}^{Md} | \beta_c^e, \beta_c) \times f(\beta_c^e | \beta_c) \times f(\beta_c)}{f(\bar{\lambda}^{Md}, \bar{\Phi}^{Md})} \quad (12)$$



où  $(\bar{\lambda}^{Md}, \bar{\Phi}^{Md})$  est la réponse structurale mesurée de la structure endommagée,  $\beta_c^e$  est le taux de dégradation de l'élément  $e$  et  $\beta_c$  est un paramètre de classe dont  $\beta_c^e$  dépend stochastiquement.

Un schéma hiérarchique fréquemment utilisé serait de supposer que le paramètre de niveau supérieur ( $\beta_c$  dans notre cas) est la valeur attendue de la PDF à partir de laquelle les paramètres de niveau inférieur (dans notre cas, les taux de dégradation  $\beta_c^e$  liés à chaque élément) sont échantillonnés. Dans ce schéma,  $\beta_c$  est une variable aléatoire.

L'approche proposée est une méthode de calcul approché bayésien hiérarchique (HABC) (Turner et Van Zandt 2014). HABC est la mise en œuvre de la méthode ABC dans un modèle hiérarchique où les paramètres sont structurés en différents niveaux dépendants. La relation entre les paramètres à plusieurs niveaux est donnée par une distribution de probabilité jointe. Cette modélisation est utilisée pour l'estimation des paramètres et permet de combiner des informations provenant de différentes sources.

Dans notre méthodologie, l'approche HABC est adoptée afin de mettre à jour l'état d'endommagement de plusieurs éléments similaires simultanément. Ces éléments peuvent appartenir à une ou plusieurs structures. Les étapes de calcul proposées sont les suivantes (Figure 2):

- 1- Classer les éléments des structures selon un ensemble de caractéristiques ;
- 2- Pour chaque classe d'éléments, postuler une distribution de probabilité *a priori* pour un paramètre  $\beta_c$ ;
- 3- Pour chaque élément de chaque structure, supposer une distribution de probabilité *a priori* paramétrée du taux de dégradation  $\beta_c^e$  en fonction de  $\beta_c$  basé sur les inspections et/ou évaluations SHM préalables;
- 4- Pour chaque classe d'éléments C :
  - a. Tirer une valeur aléatoire pour  $\beta_c$  à partir de la distribution définie à l'étape 2;
  - b. Pour chaque structure et pour chaque élément  $e$  appartenant à la classe C, tirer une valeur aléatoire de  $\beta_c^e$  à partir de la distribution de probabilité définie à l'étape 3 et basée sur la valeur de  $\beta_c$  tirée à l'étape 4-a;
  - c. A partir des valeurs  $\beta_c^e$  générées en 4-b, calculer, pour chaque structure, la distance  $\rho_s$  entre la réponse structurale observée et celle simulée (Eq. 6).
- 5- Accepter  $\beta_c$  et  $\beta_c^e$  ( $1 \leq e \leq N$ ) avec une probabilité égale à  $\psi(\rho_1, \dots, \rho_s, \dots, \rho_{NS})$ , où  $\psi$  est une fonction noyau décroissante monotone de  $\rho_s$  et  $NS$  le nombre de structures.
- 6- A partir des valeurs acceptées  $\beta_c$  et  $\beta_c^e$  ( $1 \leq e \leq N$ ), définir la distribution *a posteriori* des taux de dégradation  $f(\beta_c, \beta_c^e (1 \leq e \leq N) | \bar{\lambda}^{Md}, \bar{\Phi}^{Md})$ .

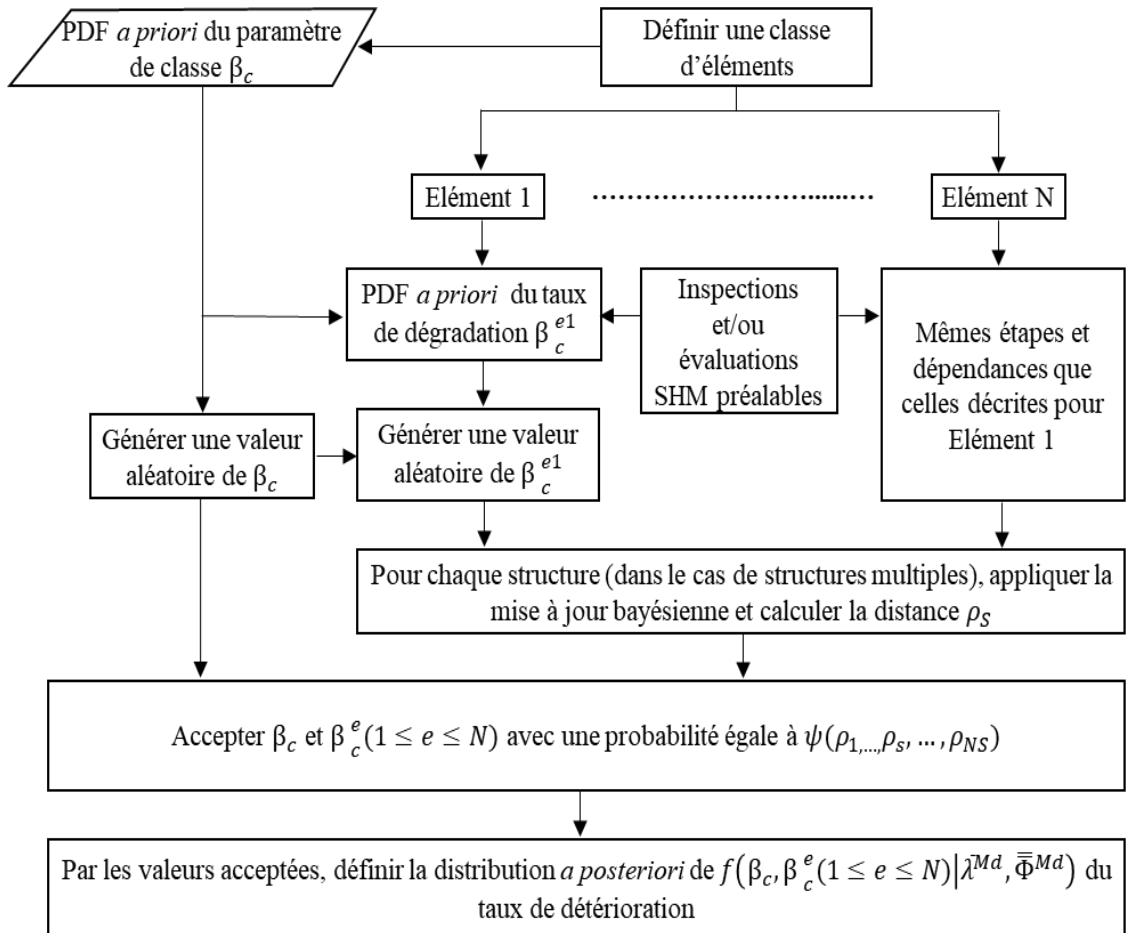


Figure 2: Organigramme de l'HABC pour les problèmes de SHM.

La méthodologie proposée a été appliquée sur deux exemples différents : quatre structures similaires de type treillis métalliques et un portique en béton à quatre étages. Les mêmes données mentionnées dans le paragraphe précédent sont prises en compte. Afin de simplifier la présentation, nous supposons (sans perte de généralité), dans les applications, que l'état initial (au temps  $t_0 = 0$ ) de la structure est exempt de défauts. Par conséquent, le taux de dégradation d'un élément entre  $t_0$  et  $t_1$  pourrait être considérée comme l'étendue de la dégradation de l'élément pendant cette période de temps. Par conséquent, on suppose que  $\beta_c^e = \alpha_c^e$ .

L'étendue de dégradation  $\alpha_c^e$  des éléments appartenant à une classe C spécifique est définie à l'aide d'un modèle multiplicatif comme suit:

$$\alpha_c^e = \alpha_e \times \alpha_c \quad (13)$$

où  $\alpha_e$  et  $\alpha_c$  sont respectivement, l'étendue de la dégradation de l'élément  $e$  et un facteur multiplicatif dépendant de la classe. La fonction a priori de ces variables est basée sur des inspections antérieures et / ou des évaluations SHM.

Les résultats obtenus ont prouvé que :

- (i) Il est possible de déterminer avec précision l'état de dégradation d'un ou plusieurs éléments d'une structure spécifique en profitant des informations obtenues à partir d'autres éléments similaires appartenant à la même structure ou à des structures différentes mais de la même classe ;
- (ii) Comparée à la méthode ABC (paragraphe précédent), la méthode proposée conduit à des résultats plus précis concernant l'étendue de la dégradation des éléments ayant de faibles effets sur la réponse structurale ;
- (iii) La méthodologie proposée est sensible aux dommages légers, modérés et graves même en cas d'erreurs de mesure élevées ;
- (iv) La distribution des capteurs sur plusieurs structures partageant des caractéristiques d'élément similaires et l'application de la présente méthodologie pour l'évaluation des dommages aboutit à de meilleurs résultats que la mise en œuvre de plus de capteurs sur chaque structure avec une évaluation individuelle de chacune d'elles.

Les principaux avantages de cette approche apparaissent dans sa capacité à: (i) prendre en compte systématiquement tout type d'incertitudes; (ii) mettre à jour l'état de dégradation des éléments, difficilement accessibles pour les SHM et / ou les inspections conventionnelles, en profitant des données provenant d'autres éléments similaires qui peuvent appartenir à des structures identiques ou différentes; (iii) réduire le nombre de capteurs mis en œuvre (d'où le coût de surveillance) tout en conservant une bonne précision des données.

## **5. Approche hybride inspection-surveillance pour une planification optimale de maintenance des structures**

L'inspection, la maintenance et la réhabilitation (IM&R) des ouvrages de génie civil a fait l'objet de recherches approfondies au cours des dernières décennies (Bastidas-Arteaga et Schoefs 2015; Stratt 2010; Atkins 2002). Les méthodologies développées dans ce domaine ont gagné l'attention des ingénieurs professionnels visant à appliquer ces méthodologies, spécialement avec le développement de technologies d'inspection de plus en plus fiables et efficaces. Néanmoins, le coût d'une inspection est une fonction croissante de sa précision et une telle approche souffre de plusieurs lacunes parmi lesquelles le fait que l'état de dégradation de la structure n'est connu qu'à des moments discrets. Tout défaut qui pourrait apparaître dans l'intervalle de temps entre deux inspections successives et qui pourrait idéalement nécessiter une action de maintenance corrective immédiate pourrait rester non détecté jusqu'à la prochaine date d'inspection. Plus récemment, la surveillance de la santé structurale (SHM) par des capteurs permanents pour mesurer plusieurs caractéristiques de la structure commence à être couramment appliquée aux structures importantes. Cependant, il n'est pas possible de s'appuyer uniquement sur des capteurs pour mesurer toutes les caractéristiques d'une structure, afin d'évaluer l'état de dégradation de tous ses éléments.

Ainsi, une planification de gestion optimale de IM&R doit pouvoir prendre en compte différents types d'informations provenant de différentes sources de données (e.g. capteurs, inspection visuelle, techniques d'inspection destructives et/ou non destructives, etc.).

Dans ce contexte, une méthodologie est proposée pour définir une planification IM&R combinant, de manière optimale, les inspections conventionnelles et l'approche SHM globale. Cette méthodologie intègre une mise à jour bayésienne dynamique de l'état de croyance de la structure, basée sur les mesures des capteurs, dans un cadre d'analyse de décision. Les incertitudes résultant du modèle, des mesures, des contrôles imparfaits et des actions de maintenance imparfaites sont explicitement prises en compte.

Similairement à l'approche de Faddoul et al. (2011), les hypothèses suivantes ont été considérées:

- 1- Un ensemble d'états possibles des éléments :  $\theta \in \Theta$  est défini. Soit  $\theta \in \Theta = \{1, 2, \dots, m\}$  une variable discrète qui décrit l'étendue des dommages d'un élément, c'est-à-dire que  $\theta$  est une cartographie de discrétisation de  $\alpha_e$ . Chaque valeur dans  $\Theta$  représente un sous-intervalle particulier du domaine de  $\alpha_e$ , c'est-à-dire un sous-intervalle particulier de  $[0, 1]$ .
- 2- La probabilité  $P(\theta = j)$  est calculée comme étant l'intégrale de la distribution *a posteriori* de  $\alpha_e$  sur le sous-intervalle correspondant. Soit  $\bar{\theta}$  un vecteur dont les composantes sont l'état de dégradation de chaque élément. Par exemple,  $\theta^e = j$  signifie que l'élément  $e$  est dans l'état  $j$ .
- 3- Les méthodes d'inspection  $i \in I = \{i_0, i_1, \dots, i_p\}$  sont imparfaites et sont sélectionnées parmi un ensemble fini d'alternatives; où  $i_0$  signifie qu'aucune inspection n'est effectuée. Soit  $\bar{i}$  le vecteur dont les composantes sont la méthode d'inspection choisie pour chaque élément. Les résultats de l'inspection sont décrits par des distributions de probabilité discrètes. L'incertitude des résultats d'inspection  $r_j \in R$  est caractérisée par une distribution de probabilité conditionnelle ( $\Pr[r_1 | \theta^e, i^e]$ ,  $\Pr[r_2 | \theta^e, i^e]$ , ...,  $\Pr[r_m | \theta^e, i^e]$ ), où  $\theta^e$  est le véritable état discrétisé de l'élément  $e$  et  $i^e$  le type d'inspection appliquée à l'élément  $e$ .
- 4- Un ensemble d'actions de maintenance possibles  $a \in A$  est défini. Soit  $\bar{a}$  le vecteur dont les composantes sont les actions choisies pour chaque élément. Les actions de maintenance  $a^e \in A = \{a_0, a_1, \dots, a_a\}$  sont imparfaites et sont sélectionnées parmi un ensemble fini d'alternatives; où  $a_0$  signifie qu'aucune action n'est effectuée. L'incertitude liée à une action de maintenance  $a^e$  est décrite par une matrice de transition carrée  $\bar{A}^e$  où chaque élément  $a_{ij}^e$  correspond à la probabilité que l'état  $\theta^e$  de l'élément  $e$  change de la valeur  $\theta^e = i$  à une nouvelle valeur  $\theta^e = j$  après l'application de l'action  $a^e$ .
- 5- Les coûts pris en considération sont :
  - $ci(i^e)$ : coût dû à l'application de la méthode d'inspection  $i^e$  sur l'élément  $e$ .
  - $ca(a^e)$ : coût de l'action  $a^e$  appliquée sur l'élément  $e$ .

$cs(\theta^e)$ : coût subi par l'utilisateur en raison de la présence de l'élément  $e$  dans l'état  $\theta^e$  calculé comme le coût prévu de la défaillance:

$$cs(\theta^e) = \text{probabilité de défaillance} \mid \theta^e \times \text{coût de la défaillance} \quad (14)$$

D'autres coûts dus à la performance réduite de la structure peuvent être inclus dans  $cs(\theta^e)$ .

Soit :

- $N$  le nombre d'éléments dans une structure.
- $P(\theta^e = i)$  la probabilité *a priori* que l'élément  $e$  soit dans l'état  $i$  ( $i = 1, \dots, m$ ).
- $P(\theta^e = i \mid R = r_j)$  la probabilité *a posteriori* que l'élément  $e$  soit dans l'état  $i$  sachant que le résultat de l'inspection est  $r_j$  ( $r_j = 1, \dots, m$ ).
- $P(R = r_j \mid \theta^e = i)$  la probabilité que le résultat soit  $r_j$  sachant que le véritable état est  $i$ . Cette probabilité représente l'incertitude sur les résultats de l'inspection.

Pour un élément  $e$  donné, la probabilité d'obtenir le résultat  $r_l$  compte tenu du type d'inspection  $i^e$ , est:

$$P[r_l] = \sum_{k=1}^m P[r_l \mid \theta^e = k, i^e] \times P[\theta^e = k] \quad l = 1, \dots, m \quad (15)$$

Étant donnée une technique d'inspection  $i^e$  et son résultat  $r_l$ , la distribution de probabilité *a posteriori* de l'état de dégradation d'un élément donné est :

$$P[\theta^e \mid r_l, i^e] = \frac{P[r_l \mid \theta^e = j, i^e] \times P[\theta^e = j]}{\sum_{k=1}^m P[r_l \mid \theta^e = k, i^e] \times P[\theta^e = k]} \quad (16)$$

Le problème d'optimisation revient à minimiser le coût total  $c \mid \bar{i}, \bar{r}, \bar{a}, \bar{\theta}$  dépendant du vecteur d'inspection  $\bar{i}$ , du vecteur résultat de l'inspection  $\bar{r}$ , du vecteur d'actions  $\bar{a}$  et de l'état du système  $\bar{\theta}$  comme suit :

$$\begin{aligned} \text{minimiser } c \mid \bar{i}, \bar{r}, \bar{a}, \bar{\theta} &= ci(\bar{i}) + \sum_{e=1}^N (ca(a^e) + \sum_k^m cs(\theta^e = k) \times a_{jk}^e) \\ \text{s.t. } \quad \bar{i} &\in I \\ \quad \bar{a} &\in A \end{aligned} \quad (17)$$

Les variables d'optimisation sont : (i)  $i^e$  indiquant le type d'inspection pour chaque élément à inspecter; et (ii)  $\bar{a}$  le vecteur d'actions à appliquer sur tous les éléments. Les contraintes du problème sont définies par les ensembles  $I$  et  $A$  de techniques d'inspection et d'actions de maintenance disponibles.

On pourrait facilement inclure, dans la formulation d'optimisation, d'autres types de contraintes telles que les contraintes budgétaires, les contraintes de niveau minimum de service, etc.

Le calcul de l'analyse de décision prend donc la forme :

$$c \mid \bar{i}, \bar{r}, \bar{a} = ci(\bar{i}) + \sum_{e=1}^N (ca(a^e) + \sum_{j=1}^m [\sum_{k=1}^m cs(\theta^e = k) \times a_{jk}^e] \times P[\theta^e = j \mid \bar{r}, \bar{i}]) \quad (18a)$$

$$c \mid \bar{i}, \bar{r} = ci(\bar{i}) + \sum_{e=1}^N \min_{a^e \in A} (ca(a^e) + \sum_{j=1}^m [\sum_{k=1}^m cs(\theta^e = k) \times a_{jk}^e] \times P[\theta^e = j \mid \bar{r}, \bar{i}]) \quad (18b)$$

$${}^*c|\bar{l} = \sum_{l=1}^m {}^*c|\bar{l}, r_l \times P[r_l] \quad (18c)$$

$${}^*c = \min_{\bar{l} \in I} {}^*c|\bar{l} \quad (18d)$$

$${}^*\bar{l} = \arg \min_{\bar{l} \in I} {}^*c|\bar{l} \quad (18e)$$

Ainsi, la méthodologie proposée pourrait être résumée par les étapes suivantes :

- 1- Obtenir, à partir de la surveillance SHM, la distribution de probabilité de l'étendue des dommages  $\bar{\alpha}$  pour tous les éléments;
- 2- À partir de la PDF obtenue, calculer la fonction de probabilité de masse (PMF) pour l'état d'endommagement discrétisé pour chaque élément ;
- 3- Pour chaque élément  $e$ , chaque type d'inspection  $i^e$  et chaque résultat possible d'inspection  $r_l$  :
  - a. Calculer le PMF *a posteriori*  $P[\theta^e | r_l, i^e]$  (Eq.16) ;
  - b. A l'aide du PMF calculée en (a), calculer la PDF *a posteriori* pour tous les éléments de la structure. Nous supposons que l'état de croyance  $P[\theta^e | r_l, i^e]$  d'un donné élément  $e$  a été obtenu après l'avoir inspecté. Cet état de croyance est imposé pour cet élément particulier dans le cadre ABC présenté précédemment. Lors de l'échantillonnage,  $\alpha_e$  pour l'élément inspecté  $e$  est échantillonné de  $P[\theta^e | r_l, i^e]$ , alors que l'échantillonnage de  $\alpha_e$  pour les éléments restants se fait à partir de leurs distributions *a priori* respectives;
  - c. Calculer une action optimale à appliquer pour chaque élément ;
  - d. Calculer le coût total qui comprend : (i) le coût d'inspection, (ii) les coûts des actions de maintenance pour tous les éléments, (iii) les coûts de l'utilisateur ;
  - e. Calculer le coût espéré de l'inspection  $i^e$ ;
- 4- Choisir la combinaison optimale d'inspection des éléments (la combinaison offrant le coût le plus bas).
- 5- Choisir les actions de maintenance optimales pour tous les éléments de la structure.
- 6- Choisir la décision optimale par l'arbre de décision: inspecter un élément suivant la combinaison choisie à l'étape 4 ou appliquer les actions de maintenance optimales sur les éléments choisies à l'étape 5. Si aucun élément n'est choisi pour l'inspection, passer à l'étape 8 ;
- 7- Appliquer l'inspection prescrite et, après avoir obtenu le résultat de l'inspection de l'élément choisi à l'étape 4, mettre à jour la PDF des dommages pour tous les éléments de la structure par mise à jour bayésienne (voir étapes 3.a et 3.b) et passer à l'étape 2 ;
- 8- Appliquer les actions de maintenance optimales pour tous les éléments de la structure.

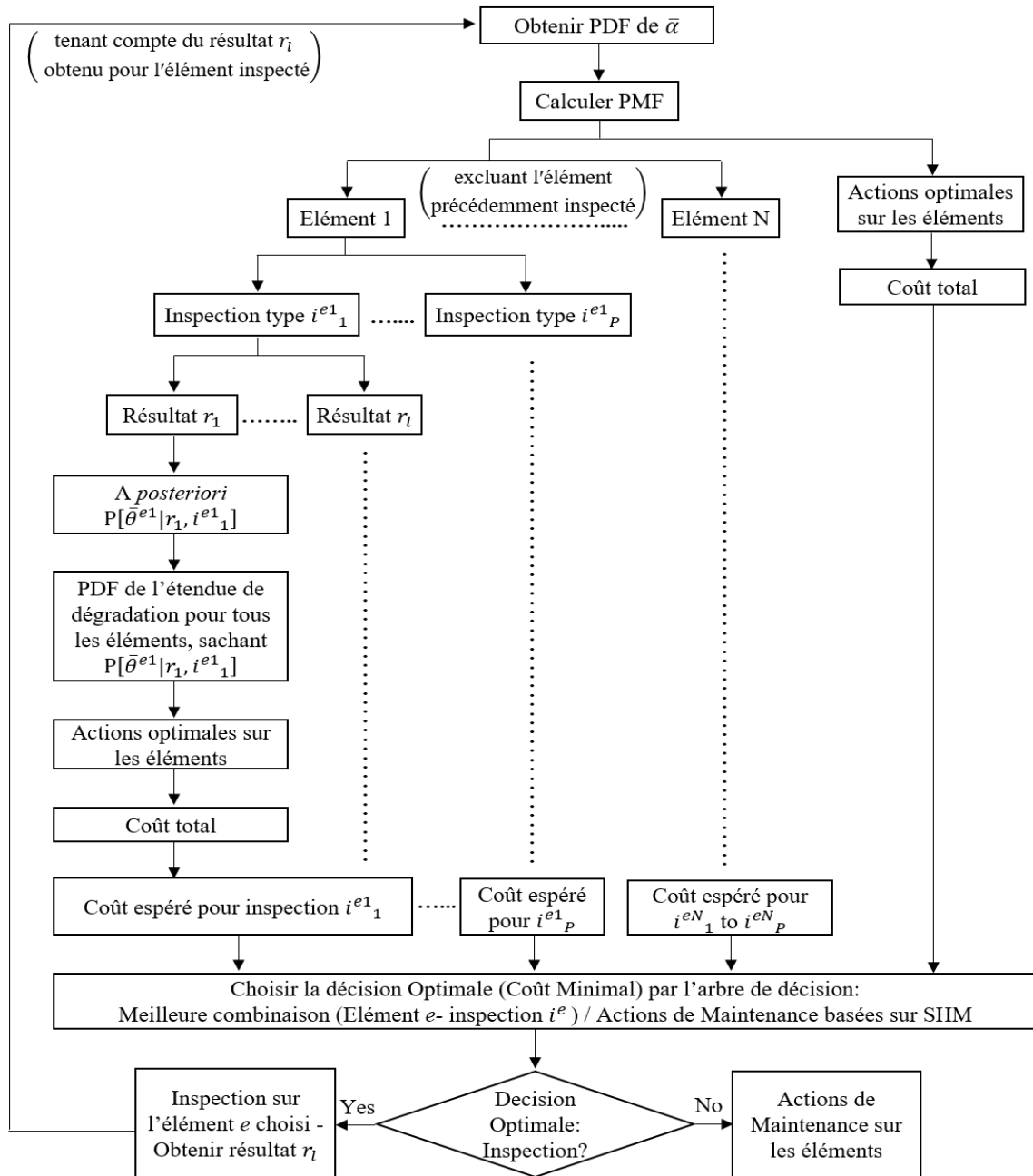


Figure 3: Organigramme de la méthodologie proposée.

Pour illustrer toutes les solutions alternatives ainsi que les résultats possibles du problème d'analyse de décision, nous choisissons la représentation de l'arbre de décision avec deux types de nœuds : (i) un nœud carré représentant un "nœud de décision" (nœud contrôlé par le décideur) suivi (ii) d'un nœud circulaire représentant un "nœud de hasard" qui est un sommet généralement incertain où le résultat dépend du processus aléatoire (Fig.4). L'arbre de décision correspondant à l'organigramme, pour un type d'inspection, est présenté dans la figure 4.

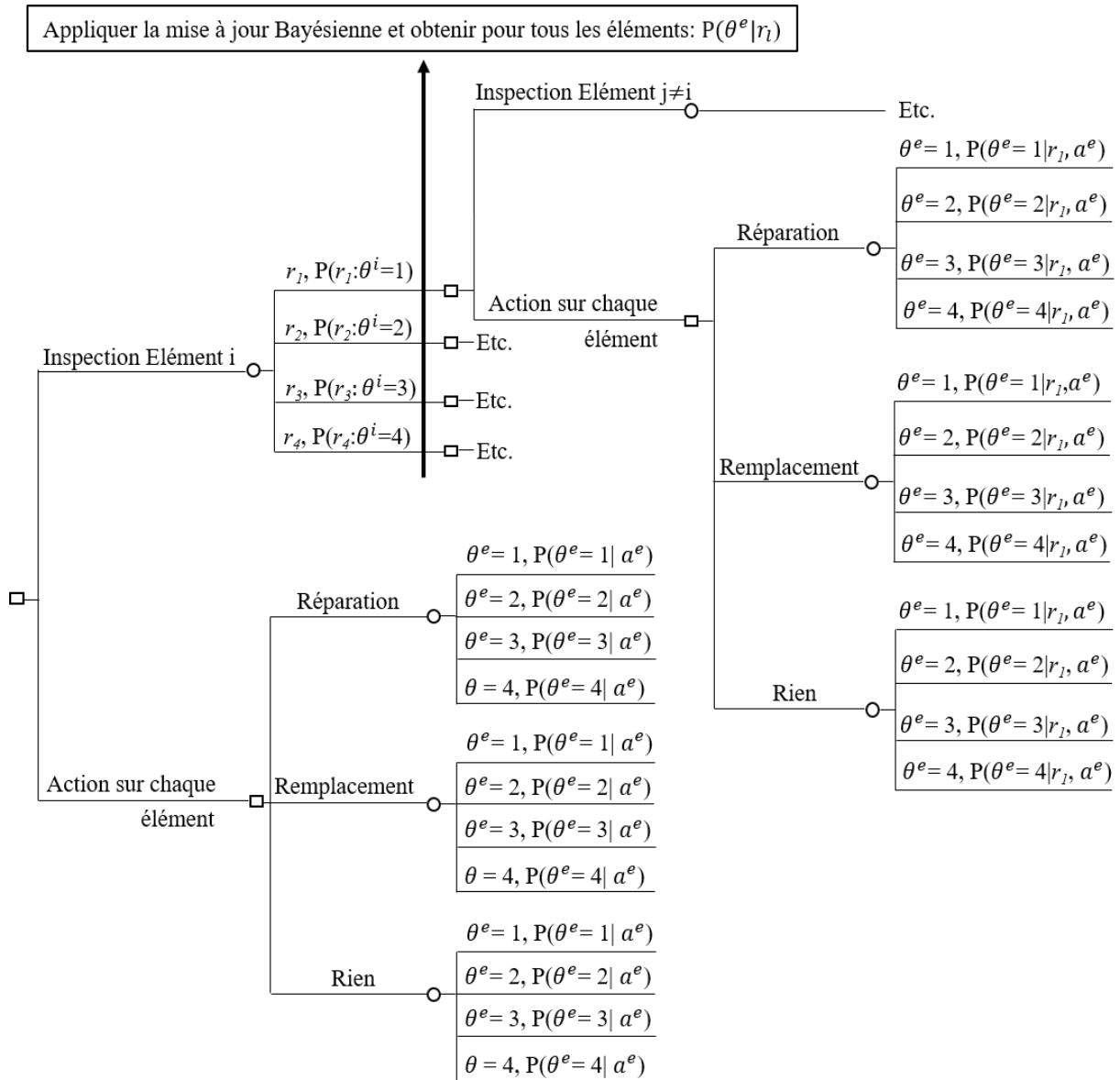


Figure 4: Disposition de l'arbre de décision.

Parmi les justifications qui favorisent cette approche, on peut mentionner les faits suivants: (i) l'inspection et/ou l'accessibilité de certains éléments peuvent être coûteuses ou difficiles. Dans un tel cas, l'inspection d'autres éléments plus accessibles et/ou moins coûteux à inspecter pourrait fournir les informations nécessaires de manière plus économique; (ii) les types de données générées par la SHM et les inspections conventionnelles sont généralement différents et complémentaires ; (iii) il ne suffit pas de s'appuyer sur des informations obtenues uniquement par la SHM pour caractériser tous les états mécaniques, physiques et chimiques d'un élément structural; iv) le recours à des inspections ponctuelles peut être dangereux et sous-optimal.

L'applicabilité et les avantages de la méthodologie proposée ont été démontrés par les deux applications numériques précédemment mentionnées, le treillis métallique et le portique



en béton. Pour chaque application, trois actions de maintenance sont prises en compte (ne rien faire, réparation, remplacement) et deux types d'inspections sont comparés. Les résultats ont montré que dans certains cas, tel que le cas des structures avec un nombre limité d'éléments, on peut s'appuyer uniquement sur les données provenant du SHM alors que pour les structures grandes et/ou complexes, il est souvent important d'inspecter un ou plusieurs éléments et de combiner les résultats provenant des deux sources. Cela permettra d'obtenir des résultats plus précis concernant la dégradation de l'ensemble des éléments de la structure et non de l'élément inspecté uniquement. La comparaison de deux types d'inspection a permis aussi de conclure que la valeur apportée en information par une technique d'inspection parfaite, ou plus précise qu'une autre, ne compense pas toujours le surcoût. Dans ce cas particulier, le choix optimal serait de choisir l'inspection moins précise étant moins coûteuse.

## **6. Optimisation de type proie-prédateur pour le placement optimal des capteurs**

La surveillance d'une structure pour prévoir l'état d'endommagement de ses éléments nécessite trois étapes principales : (i) la mise en œuvre de capteur(s), (ii) le traitement des données et (iii) l'évaluation de la santé structurale. En général, la précision des résultats augmente avec le nombre de capteurs mis en œuvre. Cela impliquerait un très grand nombre de capteurs dans une structure qui, non seulement induit un coût élevé de leur prix et de leur maintenance, mais transforme également le traitement des données en une tâche difficile. D'où l'importance de développer des méthodologies pour placer les capteurs de façon optimale. Cela permettrait aux données acquises de se traduire par une identification précise des caractéristiques structurales, et par suite d'un dommage existant, avec le moins de capteurs possibles.

Récemment, parmi les méthodologies développées dans ce domaine, l'algorithme génétique (AG) reçoit une grande importance en raison de sa capacité à traiter des problèmes complexes et de grande dimension avec une convergence rapide et une grande adaptabilité. Cependant, la plupart des recherches sont basées soit sur une situation spécifique de dommages, soit sur la maximisation de l'indépendance linéaire des informations modales dans la structure initiale. Or, dans la réalité, les capteurs doivent être en mesure d'identifier la plupart des scénarios de dommages futurs. En fonction de l'emplacement et de l'ampleur d'un dommage, son effet sur les formes modales peut différer (en termes de valeurs et de DOF affectés). Par conséquent, une configuration de capteurs optimale obtenue pour une configuration d'endommagements spécifique pourrait ne pas être optimale pour d'autres configurations d'endommagements. Ainsi, lors de l'optimisation de l'emplacement des capteurs, il est essentiel de trouver une configuration de capteurs qui soit capable de détecter le plus de configurations de dommages possibles.

Dans ce contexte, une nouvelle méthodologie est suggérée basée sur un AG de type Proie-Prédateur avec une mise à jour bayésienne des paramètres structuraux. Partant de deux populations initiales représentant les endommagements (proies) et les capteurs (prédateurs), les deux populations évoluent à travers un AG afin de converger vers la configuration

optimale de capteurs, en termes de nombre et d'emplacement. Le point fort principal de cette optimisation est sa capacité à minimiser le nombre et à trouver l'emplacement exact des capteurs tout en maximisant la probabilité de détection des dommages.

La relation proie-prédateur est une relation bilatérale correspondant à une interaction antagoniste bénéfique pour le prédateur et néfaste pour la proie. Ce type d'interaction se trouve dans tous les écosystèmes et fait l'objet de modélisations théoriques depuis de nombreuses années (Abrams 2000; Kuno 1987). Néanmoins, il pourrait être adopté aussi en optimisation afin d'atteindre la solution optimale globale sans être piégé dans une solution locale (Higashitani et al. 2006). La relation entre les capteurs et les dommages peut donc être similaire au comportement proie-prédateur.

La première étape du problème consiste à représenter les états possibles de la variable sous forme de codage. Dans notre cas, cette étape nécessite la création de deux populations qui co-évoluent: “  $P_{capteurs}$  ” représentant la configuration des capteurs et “  $P_{défauts}$  ” représentant la configuration des défauts. On modélise chaque configuration de capteurs par un chromosome de taille égale au nombre de degrés de liberté. Chaque gène du chromosome prend la valeur 1 quand le degré de liberté correspondant est observé par un capteur et 0 quand il ne l'est pas. Voici un exemple de chromosome appartenant à  $P_{capteurs}$ :

$$Ch_{capteurs} \quad \boxed{0 \quad 0 \quad 1 \quad 0 \quad 1 \quad 0 \quad 0 \quad 0}$$

Ce code, par exemple, représente une structure avec huit degrés de liberté (ddl) au total où le troisième et le cinquième ddl sont observés par des capteurs.

Par ailleurs, on modélise une configuration de défauts par un chromosome de taille égale au nombre d'éléments de la structure. Les gènes du chromosome sont des nombres réels entre 0 et 1 qui représente l'étendue du défaut. Un gène prenant une valeur 1 signifie que l'élément a conservé l'intégralité de sa rigidité initiale. Voici un exemple d'un chromosome appartenant à  $P_{défauts}$ :

$$Ch_{défauts}: \quad \boxed{0.43 \quad 0.8 \quad 0.95}$$

Ce code signifie que nous sommes en présence d'une structure à trois éléments ayant perdu respectivement 57%, 20% et 5% de leur rigidité initiale.

Chaque chromosome fournit une solution potentielle au problème. C'est la fonction d'évaluation qui évalue les performances de chaque individu pour permettre à la population d'évoluer afin d'aboutir à la meilleure solution. Dans notre problème, nous cherchons à optimiser deux fonctions. Les deux populations devraient évoluer de manière antagoniste, chacune selon sa fonction de fitness. En se basant sur les mêmes hypothèses présentées pour l'approche hybride « inspection-surveillance », les coûts relatifs aux capteurs et défauts sont alors définis par :

$$C_s = n_c \times c_c + \frac{\sum_{d=1}^{N_d} |C(*\bar{v}_d) - C_{s-IMP}(*\bar{v}_d)|}{N_d} \quad (19)$$

$$C_d = |C(*\bar{v}_d) - C_{meilleur\ capteur-IMP}(*\bar{v}_d)| \quad (20)$$

$$\text{avec } C(*\bar{v}) = \sum_{e=1}^N \min_{\bar{a}^e \in A} (c_a(a^e) + \sum_{j=1}^m (\sum_{k=1}^m c_s(\theta^e = k) \times a_{jk}^e) \times *\bar{v}_j^e) \quad (21)$$

$$\text{et } C_{IMP}(*\bar{v}) = \sum_{e=1}^N (c_a(a_{IMP}^e) + \sum_{j=1}^m (\sum_{k=1}^m c_s(\theta^e = k) \times a_{IMP-jk}^e) \times *\bar{v}_j^e) \quad (22)$$

où  $n_c$  est le nombre de capteurs installés ayant un prix unitaire  $c_c$  et  $N_d$  le nombre de configurations de défauts possibles.  $C(*\bar{v}_d)$  est le coût encouru si nous appliquons les actions optimales basées sur une information parfaite et  $C_{IMP}(*\bar{v}_d)$  le coût encouru si l'on applique les actions de maintenance optimales  $a_{IMP}$ , basées sur l'information imparfaite  $\bar{v}_d$ , sur une structure avec un vrai état certain  $*\bar{v}_d$ .

$\bar{v}$  est le vecteur dont les composantes sont les états de croyance des éléments individuels;

$$\text{i.e. } \bar{v}^e = \Pr[\bar{\theta}^e = 1], \dots, \Pr[\bar{\theta}^e = m] \quad (23)$$

$*\bar{v}$  est le vecteur dont les composantes sont les états de croyance certains des éléments individuels;

$$*\bar{v}_j^e = \begin{cases} 0 & \text{si } j \neq \text{état réel de l'élément } e \\ 1 & \text{sinon} \end{cases} \quad (24)$$

L'écart entre le coût de l'information parfaite  $C(*\bar{v})$  et le coût  $C_{IMP}(*\bar{v})$  quantifie le coût du manque d'information. Ainsi, le coût  $C_s$  est composé de deux éléments: (i) le coût des capteurs; (ii) le surcoût moyen dû à un processus de prise de décision avec des informations imparfaites (la moyenne est prise par rapport à la population de défauts).  $C_d$  est le coût supplémentaire dû aux informations imparfaites produites par la meilleure configuration de capteurs dans la population pour une configuration de défauts particulière.

Par conséquent, les fonctions d'évaluation « fitness » à maximiser sont définies par :

$$f_s = \frac{1}{c_s} \quad (25)$$

$$f_d = C_d \quad (26)$$

Le but d'un chromosome de défauts est alors d'"échapper" à toutes les configurations de capteurs, en "échappant" à la meilleure configuration de capteurs, et de se rendre plus difficile à détecter. Autrement dit, le meilleur chromosome de défauts représente la configuration la moins détectable et, par conséquent, c'est le chromosome qui augmente le plus le coût supplémentaire en raison d'informations imparfaites. A l'inverse, chaque chromosome de capteurs cherche à diminuer ce surcoût en diminuant le surcoût moyen dû à une information imparfaite par rapport à la population de défauts. Il cherche aussi à minimiser le nombre de capteurs. En d'autres termes, chaque chromosome de capteurs, représentant une configuration de capteur, tentera de détecter et de quantifier autant de configurations de défauts que possible avec un nombre minimal de capteurs.

La sélection des meilleurs chromosomes est faite par : élitisme et roulette. L'élitisme garde systématiquement le meilleur individu d'une génération à l'autre. Alors que dans la

sélection par roulette, tous les chromosomes de la population sont placés sur une roue, la place donnée à chaque chromosome étant proportionnelle à sa valeur d'adaptation représentée par le résultat de la fonction d'évaluation nommée "fitness". Les individus ayant une fitness relative élevée sont donc plus susceptibles d'être sélectionnés et reproduits.

Afin de diversifier la population, deux opérateurs ont été introduits dans la méthodologie : le croisement et la mutation. En combinant deux parents (deux chromosomes de la population) et en échangeant des informations entre eux, le croisement génère deux descendants ayant des gènes mixtes. Il pourrait être simple ou multiple. Pour un croisement simple (avec un seul point de croisement), le parent 1 (respectivement parent 2) reçoit les gènes du parent 2 (respectivement du parent 1) qui suivent le point de croisement leur permettant de produire deux descendants. Pour un croisement multiple, les chromosomes sont coupés à plusieurs points de croisement, et les gènes des deux parents sont inversés deux par deux, une coupe sur deux, pour créer deux descendants. Dans notre méthodologie, nous choisissons au hasard l'un des deux descendants. Cette combinaison est appliquée avec une probabilité de croisement  $p_c \in ]0,1[$ .  $p_c$  se situe généralement entre 0,5 et 0,9 (Rakotomahefa et al.2019). Par ailleurs, le rôle de la mutation est de modifier aléatoirement la valeur d'un gène dans un chromosome pour en former un autre qui le remplacera avec une probabilité de mutation  $p_m \in ]0,1[$  qui n'est pas assez élevée afin d'éviter de transformer l'AG en une simple recherche aléatoire.

Une seconde diversification a été imposée sur la population de défauts, le but de notre problème étant de détecter le plus de configurations possibles. Pour cette raison, il est important d'encourager les populations de défauts à rester diversifiées. Nous introduisons alors un critère de diversification dans le processus d'optimisation lors de la création de la nouvelle génération. Après avoir sélectionné les meilleurs chromosomes et appliqué les opérateurs de croisement et de mutation, le chromosome descendant obtenu (ou le parent sélectionné si la recombinaison n'a pas eu lieu) est accepté ou non dans la nouvelle population en fonction de sa proximité avec les chromosomes qui ont déjà été acceptés. Cette proximité est représentée par la distance euclidienne entre le chromosome descendant (offspring) et chaque chromosome  $Ch_i$  de la nouvelle population comme suit:

$$d_{off-Ch_i} = \sqrt{\sum_{j=1}^{N_G} (g_{j(Offspring)} - g_{j(Ch_i)})^2} \quad (27)$$

où  $g_{j(Offspring)}$  et  $g_{j(Ch_i)}$  sont les gènes  $j$  du descendant et du chromosome  $Ch_i$  de la nouvelle population respectivement, et  $N_G$  le nombre de gènes dans chaque chromosome.

Le minimum entre toutes les distances  $d_{off-Ch_i}$  est alors comparé à un nombre aléatoire:

$$offspring \text{ is } \begin{cases} \text{accepted} & \text{if } rnd \leq \min_{i \leq N_{C-acc}} d_{off-Ch_i} \\ \text{not accepted} & \text{if } rnd > \min_{i \leq N_{C-acc}} d_{off-Ch_i} \end{cases} \quad (28)$$

où  $rnd$  est un nombre aléatoire entre 0 et 1, et  $N_{C-acc}$  le nombre de chromosomes acceptés dans la nouvelle population avant l'évaluation du descendant en question.

Enfin, comme critère de terminaison, le nombre de générations est choisi pour terminer l'algorithme puisque le temps n'est pas un problème et la limite de fitness est inconnue.

On suppose que la réponse structurale est obtenue en mesurant les paramètres modaux (les valeurs propres et les vecteurs propres) et qu'un dommage structural est défini par une perte de rigidité des éléments. La méthodologie peut donc être décrite comme suit :

- 1- Créer une population de chromosomes  $N_d$  représentant les configurations de défauts;
- 2- Créer une population de chromosomes  $N_s$  représentant les configurations des capteurs;
- 3- Pour chaque configuration de capteurs et configuration de défauts, mettre à jour l'état de dégradation de chaque élément structural en se basant sur les mesures des capteurs et en appliquant le calcul Bayésien approché (ABC) ;
- 4- Pour chaque type de population (proie et prédateur) :
  - a. Évaluer les chromosomes par la fonction d'évaluation du type de population ;
  - b. Stocker le meilleur chromosome par élitisme ;
  - c. Sélectionner les meilleurs chromosomes parmi les  $N_d$  (ou  $N_s$  dans le cas des capteurs) chromosomes de la population à partir de la sélection par roulette ;
  - d. Choisir au hasard deux chromosomes parents (pour chaque population) et les recombinaison par croisement en fonction d'un taux de croisement ;
  - e. Choisir au hasard un des deux chromosomes obtenus et y appliquer une mutation en fonction du taux de mutation.
  - f. Ajouter le nouveau descendant à la population ;
  - g. Répéter les étapes (d) à (f) jusqu'à l'obtention de  $N_d-1$  (ou  $N_s-1$  dans le cas des capteurs) nouveaux individus ;
  - h. Ajouter l'individu élite pour obtenir la nouvelle population.
- 5- Répéter les étapes (3) et (4) jusqu'à satisfaction du critère de terminaison ;
- 6- Obtenir le meilleur chromosome représentant la configuration optimale de capteurs.

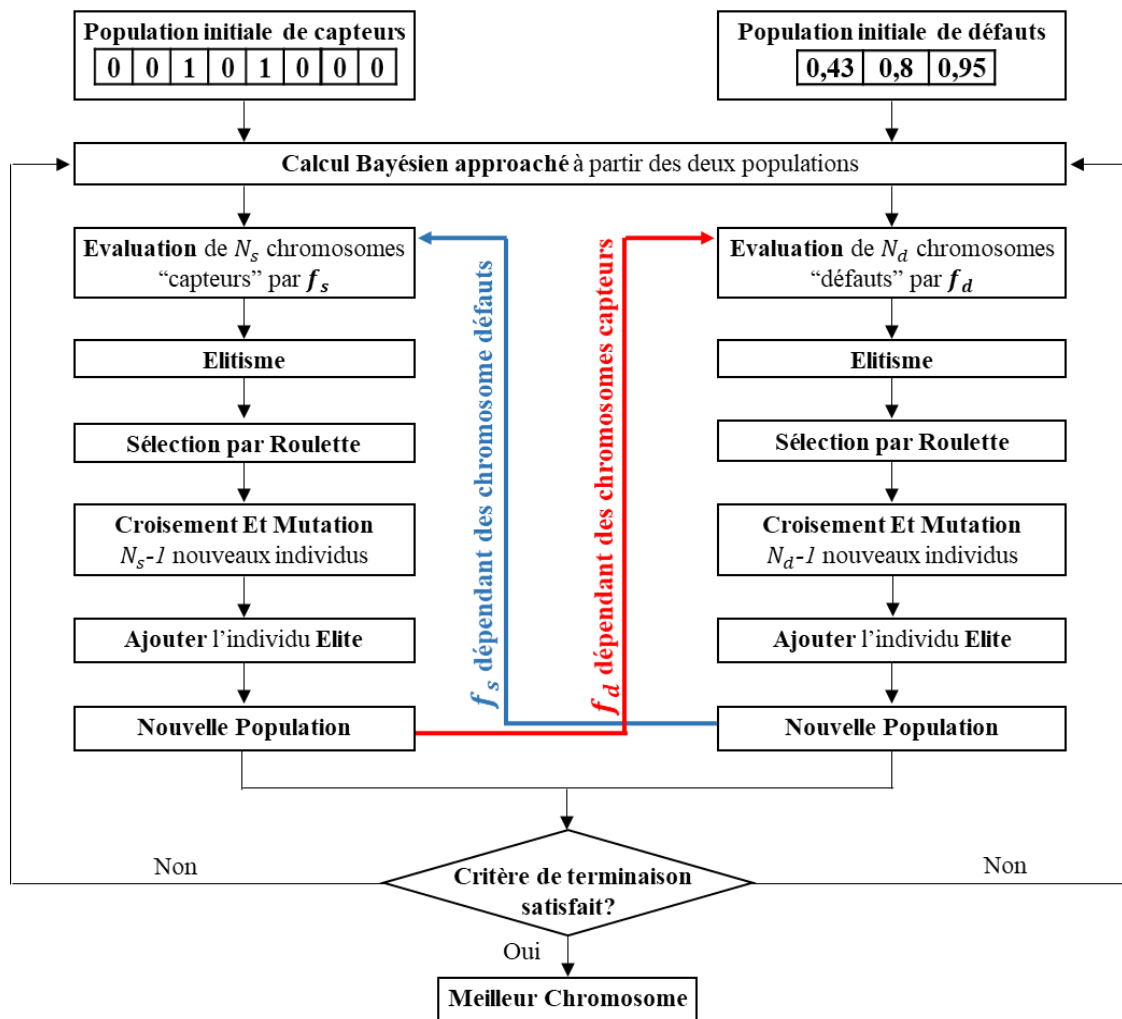


Figure 5: Algorithme Génétique type Proie-Prédateur.

La méthodologie d'optimisation est validée par deux applications numériques, à savoir un treillis métallique et un portique en béton (les mêmes que celles du paragraphe précédent). Pour les deux applications, les taux de croisement et de mutation sont, respectivement, 0,9 et 0,1. Ces applications ont révélé que : (i) le croisement et les mutations ne donnent pas toujours suffisamment de diversité à la population; il est donc important d'imposer une diversification supplémentaire sur la population de défauts pour élargir l'espace de recherche de la population de capteurs qui, à son tour, continue à chercher une meilleure configuration avec chaque apparition de nouvelles configurations de défauts; (ii) même si la précision des informations augmente généralement avec le nombre de capteurs, parfois la valeur ajoutée de l'information ne vaut pas le prix des capteurs supplémentaires, surtout s'ils ne sont pas placés de façon optimale; (iii) par contre, lorsque les capteurs sont positionnés de manière optimale, la valeur de l'information pourrait avoir un effet majeur de sorte que le prix du capteur perdrait un peu de son importance ; dans ce cas, la valeur ajoutée en information, apportée par des capteurs supplémentaires, compenserait leur prix dans une certaine mesure. Le principal avantage de la technique proposée est alors sa contribution à l'amélioration des performances

de l'AG visant à atteindre l'optimum global tout en cherchant la meilleure configuration de capteurs capable de détecter autant de configurations de défauts que possible.

## 7. Conclusions

L'objectif principal de cette thèse est de développer de nouvelles stratégies SHM pour le suivi des ouvrages de génie civil. Ce travail s'est concentré sur trois axes principaux : (i) la détection, la localisation et la quantification des dommages, (ii) la planification optimale de la maintenance et (iii) l'optimisation de l'emplacement des capteurs. En se basant sur les résultats fournis par les capteurs, les stratégies développées sont classées comme des méthodes appartenant à la classe d'analyse modale opérationnelle.

Quatre méthodologies abordant les problèmes de SHM ont été présentées :

La première méthodologie concerne l'évaluation des dommages dans une structure, sans avoir à résoudre le problème inverse qui est généralement mal défini. A partir d'un SHM permanent global et la méthode ABC, les densités de probabilité de l'étendue des dommages dans les éléments structuraux sont mises à jour en fonction d'une distribution *a priori* et des mesures de capteurs. Cette technique intègre, systématiquement, des incertitudes affectant la précision des résultats et ne nécessite pas de passer par une formulation explicite de la fonction de vraisemblance dans le processus bayésien. Son application sur deux types de structures différents, un treillis métallique et un portique en béton, a prouvé sa capacité à détecter avec précision les dommages. Pourtant, il pourrait être plus difficile de détecter de petits dommages dans des éléments qui n'ont pas d'effets majeurs sur les formes modales de la structure.

Dans la deuxième méthodologie, une technique de renforcement de l'information a été développée pour améliorer l'évaluation des dommages des éléments et/ou des structures faiblement surveillés à l'aide d'informations disponibles pour des éléments fortement surveillés et/ou les structures appartenant à la même classe. Cette approche est basée sur un calcul bayésien hiérarchique approché (HABC) qui classe les éléments selon des caractéristiques spécifiques et met à jour, simultanément, le taux de dégradation des éléments d'une même classe. La force de cette technique réside dans sa capacité à obtenir une quantité suffisante d'informations sur un grand nombre d'éléments (appartenant à une ou plusieurs structures), même ceux difficilement accessibles pour la surveillance SHM et/ou inspections conventionnels, en implémentant un nombre réduit de capteurs. La validation de cette technique à travers deux applications numériques a révélé que même les éléments endommagés qui n'affectent pas significativement les formes modales peuvent être détectés avec précision grâce à d'autres éléments bien surveillés appartenant à la même classe. En outre, dans le cas de plusieurs structures similaires, il a été montré que la répartition des capteurs sur les structures conduit à une évaluation plus spécifique de leurs états de dégradation que l'évaluation de chaque structure seule avec un nombre de capteurs plus élevé. Après avoir mis à jour l'état de dégradation des éléments appartenant à une classe spécifique, la précision des résultats obtenus a également permis d'améliorer l'évaluation des états des éléments n'appartenant à aucune classe.

Tout en se basant sur la procédure ABC développée, une approche hybride d'inspection-surveillance a été développée pour une planification optimale de la maintenance des ouvrages de génie civil, intégrant la mise à jour bayésienne dans un cadre d'analyse de décision. Le but de la méthodologie est de décider de manière optimale si une inspection est nécessaire et sur quel (s) élément (s), ou des actions de maintenance doivent être appliquées sur les éléments. Les actions de maintenance comprennent un remplacement, une réparation ou tout simplement aucune action si l'élément est en bon état. L'application de cette technique sur les structures précédemment mentionnées a démontré qu'une surveillance permanente est convenable pour les structures relativement petites avec un nombre limité d'éléments, tandis qu'une ou plusieurs inspections pourraient être nécessaires pour les structures plus grandes et /ou plus complexes. Par conséquent, pour de tels types de structures, il est important de combiner les données provenant des deux sources, les inspections conventionnelles et la surveillance permanente, pour réduire les incertitudes et obtenir des résultats plus spécifiques.

Finalement, un algorithme d'optimisation proie-prédateur a été proposé, basé sur un algorithme génétique, pour choisir de manière optimale le nombre et l'emplacement de capteurs à implémenter dans une structure. Contrairement aux AG habituels, deux populations interagissent de manière antagoniste et évoluent, chacune dépendant de son propre avantage; tandis que la population de défauts évolue en essayant d'éviter d'être détectée par les capteurs, la population de capteurs converge vers une configuration capable de détecter le plus grand nombre de défauts. Par conséquent, l'évaluation de chaque type de chromosome dépend du nombre de chromosomes qu'il peut dominer de l'autre population ce qui encouragera la population de capteurs à mieux évoluer vers une solution globale. L'application de cet algorithme d'optimisation sur la structure métallique et le portique en béton a déterminé l'importance d'optimiser le nombre et l'emplacement des capteurs. Deux facteurs ont également été étudiés dans notre travail : la diversification de la population de défauts et le coût des capteurs. Les résultats ont démontré que l'imposition d'une diversification supplémentaire sur la population de défauts est nécessaire pour élargir l'espace de recherche pour la population de capteurs. Ceci permettra d'obtenir des résultats en prenant en compte autant de configurations de défauts que possible. Ils ont également montré que la valeur ajoutée en informations fournie par des capteurs supplémentaires ne compense pas toujours leur prix, surtout s'ils ne sont pas placés de manière optimale. D'autre part, lorsque les capteurs sont localisés de manière optimale, la valeur ajoutée des informations apportées par des capteurs supplémentaires pourrait être plus importante que l'augmentation du prix des capteurs. Il est donc important non seulement d'optimiser la localisation des capteurs, mais également leur nombre.

## **8. Perspectives**

Les stratégies proposées dans cette étude pour surmonter certaines limitations de la surveillance de la santé structurale, en génie civil, ont fourni des résultats significatifs. Néanmoins, les méthodologies proposées pourraient bénéficier de la mise en œuvre de plusieurs améliorations nécessaires.



Un des inconvénients du calcul bayésien approché (ABC) est sa complexité calculatoire qui devient rapidement très élevée, même pour un nombre relativement faible d'éléments. L'algorithme de Metropolis-Hastings aurait pu être adopté. Cependant, nous avons choisi d'implémenter la formulation ABC pour éviter tout biais potentiel qui pourrait en découler (par exemple, la génération d'échantillons corrélés). De futurs travaux sont nécessaires pour évaluer la sensibilité de la méthode Metropolis-Hastings ABC et HABC à de tels biais dans un cadre SHM.

Un des facteurs qui pourrait être pris en considération lors de la mise à jour de l'état d'endommagement des éléments structuraux serait la présence d'éléments autres que les poteaux et les poutres, tels que les dalles, les cloisons, les murs porteurs, etc. La contribution de la rigidité de ces éléments structuraux pourrait affecter les résultats vibratoires et, par conséquent, contribuer à améliorer la détection des dommages dans la structure.

Il serait également intéressant de déterminer la sensibilité de la configuration des capteurs dans la localisation et la détermination des dommages en fonction de différents paramètres tels que : les facteurs environnementaux (notamment la différence de température entre le jour et la nuit, et entre les saisons), les chargements variables, etc.

En plus de la sensibilité des capteurs envers ces paramètres, on pourrait ajouter à l'étude d'autres facteurs tels que la durée de vie des capteurs et leur probabilité d'être endommagés durant une période de temps spécifique. De tels facteurs aideraient le décideur à choisir le bon type de capteurs en fonction de la situation (c'est-à-dire si la surveillance est effectuée à court terme ou à long terme).

Un autre facteur qui n'a pas été pris en compte est l'interaction sol-structure. Dans nos applications numériques, les structures sont supposées être simplement supportées. Cependant, il serait également intéressant d'étudier l'influence du matériau à partir duquel le sol est composé pour refléter la réalité et comprendre de manière plus réaliste le comportement des structures par rapport au sol qui les supporte.

# General Introduction

## Overview

Structural Health Monitoring (SHM) using permanent sensors has been a fast growing management tool during the last decade. This fast progress is mostly due to technological advances in several fields (i.e. sensors technology, data handling, efficient energy harvesting, etc.). SHM methodologies combine a variety of sensing technologies for the detection and localization of damage in order to assess the state of the structure and predict its residual life. It can be divided into two approaches:

- (i) Local SHM based on a direct evaluation of an element or a part of a structure to evaluate its state;
- (ii) Global SHM based on a mechanical modeling of the structure where few sensors (whose number and locations are to be optimized) are used to monitor the whole structure. However, limited budgets are available for the monitoring, maintenance and rehabilitation of structures and infrastructures. And till this date, the installation of sensors on every measurable feature of the structure is still being prohibitory costly. Hence, unless some critical elements are to be specifically monitored, global SHM approaches are generally used.

A four level criterion proposed by Rytter (1993) to evaluate damage detection techniques rank the methodologies according to the following levels: (i) detection of whether a damage is present in the structure; (ii) localization of the defect; (iii) estimation of the damage extent and (iv) calculation of the residual life of the structure and risk assessment. Over recent years, technological advances in civil engineering and related disciplines focused on developing damage assessment methodologies that allow one or more levels to be satisfied. One of the most adequate identification techniques for inverse problems is the Bayesian inference which provides a rational and robust tool that is able to characterize the uncertainties of the model parameters based on the available data. Yet, in most literature, assumptions are made to define appropriate likelihood functions which can be hard to express explicitly.

Furthermore, till this date, attention is only focused on assessing the condition state of a single structure, where elements can be less monitored than others due to the limited number of sensors. As such, developments are needed to take advantage of the simultaneous monitoring of several similar structures (a case in point would be identical buildings in compounds or identical bridges in a city) and/or similar elements.

Another commonly used monitoring concept is the periodical inspection starting with a visual inspection which may lead to destructive and/or non-destructive techniques. Yet, such an approach suffers from many limitations. For instance, the condition state of the structure is only known at discrete time points. Any defect that might appear between two successive inspections and which could possibly need an urgent maintenance action might remain undetected till the next inspection date. Also, some of the elements cannot be assessed due to

their limited accessibility. Moreover, the cost of an inspection technology is usually an increasing function of its accuracy. It is therefore useful to combine both concepts: the periodical inspections and the permanent monitoring.

In order to optimize the performance of an SHM system, sensors should be judiciously implemented on the structure in terms of number and location. An optimal number of sensors should be installed at optimal locations in order to: (i) minimize sensors costs, (ii) maximize the probability of damage detection, (iii) maximize the accuracy of damage localization and (iv) maximize the accuracy of damage characterization. This is an optimization problem with conflicting objectives at different levels. For example, maximizing the probability and accuracy of detection would lead to an increase in sensors costs.

## **Contribution**

This study is presented as a contribution to overcome the above listed challenges concerning damage assessment, optimal sensor placement and optimal Inspection, Maintenance and Rehabilitation (IM&R) planning.

First, an Approximate Bayesian Computation (ABC) approach is proposed in order to assess the condition state of a structure without any artificial constraint or assumption on the form of the likelihood. This approach allows to consider all uncertainties related to the degradation of elements, the mechanical model and the accuracy of sensors measurements. The ABC is considered as the general framework of the thesis, as it is the basis of all developed methodologies.

This approach is further developed to extract information from well monitored elements/structures in order to amplify the information about less monitored elements/structures. A Hierarchical Approximate Bayesian Computation (HABC) for borrowing strength is then proposed to update the condition state of an element and/or structure based on data generated from monitoring similar elements and/or structures. This technique would contribute in strengthening the assessment of structures and reducing the number of sensors needed to monitor several elements and/or structures.

Another contribution is the combination of data coming from different sources such as permanent monitoring and conventional inspection techniques to define an optimal Inspection, Maintenance and Rehabilitation planning for structures. This procedure integrates the ABC approach in a decision analysis framework. It gives the decision maker the opportunity to optimally choose, at a specific time, whether it is necessary to inspect a particular element or it is preferable to directly apply maintenance actions (i.e. repair or replacement) on elements based on SHM results only. When an inspection is needed, its results are injected in the SHM procedure, which contributes in reducing the uncertainty affecting the assessment of damage.

A part of the work has also focused on devising a suitable genetic algorithm for optimal sensor placement. The proposed scheme belongs to the more general concept of predator-prey modelling. This method allows an antagonist coevolution of the population of sensors and the population of defects, each population evolving depending on the evolution of the other

population. It therefore results in finding an optimal sensor configuration able to detect the widest range of possible damage configurations. One advantage of the proposed methodology is its capacity to increase the focus of the resulting SHM on some predefined critical elements.

## **Thesis Outline**

The thesis is organized around five chapters which are organized as follows:

Chapter 1 presents a literature review on a representative set of previous works that have tackled issues related to the monitoring of civil engineering structures. The objective of this bibliographic research is to explore the various methods commonly used and to identify their advantages and disadvantages. These methods are classified into two main categories: (i) damage detection and localization and (ii) optimal sensor placement. The basic concepts of structural health monitoring and the operational modal analysis are also summarized.

Chapter 2 describes a new methodology for damage detection and localization in civil engineering structures based on operational modal analysis and Bayesian inference approach. The proposed approach estimates the damage extent of each element by updating its condition state. All uncertainties that come into play are taken into consideration using an Approximate Bayesian Computation (ABC) framework.

Chapter 3 proposes a Hierarchical Approximate Bayesian Computation (HABC) for borrowing strength to strengthen the damage assessment of similar elements belonging to the same structure or multiple structures. Using a classification scheme, less monitored elements can borrow information from well monitored elements belonging to the same class (but not necessarily to the same structure) in order to update their condition state through a Bayesian hierarchical model.

Chapter 4 suggests an optimal planning of Inspection, Maintenance and Rehabilitation (IM&R) of civil engineering structures by optimally combining conventional inspection techniques and permanent monitoring in a decision analysis framework. This methodology integrates a dynamic Bayesian update of the belief state of the structure, based on sensor readings and inspection outcomes. Decision tree calculations are therefore detailed in this chapter and a particular emphasis is given for the value of information which shows the importance of the data fusion.

Chapter 5 aims at finding a cost-effective sensor configuration for the monitoring of structures by optimizing the number and location of sensors. A genetic algorithm of type predator-prey, integrating the methodologies described in chapters 2 and 4, is then proposed to maximize the probability of detecting damage with a limited budget. The degree of importance of the different damage scenarios and the types of available inspection and maintenance techniques are taken into account in the proposed sensor optimization.

The applicability of the above-mentioned methodologies is demonstrated through two numerical applications on different types of structures: (i) a steel truss and (ii) a multistory concrete frame.

## **Chapter 1: Literature Review**

### **1.1 Introduction**

After having introduced the research topic and outlined the key characteristics and the objectives of this study, this chapter provides an overview of prior research concerning structural health monitoring of civil engineering structures. Such a review is essential in order to identify potential gaps and shortcomings that may affect the efficiency of existing methodologies in the specialized literature. Therefore, this chapter summarizes the general concepts and approaches in structural health monitoring. It introduces the aspects of operational modal analysis and discusses damage detection methods that are mostly used. A particular emphasis will be put on methods based on the Bayesian probabilistic approach. Moreover, recent developments concerning optimal sensor placement are discussed with a focus on genetic algorithms.

### **1.2 Structural Health Monitoring**

Nowadays, lots of in-service structures fall below the minimum level of safety required to meet relevant standards. Therefore, one of the most important issues in civil engineering is the detection of structural damage, defined as changes in material properties and boundary conditions which adversely affect the system performance. The most frequently used monitoring concept, until now, remains the periodical inspection approach which consists of a visual inspection that can be potentially followed by destructive or non-destructive investigations. However, some structures might need to be monitored continuously, in a cost-effective way, by using sensors with a high degree of automation. Such problems can be tackled by resorting to the Structural Health Monitoring (SHM) which is a set of techniques and methodologies for detection, localization, characterization and quantification of damage and damaging phenomena. These techniques are used, among others, to predict the residual life of the structure.

#### **1.2.1 Monitoring Concepts: Inspection and Continuous Monitoring**

Monitoring a structure involves two main concepts: Inspection and Continuous monitoring. Inspection is usually used for a direct evaluation of a structural element at a specific time, while continuous monitoring can give information about the structure at any point in time.

Historically, detecting structural damage was highly dependent on on-site visual inspections followed, when needed, by destructive and non-destructive testing to evaluate the properties of a material and component or system. For an optimal inspection outcome, a description of the structure with its historical data (i.e. previous inspection reports, modifications in the structure, etc.) is needed.

According to Santa et al. (2002), the assessment of an existing structure follows a seven step process:

- 1- Review of all related documentation;
- 2- Visual on-site inspection;
- 3- On-site testing and measurements;
- 4- Analysis of collected data to improve the probabilistic models for structural resistance;
- 5- Analysis of the structure with updated loading and resistance parameters;
- 6- Structural reliability and decision analysis;

This subject has been also tackled by the Joint Committee on Structural Safety (JCSS) in a document that presents general guidelines, recommendations and reliability methods useful for the assessment of existing structures (Diamantidis 2001). The JCSS divided this type of assessment into three phases:

- Phase 1: Preliminary Evaluation.
- Phase 2: Detailed Investigation.
- Phase 3: Calling a Team of Experts.

In phase 1, a preliminary assessment is done using simple methods such as visual inspections, review of existing documentation and a simplified assessment of the actual state of the structure (e.g. age, loading changes, structural system modifications, etc.).

In phase 2, a more detailed assessment is done by investigating the site with inspections (including testing), updating the structural information accordingly using statistical procedures and carrying out detailed structural and reliability analysis. In this phase conclusions are made and decisions are made.

In case these decisions are of large consequences (in terms of risk and cost), one should move to phase 3 where experts are called to carefully make the best decisions.

Depending on each phase results, one could take action or move to the next phase.

Visual on-site inspection provides a global impression about the condition of a structure. It gives an idea about the deterioration symptoms along with their probable sources. This type of inspection intervenes as a main component in two categories of inspections: Routine and in-depth inspections.

Routine inspection is defined as regular visual inspection of the structure as a whole to ascertain its condition state and identify significant damage at the time of inspection. Examples of deterioration symptoms noted by a routine inspection are: cracks, rust stains, delamination and corrosion.

In-depth inspection is considered as a follow-up to a routine inspection for a more precise identification of a detected damage (Bergmeister 2003). It is used to identify damage that are not easily detected by routine inspection, using destructive and non-destructive testing. Among these testing methods, one can cite testing samples for compressive strength, load testing, measuring depth of carbonation, Penetrant Testing, Radiographic Testing (RT) and Ultrasonic Testing, Acoustic Emission (Helal et al. 2015; Ohtsu 2015; Gholizadeh 2016). The use of such techniques, aiming at a better knowledge of the real condition state of a

structure and leading to the diagnosis of its pathology, is referred to as “auscultation” according to fascicle 03 of the ITSEOA (ITSEOA (Fascicule 03) 2010). A state of the art on the auscultation and instrumentation methods is presented in a technical guide published by IFSTTAR and CEREMA as a reference document for the auscultation of structures (IFSTTAR & CEREMA 2015). However, even though inspections are able to assess damage, they might require the removal of obstacles that might impair good visual access. They might also interfere with the usage of the structure and/or be dangerous for the inspectors. Moreover, defects are only assessed at the inspection time, any significant defect that might appear between two consecutive inspections may not be identified on time.

Hence, due to the above limitations, continuous monitoring technique has received lots of attention during the last decades. This type of monitoring can be conceptually divided into three levels (Figueiredo 2010):

- Damage detection.
- Damage diagnosis.
- Damage prognosis and Risk assessment.

Detecting, locating and quantifying a damage can be done through a two-step process: First, sensors and a data acquisition system are installed in order to measure a specific property of the structure (e.g. stresses, deflections, accelerations) and measurements are collected. A measured structural property could derive from a static or a dynamic response of the structure. Then, the collected information is analyzed and interpreted to assess the condition state of the structure.

After the detection and characterization of the damage, a damage prognosis and risk assessment could be done. At this level, the remaining useful lifetime of a structure and the likelihood of a failure scenario happening with its consequences are evaluated. This would allow the assessment of risk and the choice of adequate decisions concerning future inspections and/or maintenance actions to be done on the structure (Lynch et al. 2016). However, till this date, the first two levels are given more importance than the third one.

The main advantage of monitoring a structure on a continuous time basis relies in the fact that it detects a damage at an early stage with minimal human involvement. This results, amongst others, in reducing the margin of human error, the potential of dangerous situations for the inspectors, preventing catastrophic failures and saving maintenance costs. It also plays a role in extending the lifetime of structures. This subject has been tackled by Orcesi and Frangopol (2011) where it has been shown that optimizing M&R strategies using monitoring information helps avoiding selecting solutions that highly overestimate the real performance of the structure. Using information coming from SHM reduces the uncertainty affecting reliability assessment and helps in keeping the structure at the maximum level of functionality. Okasha et al. (2012) proposed a methodology to integrate information coming from SHM in a structural reliability analysis and it has been shown that using SHM increased the accuracy of the reliability analysis. Based on SHM outcome, preventive maintenance strategies and inspections could be planned. Unlike other methods (e.g. inspections), SHM

enables to update the integrity of the structure continuously. It facilitates and ensures the assessment of damage in inaccessible areas. It also helps in eliminating/reducing downtime and service interruption.

### **1.2.2 Global and Local Monitoring**

The presence of a damage on any structural element does not affect only the element itself, but the global behavior of the structure (except in the case of isolated elements). Its impact on the whole structure depends on its location and severity. Hence, damage identification methods are divided into two main approaches: (i) Local SHM and (ii) Global SHM.

Local SHM techniques rely on a direct evaluation of a structural member to evaluate its state with respect to different possible defects and degradation types (e.g. strain measurement at a precise location). Intermittent structural evaluation by means of visual inspection or various Non Destructive Evaluation (NDE) techniques that are applied directly by inspectors on specific elements belong to the local approach. Local SHM techniques can be used: (i) to detect an existing defect (e.g. cracks) (Wang et al. 2016) or a short-term deformation (e.g. impact due to earthquakes) or (ii) to monitor long-term deterioration process (e.g. deflection, foundation settlement). Assessing an existing structure is essential not only to detect damage, but also make decisions about the repair and rehabilitation. In a short-term monitoring, sensors are installed on the structure's surface. An example of such a case is monitoring the static behavior of a bridge during the construction phase (Enckell 2006). As for the long-term continuous monitoring, sensors are embedded or attached to the structural member to evaluate the evolution in time of a specific performance parameter of the member. Examples of such a case is monitoring a bridge pile for tilting or a bridge deck girder for excessive deflection, during its service lifetime, using deflectometers or long base deformation sensors (Rodrigues 2010; OBrien 2016). Another example is monitoring a rebar corrosion at early stages using acoustic emission transducers (Zdunek 1995).

But, even though local monitoring is considered a good indicator of structural health condition, it does not provide any data concerning the global behavior of the structure and consequently, it will be hard to estimate its remaining useful life (Abdo 2014). While providing relatively precise measurements for performance parameters, this approach is not practical for complex structures having numerous structural members. The exhaustive instrumentation of such a structure would not be economically feasible most of the time. Some structures may also include features that cannot be directly accessed and/or measured. In such cases the performance of the related structural members must be assessed indirectly by means of global SHM techniques. Chang et al. (2003) published a review of global and local monitoring techniques for civil engineering infrastructure where they discussed the limitations of existing methods and highlighted new research directions.

In global SHM, the structural overall behavior is assessed using the static response (e.g. deflection, stiffness, strain) or the dynamic response (i.e. modal parameters such as frequency, mode shapes and modal flexibility) of the structure. Between both techniques, the dynamic techniques gained greater acceptance among engineers and have been successfully applied to



real-life structures. Global SHM can therefore identify damage affecting the overall structure. This approach involves a few sensors whose types, number and location must be judiciously chosen, used to monitor a structure for the advent of specific failure modes. The parameters of the sensing scheme (types, numbers and location) must be optimized in order to maximize the following objectives:

- 1- Increase the probability of defect detection;
- 2- Increase the reliability and precision of defect localization;
- 3- Increase the precision in evaluating the extent of the defect.

Global SHM can be also used for short-term and long-term. In the first case, this approach is usually employed to detect existing defects or to study the behavior of the structure in a short period of time under specific loadings. For instance, Guzman-Acevedo et al. (2019) tackled the problem of short-term deformations in a bridge since these deformations can be more relevant in bridges. In their paper, they studied the dynamic displacement of the bridge that can be caused by, among others, traffic, people or earthquake activity. Aasim et al. (2021) evaluated the condition state of a deteriorated bridge for a specific period of time using the vibration-based damage detection. On the other hand, long-term global SHM tends to be more commonly used in order to early detect any future degradation of the structure during its lifetime. This would ensure safety and contribute in future decisions regarding inspection and maintenance strategies. It is also useful to predict and extend the lifetime of a structure. This type of monitoring is very popular in bridges because a collapse in bridges may result in high consequences. Example of bridges subjected to continuous monitoring are the TsingMa Bridge with a total of 786 sensors (Dongsheng 2011) and the Dowling Hall footbridge at Tufts University (Behmanesh and Moaveni 2014). Using a long-term SHM global would allow also studying the behavior of the structure towards changes in environmental conditions (Borah et al. 2021).

Global SHM approaches can be further divided into (i) direct methods and (ii) indirect methods.

In direct Global SHM methods, measurement datasets are used directly to ascertain the above-mentioned three objectives. These methods train a model on several patterns such as damage configurations from which dynamic characteristics are predicted and compared to the measured data. They are qualified of “direct” because damage are identified by matching observed structural response to a predefined set of failure modes. Such methods usually involve one or several of the following techniques: pattern recognition, machine learning, classification algorithms etc.

A typical direct global SHM scenario consists then broadly of the following steps:

- 1- A set of different failure modes is identified by one or several experts based on an analytical and mechanical investigation and/or on historical behavior of similar structures;
- 2- For each failure mode specified in the first step, corresponding predicted sensor measurements are calculated (e.g. via analytical models);

- 3- Measured variables are compared (using for example pattern recognition techniques) to the variables calculated in step 2. Depending on the obtained degree of similarity, one can infer about the occurrence of the corresponding failure mode.

However, direct SHM methods requires a very large unbiased data set to train on. It is also time consuming since the algorithm takes time to learn and be trained in order to be able to accurately detect a good amount of failure modes. Otherwise, the algorithm might not be able to detect uncommon failure modes for which he hasn't be trained.

For these reasons, it might be better to use indirect SHM methods. The underlying rationale behind global indirect SHM methods is the fact that under unchanging load conditions, any changes in variables measured by the sensors, is due to changes in the underlying structural characteristics (changing material properties, boundary conditions, etc.). Global indirect SHM methods focus on updating our knowledge of structural characteristics given measured data. It is based on inverse problems where inverse functions are used to determine the cause at the origin of the changes in measurement data. These functions are based on minimizing the error function between measured and simulated. The great advantage of indirect methods is their ability to systematically and transparently take into consideration all uncertainties that affect the structural system as well as the measuring system. For example, one might face the following uncertainties in SHM problems:

- 1- Uncertainties related to the true values of structural parameters (Young modulus, stiffness, geometrical dimensions, etc.)
- 2- Structural Model uncertainties that may affect predicted behavior of the structure for a given set of structural parameters values;
- 3- Measurement uncertainties that may veil the true values of measurement variables;

A natural methodology that one might use in order to take into account the above mentioned uncertainties would be a Bayesian updating approach (Section 1.4.3). This methodology would take as a first step an initial subjective probability distribution of the structural parameters, and then, as new data becomes available the initial probability distribution will be updated accordingly.

### **1.2.3 Passive and Active Monitoring Approaches**

A Structure Health Monitoring system can be implemented in a structure using active, passive or active/passive sensing techniques (Figure 1.1).

Passive monitoring is the action of monitoring a structure only by the use of embedded sensors that “listen” to the structural response caused by ambient vibration. In passive monitoring, a damage is identified by analyzing a signal measured from sensors under unknown input. Certain assumptions must therefore be made as to its nature. One of the commonly use assumptions states that the ambient excitation is a stationary stochastic process with a frequency band sufficiently wide so that all the relevant eigenfrequencies of the

structure are excited. In such a case, only the response of the structure is useful to estimate the dynamic parameters of the structure.

The well-known equation of motion of a structure can be written as follows:

$$\bar{M}\ddot{\bar{u}} + \bar{C}\dot{\bar{u}} + \bar{K}\bar{u} = \bar{p}(t) \quad (1.1)$$

where  $\bar{M}$ ,  $\bar{C}$  and  $\bar{K}$  are respectively the mass, damping and stiffness  $N \times N$  matrices,  $\bar{p}(t)$  is the  $N$ -dimensional vector of external forces applied to the structure,  $\bar{u}$ ,  $\dot{\bar{u}}$  and  $\ddot{\bar{u}}$  are respectively the displacement, velocity and acceleration  $N$ -dimensional vectors.

When dealing with a global passive monitoring,  $\bar{p}(t)$  is assumed to be unknown and the dynamic properties are extracted from output-only data.

This methodology has attracted many researchers who have developed this approach based on local and global methods such as passive imaging methods (Zhang et al. 2014), acoustic emission (Kral et al. 2013), operational modal analysis (Gentile and Saisi 2007), etc. The acoustic emission is considered one of the most popular passive monitoring. The advantage of using such an approach lies in the fact that it does not require any artificial excitation (active source) of the structure and the measured response is representative of the real operating conditions of the structure. However, this type of sensing induces small signal-to-noise ratios.

Active monitoring takes place when perturbations of the structure are generated by actuators, and the structural response is monitored by sensors. Hence, in this type of monitoring, the external force (input) is known, with a limited frequency range, and the response depends on the input. In such a case, and using a global monitoring scheme, the dynamic properties are extracted using the equation of motion of the forced vibration response (Eq. 1.1). This type of monitoring, often using classical modal analysis, can detect damage including cracks, corrosion, delamination, etc. It has the advantage of controllable excitation source and reproducible results. Commonly used methods are the ElectroMechanical Impedance (EMI) [6] and guided ultrasonic wave methods (Giurgiutiu 2007).

Recent studies have also focused on exploring the potentials of both monitoring methods (Yu et al. 2012) and on merging them. By combining active monitoring and passive monitoring technologies, a comprehensive scheme can be provided to detect any structural abnormality in real time. For example, Nasrollahi et al. (2018) developed a SHM system based on an array of wafer transducers and a smart data acquisition system able to run passive sensing based on acoustic emission where transducers detect signals emitted by the appearance of new damage or the expansion of previous ones, and active sensing based on electromechanical impedance and guided ultrasonic waves.

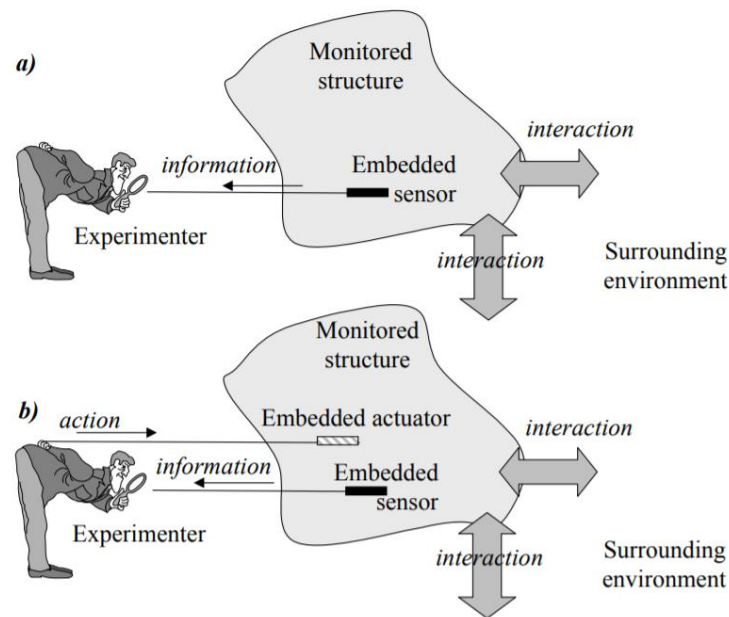


Figure 1.1: Representation of the sensing techniques: a) passive and b) active (Balageas 2006).

#### 1.2.4 Data Interpretation Approaches

After having obtained the information from the implemented sensors, data should be analyzed in order to judge whether a damage has occurred or not. Many algorithms and methods are presented in the literature for data analysis and interpretation. These methods are divided into two main categories which differ by the use of a physics-based model. These two main types of data interpretation approaches are model-based (used by indirect methods) and model-free data interpretation (used by direct methods). Catbas et al (2008) provided an overview of the strengths and weaknesses of each approach.

In model-based data analysis, the structural response obtained from measurements is compared to the predicted responses given by behavior models. This type of interpretation is usually expensive but, easy when the relationship between measurements and potential causes is explicit (Catbas et al. 2008) and more reliable information is obtained because it analyzes the changes between the numerical models in reference state, current state and damaged state. It is able to estimate future behavior of the structure when precise model is developed. However, in case of errors in the model and/or measurements, it may fail to identify the right damage. In some cases, such as complex structures, a high number of models may be required, difficulties and uncertainties increase as well. One solution to these limitations was proposed by Reynders et al. (2010) who applied the so-called *Operational Modal Analysis with eXogenous forces* (OMAX) to identify a finite element model that accounts for two different excitation sources: an unmeasured ambient vibration and measured artificial forces. Their approach was able to detect a loss of stiffness in a pier of a real three-span bridge. But despite all the limitations, many researchers have proven the efficiency of the model-based approaches such as Beck and Katafygiotis (1998) who presented a Bayesian statistical framework to update a structural model taking into consideration its associated uncertainties

to avoid ill-conditioning. Görl and Link (2003) was able to localize a damage and identify its extent in a steel frame structure using a reference finite element model generated from the measured response of the undamaged structure. This identification was based on the changes in stiffness between the undamaged and damaged structure. More recently, Behmanesh et al. (2015) implemented a Hierarchical Bayesian modeling to define a probabilistic finite element model for uncertainty quantification of model parameters and damage identification of civil structures under changing environmental conditions. Nozari et al. (2017) employed a finite element model updating of a four-story concrete frame building which was intensely damaged by an earthquake. Two models were created, one representing the initial state of the structure and another one updated to match the measured modal properties. The damaged states of the structural elements are therefore identified using the ratio of the elasticity modulus between both models. The same study has been extended by Akhlaghi et al. (2021) where a Bayesian updating model has been deployed to update the elasticity modulus ratio from a probabilistic perspective.

In model-free data interpretation, the analysis is only based on the recorded data without the need to develop any structural model. The basic idea of this approach consists of training the algorithm on a multitude of measured data. Damage are later identified either by recognizing the damage pattern by the trained algorithm (in supervised learning) or by identifying discrepancies between measured and predicted data (in unsupervised learning). In unsupervised learning, no prior knowledge nor experimental testing of undamaged structure is required. As it was stated by Posenato et al. (2010) “*The methodology is completely data-driven*”. This type of interpretation is more applicable when a large number of structures or when complex structures need to be monitored. However, the physical interpretation of damage (i.e. changes in stiffness) may not always be possible (Gonzalez and Karoumi 2015). In literature, various model-free damage detection methods have been used based on signal processing algorithms and machine learning techniques (e.g. wavelet transform, robust regression algorithms, support vector machine) (Santos et al. 2017, Sen and Nagarajaiah 2018, Avci et al. 2021). Among the most popular techniques are the Principal Components Analysis (PCA) and the Artificial Neural Network (ANN). PCA is a method used to reduce the dimensionality of large data sets to a smaller number of uncorrelated variables  $\psi$  while keeping as much as possible the variability of the original data. Its main objective is to obtain the most important characteristics from data. ANN is a mathematical process that imitates the human brain process. It is a collection of multiple nodes (neurons) in multiple layers where data is received by the input layer, processed by hidden layers performing mathematical computations in order to obtain the output data we are seeking. Azim and Mustafa (2020), for instance, identified damage in steel truss railroad bridges using the PCA of strain response. After having obtained the two principal components (eigenvectors of the covariance matrix obtained from the collected data) from measured data for the baseline and damaged bridges, authors defined a damage indicator as:

$$DI^i = \left| \frac{D_b^i - D_d^i}{D_b^i} \right| \times 100, \quad i = 1, 2, \dots, N_S \quad (1.2)$$

where  $N_s$  is the number of sensors,  $D_b$  and  $D_d$  are the distances for baseline and damaged bridge principal components given by:

$$D^i = \sqrt{(\psi_1^i)^2 + (\psi_2^i)^2} \quad (1.3)$$

where  $\psi_1^i$  and  $\psi_2^i$  are the first two principal components.

A damage is therefore located where high values of DI are obtained.

Ruffels et al. (2020) adopted the ANN to detect damage in a laboratory model of a steel arch bridge. Having collected accelerations from the bridge in its healthy state, the ANN was trained using the Root Mean Square Error:

$$RMSE = \sqrt{\frac{\sum_{i=1}^T (output_i - target_i)^2}{N}} \quad (1.4)$$

where  $output_i$  and  $target_i$  are, respectively, the measured acceleration and the predicted acceleration by ANN at instant  $i$ , and  $N$  the total number of samples in a run.

The ANN is trained in such a way to minimize the RMSE so it can predict the actual value of acceleration. A reference set of data and unseen data are then given to the ANN in order to predict the accelerations for each set, and the RMSE are calculated accordingly. The comparison between the distributions of the RMSEs will indicate the presence of a damage. Therefore, a high RMSE far from the RMSE of the reference state will be considered as an outlier and reveals the presence of a damage.

### 1.3 Operational Modal Analysis (OMA)

Going through vibration testing to study the dynamic behavior of a system and identify its structural parameters can be performed using two main types of modal analysis: The Experimental Modal Analysis (EMA) and the Operational Modal Analysis (OMA).

EMA identifies a structural dynamic properties using its response to vibrations induced by controlled input forces applied on it (i.e. artificial excitation using shakers, controlled blasts, drop weights, etc.). Thus, using the EMA in structural health monitoring is an example of active monitoring (section 1.2.2). EMA is useful for small and medium size structures (Brincker and Ventura, 2015) due to the complexity in applying controlled and measurable excitation on large and massive structures which require heavy and expensive devices.

To tackle this issue, studies have been focusing on operational modal analysis which take advantage of the ambient forces and uncontrolled forces (i.e. wind, waves, vehicle traffic, etc.) to excite the structure with free artificial and/or natural vibrations. The idea behind OMA is that the structure is being tested using excitations having, nearly, the same characteristics of the white noise, which means that it covers a wide frequency range including the frequency range of the modal characteristic of the structure. The advantages of such a technique relies in the fact that: (i) it reflects the actual behavior of the structure under real conditions, (ii) OMA tests are considered cheap and fast, (iii) OMA tests do not interrupt the normal

operation or normal use of the structure. However, it requires the implementation of very sensitive sensors. Another limitation arises in the presence of a lack of excitation of some modes which may keep some of these vibration modes unidentifiable from the data. Identifying a damage through an operational modal analysis is considered as a passive global monitoring (section 1.2.2) since the input is not measured, only measurements of the structural response to external forces (ambient forces) are employed.

This technique is also known as “output-only modal analysis” (since the input is unknown) where some assumptions are needed as stated by Rainieri and Fabbrocino (2014):

- 1- Linearity: Given a combination of inputs, the response of the system to this combination is equal to the same combination of the corresponding outputs.
- 2- Stationarity: The dynamic characteristics of the structure are not function of time.
- 3- Observability: The sensors are implemented such as the modes of interest are well observed.

A typical damage assessment using OMA in a model-based analysis, for instance, includes the following steps:

- 1- Develop a finite element model (FEM) to predict the modal parameters;
- 2- Implement sensors on a structure and collect information (i.e. acceleration, velocity) using ambient vibration testing;
- 3- Proceed with an OMA to extract the modal parameters such as natural frequencies, mode shapes and damping from the experimental data;
- 4- Compare the theoretical results (using FEM) with experimental results and update the model accordingly until reaching the optimal model with a maximum correlation between both results;
- 5- Once the difference between theoretical and experimental modal behaviour has been minimized, identify the uncertain structural parameters, such as Young’s modulus, to evaluate the damage and assess the structural safety.

Since damage cannot be directly measured by sensors, collected data is converted into damage information through: 1) time-domain identification methods based on correlation functions or the analysis of response time histories; 2) frequency-domain identification techniques based on spectral density functions. Among the well-known time domain methods are the stochastic subspace identification (SSI), the Eigensystem Realization Algorithm (ERA) and the Auto-Regressive (AR) models (Rainieri and Fabbrocino 2004, He and Fu 2001). While the frequency domain decomposition (FDD) is the most commonly used technique in the frequency approach, authors tend to adopt the time-domain techniques due to the fact that they can handle noise data better than frequency-domain methods thus bias-free data are more easily obtained.

In SHM, OMA has been adopted in direct and indirect monitoring (section 1.2.3). As an example of a global indirect monitoring, Gentile and Saisi (2007) applied an OMA-based SHM aiming at evaluating the structural condition of a masonry bell-tower. After having

identified five vibration mode shapes from the ambient vibration data and compared responses, given by the finite element results, to the measured responses, authors could identify Young's modulus in different regions of the tower. Hence, regions with relatively low Young's modulus in the model revealed the occurrence of a damage.

Altunışık et al. (2017) extracted the dynamic characteristics of a cracked cantilever beam using the enhanced frequency domain decomposition and the SSI and compared them to numerically calculated results using finite element models. The difference between experimental and calculated dynamic properties was further minimized, using the modal sensitivity method based on Bayesian parameter estimation, in order to detect damage in the beam. A good correlation was shown between the results. However, particular attention should be paid in model updating so that the numerical model represents the same boundary conditions as the experimental ones.

On the other hand, as an example of a global direct monitoring, Zhang (2007) performed damage diagnosis in a bridge by defining a statistical measure based on damage features extracted from a large data sample of the measured response under ambient excitation. The effects of the different environmental conditions on results was reduced due to a data normalization process. Thus, results were very similar with or without noise-contaminated measurements. Yet, the probability of occurrence of a damage was not only high at the damage location, but also on the nodes close to it which results in a false identification. It was also observed that abnormality is detected only when sensors are close to the damage.

## **1.4 Damage Detection**

### **1.4.1 Introduction**

Detecting, localizing and quantifying a damage constitute the three pillars of structural health monitoring. A structural damage is characterized by the appearance of permanent alterations (e.g. cracks, deflection, corrosion) in a structural element causing a reduction in its rigidity. This leads to a degradation of the physical behavior of the structure and may end up with a failure if the damage hasn't been detected on time. The cause of a damage may arise from several factors such as external loadings, environmental conditions (e.g. wind, earthquake, temperature, chemical attacks) or even poor construction and quality. Changes in the physical or mechanical behavior of a structure, due to a damage, must be detectable through changes in modal parameters between the healthy and damaged state of structure. For instance, the eigenvectors and eigenfrequencies depend, in particular, on the rigidity of the structure. Hence, a defect resulting in a stiffness reduction will lead to changes in these two parameters.

Many methods have been developed in literature to detect damage based on the modal properties of the structure. These methods could be employed using model-free and/or model-based approaches (section 1.2.4). The following sections provide a review of some detection techniques, and present examples of model-free and model-based approaches.



## 1.4.2 Damage Detection Methods

Among all damage detection methods, the vibration-based methods are the most widely used approaches in SHM because they allow for a local and a global evaluation of the condition of the structure (Das et al. 2016; Farrar and Doebling 1997). These methods can be divided into two main classes:

- The signal-based techniques: which consist in defining the damage by indices and comparing structural responses before and after damage. they are appropriate for detecting damage locations.
- The model-based techniques: which detect both the damage locations and the severities by updating the structural mathematical model.

They are mostly based on one or several of the following sets of modal parameters:

- The natural frequency
- The mode shape
- The modal curvature
- The modal strain energy
- The modal flexibility

These global parameters may not be always sufficiently sensitive to minor damages (Fan et al., 2021). For this reason, local damage detection methods (mostly using nondestructive testing) have been developed by researchers. An example of such methods is the Electromechanical Impedance (EMI)-based method using piezoelectric transducers. In the following, a review of the modal-based and the EMI-based methods is presented.

### 1.4.2.1 Modal-based methods

#### 1.4.2.1.1 Natural Frequency

The earliest technique among all vibration-based methods for the detection of a damage, relied on the eigenfrequencies analysis of a system. This approach is based on the assumption that frequencies are sensitive indicators of a damage. This is due to the fact that a damage causes changes in structural properties which in turn lead to changes in the natural frequencies of the structure. Taking the example of an undamped multi degree-of-freedom systems with free vibration, the equation of motion is written as:

$$\bar{M}\ddot{\bar{u}} + \bar{K}\bar{u} = 0 \quad (1.5)$$

where  $\bar{M}$  and  $\bar{K}$  are respectively the mass, damping and stiffness matrices;  $\bar{u}$  and  $\ddot{\bar{u}}$  are respectively the displacement and acceleration vectors.

The modal characteristics of a structure are then obtained using the equation:

$$(\bar{K} - \bar{M}\omega_j^2)\bar{\Phi}_j = 0 \quad (1.6)$$

where  $\omega_j$  is the eigenvalue or the pulsation frequency and  $\bar{\Phi}_j$  the eigenvector or the mode shape vector.

The eigenfrequencies  $\lambda_j = \frac{\omega_j}{2\pi}$  of the non-damped system and its eigenvector depend then on the mass and stiffness matrices. A change in the values of these modal characteristics between two states of a structure will therefore indicate a change in the mass and/or stiffness matrix probably due to a damage.

The frequency measurement principle was initially proposed by Adams et al. (1978) for structures which could have a one-dimensional representation. The position  $x$  of the damage is calculated using the following equation:

$$f(x)_i \Delta\lambda_i = f(x)_j \Delta\lambda_j \quad (1.7)$$

$$\text{where } f(x)_n = \frac{\partial(\beta_{xx} + \gamma_{xx})}{\partial \lambda} \quad (1.8)$$

where  $\beta_{xx}$  and  $\gamma_{xx}$  are respectively the direct receptances of the parts of the bar on either side of the damage and are continuous functions of  $\lambda_n$  the natural frequency of the bar,  $\Delta\lambda_i$  and  $\Delta\lambda_j$  are the frequency changes at modes  $i$  and  $j$ .

Their methodology was tested on aluminium bar with a saw cut, on bars with more realistic forms of damage, a tapered bar and on a camshaft. Results showed that a damage, at a single point, equivalent to a minimum of one per cent of removed area of the cross-sectional area of the structure could be found by detecting changes in the natural frequencies of the structure. Very small and very severe damage could not be detected. In some cases, the degree of asymmetry of a structure could be insufficient to determine accurately the damage site; it could indicate many possible sites.

This study has been extended by Cawley and Adams (1979) to two- and three-dimensional structures using a sensitivity analysis. Authors located a damage by minimizing the error in assuming it to be at a position  $x$ , given frequency changes  $\delta\lambda_i$  and  $\delta\lambda_j$  and the sensitivities  $S_{ri}$  and  $S_{rj}$  in modes  $i$  and  $j$ , respectively. The error is then a function of the frequency ratio  $\delta\lambda_i/\delta\lambda_j$  and the sensitivity ratio  $S_{ri}/S_{rj}$ . A rough estimation of the damage magnitude was also proposed by comparing, for each mode, frequency changes due to a hole of area  $A$  and the measured frequency change at the predicted damaged location. A damage is then quantified by the size of the predicted hole. Results were successful when only one damage site is present yet, erroneous results were produced in the case of a damage at two or more locations. Also, the severity of a damage was not always successfully identified. Cuts of similar length but different directions were identified by damage with different magnitudes.

Behtani and Bouazzouni (2011) proposed the use of the Local Frequency Change Ratio (LFCR) to detect and localize defects in laminated beams defined by:

$$LFCR = \frac{|LF_{ij}^d - LF_{ij}|}{LF_{ij}} \quad (1.9)$$

with  $LF_{ij} = \frac{\bar{\Phi}_i^t \bar{K}_j \bar{\Phi}_i}{\bar{\Phi}_i^t \bar{M}_j \bar{\Phi}_i}$  and  $LF_{ij}^d$  are the local frequencies of, respectively, the undamaged and damaged state of the structure in mode  $i$  at the  $j$ -th element in the structure .

A damage is then defined by the element for which the ratio LFCR is the highest. In the case of a unidirectional beam, damage could be successfully located at different locations of the beam with LFCR being much higher at the damage location. However, in the case of a laminated beam with 3 discretized layers, many false peaks appeared when a single damage was applied and a random distribution of LFCR has been given when applying multiple damage. Hence, their methodology could only be applied in case of unidirectional structures.

Calculating the correlation between natural frequencies is another common way used to locate damage. Mohan et al. (2014) studied the correlation between experimental and numerical frequency change ratios to detect and localize damage. Their method was based on the damaged location assurance criterion (DLAC) defined by:

$$DLAC(j) = \frac{|\overline{\Delta\lambda}^T \cdot \{\delta\lambda_j\}|^2}{(\overline{\Delta\lambda}^T \cdot \overline{\Delta\lambda})(\delta\lambda_j^T \cdot \delta\lambda_j)} \quad (1.10)$$

where  $\overline{\Delta\lambda}$  and  $\delta\lambda_j$  represent, respectively, the observed frequency change vector and the hypothesis frequency change vector at the  $j$ -th location between the undamaged and damaged structure.

By simulating damage at multiple locations, one at a time, and comparing the hypothesis frequency change vector to the observed one, a damage is localized where the DLAC gives a value 1. In such a case, a good correlation appears between the observed and hypothesis frequency change vectors. Results using the first four modes proved that this criterion is effective in the case of a single damage provided that it is not located near a support. The influence of the support led to an identification of multiple damage sites while, in reality, there is only one. Such a method can be used to simulate multiple possible damage scenarios and locate a damage on an actual structure if a strong correlation exists between the actual structure and a simulated damage case. However, the DLAC can only be used for a single damage location. Otherwise, the problem becomes computationally complex.

The case of single and multiple damage detection using relative natural frequency changes ratio (RNFC) has been tackled by Sha et al. (2019). The RNFC is calculated as:

$$\Delta\lambda_{ij} = \frac{\lambda_j - \lambda_{ij}^d}{\lambda_j} \quad (1.11)$$

where  $\lambda_j$  and  $\lambda_{ij}^d$  the  $j$ -th natural frequency of, respectively, the intact structure and the damaged structure when damage is at  $i$ -th element.

A comparison between the RNFC of the actual damage and the simulated damage in a beam reveals the damage location. A damage severity estimation is also given in the paper based on the RNFC. From multiple damage scenarios, results showed that this technique was able to identify the actual defect location and severity, however, other non-damaged locations were also identified as damaged ones. The false positives occurred at locations which are

symmetrical to the damaged elements. Having studied the effect of temperature variations on the results, it was concluded that even though natural frequencies decrease when temperature increases, the method can still localize damage under varying temperatures. Hence, this method is able to define the most probable damage locations yet, it is unable to give a unique solution.

The above-mentioned studies considered the case of simple structures. Yet, applying them to localize damage in large scale structures is a very complex task requiring a large number of measurements. Hence, when using natural frequencies, authors may resort to combining it with other methods.

Frigui et al. (2018) proposed a methodology to detect damage through changes in natural frequencies and then locate it through mode shape derivatives. Frequency shifts that exceeds 5% reveals the presence of a damage while those that are lower than 5% are considered to be caused by other factors such as environmental conditions (Salawu 1997). Using the first two bending modes, the application of this method on an 18 storey building showed that only severe damage (50% stiffness reduction) could be detected using frequency changes. With less severe damage (25% stiffness reduction), the obtained frequency shift was lower than 5%. In this case, authors proposed using mode shapes for the damage detection.

Therefore, studies showed that natural frequencies are not always sensitive to damage, especially for large and/or complex structures where damage may cause very small changes to the natural frequencies. In such cases, it might be also a very complex task to localize damage, when detected, since a very large number of measurements is needed to identify, at least, the most probable damage locations. For the case of more simple structures, damage could be located however the solution is very susceptible to false positives which leads to a non-uniqueness of the results.

#### 1.4.2.1.2 Mode Shape and Curvature Mode Shape

The second dynamic property that can be affected by a damage in a structure is the mode shapes (Eq. 1.6). These modal properties are believed to be more sensitive to damage than frequencies since they could provide spatial information. To study the feasibility of both methods in assessing damage in a structural system, Srinivasan and Kot (1992) conducted a study on a cylindrical shell where changes in frequency and mode shapes are measured. Mode shapes of undamaged and damaged shells are compared using plotting deformed shapes and the diagonal terms of the Modal Assurance Criterion Matrix (MAC).

The equation of MAC is usually defined by:

$$MAC_{ij} = \frac{(\bar{\Phi}_i^T \bar{\Phi}_j)^2}{(\bar{\Phi}_i^T \bar{\Phi}_i)(\bar{\Phi}_j^T \bar{\Phi}_j)} \quad (1.12)$$

where  $\bar{\Phi}_i$  and  $\bar{\Phi}_j$  represent two vectors. The MAC values vary between 0 and 1; a MAC value of 1 shows a perfect correlation between both vectors while a MAC value of 0 indicate no correlation.

In Srinivasan and Kot's methodology,  $\bar{\Phi}_i$  and  $\bar{\Phi}_j = \bar{\Phi}_i^d$  represent respectively the undamaged and damaged mode shape vectors in mode  $i$ . A damage appears where there is a poor correlation between both vectors (a MAC value shifting from 1 towards 0) and hence, a high deviation. Out of 52 modes, at least 10 modes presented high deviations between both states which indicates the presence of a damage. Yet, for the same modes, changes in the corresponding frequencies were negligible. Hence author deduced that mode shapes are more sensitive than modal frequencies to the presence of damage. Even if changes did not appear in all modes, the sensitivity of some of them could still be an indication.

The Modal Assurance Criterion was later applied by Zhao and Zhang (2012) to detect damage while analyzing the sensitivity of mode shapes to damage. In their paper, authors analyzed the correlation between the mode shapes of undamaged and damaged structures. As it was shown in Srinivasan and Kot (1992), deviations in MAC don't appear in all modes. Therefore, for a better identification and localization, authors compared the MAC values in all modes and chose the modes having the smallest values to locate the damage and estimate its severity. Their method has proved to be effective however, both states of the structure were simulated without taking into account any noise or measurement errors.

MAC was therefore able to accurately detect damage however, it cannot be used directly to localize damage. For this purpose, another index has been used by Tatar et al. (2017), the Coordinate Modal Assurance Criterion (COMAC), to locate damage in a concrete building retrofitted after an earthquake. Authors therefore applied the MAC and COMAC to identify and locate damage in a building. COMAC is defined by:

$$COMAC_j = \frac{|\sum_{i=1}^N \bar{\Phi}_{ij} \bar{\Phi}_{ij}^d|^2}{\sum_{i=1}^N \bar{\Phi}_{ij}^2 \sum_{i=1}^N \bar{\Phi}_{ij}^{d2}} \quad (1.13)$$

where  $\bar{\Phi}_i$  and  $\bar{\Phi}_i^d$  are the  $i$ -th mode shapes of, respectively, the healthy and damaged structure,  $j$  a measurement point and  $N$  the number of modes.

A value of 0 characterizes the most likely damage location and a value of 1 characterizes a location with no apparent damage. Results for two different sensor layouts proved that MAC and COMAC are able to accurately detect damage however, the accuracy of locating a damage depends on the sensor layout. With less number of sensors, COMAC could roughly locate damage.

Shi et al. (2000) conducted a sensitivity- and statistical-based method where incomplete mode shapes are directly used to localize a structural damage. To do so, their methodology was based on the Multiple Damage Location Assurance Criterion (MDLAC) developed by Messina et al. (1998). However, instead of using modal frequency, they applied the correlation parameter MDLAC using incomplete mode shapes as follows:

$$MDLAC(\alpha_j) = \frac{|\Delta \bar{\Phi}^T \cdot \delta \bar{\Phi}(\alpha_j)|^2}{(\Delta \bar{\Phi}^T \cdot \Delta \bar{\Phi}) \cdot (\delta \bar{\Phi}(\alpha_j)^T \cdot \delta \bar{\Phi}(\alpha_j))} \quad (1.14)$$

where  $\Delta\bar{\Phi}$  is the measured mode shape change vector,  $\delta\bar{\Phi}$  is the analytical mode shape change and  $\alpha_j$  is the damage size at location  $j$ .

This parameter is calculated for a single damage element, one at a time for all elements, and the damage sites are identified as those having the highest MDLAC values. Results proved that a single damage is well detected. However for multiple ones, although these damage are being observed, higher values of MDLAC can be obtained for non-damaged sites which may lead to erroneous conclusions. In such a case, potential damage sites can be defined yet one may not be able to differentiate between the true positive and the false positive results. For better results, one should repeat the procedure many times using the suspected potential damaged elements identified previously.

Another sensitivity-based method was developed by Parloo et al. (2003) to localize and quantify damage in a structure using mode shape sensitivities to changes in stiffness (or mass) without the need of a prior finite element model. For each mode  $j$ , and depending on changes in mass or stiffness, damage parameters  $p$  are obtained by solving the following equation:

$$\bar{\Phi}_j^d - \bar{\Phi}_j = \bar{S}_j \Delta p \quad (1.15)$$

where  $\bar{\Phi}_j^d$  and  $\bar{\Phi}_j$  are the mode shape vector  $j$  for, respectively, the undamaged and damaged structure, and  $\bar{S}_j = [\frac{\partial \bar{\Phi}_j}{\partial p_1} \dots \frac{\partial \bar{\Phi}_j}{\partial \alpha_{Np}}]$  is the sensitivity matrix.

By using this method, mode shapes which are not affected by the occurrence of a damage do not negatively affect the results since their sensitivities are small comparing to other mode shapes. But the problem is the dependence between the number of elements where damage can be identified and the number of mode shapes used because sensitivities are obtained from a linear combination of the number of mode shapes. Hence, a minimum number of mode shapes is required to keep the set of equations in Eq. (1.15) well-conditioned.

To overcome this limitation, a damage indicator could be used where no conditions are required on the mode shapes. Hu et al. (2006) suggested a statistical algorithm to identify a defect in timber using difference in mode shapes. To assess a damage, authors proposed a standard normal indicator value as follows:

$$DI_{ij} = \frac{|l_{ij} - \mu_i|}{\sigma_i} \quad (1.16)$$

where  $l_{ij}$  is a discrete Laplacian transform operated on the difference between damaged and undamaged mode shapes  $i$  at the  $j$ -th measurement point, and  $\mu_i$  and  $\sigma_i$  are the mean and the standard deviation of  $l_{ij}$  at all measurement points.

A damage is identified where  $DI_{ij}$  exceeds a certain threshold. The method was able to successfully locate the damage in a single and multiple points using the first two modes. However, the indicator does not take into consideration the severity of the damage and therefore, its application is limited.

Other authors have also addressed the damage identification problem in bridges, through changes of mode shapes, using responses from passing vehicles (Obrien and Malekjafarian (2016), Oshima et al. (2014) and Zhang et al. (2012)).

Even though mode shapes have been used for damage identification, damage may not influence significantly mode shapes of the lower modes, which are usually measured from vibration tests of large structure. For such structures, it may be also difficult to generate high mode shapes (third and above) due to the noise in the response signal. To enhance the sensitivity of mode shape data to the damage detection, other modal derivatives might be used such as the modal curvature. Changes in the higher order mode shape derivatives such as modal curvature are more specific damage detectors since they show discontinuities at damage locations.

A curvature mode shape is directly related to the stiffness of an element by the equation:

$$\Phi'' = \frac{\mathcal{M}}{EI} \quad (1.17)$$

where  $\mathcal{M}$  is the bending moment at a section,  $E$  the modulus of elasticity and  $I$  the second moment of the cross-sectional area. So, when a damage occurs, the stiffness of the damaged section is reduced thus, the magnitude of the curvature is increased at that section.

To calculate the modal curvature for a mode shape  $i$  at  $j$ -th measurement point, the central finite difference approximation is usually applied as follows:

$$\Phi''_{ij} = \frac{\bar{\Phi}_i(j-1) - 2\bar{\Phi}_i(j) + \bar{\Phi}_i(j+1)}{h^2} \quad (1.18)$$

where  $\bar{\Phi}_i(j)$  is the  $i$ -th mode shape at measurement point  $j$  and  $h$  the length between two measurement points.

The so-called ‘‘curvature mode shape’’ technique has been first introduced by Pandey et al. (1991). In their paper, authors identified a damage by the location  $j$  where the maximum absolute differences between intact and damaged curvature mode shape is obtained. They showed that this method is more sensitive for damage detection than using the displacement mode shape. Nevertheless, results show, sometimes, small peaks at undamaged locations for the higher modes which may be confusing. The main drawback of this method is that it needs a full set of readings on a structure to obtain the curvature mode shape. To reduce the needed amount of readings, he suggested a combination of two methods: the natural frequencies to detect the presence of the damage and the curvature mode shapes to locate it.

Wahab (1999) developed the method proposed by Pandey et al. (1991) and defined a damage indicator ‘‘Curvature Damage Factor’’ (CDF) to study the accuracy of the central difference approximation to compute the modal curvature. The CDF is a clear indicator of the damage location when a structure has many faults and is defined by:

$$CDF = \frac{1}{N} \sum_{i=1}^N |\Phi''_{oi} - \Phi''_{di}| \quad (1.19)$$

where  $N$  is the total number of modes to be considered,  $\Phi''_{oi}$  and  $\Phi''_{di}$  are the curvature mode shapes of, respectively, the intact and damaged structure.

Using the CDF indicator, locating multiple damage in a structure has become possible but at the same time, high irregularities appear in the measured high mode shapes which prevents us from identifying the location of a damage. In this case, many CDF peaks appear and the real location data is lost. Therefore, a smoothing technique should be used for such cases.

The CDF indicator has been used by Lestari et al. (2005) to assess damage in FRP honeycomb sandwich structures in highway bridges, using piezoelectric sensors. After having extracted the modal curvature of the first six modes, the CDF and the absolute difference between the modal curvatures of undamaged and damaged structures have been studied. Having plotted both curvature mode shapes, authors found that at higher modes (4<sup>th</sup> mode and above), the nodal points of the damage curvature shift from those of the undamaged modes. This phenomenon might be the reason behind the erroneous peaks in the curvature difference that was also found in Wahab (1999) since the shifting causes significant differences even at a non-damaged location. It also influences the CDF curve with small misleading peaks yet, a good prediction of the damage location was provided with two high peaks at the damage boundaries. Based on the obtained curvature mode shapes, authors quantified damage using a damage magnitude estimation in the form of stiffness loss. However, the quantification was not successful due to the fact that: (i) values highly differ from a mode to another; (ii) a range of stiffness loss values is given, not a specific value, resulting from the presence of two high peaks in the modal curvature curve at the damage boundaries; (iii) unacceptable results are given for modes having a nodal point close to the damage location. Hence, when assessing damage using curvature mode shapes, it might be better to only deal with lower modes in order not to be misled by false peaks.

A comparison between the performance of CDF (using mode shape curvatures) and MAC (using mode shapes) is presented in Oyarzo-Vera and Nawawi (2017) for the identification of damage in unreinforced masonry panels. From a numerical simulation and an experimental test, authors showed that MAC was able to successfully detect damage and represent the progression of their severity. Using multiple damage schemes representing a growing expansion of a damage, MAC values representing the correlation between undamaged and damaged structures decreased with the development of damage. In contrast, for the same number of measurement points, CDF roughly identified the damaged spatial distribution and were more sensitive to noise. Their results were improved when using high instrumental densities which is often impractical in reality.

According to Cao et al. (2014), erroneous results are due to the fact that modal curvatures are generated from the second-order central difference which in turn amplifies any slight noise in mode shapes. Hence they focused their research on reducing errors in second-order spatial derivatives and improving the identification of damage in noisy conditions. Instead of using the classical equations of modal curvatures, they defined a TEO-WT modal curvature based on a wavelet transform incorporating the Teager Energy Operator. Their



method was able to eliminate noise interference and accurately locate a damage by a unique singular sharply peak in the modal curvature. However, it was just tested on cases with one slight crack on a beam. It cannot be applicable, as it is, for large structures where it is impossible to take measurements on each element.

Rucevskis et al. (2016) proposed a mode shape curvature-based method to localize damage in plate-like structure using only the damaged data. The smooth modal curvature surface of the healthy structure is estimated based on a regression analysis with a polynomial approximation. The damage is then obtained by comparing the measured curvature and the estimated one for each mode  $i$  as follows:

$$DI_{i-u,v} = |(\Phi''_{i-u,v})_x^2 - (k_{i-u}^2)| + |(\Phi''_{i-u,v})_y^2 - (k_{i-y}^2)| \quad (1.20)$$

where  $u$  and  $v$  are numbers of grid point in  $x$  and  $y$  directions of a two-dimensional space,  $(\Phi''_{xy})_x$  and  $(\Phi''_{xy})_y$  the measured modal curvature in both directions and  $k_x$  and  $k_y$  the smoothed mode shape curvature surfaces in both directions.

In order to overcome the above mentioned problems about false peaks, authors proposed an average summation and normalization of the damaged index defined by:

$$DI_{u,v} = \frac{1}{N} \sum_{i=1}^N \frac{DI_{i-u,v}}{DI_{max}} \quad (1.21)$$

where  $N$  is the number of modes and  $DI_{max}$  the largest value of each mode.

Results on a simulated test case and an experimental case showed that damage are detected and located by almost half of the mode shapes. However, the efficiency of the results highly depends on the sensor placement, measurement noise and damage severity. Damage are less likely to be localized when spacing between sensors increases and/or with high measurement noise. Moreover, the proposed method has shown successful results only in the case of relatively high damage, it cannot be applicable to slight to moderate damage.

To sum up, a common problem afflicting the majority of the methods based on modal curvature was the lack of reliability in locating the damage due to the “false” peaks appearing in the results especially in higher modes. Another problem arises from the large number of measurement points needed to assess a damage.

#### 1.4.2.1.3 Modal Strain Energy

Stubbs et al. (1995) introduced a method, for damage location, based on a modal strain energy method. This method was developed for Bernoulli-Euler beams and then extended by Cornwell et al. (1999) for plate structures. It takes into consideration only the mode shapes and elemental stiffness matrices without external and/or environmental influence.

The fractional strain energy of an undamaged ( $FSE_{ij}$ ) and damaged structure ( $FSE_{ij}^d$ ), for a particular mode shape  $\bar{\Phi}_i$ , found out by Cornwell et al. (1999) is given by:

$$FSE_{ij} = \frac{U_{ij}}{U_i} = \frac{\frac{1}{2} \int_{a_j}^{a_{j+1}} (EI)_j \left( \frac{d^2 \bar{\Phi}_i}{dx^2} \right)^2 dx}{\frac{1}{2} \int_0^l EI \left( \frac{d^2 \bar{\Phi}_i}{dx^2} \right)^2 dx} \quad (1.22)$$

$$FSE_{ij}^d = \frac{\frac{1}{2} \int_{a_j}^{a_{j+1}} (EI^*)_j \left( \frac{d^2 \bar{\Phi}_i^d}{dx^2} \right)^2 dx}{\frac{1}{2} \int_0^l EI^* \left( \frac{d^2 \bar{\Phi}_i^d}{dx^2} \right)^2 dx} \quad (1.23)$$

where  $U_i$  and  $U_{ij}$  are the energies due to the  $i$ -th mode shape  $\bar{\Phi}_i$  associated with, respectively, the whole structure and a sub-region  $j$  of the structure,  $EI$  and  $EI^d$  are the flexural rigidity of, respectively, the undamaged and damaged elements,  $j$  is a sub-region of the structure between  $x=a_j$  and  $x = a_{j+1}$ ,  $\bar{\Phi}_i^d$  is the mode shape  $i$  of the damaged structure.

By considering the flexural rigidity constant on all the structure and comparing the sum of  $FSE_{ij}$  and the sum of  $FSE_{ij}^d$  on all modes for a specific sub-region  $j$ , this method could locate a damage even for a stiffness reduction of 10%, requiring the mode shapes of the structure without the need of any normalization. Nevertheless, it presents many false positives, especially near/or at the nodes, which will make it impossible to define the real damage without a prior knowledge. Additional problem occurs in the inability of the method to define multiple damage locations having different degrees of severity. It can only be effective in presence of a unique damage or same damage in different locations, a very rare or quasi impossible case in reality.

Park et al. (2002) solved this problem by modifying the model and defining a normalized damage index. The performance of their method depended on the number of damaged locations and the number of modes used. In most of the damaged cases, false positives occur but the most important problem is the number of false negatives in the results when we are in presence of only one damaged location because of the impact of the noise in the measurement data on the method used.

Yan et al. (2012) also proposed an effective algebraic algorithm using the modal strain energy to detect damage on an element using the closed-form of the sensitivity of the element modal strain energy given by Yan and Ren (2011). The advantage of this technique is that it just requires one known operational mode shape and takes into consideration model uncertainties and measurement noise simultaneously. However, the problem remains the same as other methods in detecting damage near the boundaries.

Although modal strain energy is able to locate damage, positive and false negatives are very susceptible to appear especially near boundaries insensitive to the change in the element modal strain energy. Also, these methods are sensitive to noise interference, and they require data from a high number of modes.

#### 1.4.2.1.4 Modal Flexibility

The flexibility matrix is the inverse of the static stiffness matrix, and each column of it, represents the displacement pattern of the structure associated with a unit force applied at the corresponding degree of freedom. The flexibility matrix is defined by the following equation:

$$\bar{F} = \bar{\Phi} \bar{\Omega}^{-1} \bar{\Phi}^T = \sum_{i=1}^N \frac{1}{\omega_i^2} \bar{\Phi}_i \bar{\Phi}_i^T \quad (1.24)$$

where  $\bar{\Phi} = [\bar{\Phi}_1, \bar{\Phi}_2, \dots, \bar{\Phi}_n]$  is the mass-normalized mode shape matrix,  $\bar{\Phi}_i$  is the  $i$ -th mode shape,  $\bar{\Omega} = \text{diag}(\omega_i^2)$  is the modal stiffness matrix,  $\omega_i$  is the  $i$ -th eigenvalue, and  $N$  the number of mode shapes.

Pandey and Biswas (1994) suggested a damage detection method using changes in the modal flexibility of the structure. The results showed that the flexibility matrix converges quickly with increasing frequency. So damage detection and location could be estimated from the first two modes of the structure. However, it requires a full modal analysis of the structure, which can be difficult and time consuming for large structures.

Kazemi et al. (2011) developed a two-phase procedure to localize the faults and their extent in plate structures. They used a variation of the modal flexibility to define a damage indicator, and combined it with Artificial Network and Genetic Algorithm methods to determine damage severity. Their method could predict the locations and severities of damage but showed a number of false positives which could be due to a high level of noise in the measured data.

Sung et al. (2014) proposed also a new damage detection method for cantilever beam-type structure using the modal flexibility matrix to estimate damage-induced inter-story deflection. Inter-story deflection is the difference between modal flexibility-based deflections of two successive stories. Their approach directly identifies the defect location(s) without passing by a finite element model yet, it cannot be applicable to all kind of structures, it is limited to cantilever beam-type structure.

#### 1.4.2.1.5 Modal Damping

While receiving less attention than natural frequencies, modal shape or modelling by local reduction in stiffness, damping has also been investigated as a possible damage indicator. Bachman and Diertele (1981) showed that visually undetectable cracks cause negligible variation in natural frequencies but considerably increase the damping.

Under the assumption of a small damping ratio  $\zeta$ , the basic expression to identify  $\zeta$  from free vibration structural responses is:

$$\zeta = \frac{1}{2\pi m} \ln \frac{x_n}{x_{n+m}} \quad (1.25)$$

where  $x_n$  and  $x_{n+m}$  are two particular peaks in the free vibration response of the structure with  $m$  cycles between them.

A damage is then characterized by a change in this damping ratio. This is due to the fact that damage are source of energy dissipation which increase the damping ratio.

Cao et al. (2017) provide a summary about the typical method and the application of damping in structural damage detection. They have also emphasized the factors that influence the capability of damping in characterizing a damage. These factors are basically the uncertainty in damping estimation and the interference of operational factors in damping changes (e.g. age of concrete, material quality, stress distribution).

While some early studies (Salawu and Williams 1995; Kato and Shimada 1986) concluded that damping ratios are not trustworthy indicators of damage detection due to the inconsistency of their values, Razak and Choi (2001) showed that changes in modal damping of the second and third modes were consistent with the severity of the damage in the case of corroded reinforced concrete beams. According to authors, the inconsistency of the values of the first mode is probably due to the accumulation of rust at the steel–concrete interface.

Curadelli et al. (2008) described a new approach to detect structural damage through instantaneous damping coefficient identification using a wavelet transform. They studied the evolution of the undamped natural frequency and the damping coefficient of the system with increasing damage. Still, the limitation of such a technique is that wavelet transform can only analyze a signal locally hence, for many degrees of freedom, the system should be decoupled into single degrees of freedom which increases the computational time and effort.

Other different techniques were developed to monitor damping in bridges using acceleration measurements from a moving instrumented vehicle and a dynamic truck-trailer vehicle model (Keenahan et al. 2014; González et al. 2012). For instance, Keenahan et al. (2014) used the power spectral density of accelerations for truck-trailer vehicle system to detect changes in the damping of a bridge in order to assess its deterioration state. Their method was able to remove much of the influence of the road profile on the results however, the trailer axle accelerations should be subtracted from one another in order to have accurate results. The method is also much affected by many factors such as the measurement noise.

Therefore, the uncertainty of damping estimation and the interference of operational factors are the major obstructing factors for the use of damping to characterize damage. It has been also shown that damping is more likely to be affected by a noisy environment than natural frequencies and mode shapes (Cao et al. 2017).

#### **1.4.2.2 Electromechanical Impedance-based method**

The electrical impedance of the piezoelectric transducer (PZT) is related to the mechanical properties of the host structure and is named electromechanical impedance. Variations of dynamical parameters of the structure, as a result of damage, influence the measured impedance plots.

The electromechanical impedance (EMI) method was initially introduced by Liang et al. (1994) who analyzed the dynamics of active material systems with integrated actuators. After having compared the static, the dynamic finite element and the EMI method, it was

concluded that the latter can provide more information than the others since it reflects the physical essence of the mechanics of active material systems.

Recently, Tseng and Wang (2004) investigated, numerically and experimentally, the application of the EMI-based method to detect damage in plain concrete beams. The damage was quantified through the Root-Mean Square Deviation (RMSD) which shows the difference in the electric admittance before and after damage as follows:

$$RMSD (\%) = \sqrt{\frac{\sum_{i=1}^N (M_i^d - M_i)^2}{\sum_{i=1}^N (M_i)^2}} \times 100 \quad (1.26)$$

where  $M_i^d$  and  $M_i$  are the conductance (real parts of the electric admittance) of respectively the damage and undamaged state at the  $i$ -th frequency.

The method was able to detect the growth of damage extent in a one-dimensional structure. For a three-dimensional structure, the mechanical coupling between vibrations should be considered which complicate the calculations. Moreover, damage too close or too far from the PZT transducers are not identified which means that it is a hard task to optimize the placement of transducers to monitor a structure.

Yang and Divsholi (2010) suggested a new method to reduce uncertainties in damage identification, a sub-frequency interval approach RMSD-S which consists in dividing the large frequency into sub-frequency intervals and calculating their RMSD in order to correlate the frequency range with the sensing region. It was deduced that damage close to PZT change significantly the RMSD-S at high frequency range while damage far from PZT change it at low frequency. But the same problem of sensing area remains because the changes in far damage are not that significant which could be misleading.

Wang et al. (2013) developed another technique using electromechanical admittances of multiple PZT and defining a new damage index called Cross-Correlation Coefficient (CC). It has been found that the electromechanical curve of a PZT changes near damage and the CC value decreases gradually when the damage severity increases near the PZT in question. However, this method can hardly identify a damage far from a PZT so one will need a huge number of PZTs especially in a large structure.

In addition to the above-mentioned drawbacks, one of the major problems in EMI-based methods is that, most of the times, they are unable to differentiate between damage and changes in the boundary or in environmental conditions. Since so many factors can influence the EMI signature, false alarms are very susceptible to happen.

### **1.4.3 Damage Detection Approaches**

As detailed in section 1.2.4, the above-mentioned techniques can be implemented with two different approaches: Model-free (or data-driven) and model based approaches. In the following, a review of two of the most popular approaches, one in each category, is presented.

#### **1.4.3.1 Statistical Pattern Recognition**

The idea behind the statistical pattern recognition approach can be explained by the fact that the presence, type and level of damage are deduced from previously classified observed damage cases. Such a technique is called “supervised learning” where data from damaged and undamaged conditions is needed to train the model. This method has been used in many domains and recent research has proved that it can successfully diagnose damage in structures.

For example, Worden and Manson (2000) applied an outlier analysis to identify a damage using the Mahalanobis Distance. However, in their technique, the authors made a number of assumptions such as the presence of a single outlier and the use of a Gaussian distribution for the normal condition. These assumptions are not always satisfied, which makes this technique only applicable to a limited number of problems.

Nair and Kiremidjian (2007) proposed a time series auto-regressive based detection algorithm using Gaussian Mixture Models as a damage assessment method, and the Mahalanobis Distance as an indicator for the damage extent. To be effective, their methodology requires the knowledge of the material properties of the structure and its behavior under dynamic loading conditions, and the initial measurement is assumed to be for an undamaged state. Hence, incorrect results are obtained if measurements are taken after a damage has occurred.

Recently, Heo et al. (2017) investigated the impact of local damage on the performance of an entire structure in order to improve the limitations of previous studies and suggested a new Statistical Pattern Recognition Technique, defining a Revised Mahalanobis Distance. Their theory was able to assess the condition of a structure under external loads with high fluctuations (i.e. seismic loads) which could not be done with the classical Mahalanobis Distance theory, yet, the damage could not be located using this technique.

A statistical pattern recognition approach tends to be suitable especially where clear physical basis is unavailable. In such a case, it might be difficult to construct a well correlated finite element model. It has then the advantage of not inducing model errors. However, with high-dimensional features or big data, this approach might be complex and time consuming, especially in the feature extraction and/or statistical decision-making.

#### **1.4.3.2 Bayesian Probabilistic Approach**

##### **1.4.3.2.1 Classical Bayesian Framework**

Probabilistic Bayesian model updating technique is often used to characterize modeling uncertainties associated with a structural system. Bayesian update based on measured data is becoming more and more popular in structural health monitoring domain to identify the condition state of a structure and detect damaged elements through model updating.

The well-known Bayesian update formula that defines the posterior distribution is given by:

$$f(x|D) = \frac{f(D|x) \times f(x)}{f(D)} \quad (1.27)$$

Where  $x$  is the parameter to be identified,  $f(x)$  is the prior knowledge distribution of  $x$  or its belief state and  $f(D|x)$  is the likelihood function.

A typical Bayesian updating method calculates the posterior distribution according to the following steps:

- 1- Specify a prior distribution reflecting our beliefs concerning a parameter  $x$  before obtaining any data;
- 2- Choose a statistical model and derive the likelihood function reflecting our beliefs about the data given the parameter  $x$ ;
- 3- Update the probability density function of the parameter  $x$  after having observed the data by calculating the posterior distribution  $f(x|D)$ .

If the posterior distribution  $f(x|D)$  is in the same probability distribution family as the prior probability distribution  $f(x)$ , the prior and posterior are then called conjugate distributions, and the prior is called a conjugate prior for the likelihood function  $f(D|x)$ . For instance, a beta prior distribution is conjugate for a Bernoulli or a binomial likelihood distribution, a normal prior distribution is conjugate for a normal likelihood distribution, a gamma prior is conjugate for a Poisson likelihood distribution, etc.

Many authors have used Bayesian updating for structural health monitoring and reliability assessment. Vanik et al. (2000) discussed in their paper the problems related to uncertainties in applying SHM to real structures and studied the variation in time of a probabilistic damage measure using the Bayesian approach. They were able to detect damage in most cases except the cases with limited number of modal data sets where a false alarm was triggered.

Ching and Beck (2004) proposed a two-step approach for probabilistic SHM based on a new Bayesian model updating algorithm to solve problems related to incomplete mode shape information as shown in figure 1.2. The most probable values of the stiffness parameters were determined by the Expectation-Maximization algorithm. The probability of a damage in each sub-structure  $i$  was represented by:

$$P_i(\alpha_i) \approx F_G \left( \frac{(1-\alpha_i)K_i - K_i^d}{\sqrt{(1-\alpha_i^2)(\hat{\sigma}_i)^2 + (\hat{\sigma}_i^d)^2}} \right) \quad (1.28)$$

where  $\alpha_i$  is a specific fraction of the stiffness of the undamaged structure,  $F_G$  is the standard Gaussian cumulative distribution function,  $K_i$  and  $K_i^d$  denote the most probable values of the stiffness parameters for, respectively, the undamaged and possibly damaged structure and  $\sigma_i$  and  $\sigma_i^p$  are the corresponding standard deviations.

For a full-sensor case, where measurements have been taken on each floor of a four-storey model structure, only one false detection was identified while for a partial-sensor case, where measurements are only taken at the third floor and the roof, there were many false detections. So in order to have increase results accuracy, sensors should be placed on all degrees of freedom which can be very costly.

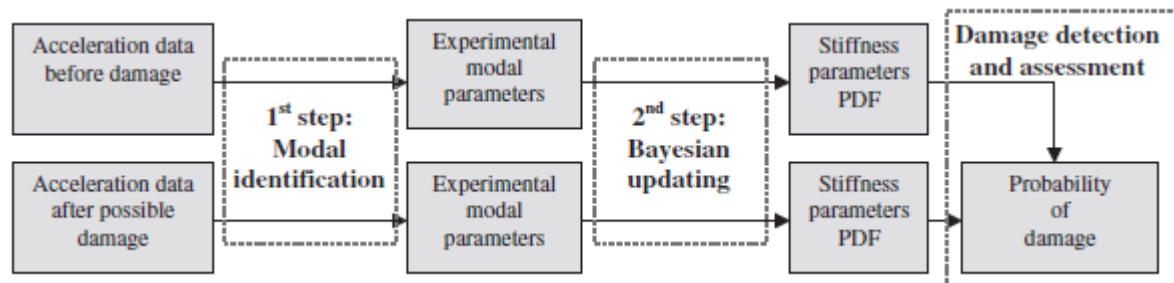


Figure 1.2: A schematic of the two-step procedure for damage detection and assessment. (Ching and Beck, 2004)

Strauss et al. (2008) presented a new method integrating monitoring data in structural reliability assessment using Bayesian updating to include prior information in the estimation of parameters like the mean and standard deviation of the reliability index, and subjective judgments with the observed data. The benefit of using the Bayesian approach lies in the fact that any prediction of future structural performance is based on past monitored data. Compared to gathering data from successive monitoring periods for the prediction of structural performance, authors stated that the Bayesian approach use less saving space since all the past information is included in the prior distribution so there is no need to save past monitored data.

Ntotsios et al. (2009) identified the location and the severity of damage using measured modal characteristics in a Bayesian inference framework. Their technique was based on finite element models and data collected before and after damage. Using a Bayesian approach, the most probable model class is selected from a family of competitive parameterized model classes which will indicate the damaged substructure. A model class is defined, in this paper, by a finite element model parametrized by structural modal parameters, each parameter associated to a damage in a substructure. Hence, each model class represent a damage scenario. The best model class is the one that is able to predict the actual damage scenario and that best fit the data. This implies that model classes should be defined beforehand and at least one of them should contain the actual damage scenario. In addition, sensors must be judiciously placed in order to provide information about all model classes simultaneously and estimate the damage severity. Due to measurement and model errors, some sensor configurations might give insufficient information for the identification of relevant model classes which could result in selecting the wrong model.

Rabiei and Modarres (2013) developed a recursive Bayesian framework combining information from online monitoring and periodic inspections and using data from direct damage observation and/or damage growth rate estimates to update crack size distribution



and parameters for an empirical crack growth model. However, the effectiveness of their approach depends on the performance of the individual techniques fused together, which means that it is necessary to develop models to better correlate both techniques.

Behmanesh and Moaveni (2014) identified damage using Bayesian finite element model updating on the Dowling Hall footbridge. Their probabilistic model updating framework quantify the uncertainty of damage identification. It was concluded that, for an accurate damage detection, it is recommended to use probabilistic FE model updating technique with several sets of measurements. But the main limitation of this method is its high dependency on the accuracy of the initial finite element model, the discretization scheme of the updating parameters and the considered residuals and their weights in the objective function. Hence, for a better damage identification, a meta-Bayesian updating could be used to select the best model class between a set of model classes, each defining a combination of factors such as initial models, objective functions, updating parameters, etc.

#### 1.4.3.2.2 Approximate Bayesian Computation

In some cases, such as non-linear models or FEM, the analytical formula of the likelihood function might be hard to find either for mathematical reasons or for computational reasons. To bypass such a problem, one can resort to the so-called Approximate Bayesian Computation (ABC), a rejection algorithm where an approximation of the posterior distribution is found without explicitly using the likelihood function but instead, generating sample data sets from the model. The steps of an ABC algorithm can be described as follows:

- 1- Given a prior distribution of a parameter  $x$ , and a specific model, a dataset  $\hat{\mu}$  is simulated.
- 2-  $\hat{\mu}$  is compared to the observed dataset  $\mu$  with a specified acceptance tolerance. If the distance measure defining the difference between datasets is within the tolerance,  $\hat{\mu}$  is accepted and thus its associated  $x$ . Otherwise,  $\hat{\mu}$  is rejected.
- 3- Step 2 is repeated for  $N$  number of simulations;
- 4- An approximate posterior distribution of the parameter  $x$  is then defined from the accepted parameter values.

Sunnåker et al. (2013) summarized the algorithm by an illustration represented in figure 1.3 (the parameter  $x$  is represented by the symbol  $\theta$  in the original version).

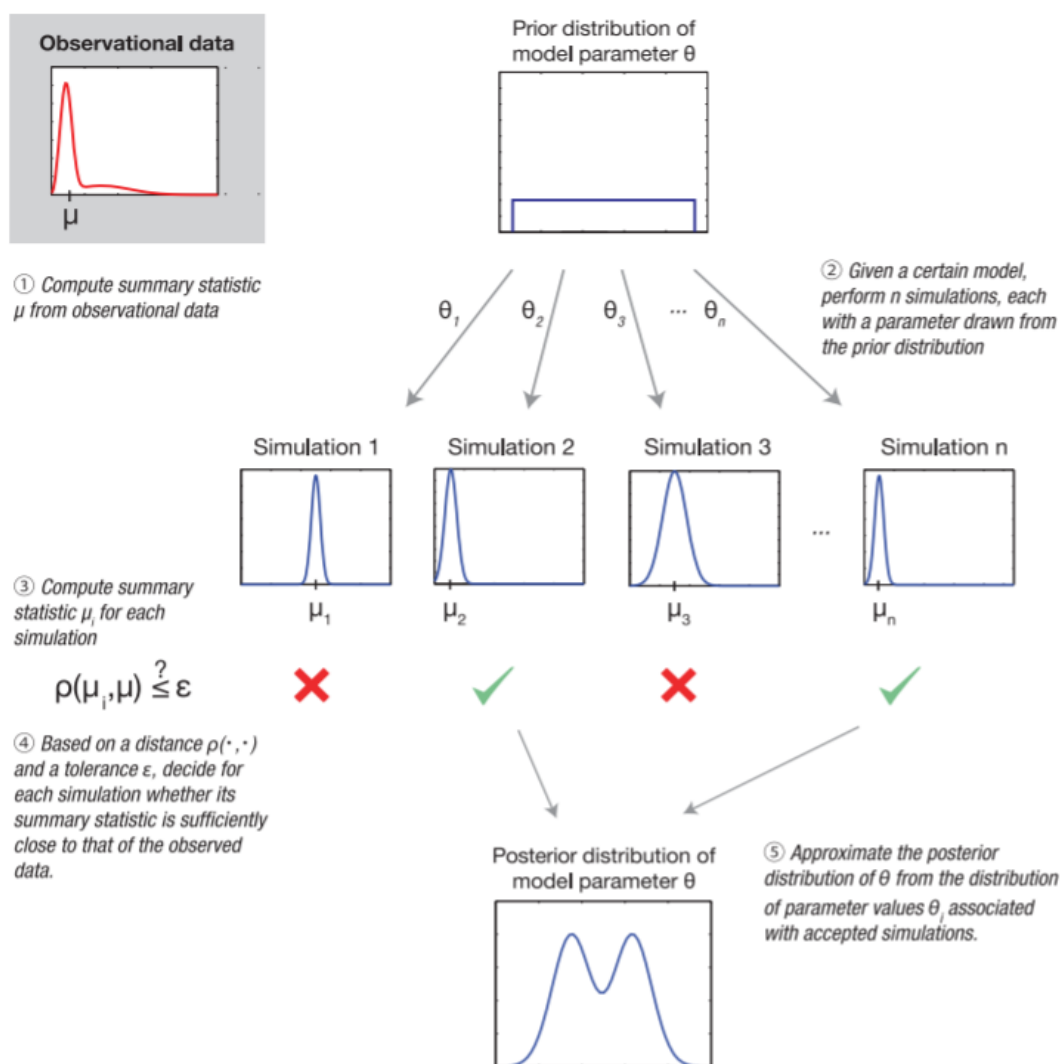


Figure 1.3: Parameter estimation by Approximate Bayesian Computation: a conceptual overview. (Sunnåker et al. 2013)

To improve computational efficiency, many authors have combined the ABC with sequential algorithms such as the partial rejection control (Sisson et al., 2008), the sequential Monte Carlo (Del Moral et al., 2012; Toni et al., 2008), the Markov Chain Monte Carlo (Wegmann et al. 2009; Marjoram et al. 2003), the subset simulation (Vakilzadeh et al. 2017; Chiachio et al. 2014) and the Metropolis Hastings sampling (Fang et al. 2019). In their article, Marin et al. (2011) provided a survey about the ABC methods which are considered as an extension to the original method. However, this technique has not been much explored yet in the structural damage assessment.

#### 1.4.3.2.3 Hierarchical Bayesian Framework

A Bayesian framework also involves a hierarchical model where the prior is a joint distribution derived from a product of conditional distributions (Congdon 2010; Robert 2006). Among others, this type of modelling is applied when observations have some kind of a natural hierarchy, when measurements are taken repeatedly at different conditions or at

different times, when data is collected from multiple sets or to take into account the prediction error parameters for a more robust identification. The hierarchical Bayesian modelling consists of multiple levels where the parameters of the prior distribution are called hyperparameters and their distributions hyperpriors. If we consider for instance  $x$  a parameter,  $y$  a hyperparameter and  $D$  the observation, the joint posterior distribution in the hierarchical model is represented by:

$$P(x, y|D) = \frac{P(D|x, y)P(x|y)P(y)}{P(D)} \quad (1.29)$$

and the marginal posterior distribution becomes:

$$P(y|D) = \int P(x, y|D)dx = \frac{P(D|y)P(y)}{P(D)} \quad (1.30)$$

Hierarchical Bayesian models have been adopted by authors to take into account uncertainties due to poor prior knowledge of hyperparameters (Wang and Zabarar 2004) and to quantify parameters uncertainties in a multilevel model (Behmanesh et al. 2015; Jiang and Mahadevan 2009). As deduced by Behmanesh et al. (2015), this technique is more suitable than the classical Bayesian framework to assess damage in operational civil structures since identified damage are associated with uncertainties coming from multiple sources, such as, from changing environmental conditions (which can significantly affect the results).

#### 1.4.4 Synthesis

Assessing damage in a structure can be done using several detection techniques and approaches. Among the most common used techniques are the modal-based methods and the electromechanical impedance. After having given a brief review of the work previously done on these methods, the following conclusions could be made:

- The natural frequency method is suitable for simple structures with regular geometries however, they can hardly identify damage in large and complex structures and/or with multiple damage. This technique suffers from a non-uniqueness of the solution since it is very susceptible to false positives;
- Mode shapes method can assess damage better than natural frequencies since they contain spatial information useful for damage localization. They are less influenced by environmental effect, yet, the changes in mode shapes still depends on the noise level and on the sensor placement;
- Mode Shape Curvature method requires a large number of sensors to be able to locate a damage and its performance depends on the number of modes considered. Also, the fact that curvatures are calculated from displacement mode shapes using the central difference approximation intrinsically induces errors and amplifies any slight noise in mode shapes. For these reasons this method is not recommended to be used alone for damage identification (Moughty and Casas 2017);

- Modal Strain Energy is effective for damage detection yet, its efficiency depends on the number of modes defined. Being based on modal curvatures, it is also affected by the same intrinsic error;
- Modal flexibility has higher damaged sensitivity in lower modes (which are more easily extracted) however, it is hardly applicable in unknown conditions (e.g. ambient). This is due to the fact that it uses mass-normalized mode shapes which require a previously known load effect;
- Modal damping is more likely to be affected by a noisy environment than natural frequencies or modal shapes. The expected deterioration should be also considered when using modal damping since damping values might increase or decrease depending on the damage type;
- Electromechanical impedance methods are able to identify damage if located near the sensor which may result in a large number of sensors for an accurate detection. They are also highly affected by environmental conditions.

In the following chapters we will be using the mode shapes method, being a simple technique which reflects the behavior of the structure in its entirety. It is easy to implement since mode shapes can be easily extracted from the dynamic response of the structure and effective at the same time.

Regarding the two different approaches that have been presented in section 1.4.3, statistical pattern recognition has an advantage of not requiring a model to be based on and therefore, no model errors are induced. However, its performance highly depends on the training data set. In order to detect an existing damage, the model must be well trained to that particular pattern damage. Also, insufficient training samples may result in over-fitting problems (Hou and Yong 2020). This process might therefore be time consuming. Hence, even though using a Bayesian probabilistic approach needs a model to be based on (which may induce model errors), it has the ability to take into consideration, intrinsically, any type of errors (e.g. model and measurement errors). It has also the advantage of including all relevant information about the unknown parameters in the prior probability. It provides a probability distribution for the unknown parameters instead of being limited to point estimations (which is often not reliable due to the presence of modeling uncertainties). And it can combine different types of information from the past and the present to update the probability distribution of the unknown parameters.

## **1.5 Optimal Sensor Placement**

### **1.5.1 Introduction**

A structural health monitoring problem has generally several main objectives: (i) maximize the reliability of damage detection; (ii) accurately localize the damage(s); (iii) precisely evaluate the extent of the damage(s); (iv) and last but not least minimize the costs. To obtain reliable information about the degradation of a structure, sensors might be required to be

installed on a large number of degree of freedom. However, often, this might be very costly and impractical. Therefore, in order to reduce costs and circumvent the need to measure inaccessible DOF, sensors optimization is essential. For instance, in mode shape based identification, sensor placement is important in order to obtain orthogonal measurements and a high signal to noise ratio. The problem can be therefore divided into two interrelated parts: (i) finding the optimal (minimum) number of sensors needed and (ii) finding the best position of the sensors.

The main objective of an optimal sensor placement for damage detection is then to (i) maximize the probability of damage detection, (ii) maximize the accuracy of damage localization, (iii) maximize the accuracy of damage quantification, (iv) while minimizing the number of sensors to be implemented.

## **1.5.2 Optimal Sensor Placement Techniques**

### **1.5.2.1 Particle Swarm Optimization**

The Particle Swarm Optimization (PSO) is an optimization process aiming toward moving a population of candidate solution (the particles), iteratively, so they can find their best positions in the search space. At each iteration, each particle moves around in the search space depending on its local best position, best position found in their vicinity and velocity.

The PSO concept was first introduced by Kennedy and Eberhart (1995). It has been then applied and improved by authors for optimal sensor placement. Ngatchou et al. (2005) have developed, for example, a Sequential Particle Swarm Optimization (S-PSO) in which they modified the PSO in order to shorten the computational run-time and improve the convergence performance. In this method, the selection is pseudo-random to avoid local optima, and the computation of the signal excess is exploited by the placement step to make some computational savings. S-PSO uses random subspaces smaller than the search space of a standard PSO and a deterministic number of iterations.

He et al. (2014) proposed another form of the PSO by applying an Integer-encoding Multi-swarm Particle Swarm Optimization (IMPSO) algorithm to optimally locate multiaxial sensors on large structures for modal identification. Their algorithm consists of dividing the population into three separate species: one elite population with smaller scale and higher fitness, and two civilian populations with larger scale and lower fitness. The IMPSO has the advantage of converging faster than other algorithms to the global optimum for large structures but this fast convergence may sometimes lead to being trapped in a local minimum.

Li et al. (2015) combined the dual structure coding and the mutation particle swarm optimization to determine the optimal sensor configuration. The dual structure coding helps in fixing the number of sensors and overcome the constraint of previously determined fixed number of sensors. They showed that this combination provides better results than the standard PSO.

The advantages of using the PSO rely in the fact that it is easy to implement with few parameters to adjust. PSO has proved a high efficiency in finding the global optima with a

rapid convergence. However, it can be difficult to define the initial parameters. A poor initialization of PSO parameters might induce a premature convergence and lead the solution to a local optimum, especially in complex problems (Abdmouleh et al., 2017).

### 1.5.2.2 Sequential Sensor Placement

The Sequential Sensor Placement (SSP) algorithms constitute a systematic and efficient way to construct sub-optimal sensor configurations that can be very good approximations of the optimal sensor configuration, using the estimation of a physical model parameter such as the information entropy. These algorithms can be divided into two main categories: (i) the Forward Sequential Sensor Placement (FSSP) algorithm and (ii) the Backward Sequential Sensor Placement (BSSP) algorithm. Both methods follow the same steps but in an inverse order. For example, in a FSSP, sensors are placed one at a time in the structure at a position that results in the highest reduction in information entropy while in a BSSP, sensors are placed at all degrees-of-freedom (DOF) and removed successively one at a time from the position that results in the smallest decrease in the information entropy.

Papadimitriou (2004) proposed the aforementioned algorithms to find near optimal sensor configurations. Results showed that both correctly pick the optimal sensor locations for the majority of sensors. However, the FSSP is computationally more effective than the BSSP needing one order of magnitude less computational effort. It has been observed that: (i) the lower and upper bounds of the information entropy are decreasing functions of the number of sensors to be placed; (ii) the difference between the upper and lower bounds of the information entropy, reflecting the “maximum improvement” obtained by the optimization process, decreases when the number of sensors increases; (iii) few sensors placed at their optimal locations provide better information than lots of sensors arbitrarily distributed on the structure.

In Papadimitriou’s method, the number of sensors to be placed must be known in advance. However, constraining the problem by this assumption usually leads to suboptimal solutions. Hence, Yi et al. (2011) developed a method to initialize the selection of the sensor set with a small set of locations before applying the Sequential Sensor Placement (SSP) algorithm to define the optimal number of sensors and involve it in a generalized genetic algorithm to optimize the sensor locations. The main difference between their application of the SSP and the one applied by Papadimitriou is that, in this paper, sensors are placed one at a time at a position giving the highest reduction in the maximum off-diagonal element of the MAC (Modal Assurance Criterion) between two mode shapes vectors (Eq. 1.12). The MAC equation should be updated each time a sensor is added. The application of the methodology on the Guangzhou New TV Tower confirmed that each increase in the number of sensors results in a decrease in the maximum off-diagonal elements of the MAC. However, due to economical reason, the optimal sensor number has been chosen as the number after which the maximum off-diagonal decrease has slowed down. But even though the SSP could give a good sensor configuration, it still is a suboptimal configuration which could not necessarily be the global optimal one due to the iteration process. For this reason, sensor locations are better

obtained by applying the generalized genetic algorithm where solutions tend to be closer to the global optimum.

Zhang et al. (2017) suggested a new strategy to optimize, simultaneously, reference and roving sensors in large structures using a computational algorithm based on the backward sequential placement algorithm with the information entropy index as a criterion. This technique has shown that it is best to choose a number of reference sensors greater than the number of modes to be identified. However, when it is not the case, it is preferable to implement the maximum possible number of reference sensors and to uniformly distribute the roving sensors.

The SSP algorithm is therefore computationally efficient to obtain a good sensor placement, having a deterministic number of computations. Yet, they are sensitive to the number of sensors and the initial candidate locations. Also, multi-objective optimization may not be implemented easily using the SSP. For these reasons, the SSP has gained less interest compared to other optimization algorithms.

### **1.5.2.3 Simulated Annealing**

Simulated annealing is a probabilistic optimization technique based on an analogy of physical annealing where the cooling of a material is controlled to reduce its energy and hence its defects. It is often used when the search space is discrete to approximate the global optimum of a certain function. At each step, the simulated annealing considers some neighboring state  $s'$  of the current state  $s$ , and probabilistically decides between moving the system to the state of lower energy or staying in the current state. This step is repeated until the system reaches a state where the objective function is satisfied.

Chen et al. (1991) applied simulated annealing to find the optimal placement of active structural members with built-in sensing and passively damped members in two complex truss-type structures. The selection procedure used the finite-time energy dissipation criterion and the measure of optimality was the maximization of the cumulative energy dissipated over a finite time interval. Even though this procedure is computationally efficient for nearly optimal solutions, it does not guarantee the global optimality. For large structures, many near-optimal solutions appear thus, the algorithm must be repeated with different starting configuration in order to identify truly optimal selected locations.

Chiu and Lin (2004) solved a combinatorial optimization problem through the application of the simulated annealing. The purpose of their study was the sensor placement for target location, in a grid based scenario, by minimizing the maximum distance error between two indistinguishable grid points in a sensor field under cost and coverage constraints. Compared to random placement, the sensor density of the adopted approach was reduced. However, a predetermination of the structure properties and a planned sensor network are required. Also, the stopping criterion used in the algorithm does not guarantee an optimal solution.

Tong et al. (2014) proposed an optimal sensor placement strategy using an improved simulated annealing algorithm with three different objective functions based on: the Fisher

information matrix (FIM), the modal assurance criterion (MAC) and the mean square errors (MSE). When using a decimal encoding where a number defining a specific location is assigned to each sensor, the search space is limited to a one-dimensional space (longitudinal or transversal). Therefore, the authors proposed using a coordinate-based encoding where each sensor is assigned a set of coordinate parameters representing its location according to the three directions  $x$ ,  $y$  and  $z$  which will allow the search space to move in more than one direction. A comparison between the simulated annealing using a decimal encoding and using the coordinate-based encoding proved that the latter, for the three objective functions, provided a better convergence and a more efficient solution. Another comparison between the three objective functions revealed that the MAC and MSE perform better than the FIM (and especially the MAC for a large number of sensors) due to the fact that the FIM groups the sensors into clusters in high-excitation regions instead of distributing them.

As an optimization, the simulated annealing method provides an appropriate solution for non-linear models, for large problems and with noisy data. It is easy to implement, flexible and work well with both combinatorial and continuous optimization (Préaux, 2018). However, if the computation time is short, the algorithm might be stuck in a metastable state relatively far from the state of least energy. Numerous tests might be sometimes needed to ensure the optimality of the results. Moreover, several conditions on parameters are required in order to guarantee the convergence which makes them hard to adjust.

#### **1.5.2.4 Harmony Search**

The Harmony Search (HS) technique is an intelligent optimization algorithm in which each harmony corresponds to a vector of  $k$  decision variables. The harmony memory (HM) represents the population and its size is called Harmony Memory Size. HS algorithm tries to find a vector  $x$  which optimizes an objective function. After having initialized and evaluated the vectors in HM, a new vector  $x'$  is generated based on a Harmony Memory Considering Rate (HMCR) and a Pitch Adjusting Rate (PAR). If  $x'$  is better than the worst vector in HM, it replaces it. The procedure is repeated until the termination criterion is satisfied.

The main drawback of this method arises from the large number of iterations needed to reach an optimal solution. For this reason, Mahdavi et al. (2007) improved the fine-tuning characteristic harmony search algorithm to increase its accuracy and convergence rate and introduced the so-called “Improved Harmony Search”. His work was based on changing the Pitch Adjusting Rate from fixed values to variables changing with the generation number.

Yadav et al. (2012) suggested an Intelligent Tuned Harmony Search algorithm to enhance the explorative behavior of the algorithm by automatically selecting the appropriate pitch adjustment strategy. Their method consists of dividing the harmony memory into two groups to enhance the balance between diversification and intensification. It has shown higher robustness and faster convergence than other HS variants however, its performance depends on some parameters such as the harmony memory size and the harmony memory considering rate.



In a review of the recent literature on the application of the harmony search, Manjarres et al. (2013) concluded that the algorithm has a good potential when searching near-optimal solutions to computationally hard optimization problems. Yet, more researches should be done to speed up the performance of the algorithm and reduce the computation time.

Another research done by Jin et al. (2015) was based on an improved harmony search algorithm to investigate the optimization problem of sensor placement on gantry crane structures. Their fitness function aimed at minimizing the maximum value of the MAC by selecting a subset of measurement points from potential locations. To reduce the number of generations to find an optimal solution, the authors integrated a New Harmony Memory as a parameter generated in each iteration and the New Harmony Memory Size refers to the number of new solution vectors improvised in each generation. This New Harmony Memory Size improved the HS algorithm however, its reasonable values should be more explored because they depend on the Harmony Memory Size and the complexity of the problem in practice.

Hence, the advantages of this method resides in the fact that it is an efficient method easy to implement. It may be used for discrete and continuous variables. However, it might need a large number of iterations to converge to a global optimum and may come across iterations that don't show any improvement.

### 1.5.3 Genetic Algorithm

The Genetic Algorithms (GA) were firstly introduced by Holland (1975) who was inspired by the Darwinian principle of natural selection to develop a tool that can import the mechanisms of natural adaptation into computer systems. GA is a search procedure that uses the mechanics of natural selection and natural genetics where chromosomes can be coded in two different ways: either as binary vectors or as real vectors. The bits representing one search variable, are called "gene", and all the genes collected in a binary vector are called "chromosome".

A genetic algorithm is basically defined by four components (Lerman and Ngouenet 1995):

- Individual (chromosome): a potential solution to the problem corresponding to a coded representation of the variable(s) in question.
- Population: a set of chromosomes in the search space.
- Environment: a search space.
- Fitness function: the - positive - function that we seek to optimize because it represents the adaptation of the individual to his environment.

In what follows, a typical genetic algorithm is described (Figure 1.4):

For the initialization, a starting population  $P(t = 0)$  of  $N_c$  chromosomes is stochastically generated based on uniform probability within the given bounds, representing the possible solutions to a given problem. The chromosome is therefore a potential solution for a given problem, combining a set of model parameters to be optimized.

Each chromosome of the population is then evaluated based on an objective function which assigns to each individual a "fitness value". This objective function is a fitness function that one seeks to optimize; it represents the adaptation of the individual to his environment.

To evolve towards the next generation of generally better solutions, the GA selects candidates from the current generation having the highest fitness values which allows the conservation of individuals with high potential. During the selection process, the best performing individuals have greater probability of being preserved, while the poorly adapted individuals will be gradually eliminated. Many types of selection could be used in the GAs such as the roulette wheel selection, the tournament selection or the truncation selection. For instance, when using the roulette wheel selection, the probability of an individual being selected is proportional to its fitness while in the tournament selection several individuals are randomly chosen from the population and among these individuals, the best one(s) are kept. The truncation selection sorts the individuals according to their fitness values and selects a certain proportion (e.g. 1/2, 1/3) of best individuals from the population.

After the selection process, the best solutions are then recombined with each other through an operation called "crossover" to form some new solutions which are used to replace the poorer of the original solutions. This type of recombination is defined by two steps:

- at first individuals chosen for the recombination are mixed and then two by two individuals are chosen as parents;
- in the second step the parents' chromosomes are recombined according to different crossover schemes.

Another type of recombination is the mutation which aims at finding a new region of the search space and avoiding the convergence to a suboptimum by exchanging values in the chromosome.

In general, the population size is kept constant. So it is necessary to decide which individuals should survive or be substituted for the next generation, this step is called "substitution". Therefore, the offspring are also evaluated and kinds of substitutions can then be applied such as the elitism (allowing the conservation of the best parents and the best offspring) or cancellation of  $N$  worst elements or cancellation of  $N$  stochastically chosen individuals, etc. The process is then repeated until the desired fitness value is reached or until reaching a certain number of iterations.

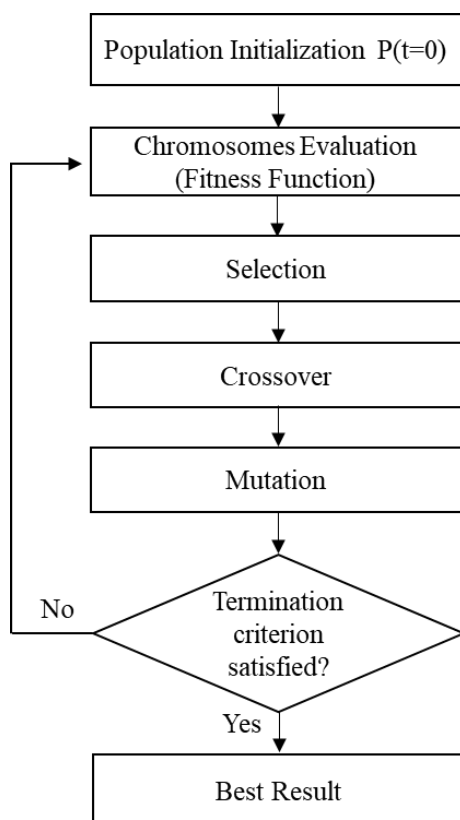


Figure 1.4: General Scheme of a Genetic Algorithm.

Yao et al. (1993) have successfully applied the GA to optimally place sensors on a large space structure for modal identification. In order to find the best locations for  $k$  sensors, each candidate solution (chromosome) consists of  $k$  genes, each gene containing an integer corresponding to a specific sensor location. To improve the convergence of the fitness, they introduced, in addition to the natural mutation, a forced mutation applied on chromosomes with redundant genes which consists of replacing one of the identical genes in the chromosome with any value different from the other genes. The fitness that has been used is the determinant of the Fisher information matrix. According to authors, GA gives higher accuracy in optimization especially with the modification they made. However, the main drawback of this method is its computational complexity coming from various factors such as the difficulty in choosing when to end the algorithm since the real maximum of the fitness value is unknown in advance and the long running time.

Zhang et al. (2000) worked on a Float-encoded Genetic Algorithm (FGA) to optimally locate piezoelectric actuators and sensors and provide their optimal gain and performance based on the minimization of energy dissipated by the active controllers. They have modified the crossover and mutation operations to avoid being trapped in a local minima and accelerate the process of convergence. Based on examples given by others, it has been shown that the FGA gives the same result as the standard genetic algorithm with a reduction in the computational requirements. But it was only tested on collocated actuators and sensors with a predetermined number.

Wongprasert and Symans (2004) identified the optimal damper distribution to control the seismic response of a 20-story benchmark building via the genetic algorithm. The optimization was achieved by minimizing four different frequency-domain objective functions. Results differ depending on the objective function used yet, most of the dampers tend to be concentrated on the lowermost and uppermost stories. All configurations provided an improvement in the seismic response however, the choice of the best depends on the criteria given the highest priority.

Liu et al. (2008) presented an improved genetic algorithm to find the optimal sensor location on a spatial lattice structure. They introduced some innovations to the GA such as the decimal two-dimension array coding system (instead of the binary code) to code the solutions and the forced mutation operator. In a population of  $m$  individuals representing the sensors locations, each individual is a chromosome having a size equal to the number of sensors to be placed where each gene is an integer defining a DOF (a specific sensor location). The maximum value a gene can take is the total number of DOFs. If in the same chromosome two genes contain the same value, one of them undergoes a forced mutation to a value that is not taken by the other genes. Conclusions revealed that the decimal two-dimension array coding system presents far less storage space than the binary coding methods because the length of a chromosome is reduced from the number of total DOFs to the number of sensors to be placed with an integer gene, and that the convergence of the modified GA gives better results. But the disadvantage of such a method is that we should, at the beginning, specify the number of sensors to be implemented and then optimize their location.

Yi et al. (2011) suggested an enhanced genetic algorithm, the “Generalized Genetic Algorithm” to optimally locate sensor on high-rise structures. Their method differs from the basic GA algorithm mainly in the evolutionary process, during the process of crossover and mutation. They added a two-quarter selection to the algorithm which allows parents to compete with the children during the process of crossover and mutation, and the best one is kept for the next competition. These changes, in addition to the use of a dual-structure coding method, improved the algorithm in finding the global optimum with lower computational iterations. A dual-structure encoding consists of a chromosome composed of two rows: a row defining the append code representing the DOFs and another row defining the variable code where genes take the value 0 or 1 depending on the measured DOF (a value of “1” means that the corresponding DOF in the upper row correspond to a sensor location). When the number of sensors is predefined, the variable code is fixed and the genetic operators (crossover and mutation) only operate on the append code.

Jung et al. (2015) improved the modal identification of flexible structures by optimizing the sensor placement via a genetic algorithm. The problem consists of finding the vector of positions ( $X$ ) of  $N$  vibration sensors by using, as objective function, the arithmetic sum of the off-diagonal terms in the modal assurance criterion:

$$F(X) = \sum_{i,j=1,i < j}^N MAC_{ij}(X) \quad (1.31)$$

Minimizing the off-diagonal terms increases the orthogonality between the reduced numerical modes extracted from the original natural mode obtained from a finite element modal analysis. In the GA algorithm, the fitness was calculated by reversing the objective function. After comparing the developed GA using reduced numerical modes to other methods based on the information of the original mode shapes (e.g. effective independence), it has been proven that the smallest off-diagonal MAC values has been given by the authors' method and that the configuration of sensors obtained by this method gives the most accurate vibration pattern (which is influenced by the accuracy of the natural modes).

Hou et al. (2019) worked on minimizing the mutual coherence of the sensitivity matrix of mode shapes in a genetic algorithm framework to explore the optimal placement of sensors used for damage detection. In addition to the classical GA algorithm, authors have forced a mutation on the chromosomes where the number of measured locations (genes with a value 1) is different than the number of sensors fixed at the beginning. The forced mutation is applied after the natural crossover and mutation and its aim is to keep the number of sensors constant in the chromosomes. The advantages of their optimization method is its fast convergence to the solution and the consistency of the results even with different initial populations however, the number of sensors must be previously fixed. After having compared results using optimal sensor placement and uniformly selected sensor locations for the same number of sensors, it was concluded that the former can identify more accurately damage location and severity.

Chapoulade et al. (2019) optimized the configuration of Vibrating Wire Extensometers (VWE) in a tunnel cross-section, using a GA algorithm combined to Bayesian updating. Their methodology starts by generating a strain database for multiple horizontal stress values  $\sigma_{h\ target}$  using finite element analysis. For each measured strain, the most probable horizontal stress is calculated using Bayesian updating, and is used by the fitness function of the GA algorithm. The fitness function depends on a weighted sum of two components; namely: the inverse model results and their dispersion. The best VWE configuration is found as the one that predict best the horizontal stress  $\sigma_{h\ target}$ . Yet, the optimal sensor placement depends on the weight of each of the two components of the fitness function.

Genetic algorithms are often used for sensor configuration optimization, they are particularly efficient for the exploration of large search space and offer a great adaptability. However, GAs might converge prematurely thus they do not guarantee that the obtained solution is the true global optimal solution. Variations and extensions designed to tackle premature convergence (and other issues) are continuously reported in the literature.

#### 1.5.4 Synthesis

Optimizing a sensor configuration for damage assessment can be done using several optimization techniques. Among these are the previously discussed ones, namely the Particle Swarm Optimization (PSO), Sequential Sensor Placement (SSP), Simulated Annealing (SA), Harmony Search (HS) and Genetic Algorithm (GA). The following conclusions can be drawn on the performance of these techniques:

- PSO is easy to implement, provides a rapid convergence and tends to be very efficient in finding the global optima with a short computational time. However, the setting of initial parameters highly affects the results and might be a difficult task;
- SSP is computationally efficient but it may not be suitable for multi-objective optimization;
- SA is an efficient method for non-linear models and large problems, easy to implement and flexible. However, as it is the case for PSO, the initial parameters might be hard to adjust. The computational time tends also to be higher than others methods in order to ensure the optimality of the results;
- HS has the advantage of being efficient and easily implemented. Yet, the algorithm may come across iterations with no improvement.
- GA is very efficient for solving complex problems and large search spaces with a rapid convergence, a great adaptability and without the need of calculating the derivative of an objective function to find a solution to the optimization problem. However, it might be time consuming for large and complex problems and the initial parameters might be also hard to define.

These methods have a common limitation, which is the tendency to converge prematurely to a local optimum and get stuck in it. Several techniques might be used to avoid or minimize this shortcoming such as launching several runs and choosing the suboptimal solutions to define the initial population for a last run which aims at finding the global solution.

Between the presented methodologies, the SSP tends to be the less popular one being limited in terms of application. As for the others, a review of comparison studies between PSO, SA, and GA has been presented in Chapoulade (2019). It was concluded that the AG and PSO are more robust and precise than SA converging with much less iterations. Yet AG needs less parameters to adjust. The same conclusion can be made regarding the comparison between AG and HS.

## **1.6 Conclusion**

An overview of structural health monitoring concepts and techniques required by structural damage assessment has been given in this chapter.

The state-of-art of these topics has been reviewed showing various methods that have been proposed and developed to optimize the detection process spanning from the choice of the optimal sensor configuration to the identification and quantification of the damage.

Among all the techniques used for damage assessment, Bayesian updating has proved its efficiency when dealing with inverse problems in structural system identification. However, even though the likelihood function might be implicit and hard (or impossible) to express analytically, authors tend to assume a Gaussian likelihood function (representing the correlation between the predictions and observations). This assumption might not be valid in

some settings, therefore, in such cases, it is preferable to use a likelihood-free Bayesian method such as the Approximate Bayesian Computation.

Most authors have also tackled the problem of damage detection in the case of a single structure. Yet, sometimes one is in presence of multiple similar structures such as similar buildings in a compound or similar bridges. In such situations, one could take advantage of the similarity between structures. Using information generated by sensors implemented on a structure, one could amplify the available knowledge about the condition state of elements belonging to similar structures. Such a scheme maximizes the yield of information with less sensors. When the number of sensors is limited, it might be also useful to borrow information from well monitored elements to less monitored ones within the same structure.

SHM outcomes are also used in Inspection, Maintenance and Rehabilitation (IM&R) problems. When an anomaly is detected by a SHM system, an inspection of one or several elements might be prescribed based on the SHM outcome. The inspection results would normally be used to plan structural maintenance. Inspection results obtained for an element can be used, along with the SHM, to update the condition state of the remaining elements. This fusion of data might be useful for an optimal IM&R planning in order to maximize the amount of yielded information, reduce the uncertainties, and minimize inspection costs.

Moreover, sensor placement is a key component in SHM design, having major effects on damage detection and localization performance. Genetic algorithms are considered as popular techniques for optimal sensor placement, being adaptive, stochastic and easily parallelized optimization methods. They are able to efficiently search complex and large solution spaces. Yet, often researchers focus on optimizing sensors' positions with a predetermined number of sensors. The influence of their number is rarely assessed and measurement noise is not always taken into consideration which may lead to false alarms and/or reduced sensitivity. Moreover, an optimal sensor configuration is usually found using specific damage configurations or based on the modal information in the initial structure. However, in real cases, an optimal sensor configuration should be able to identify most of the possible future damage configurations. Hence, in order to optimally choose the number and position of sensors for damage assessment, genetic algorithms could be improved by taking into account all uncertainties and involving as much damage configurations as possible.

The following chapters discuss some improvements and new methods to tackle these limitations.

## Chapter 2: Bayesian updating of the condition state of a structure

### 2.1 Overview

As previously discussed in the first chapter, detecting, locating and evaluating anomalies are the three main pillars of structural health monitoring. They belong to the damage diagnosis part which uses damage identification techniques and sensor data to assess the condition state of a structure. Identifying the stiffness parameters of healthy and damaged structures using collected vibration data is a very common way to detect a damage. In such cases, a damage is defined by stiffness reduction (Ching and Beck 2004). This issue has been the point of interest of many researchers who have developed different techniques to detect damage in a structure by comparing the vibrational response of the structure before and after a damage has occurred (Das et al. 2016; Liu and Chen 2002; Hu and Afzal 2006). Among all these techniques, Bayesian updating based on an inverse system identification approach has proved to be very effective in identifying damage in a structure using vibration data. The postulated prior distribution of a system parameter, which can be informative or non-informative, is updated with each new information obtained from the sensors. This type of problem is addressed by authors such as Beck and Katafygiotis (1998), Vanik et al. (2000) and Behmanesh et al. (2015). However, in most literature, assumptions are being made to formulate a suitable likelihood function which is, in many cases, hard to express explicitly.

In this chapter, a methodology is developed to update the condition states of a structure without the need to make assumptions and pass through explicit likelihood functions. The proposed technique is classified as an output-only modal identification method, belonging to the class of operational modal analysis (Rainieri and Fabbrocino 2014, and Brincker and Ventura 2015). The degree of damage of the structural members is assessed using a hierarchical Approximate Bayesian Computation (ABC) framework. It explicitly takes into consideration all uncertainties associated with the precision of the sensors, the lack of data due to the fact that not all degrees of freedom are measured, the mechanical model and the degradation of the elements. This chapter is organized in three main sections over eight paragraphs. A quick review is first given on modal analysis calculations followed by the damage and uncertainties definitions. Secondly, the ABC method is presented to update the belief states of the structural elements with the adopted evaluation function. In the last section, two numerical applications demonstrating the proposed approach are presented.

### 2.2 Modal Analysis of a structure

An Operational Modal Analysis (OMA) problem entails identifying the dynamic characteristics of a structure through the identification of its natural modes of vibration (Chapter 1, section 1.3). Each of these modes has three specific properties: a natural frequency, a mode shape representing the spatial distribution of movement over the structure and a damping factor which in some cases may be negligible. These properties can be defined



for a real structure having a linear elastic behavior by modelling it as a multi degree-of-freedom system (MDOF) having  $N$  independent degrees of freedom.

The well-known equation of motion of a MDOF system can be written as follows:

$$\bar{M}\ddot{\bar{u}} + \bar{C}\dot{\bar{u}} + \bar{K}\bar{u} = \bar{p}(t) \quad (2.1)$$

where  $\bar{M}$ ,  $\bar{C}$  and  $\bar{K}$  are respectively the mass, damping and stiffness  $N \times N$  matrices,  $\bar{p}(t)$  is the  $N$ -dimensional vector of external forces applied to the structure,  $\bar{u}$ ,  $\dot{\bar{u}}$  and  $\ddot{\bar{u}}$  are respectively the displacement, velocity and acceleration  $N$ -dimensional vectors.  $\bar{M}$ ,  $\bar{C}$  and  $\bar{K}$  are symmetrical matrices formed by real constant coefficients.

The damping ratio being normally less than 20%, the modes of the damped and undamped structure coincide. The solution of the Eq. (2.1) can be found then by neglecting the effect of damping on frequencies and mode shapes (Capra and Davidovici 1982). Therefore, we consider, in this paragraph, the case of undamped MDOF systems with free vibration where there are no external forces  $\bar{p}(t)=0$ . In such a case, Eq. (2.1) becomes:

$$\bar{M}\ddot{\bar{u}} + \bar{K}\bar{u} = 0 \quad (2.2)$$

This equation has a particular solution in the form of:

$$\bar{u}(t) = a\bar{\Phi}\sin(\omega t + \theta) \quad (2.3)$$

where  $\bar{\Phi}$  is a  $N$ -dimensional mode shape vector,  $a\bar{\Phi}$  is a vector representing the amplitudes,  $\omega$  is a pulsation frequency and  $\theta$  is a phase shift.  $a$  and  $\theta$  are constants determined by the boundary conditions.

Replacing  $u$  and  $\ddot{u}$  by their values in equation (2.2), the mathematical solution is conditioned by the expression:

$$|\bar{K} - \bar{M}\omega^2| = 0 \quad (2.4)$$

When developing this determinant, we obtain an equation of degree  $N$  of the eigenvalues  $\omega^2$ . By resolving this equation, we obtain the values of  $\omega_1, \omega_2, \omega_J \dots \omega_N$  relative to the  $N$  possible modes of vibration.

The mode shape vector  $\bar{\Phi}_J$  corresponding to the vibration mode  $J$  having a pulsation frequency  $\omega_J$  is given by:

$$(\bar{K} - \bar{M}\omega_J^2)\bar{\Phi}_J = 0 \quad (2.5)$$

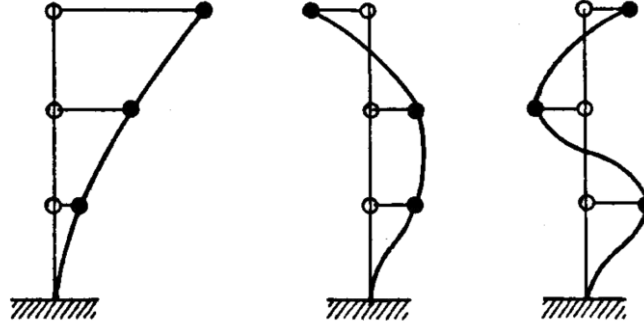


Figure 2.1: Example of vibration modes for a MDOF with 3 nodes.

These modal vectors  $\bar{\Phi}_j$  satisfy the following orthogonality properties:

$$\begin{cases} \bar{\Phi}_j^t \bar{K} \bar{\Phi}_l = 0 & \text{if } l \neq j \\ \bar{\Phi}_j^t \bar{M} \bar{\Phi}_l = 0 & \text{if } l \neq j \\ \bar{\Phi}_j^t \bar{\Phi}_j = 1 \end{cases} \quad (2.6)$$

$\bar{\Phi}_j^t$  being the transpose of the modal vector  $\bar{\Phi}_j$ .

The deformed shape of the structure, a sinusoidal function of time with an amplitude  $a_j \bar{\Phi}_j$ , is given by the equation:

$$\bar{u}_j(t) = a_j \bar{\Phi}_j \sin(\omega_j t + \theta_j) \quad (2.7)$$

The motion is periodic with a period:  $T_j = \frac{2\pi}{\omega_j}$  (2.8)

Therefore, the eigenvalues are defined, for each mode J, by:

$$\omega_j^2 = \frac{\bar{\Phi}_j^t \bar{K} \bar{\Phi}_j}{\bar{\Phi}_j^t \bar{M} \bar{\Phi}_j} \quad (2.9)$$

The  $N$  eigenvalues are organized in a diagonal matrix  $\bar{\omega}_N^2$  and their corresponding mode shapes constitute the columns of the mode shape matrix  $\bar{\Phi}_N$ . For the rest of the chapter, we shall represent the eigenfrequencies by  $\lambda_j = \frac{\omega_j}{2\pi}$ .

### 2.3 Definition of a damage

To define a damage, we consider a frame structure. We represent this structure by a finite element model (FEM). Frame elements are able to carry both axial force and shear force, and bending moment. Therefore, a frame element is seen to possess the properties of both truss and beam elements. The general stiffness matrix for a frame element is a 12x12 matrix.

Damage is characterized by a loss of the stiffness matrix of one or more elements in the structure. This change affects the stiffness matrix elements unequally, depending on the damage type, source, and local spread pattern (e.g. section loss due to corrosion, cracks due

to fatigue, etc.). Hence, we define the deterioration extent vector  $\bar{\alpha}_e$  of an element as a vector whose components represent alterations to various properties (Young modulus, area moment of inertia, etc.) of element  $e$ .

By adopting the notation of Shi et al. (2000), one can write:

$$\bar{K}^d = \bar{K} + \sum_{e=1}^N \bar{\Delta K}_e \quad (2.10)$$

where  $\bar{K}$  and  $\bar{K}^d$  are the stiffness matrices of the undamaged and damaged structure respectively,  $N$  is the number of elements and  $\bar{\Delta K}_e$  is the elemental stiffness matrix perturbation caused by a damage of element  $e$ .

$$\bar{\Delta K}_e = f(\bar{\alpha}_e) \quad (2.11)$$

Any prior information about the damage extent can be expressed by the prior probability distribution of  $\bar{\alpha}_e$ . Choosing the bounds zero and one for the components of  $\bar{\alpha}_e$ , can be considered as injecting engineering knowledge in the model (i.e. element stiffness is a non-negative monotone decreasing function in terms of deterioration, as long as no maintenance is done).

## 2.4 Model and Measurement Uncertainties

The purpose of the methodology presented in this chapter is to update the structural properties of the elements of a structure based on its observed modal properties. Hence, the proposed methodology can be considered, as an inverse problem where we are determining a system (structural parameters) from its “input → output” correspondence. The knowledge of these structural parameters values would serve as the basis for Inspection, Maintenance & Rehabilitation (IM&R) optimal decision making. Failing to properly account for different types of uncertainties affecting these parameters, identifying their sources and their propagation throughout the model would lead to suboptimal decision making.

The uncertainty of the estimated system parameters is generally due to: (i) model imperfection and simplification, (ii) intrinsic aleatory uncertainty of some variables, (iii) numerical errors and approximations, (iv) measurement uncertainties, (v) partial observability of the system. The last two types of uncertainties are specifically related to the inverse model calculations.

### 2.4.1 Model imperfection and simplification

Simplifications are compulsory for any physical model, of the reality, to be tractable. These simplifications are usually related to: (i) a reduced set of relevant input variables, and/or (ii) a simplified mathematical structure of the problem. Model uncertainty may arise also from an unwanted and overlooked model inadequacy. For example, among the many simplifications assumed in the numerical application presented in the last section of this chapter we presume that the structure has a linear elastic behaviour and that the ground is motionless rigid material, etc.

### **2.4.2 Intrinsic aleatory uncertainty of some variables**

Some input variables may be qualified as intrinsically uncertain in the sense that their uncertainty cannot be reduced by acquiring more knowledge or conducting more experiments and/or inspections. For example, wind speed at a specific location and at a future point in time has an uncertainty, which is at least partially intrinsic. i.e. it cannot be eliminated by any amount of additional inquiries. The exact properties of structural material (e.g. concrete and steel) are usually considered as spatially epistemic random variables while future loads are usually considered as intrinsic random variables.

### **2.4.3 Numerical errors and approximations**

Apart from very simple models, the actual computation of a mathematical model requires the use of numerical methods and algorithms, introducing numerical errors and approximations. For example, running algorithms on digital computers result usually in floating numbers errors. Also, in the numerical applications at the end of this chapter, we use Approximate Bayesian Computation to calculate the posterior PDF of structural parameters. We will show that under some general conditions, our proposed methodology practically eliminate the uncertainty of ABC for structural Bayesian updating.

### **2.4.4 Measurement uncertainties**

Any model requiring observable variable as input must account for any potential measurements uncertainties. This uncertainty is epistemic in the sense that its magnitude depends on the available technology and on the effort dedicated for the measurements. For example, in the numerical application at the end of this chapter we consider that the acceleration time series obtained from the sensors are uncertain and that the uncertainties are modelled as zero mean uniform distributions.

### **2.4.5 Partial observability of the system**

For inverse problems identification, one need to observe (and/or simulate) the output-input relationship in order to identify the system constitutional parameters. For deterministic systems, if we assume that there is no measurement or model uncertainties and that the excitation-response (i.e. input-output) of the system is exhaustively observed then, at least theoretically, one can uniquely identify the problem. The underlying assumption in that case is that there exists a bijective relationship between the input and output variables for a fixed system configuration or between the system configuration and the output variables for a fixed system configuration. However, often, not all the input or output variables can be practically or even feasibly observed. For example, in a global SHM problem, one need to exhaustively observe the infinite space of degrees of freedom in order to fully characterize the system response. As such, global SHM can only partially observe a system. Therefore, the input-output relationship can no longer be bijective i.e. for a given partial response there exist multiple system configurations that can account for it. Such a problem is qualified as being ill-posed.

Not taking into account, in the mathematical modelling, the above-mentioned uncertainties boil down to neglecting some of the available information. As such, any decision-making process based on the model would produce suboptimal solutions. In what follows, we state a mathematical model that account for the above-mentioned uncertainties. In subsequent sections and chapters, we will build upon this model to (i) develop extensions and algorithms that allows to further take into account additional relevant information and (ii) to develop decision making optimization algorithms for the IM&R planning.

Let:

- $\bar{\lambda}$  and  $\bar{\lambda}^d$  be the eigenfrequency vectors of, respectively, the undamaged and damaged structure.
- $\bar{\Phi}$  and  $\bar{\Phi}^d$  the eigenvectors matrices of, respectively, the undamaged and damaged structure.
- $\bar{\varepsilon}_{Mo}$  be a random vector representing model uncertainty.
- $\bar{\varepsilon}_{Me}$  be a random vector representing measurement uncertainty.

The structural response of the structure is described by:

$$\bar{\lambda}^d = \bar{\lambda} + \Delta\bar{\lambda} \quad (2.12)$$

$$\bar{\Phi}^d = \bar{\Phi} + \Delta\bar{\Phi} \quad (2.13)$$

The mechanical behaviour of the damaged structure can be formulated as:

$$(\bar{\lambda}^d, \bar{\Phi}^d) = \xi(\bar{K}^d) \quad (2.14)$$

where  $\xi()$  is a stochastic multidimensional function which must account for model uncertainty.

In our case, model uncertainty might originate from the discretization of the FEM, from the inadequacy of the simplified mechanical assumptions, from geometrical uncertainties, etc. Equation (2.14) can then be written:

$$(\bar{\lambda}^d, \bar{\Phi}^d) = g(\bar{K}^d, \bar{\varepsilon}_{Mo}) \quad (2.15)$$

where  $g()$  be a deterministic function depending on an additional random vector  $\bar{\varepsilon}_{Mo}$ . In our numerical application,  $g()$  represents the FEM algorithm.

In addition to model uncertainties, noise and measurement errors are other types of uncertainties affecting the structural system by widening the gap between the measured structural response  $(\bar{\lambda}^{Md}, \bar{\Phi}^{Md})$  and the actual response  $(\bar{\lambda}^d, \bar{\Phi}^d)$ . Hence:

$$(\bar{\lambda}^{Md}, \bar{\Phi}^{Md}) = w(\bar{\lambda}^d, \bar{\Phi}^d, \bar{\varepsilon}_{Me}) \quad (2.16)$$

where  $w()$  be deterministic function depending on an additional random  $\bar{\varepsilon}_{Me}$ .

From (2.15) and (2.16), one can write:

$$(\bar{\lambda}^{Md}, \bar{\Phi}^{Md}) = w(g(\bar{K}^d, \bar{\varepsilon}_{Mo}), \bar{\varepsilon}_{Me}) \quad (2.17)$$

From (2.10) and (2.17) we get:

$$(\bar{\lambda}^{Md}, \bar{\Phi}^{Md}) = w(g(\bar{K} + \sum_{e=1}^N \bar{\Delta K}_e, \bar{\varepsilon}_{Mo}), \bar{\varepsilon}_{Me}) \quad (2.18)$$

It is considered herein that  $\bar{K}$  is a random matrix and all the variables are random variables. Hence, any prior information about the probability distribution of  $\bar{K}$  can be taken into account by equation (2.18).

## 2.5 Approximate Bayesian Computation for a single structure

Often a limited number of sensors is implemented on the structure and therefore, because the information coming from collected data is insufficient to determine a realistic model of the structure, such problems are ill-conditioned and ill-posed when treated deterministically. Some uncertainties should also be taken into account, such as model uncertainties, sensors noise, simplifying approximations, etc. Therefore, the objective of the detection should not be limited to a single optimal parameter vector but, rather, attempt to find a probability distribution of the model parameters based on the available data. For these reasons, one of the most adequate identification techniques for inverse problems is the Bayesian updating which provides a rational and robust tool that is able to handle the difficulty of non-unique solutions.

In our problem, the purpose of the Bayesian updating is to calculate the posterior Probability Density Function (PDF) of the damage extent  $\bar{\alpha}_e$  for each element after observing the structural response  $(\bar{\lambda}^{Md}, \bar{\Phi}^{Md})$ . In what follows, to simplify the presentation, we shall reduce  $\bar{\alpha}_e$  to one scalar component  $\alpha_e$ .

$$f(\bar{\alpha} | \bar{\lambda}^{Md}, \bar{\Phi}^{Md}) = \frac{f(\bar{\lambda}^{Md}, \bar{\Phi}^{Md} | \bar{\alpha}) \times f(\bar{\alpha})}{f(\bar{\lambda}^{Md}, \bar{\Phi}^{Md})} \quad (2.19)$$

where  $\bar{\alpha}$  is a vector whose components are the damage extents  $\alpha_e$  of each element,  $f(\bar{\alpha})$  is the prior distribution,  $f(\bar{\alpha} | \bar{\lambda}^{Md}, \bar{\Phi}^{Md})$  is the posterior distribution given the observed data  $\bar{\lambda}^{Md}, \bar{\Phi}^{Md}$  and  $f(\bar{\lambda}^{Md}, \bar{\Phi}^{Md} | \bar{\alpha})$  is the likelihood function.

The Bayesian updating of equation (2.19) can be conceptually partitioned into a hierarchical Bayesian updating as follow:

$$f(\bar{\lambda}^d, \bar{\Phi}^d | \bar{\lambda}^{Md}, \bar{\Phi}^{Md}) = \frac{f(\bar{\lambda}^{Md}, \bar{\Phi}^{Md} | \bar{\lambda}^d, \bar{\Phi}^d) \times f(\bar{\lambda}^d, \bar{\Phi}^d)}{f(\bar{\lambda}^{Md}, \bar{\Phi}^{Md})} \quad (2.20a)$$

$$f(\bar{K}^d | \bar{\lambda}^d, \bar{\Phi}^d) = \frac{f(\bar{\lambda}^d, \bar{\Phi}^d | \bar{K}^d) \times f(\bar{K}^d)}{f(\bar{\lambda}^d, \bar{\Phi}^d)} \quad (2.20b)$$

$$f(\bar{\alpha} | \bar{K}^d) = \frac{f(\bar{K}^d | \bar{\alpha}) \times f(\bar{\alpha})}{f(\bar{K}^d)} \quad (2.20c)$$

An analytical solution for problem (2.20) is generally not possible. Even numerical approaches such as the one using Markov Chain Monte Carlo (MCMC) methods cannot be used because some of the likelihood functions are usually implicit; e.g. the relation between structural parameters ( $\bar{K}^d$ ) and the structural response ( $\bar{\lambda}^d, \bar{\Phi}^d$ ) is usually described by numerical methods such as FEM. The approach adopted in this chapter makes use of the Approximate Bayesian Computation (ABC) algorithm (Wilkinson 2013, Wegmann et al. 2009) to calculate a posterior probability distribution of the vector  $\bar{\alpha}$  after observation of the measured structural response ( $\bar{\lambda}^{Md}, \bar{\Phi}^{Md}$ ). Instead of explicitly using likelihood functions, ABC (or likelihood-free inference) yield the posterior distribution by generating sample data sets from a model.

ABC algorithms were basically developed based on rejection sampling algorithms where generated samples of unknown parameters are accepted or rejected depending on a specific criterion evaluating the similarity between the simulated data given a certain sample and the observed data. In our problem, the ABC algorithm is essentially composed of the following 5 steps:

- 1- Generate  $\bar{\alpha}$  from a suitable prior distribution of the damage extent.
- 2- Using the generated  $\bar{\alpha}$ , simulate ( $\bar{\lambda}^{SMd}, \bar{\Phi}^{SMd}$ ). For the calculation of ( $\bar{\lambda}^{SMd}, \bar{\Phi}^{SMd}$ ), one can optionally add noise at any calculation step to account for model uncertainties, other than the ones taken in account by the threshold  $\varepsilon$  described below.
- 3- Calculate some metric  $\rho$  between the observed structural response ( $\bar{\lambda}^{Md}, \bar{\Phi}^{Md}$ ) and the simulated one ( $\bar{\lambda}^{SMd}, \bar{\Phi}^{SMd}$ ).
- 4- Accept  $\bar{\alpha}$  with probability  $\psi(\rho)$ . Where  $\psi$  is a monotone decreasing kernel function of  $\rho$ . If  $\psi(\rho)$  is the uniform distribution then the acceptance rule reduces to : if  $\rho \leq \varepsilon$  where  $\varepsilon$  is a small chosen acceptance threshold.
- 5- Define a posterior distribution of the damage extent based on the set of accepted  $\bar{\alpha}$ .

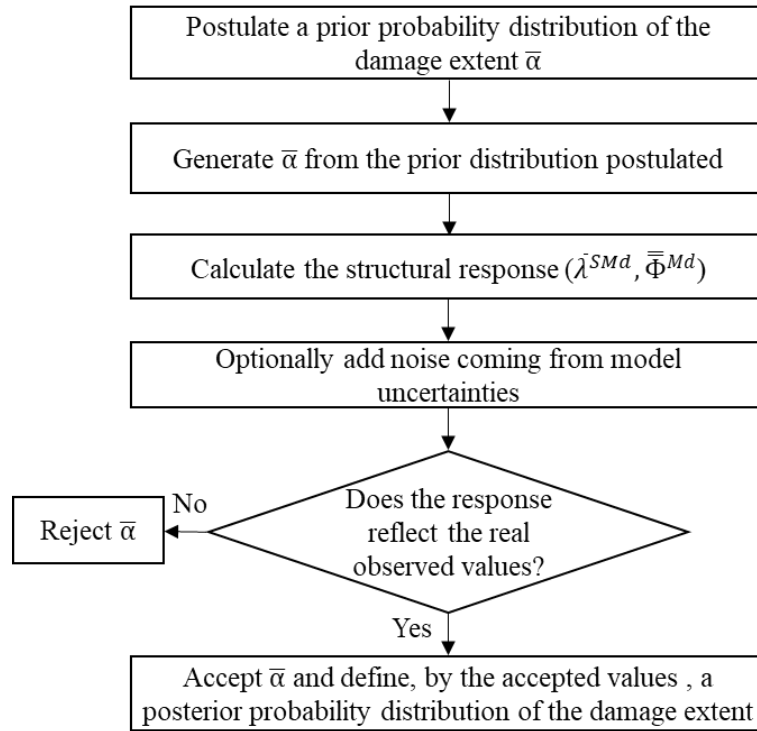


Figure 2.2: Flowchart describing the Bayesian update of a structure.

In a general setting, accepted values of  $\bar{\alpha}$  form an approximation of the true posterior unless  $\varepsilon = 0$  or  $\varepsilon = \infty$ . In the former case, the true posterior distribution is defined since exact values are accepted while in the second case,  $\varepsilon$  is large enough to accept all generated values which will reflect the prior distribution. Hence, an acceptance threshold  $\varepsilon$  greater than zero introduces a bias into the computed posterior distribution. The smaller the value  $\varepsilon$ , the smaller is the number of accepted samples. In such a case, results are less biased but, a larger sample size is needed which will require a higher computational time. However, Wilkinson (2013) showed that if model and/or measurement errors are modelled as a uniformly distributed random variable with a support of  $[-\varepsilon, \varepsilon]$ , then the computed posterior distribution will be exact. He also presented an extension to the original ABC where the model and/or measurement errors can have any given probability distribution.

The choice of the prior of  $\bar{\alpha}$  depends on the information available to the decision maker about the condition state of the structure. One example of such knowledge is the fact that the rigidity of a structural element is a monotone decreasing function of time if no maintenance is done between readings. Another example would be the knowledge of the manager of the structure about the rate of the deterioration of some elements of the structure. In fact, the sensors implemented on the structure might give us indications about the levels of stress and their frequency for some of the structural elements during the normal functioning of the structure. Such information can be used to predict fatigue occurrence, plastic deformations, etc. Therefore, prior information on the alterations undergone by the structural parameters might be available to the decision maker. Moreover, oftentimes the manager of the structure might have relevant information about the deterioration of the structure affecting the structural



parameters. For example, the results from previous inspections performed on the elements of the structure. These results can be taken into consideration by integrating them in the prior probability distribution of the structural parameters.

## 2.6 Evaluation Metric $\rho$

When applying the ABC algorithm on the structure, the simulated and observed structural responses are compared, using some metric  $\rho$ , in order to update the model and identify damage. When dealing with mode shapes, authors have often used the modal assurance criterion (MAC) which measures the correlation between two data sets or two vectors (Prado et al. 2016; Pastor et al. 2012; Allemang and Randall 2003). The criterion is a scalar constant determining the deviation between two modal vectors, in our case  $\bar{\Phi}^{Md}$  and  $\bar{\Phi}^d$ , and is defined by the following equation:

$$MAC_{i,i} = \frac{[\bar{\Phi}^{Md}_i{}^H \bar{\Phi}^d_i]^2}{[\bar{\Phi}^{Md}_i{}^H \bar{\Phi}^{Md}_i][\bar{\Phi}^d_i{}^H \bar{\Phi}^d_i]} \quad (2.21)$$

where  $H$  represents the complex conjugate transpose (Hermitian) which can be replaced by the transpose  $T$  when the modal vectors are real valued vectors and  $i$  defines the mode of vibration. The conjugate transpose (Hermitian transpose) of a matrix  $\bar{A}$  is obtained by first calculating the transpose matrix  $\bar{A}^T$  of the matrix  $\bar{A}$  (by interchanging the rows and columns of the matrix) and then replacing each element of  $\bar{A}^T$  by its complex conjugate.

The MAC values vary between 0 and 1. An absence of correlation is reflected by a null value while similar mode vectors lead to obtaining unity. This criterion was initially used in our methodology as the ABC metric  $\rho$ . However, it was a rough approximation because for the ABC algorithm to be considered an exact Bayesian updating tool,  $\rho$  must be a distance measure that could be comparable to the measurement error  $\bar{\epsilon}_{Me}$ . Moreover, when using the MAC, slight damage may remain undetectable since the computation is dominated by the largest differences between modal vectors.

Consequently, we propose to replace the MAC by the Maximum Sum of Absolute Differences (MSAD) and use it as the metric required by the steps of the ABC algorithm as follows:

$$\rho = \max_{mDOF} \sum_{i=1}^M |\bar{\Phi}^{Md}_{DOF-i} - \bar{\Phi}^d_{DOF-i}| \quad (2.22)$$

where  $M$  represents the number of modes of vibration and  $mDOF$  the measured degrees-of-freedom.

For each measured degree-of-freedom and for each mode of vibration, the absolute difference between the observed and simulated mode shape values are calculated. These differences are then summed up on all the modes of vibration. The maximum value of summation between all the measured degrees-of-freedom is accepted with probability  $\psi(\rho)$ . The kernel function

$\psi(\rho)$  represents the PDF of the measurement errors. If  $\psi(\rho)$  is a uniform PDF, then the acceptance probability is equivalent to the following:

$$p = \begin{cases} 1 & \text{if } \rho \leq \varepsilon \\ 0 & \text{if } \rho > \varepsilon \end{cases} \quad (2.23)$$

where  $\varepsilon$  is a measurement error on the data which depends on the sensing technology used.

## 2.7 Numerical Applications

To demonstrate the applicability of the above-proposed methodology, the Bayesian updating has been applied to two types of structures: (i) a steel truss structure and (ii) a 4-story concrete frame structure.

Without loss of generality, we suppose in both applications that there is no prior information about the structure. Accordingly, the prior probability distribution of the degradation of all the elements is considered as a non-informative uniform distribution. Measurement error is taken as a uniform random variable having a zero mean and a range equal to  $0.15 \text{ m/s}^2$ . The model errors are assumed to be uniformly distributed within 10% of the true value.

The continuous damage space  $[0, 1]$  of each element is discretized into four ordinal states  $\{1, 2, 3, 4\}$  (Table 2.1) where 1 stands for the best condition state, i.e. degradation extent is between 0% and 25%, and 4 stands for the worst condition state, i.e. degradation extent is between 75% and 100%. In table 2.1,  $\theta^e = j$  is a possible element condition state representing a particular subinterval from the domain of  $\alpha_e$ .

Table 2.1: Mapping between the continuous damage state extent and the discretized condition state.

$\theta^e$	Degradation extent
1	$\alpha_e \in [0,0.25]$
2	$\alpha_e \in ]0.25,0.5]$
3	$\alpha_e \in ]0.5,0.75]$
4	$\alpha_e \in ]0.75,1]$

In our algorithm, the evaluation function consists of comparing measured and simulated mode shapes using the maximum of the sums of the absolute differences over all measured degrees of freedom. The acceptance threshold  $\varepsilon_{Me}$  which is the measurement error (in  $\text{m/s}^2$ ) is assumed to be the same for all the installed sensors (i.e. the values of the components of the vector  $\bar{\varepsilon}_{Me}$  are all equal to  $\varepsilon_{Me}$ ). In order to be able to use  $\varepsilon_{Me}$  as an acceptance threshold and obtain exact results, the mode shape values will be multiplied by their corresponding  $\omega^2$ .

The acceleration being the second derivative of the displacement, Eq. (2.3) leads to the following expression:

$$\bar{\ddot{u}} = \omega^2 \bar{u} \quad (2.24)$$

The acceleration is equal to the displacement multiplied by the eigenvalue. And since the mode shape is a set of relative displacement of the DOFs, the acceleration is then proportional to the product between the mode shape and the eigenvalue and one can write:

$$\bar{u} \propto \omega^2 \bar{\Phi} \quad (2.25)$$

Eq. (2.22) will then become:

$$\rho = \max_{mDOF} \sum_{i=1}^M |(\omega^{Md_i})^2 \bar{\Phi}_{DOF-i}^{Md} - (\omega^d_i)^2 \bar{\Phi}_{DOF-i}^d| \quad (2.26)$$

where  $\omega^2_i$  is the eigenvalue relative to mode  $i$ .

Therefore, if the maximum of the sums of the absolute differences  $\rho$  does not surpass the predefined threshold  $\varepsilon_{Me}$ , the generated vector of damage extent is accepted, otherwise it is rejected.

In the following examples, the measured and simulated mode shapes and eigenvalues are given by FEM algorithms. Consequently, the real existing structure is modelled by FEM from which derives the measured structural response taking into consideration the measurement error.

### 2.7.1 Steel Truss

The first application illustrates a simply supported plane structure representing one of the four faces of a hinged steel truss structure. It includes 19 nodes, each having three degrees-of-freedom, and 33 round steel tube elements with an initial Young's modulus  $E=210$  GPa and a density  $d=7850$  kg/m<sup>3</sup> (Figure 2.3). The element cross-section properties are stated in table 2.2. The plane structure is subjected to unknown ambient excitation (from traffic, wind, wave in the case of an offshore structure, etc.). It is monitored by six horizontal accelerometers, one on each level, on nodes N5, N8, N11, N14, N16, and N19.

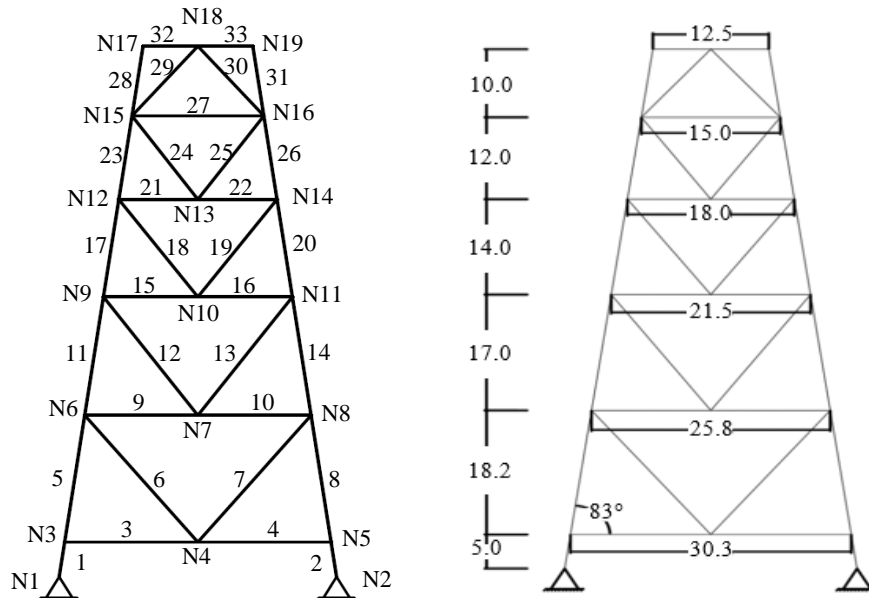


Figure 2.3: Geometry of the simply supported steel truss structure (dimensions in meters).

Table 2.2: Elements sections properties.

Elements	Section dimensions	
	Exterior diameter (mm)	Thickness (mm)
1,2,5,8,11,14,17,20,23,26,28,31	1219	25
3,4,6,7	610	10
9,10,12,13	508	10
15,16,18,19,27	457	10
21,22,24,25	406.4	10
29,30	355.6	10
32,33	323.9	10

The aim of the applied methodology is to update the state of the structural elements in order to identify the damage. We assume that a damage, resulting from various sources (i.e corrosion, fatigue cracks, etc.), is defined only by a loss of the axial stiffness since the structure behaves as a truss system. It is assumed that element 8 is 80% deteriorated (e.g. due to accidental actions or fatigue loading) which means that its remaining axial stiffness represents only 20% of its initial stiffness; however, the damage has not been detected yet.

In a real world setting, the structural parameters of the real initial structure (which may be damaged or not) do not coincide exactly with the modelled parameters. This is due to the presence of some sources of uncertainties such as geometrical imperfections, model imperfections, numerical approximations, etc. Hence, the mechanical analysis is unable to predict exactly the real behaviour of the structure. Consequently, in addition to the model and measurement errors taken into account, it is essential to apply the Bayesian updating on the initial structure to update the prior distribution of the structural parameters. Using data generated from sensors at  $t=0$  (time when sensors have been implemented), the prior distribution of the degradation of the structural elements is updated using the ABC methodology described in section 2.5. This first step is considered as a model tuning in order to improve the accuracy of the results. The obtained posterior PDFs will then be taken as a new prior distribution to detect any future deterioration in the structure. When applying the ABC methodology at  $t>0$ , this new prior distribution will be updated using data generated from sensors at time  $t$ , in order to assess the condition state of the structure.

In our case, we suppose that the initial structure (structure at  $t=0$ ) is an intact one. However, if for some reason, the updating procedure has to be applied on an already degraded structure, without any information about its undamaged state, the current state will be considered as the reference state and any future deviation from this reference will be identified as an additional damage. From the modal analysis, all the mode shapes have been taken into account. The first three mode shapes and their identified frequencies are presented in Appendix A for the intact and damaged structure.

Table 2.3 summarizes the obtained belief states of the first 10 elements for both cases, the intact and damaged structure. It shows the probability of each element being in any of the

four states (Table 2.1), after having applied the Bayesian updating on the intact structure (for the model tuning) and the damaged structure (at  $t > 0$ ). Each value,  $P(\theta^e = i)$ , is obtained by calculating the integral of the posterior distribution of  $\alpha_e$  over the corresponding subinterval (as defined in table 2.1). The table values are therefore obtained from the posterior PDFs of  $\alpha_e$  (e.g. figures 2.4 and 2.5). For instance, the first value 0.980 means that element 1 has a probability of 0.98 being in state  $\theta^e=1$  (corresponding to a subinterval  $0 < \alpha_e < 0.25$ ).

Table 2.3: Discretized belief states of steel elements 1-10 in the intact and damaged structures.

Element \ $P(\theta^e = i)$	Intact Structure				Damaged Structure			
	$i = 1$	$i = 2$	$i = 3$	$i = 4$	$i = 1$	$i = 2$	$i = 3$	$i = 4$
1	0.980	0.015	0.005	0	0.793	0.2	0	0.007
2	0.999	0.001	0	0	0.8	0.2	0	0
3	0.997	0.002	0.001	0	0.75	0.2	0	0.05
4	0.988	0.005	0.006	0.001	0.793	0.2	0	0.007
5	0.986	0.01	0.003	0.001	0.55	0.15	0	0.3
6	0.989	0.008	0.003	0	0.8	0.2	0	0
7	0.990	0.007	0.002	0.001	0.798	0.2	0.002	0
8	0.988	0.009	0.002	0.001	0.3	0.09	0.01	0.6
9	1	0	0	0	0.8	0.2	0	0
10	1	0	0	0	0.8	0.2	0	0

The updated damaged state of the structural elements showed that the majority of the elements are most probably in a good condition, with probabilities ranging from 0.55 to 0.8 for the state  $\theta^e = 1$ , while element 8 is very damaged with a probability of 0.6 being in the worst state  $\theta^e = 4$ . However, two values are to be considered: the probability of element 5 being in state 4 and the probability of element 8 being in state 1. These two probabilities have the same value, 0.3, which is quite high.

The degradation extent of elements 5 and 8 are presented, respectively, in figures 2.4 and 2.5. For illustration purposes, the degradation extent will be presented using the PDF of the remaining stiffness (relative to the initial stiffness). The most probable degradation extent value is represented by the shift of the curve's peak from the value 1 due to the fact that, in our problem, a degradation is defined by a loss of stiffness. Hence, a relative remaining stiffness equal to 1 means that the element has conserved the integrality of its initial rigidity while a value near 0 means that it has lost all its rigidity. As one can see, the distributions of the damaged elements present two peaks each, around the values 0.2 and 1. For element 5, a higher peak appears near the value 1 while for element 8 a higher peak appears near the value

0.2. If one would only make a judgement based on the highest peak, one can possibly think that element 8 is damaged having lost around 80% of its initial rigidity (state 4) while element 5 is in good condition. However, the presence of a second peak, even with a smaller amplitude, cannot be ignored. It can be therefore confusing to decide whether the elements are damaged or not, especially for element 5. In element 8 damage extent's curve, the highest peak amplitude is much higher than the second one (more than 3 times) while in the case of element 5, the difference between both peaks amplitudes is not very high. This confusion, resulting from the presence of a double peak, is due to the symmetrical position of elements 5 and 8 with respect to the geometry of the structure. These two elements may have a similar effect on certain mode shapes and therefore, in step 2 of the algorithm (section 2.5), two differently generated  $\bar{\alpha}$  might result in very similar mode shapes. An example of such a situation is generating two vectors  $\bar{\alpha}_1$  and  $\bar{\alpha}_2$  representing, 20% rigidity loss in, respectively, element 5 and element 8. According to  $\bar{\alpha}_1$ , all elements are in a good condition except element 5 while according to  $\bar{\alpha}_2$ , all elements are in a good condition except element 8. Both vectors including the same damage extent for two symmetrical elements respectively, they may have very similar effect on certain mode shapes.

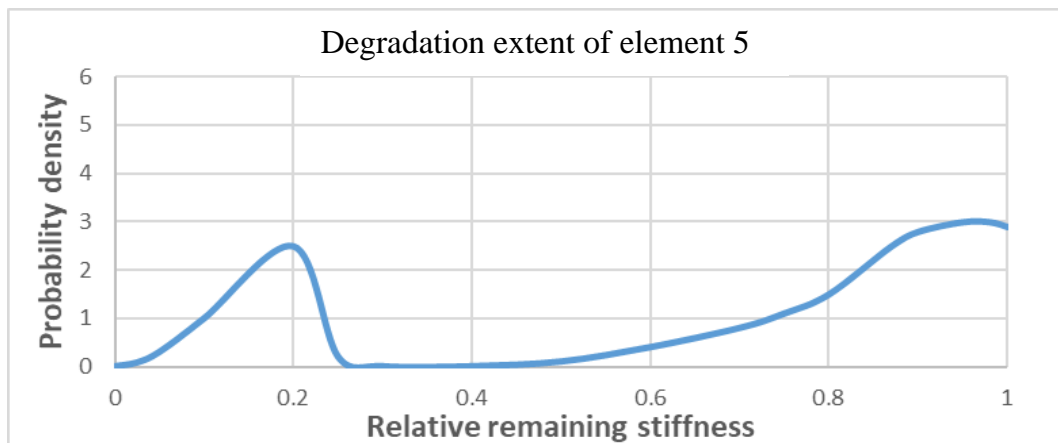


Figure 2.4: Degradation extent of element 5 in the damaged structure.

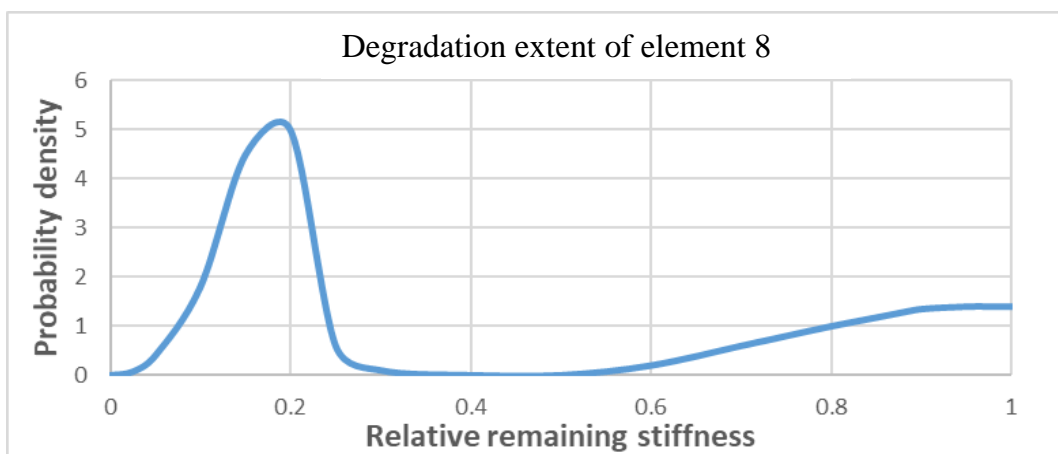


Figure 2.5: Degradation extent of element 8 in the damaged structure.

In order to better analyze the efficiency of the algorithm, the methodology has been applied on the same structure with a measurement error equal to  $0.1 \text{ m/s}^2$ . The posterior PDFs of elements 5 and 8 are shown in figure 2.6. An improvement in the accuracy of the results is noticed. With better measurement precision, one can be almost confident that element 8 is highly damaged (with around 80% deterioration), while elements 5 is in good condition.

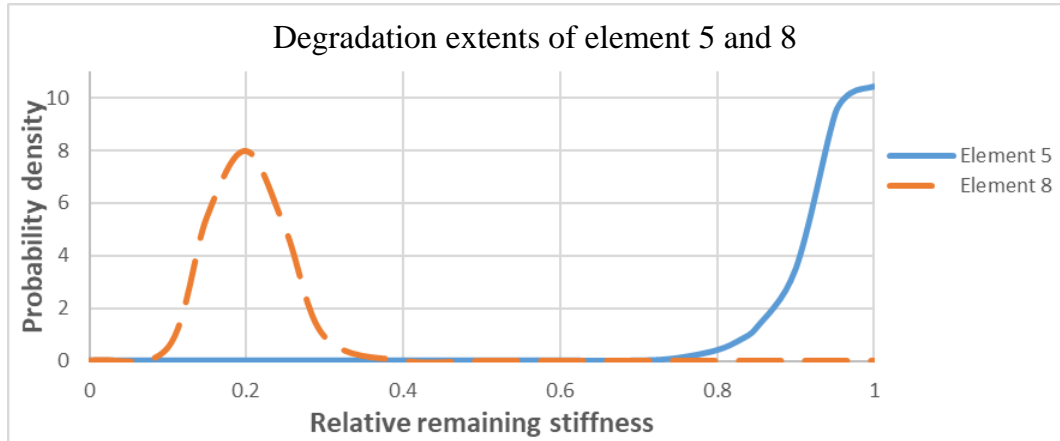


Figure 2.6: Degradation extent of elements 5 and 8 in the damaged structure (measurement error= $0.1 \text{ m/s}^2$ ).

The proposed algorithm was therefore able to detect a damage, locate it, and assess its deterioration extent. However, when the measurement error is relatively high, false peaks might be seen. In our example, even with the presence of a false peak, a significant change is noticed in the degradation extent of element 8, the highest peak being significantly shifted from the value 1. Yet, more serious doubts are raised about the degradation of a healthy element (element 5) being symmetrically positioned to element 8. When measurement precision cannot be enhanced, this shortcoming can be mitigated by a judicious placement of sensors as it will be shown in Chapter 5.

### 2.7.2 Multistory Concrete Frame

The ABC algorithms has also been performed on a 4-story concrete frame structure in order to prove the efficiency of the algorithms on any type of structure. The presented frame is simply supported with 20 elements and 15 nodes (Figure 2.7), thus it includes a total of 39 degrees-of-freedom. It is subjected to unknown ambient excitation. The density and the initial Young's modulus of the concrete elements are evaluated as  $d=2500 \text{ kg/m}^3$  and  $E=33 \text{ GPa}$ , respectively. Columns and beams have rectangular cross-sections with dimensions  $40 \times 60 \text{ cm}$  and  $40 \times 70 \text{ cm}$ , respectively. The beam-to-column connection is supposed to be rigid. The span length is equal to  $6 \text{ m}$  and the height of each level is  $3.5 \text{ m}$ .

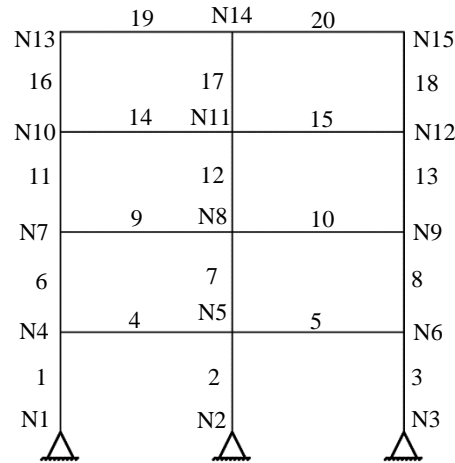


Figure 2.7: Simply supported concrete frame structure.

Unlike truss members, elements of a frame structure are subjected to axial forces and bending moments. Therefore, element degradation is described by a loss of the initial rigidity (axial and flexural rigidity) or in other words by a change of the stiffness matrix of that element. In this numerical application, elements 1 and 10 are considered as damaged with a loss of respectively 40% and 25% of their initial stiffness. A reduction as high as 40% can correspond to an accidental action or, for instance, to the elastic modulus reduction of an old concrete column exposed to fire (Frigui et al. 2018, Bikhiet et al. 2014). The purpose of this study is to evaluate the algorithm's performance in the case of severe and less severe damage. The frame structure is monitored by three horizontal accelerometers on nodes N4 in the first story, N9 in the second story and N13 in the last story. This example aims at finding the damage in elements 1 and 10 by applying the ABC algorithm for a single structure.

The tuning of the model on the initial structure, and the ABC procedure applied on the damaged structure will be done as detailed in the previous numerical application. The results obtained from applying ABC are presented in table 2.4 in the form of updated belief states of the elements for the intact and deteriorated structure. From the modal analysis, all the mode shapes have been taken into account. The first three mode shapes and their identified frequencies are presented in Appendix A for the intact and damaged structure.

As stated in section 2.4, even if the structure is a new one, it is impossible to obtain a deterministic value of the damage extent. However, a range within which the true value is believed to lie is given. As one would expect, the discretized belief states of the elements in the intact structure revealed that all the elements are in very good condition. A very high probability, around 0.99, was found for  $\theta^e = 1$  in the whole structure which shows that any future significant divergence of this value would probably reflect the presence of a damage.



Table 2.4: Discretized belief states of the concrete elements in the intact and damaged structures.

Element \ $P(\theta^e = i)$	Intact Structure				Damaged Structure			
	$i = 1$	$i = 2$	$i = 3$	$i = 4$	$i = 1$	$i = 2$	$i = 3$	$i = 4$
1	0.997	0.003	0	0	0.154	0.80	0.046	0
2	0.989	0.011	0	0	1	0	0	0
3	0.99	0.010	0	0	0.89	0.03	0.08	0
4	0.995	0.005	0	0	1	0	0	0
5	0.964	0.034	0.002	0	0.97	0.03	0	0
6	0.984	0.014	0.002	0	0.96	0.04	0	0
7	0.998	0.002	0	0	0.97	0.03	0	0
8	0.982	0.018	0	0	0.94	0.03	0.03	0
9	0.976	0.013	0.011	0	0.86	0.11	0.03	0
10	0.964	0.033	0.003	0	0.7	0.27	0.03	0
11	0.989	0.011	0	0	1	0	0	0
12	0.997	0.003	0	0	1	0	0	0
13	0.986	0.014	0	0	0.95	0.05	0	0
14	0.982	0.015	0.003	0	1	0	0	0
15	0.985	0.014	0.011	0	1	0	0	0
16	0.999	0.001	0	0	0.97	0	0.03	0
17	0.995	0.005	0	0	1	0	0	0
18	0.995	0.005	0	0	1	0	0	0
19	0.998	0.002	0	0	1	0	0	0
20	0.999	0.001	0	0	1	0	0	0

When running the update on the damaged structure a significant decrease of the probability values was noticed for elements 1 and 10 in the category  $\theta^e = 1$ . For element 1, this diminution was basically compensated by an increase in the probability of this element being in the state  $\theta^e = 2$  from 0.003 to 0.8. That is, the structural performance of element 1 has been reduced by a factor in the range  $[0.25, 0.5]$ . This conclusion meets our expectation since element 1 is supposed to be 40% damaged. Figure 2.8 illustrates the degradation extent of element 1 in the damaged structure. For illustration purposes, the degradation extent will be represented in the following graphs using the PDF of the remaining stiffness (relative to

the initial stiffness). The most probable degradation extent value is represented by the shift of the curve's peak from the value 1 due to the fact that, in our problem, a degradation is defined by a loss of stiffness. Thus, a relative remaining stiffness equal to 1 means that the element has conserved the integrality of its initial rigidity while a value near 0 means that it has lost all its rigidity. As it is shown, the distribution of the degraded element reaches a peak at the value 0.6 and then decreases again which indicates that the element is damaged with a degradation extent equal to 0.4.

For element 10 in its damaged state, a smaller change was observed in the state  $\theta^e = 1$  (a probability decrease from 0.964 to 0.7). However, it was also compensated by the following state  $\theta^e = 2$  where the probability increased from 0.033 to 0.27. These values can be confusing since the difference is neither too small nor too high. According to the belief states of the elements in the damaged structure (Table 2.4), element 10 is probably in good condition yet, the probability of the same element being in the second state is also to be considered. Even if we look at the degradation extent of element 10 in figure 2.9, one can see that the distribution of the degraded element does not present a clear peak. Although its distribution converges to the value 1, it presents almost a high plateau between the relative remaining stiffness's 0.6 and 0.75 which may indicate that this element could be deteriorated and belong to the category  $\theta^e = 2$ . The confusion in this case comes from the fact that element 10 is a beam which may not have a major effect on the structural performance. If a beam is slightly damaged, it will undergo a redistribution of forces and internal stresses and therefore, it might not significantly affect the mode shapes of the structure. It is then harder to detect, in our case, a slight to moderate damage in the beam 10.

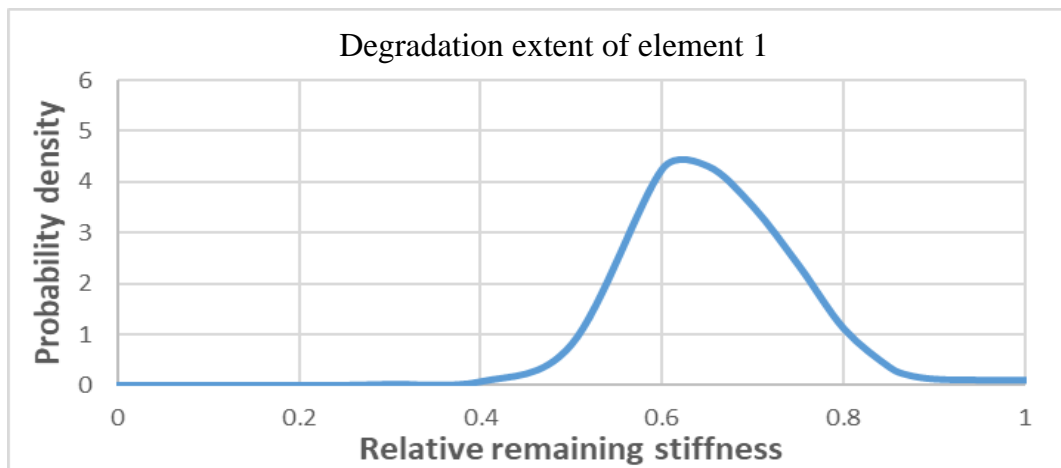


Figure 2.8: Deterioration extent of element 1 in the damaged structure.

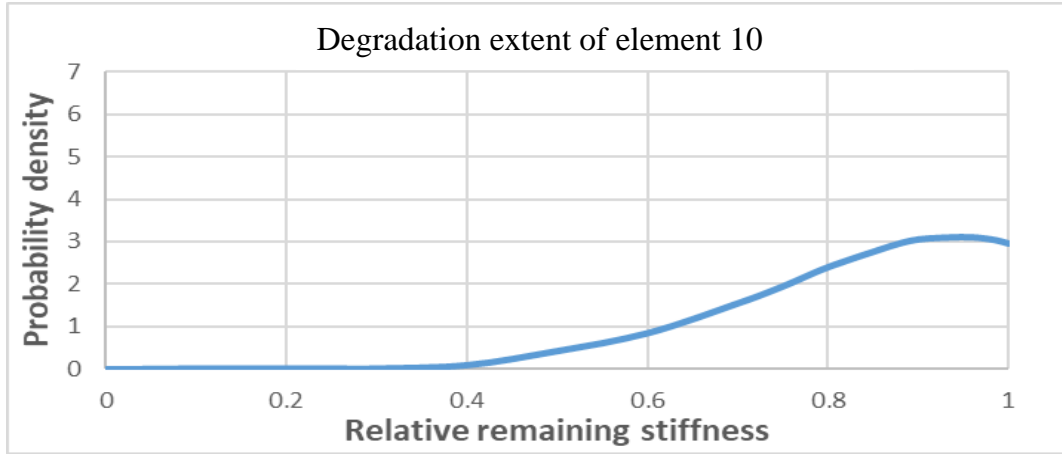


Figure 2.9: Deterioration extent of element 10 in the damaged structure.

As done for the previous example, a case is considered where measurement error  $\varepsilon_{Me}$  is supposed to be equal to  $0.1 \text{ m/s}^2$ . The posterior PDF of element 10, in its damaged state, is shown in figure 2.10. As observed, with a higher measurement precision, the algorithm could accurately detect mild damage in beam 10.

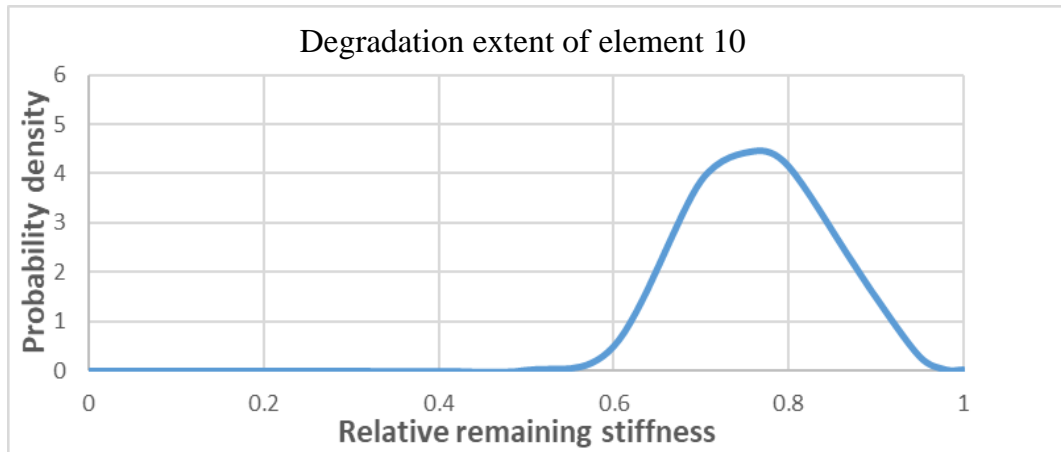


Figure 2.10 Deterioration extent of element 10 in the damaged structures ( $\varepsilon_{Me}=0.1 \text{ m/s}^2$ ).

### 2.7.3 Sensitivity analysis on damage detection

The damage detection performance of an algorithm depends on multiple factors. Among the most important factors are: (i) damage location, (ii) damage extent, (iii) sensor number and (iv) measurement precision.

In order to evaluate the effect of these parameters on the proposed algorithm, a sensitivity analysis is conducted on both numerical applications: (i) Steel truss and (ii) Multistory Concrete Frame. For each application, different parameters combinations have been considered and results have been evaluated according to two measures:

- Mean of the damage extent PDF distribution calculated, for each element, by:

$$Mean(\alpha_e) = \frac{\sum Accepted \alpha_e}{N_{\alpha_e}} \quad (2.27)$$

where  $N_{\alpha_e}$  is the number of accepted  $\alpha_e$  (refer to section 2.5).

- Average Root Mean Square Deviation between the accepted  $\alpha_e$  and the actual damage extent  $\alpha_{e(Actual)}$  on all the elements defined by:

$$Average RMSD = \frac{\sum_{N_e} \sqrt{\frac{1}{N_{\alpha_e}} \sum_{i=1}^{N_{\alpha_e}} (\alpha_{ei} - \alpha_{e(Actual)})^2}}{N_e} \quad (2.28)$$

where  $N_e$  is the number of elements in the structure.

For both applications, the remaining stiffness (quantifying the damage extent) and measurement precision variations have been taken as follows:

- Remaining stiffness (for each element, one at a time): 99% - 95% - 90% - 80% - 50% (corresponding to, respectively, 1%, 5%, 10%, 20% and 50% damage extents);
- Measurement error ( $\varepsilon_{Me}$ ): 0.05 m/s<sup>2</sup> - 0.15 m/s<sup>2</sup>.

### 2.7.3.1 Steel Truss

In the case of the steel truss structure, the remaining parameters variations have been taken as follows:

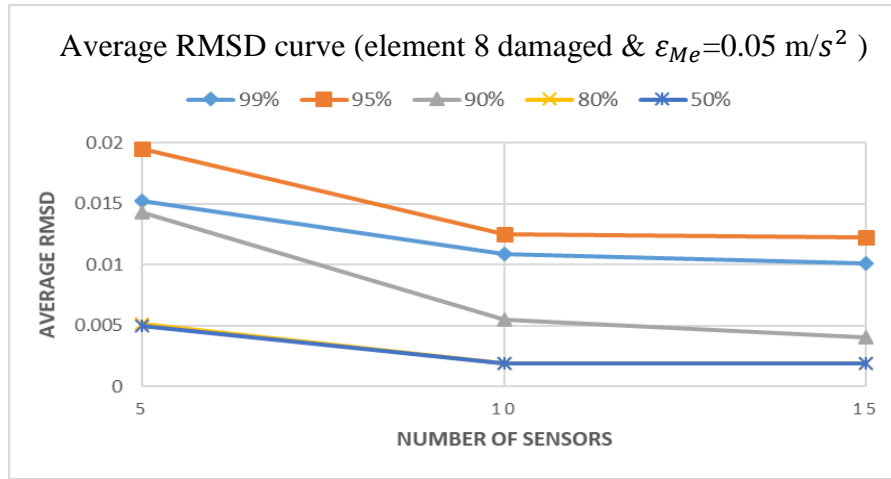
- Damage location: Element 8 – Element 15 – Element 25;
- Sensors number, location (N: Node) and direction (H: Horizontal – V: Vertical):
  - 5 sensors: H: N3 – N6 – N9 - N12 - N17;
  - 10 sensors: H: N3 – N6 – N9 - N12 - N17;  
V: N4 – N7 – N10 – N13 – N18;
  - 15 sensors: H: N3 – N5 – N6 – N8– N9 – N11 - N12 – N14 – N16 - N17;  
V: N4 – N7 – N10 – N13 – N18;

In table 2.5, the means of the damage extent distributions of element 8 and the average RMSD are stated for the different damage extents of element 8 for  $\varepsilon_{Me}=0.05$  m/s<sup>2</sup> and  $\varepsilon_{Me}=0.15$  m/s<sup>2</sup>. The average RMSD curves are illustrated in figures 2.11 a-b for  $\varepsilon_{Me}=0.05$  m/s<sup>2</sup> and  $\varepsilon_{Me}=0.15$  m/s<sup>2</sup>.

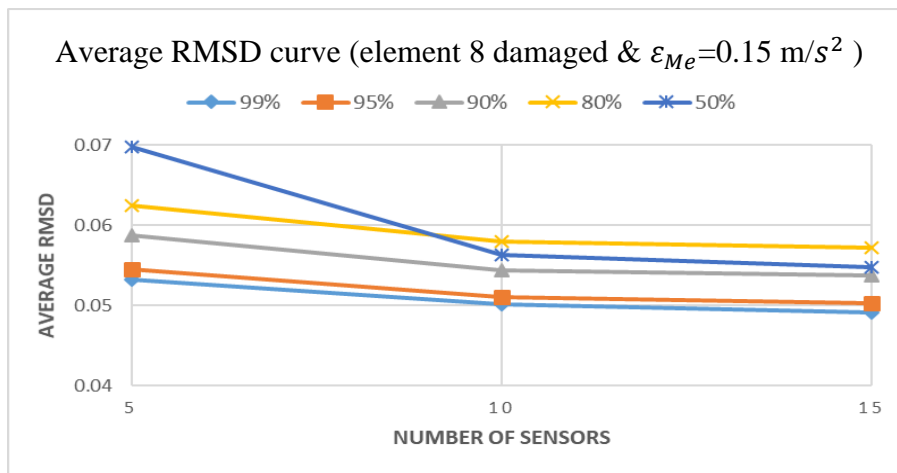
Results for elements 15 and 25 are summarized in Appendix B.

Table 2.5: Mean of the damage extent distributions of element 8 (and average RMSD) for different damage extents, number of sensors, and measurement error  $\epsilon_{Me}$ .

Element 8										
	$\epsilon_{Me} = 0.05 \text{ m/s}^2$					$\epsilon_{Me} = 0.15 \text{ m/s}^2$				
Remaining Stiffness \diagdown	99%	95%	90%	80%	50%	99%	95%	90%	80%	50%
Number of Sensors										
5 sensors	0.995 (0.015)	0.992 (0.019)	0.891 (0.014)	0.797 (0.005)	0.508 (0.005)	0.995 (0.053)	0.993 (0.055)	0.973 (0.059)	0.957 (0.62)	0.528 (0.070)
10 sensors	0.993 (0.011)	0.991 (0.013)	0.892 (0.005)	0.798 (0.002)	0.504 (0.002)	0.995 (0.050)	0.994 (0.051)	0.971 (0.055)	0.945 (0.58)	0.527 (0.056)
15 sensors	0.993 (0.010)	0.991 (0.012)	0.892 (0.004)	0.798 (0.002)	0.504 (0.002)	0.996 (0.049)	0.994 (0.050)	0.971 (0.053)	0.942 (0.57)	0.527 (0.054)



(a)



(b)

Figure 2.11: Average RMSD distribution for the different damage extents in element 8, different sensor numbers (5, 10 and 15) for: (a)  $\epsilon_{Me}=0.05 \text{ m/s}^2$  and (b)  $\epsilon_{Me}=0.15 \text{ m/s}^2$ .

Looking at the results for  $\varepsilon_{Me}=0.05 \text{ m/s}^2$ , one can notice that the proposed algorithm is able to locate and quantify damage with a 10% stiffness reduction or more. In such cases, the mean of the obtained damage extent distribution is very close to the mean of the real damage. For instance, in the case of a 10% damage with 5 implemented sensors, the mean of the obtained distribution is 0.891 whereas the remaining stiffness resulting from the real damage is 0.9. Nevertheless, the mean cannot be the only indicator. A distribution could have a mean close to the actual remaining stiffness and, at the same time, be wide enough to have values very far from the exact one. Hence, it is important to calculate the RMSD between the predicted values and the actual value. This would allow us to understand how far the damage extent distribution reflects the actual damage. For instance, for a damage extent equal to 10% and above in element 8 (i.e. 90%, 80% and 50% remaining stiffness), the maximum average RMSD for that specific element is 0.014. This is an indication that the simulated damage extents values are close to the true value. Yet, 1% and 5% damage (i.e. 99% and 95% remaining stiffness) are hardly detected even for  $\varepsilon_{Me}=0.05 \text{ m/s}^2$ . The reason behind it, is that measured mode shapes are less sensitive to low level damage especially in a noisy environment where it may be hard to distinguish between the noise effect and the slight damage.

As for the case of a measurement error as high as  $\varepsilon_{Me}=0.15 \text{ m/s}^2$ , the high level of uncertainty is reflected on the results. As observed in table 2.5, among the proposed damaged extents, only a 50% damage can be detected with a mean around 0.527 and average RMSD values between 0.054 and 0.070. Yet, even though 10% and 20% damage are not accurately quantified, the corresponding means might be an indication of a damage occurrence. For a healthy element, the mean of the damage extent distribution should be close to 1. Table 2.6 shows the mean of the damage extent distributions of element 8 in its healthy state. Hence, a mean with a value 0.971 (for a 10% damage with 15 sensors) or 0.942 (for a 20% damage with 15 sensors) should raise doubts about the presence of a damage.

Table 2.6: Mean of the damage extent distributions of element 8 in its healthy state, for  $\varepsilon_{Me}=0.15\text{m/s}^2$ .

<b>Element 8</b>	
Number of Sensors	Mean ( $\alpha_e$ )
5 sensors	0.997
10 sensors	0.998
15 sensors	0.998

Similar results were obtained for elements 15 and 25. In terms of RMSD, the evolution of the results accuracy with the number of sensors might differ from an element to another. This is due to the fact that, depending on a damage location and severity, some measurement points might be affected more than others. In addition, in some cases, the mean does not give enough information about the damage extent distribution yet, the distribution itself might give better

information. For instance, for the case of 50% damage in element 15 with 15 sensors, the mean of the damage extent distribution is 0.704. Yet, the mode (highest peak) of the distribution is at 0.5 (Figure 2.12). The difference between the mean and the actual damage value is due to the presence of a double peak in the distribution. Hence, in this case, the algorithm was able to identify the presence of a damage and its most probable severity. But in order to obtain more exact results, one may resort to an inspection for example (as will be seen in Chapter 4) or to a borrowing strength technique (as will be seen in Chapter 3).

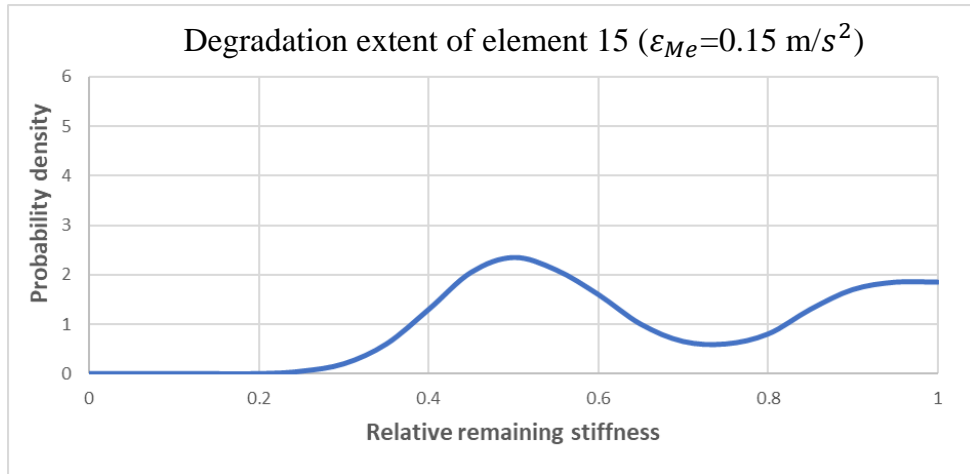


Figure 2.12: Degradation extent of element 15 with 15 sensors ( $\epsilon_{Me}=0.15\text{m/s}^2$ ).

Moreover, it can be noticed that for both measurement errors, the rate of decrease of the average RMSD is slowing as the number of sensor increases. This is due to the increase redundancy in the measurements. However, one can note that the rate of decrease would depend also on the sensors locations. For instance, in figures 2.11 a-b, one can notice that the average RMSD curve is significantly steeper when the number of sensors increases from 5 to 10. This is probably due to the fact that the additional five sensors measured some degrees-of-freedom that were highly affected by the damage. Also, as expected, the average RMSD values considerably increase with the measurement errors. As seen in the above figures, for  $\epsilon_{Me}=0.05\text{m/s}^2$ , the average RMSD values lie between 0.004 and 0.019 while for  $\epsilon_{Me}=0.15\text{m/s}^2$ , they lie between 0.049 and 0.07. Comparing the results obtained for elements 8, 15 and 25 (Appendix B), one can note that the accuracy of quantification depends on the damage location and extent. Therefore, the effect of the sensor number on the damage detection depends on the sensors location and the damage location and extent.

### 2.7.3.2 Multistory Concrete Frame

For the case of the concrete frame structure, the changes in damage location and sensors number are taken as follows:

- Damage location: Element 1 – Element 10 – Element 17;
- Sensors number, location (N: Node) and direction (H: Horizontal – V: Vertical):
  - 1 sensor: H: N9;
  - 3 sensors: H: N4 – N9 - N13;
  - 6 sensors: H: N4 – N9 - N12 – N13  
V: N7 – N13;

Results obtained for element 1 are presented in table 2.7 and figures 2.13 a-b for the different damage extents, sensor number and measurement precision. Table 2.7 resumes the means of the damage extent distributions of element 1 and the average RMSD for  $\varepsilon_{Me}=0.05$  m/s<sup>2</sup> and  $\varepsilon_{Me}=0.15$  m/s<sup>2</sup>. Figures 2.13 a-b represent the average RMSD curves for the same measurement precisions.

Results for element 17 are also presented in table 2.8 (for  $\varepsilon_{Me}=0.05$  m/s<sup>2</sup> and  $\varepsilon_{Me}=0.15$  m/s<sup>2</sup>) and figures 2.14 a-b.

Results for element 10 are presented in Appendix B.

Table 2.7: Mean of the damage extent distributions of element 1 (and average RMSD) for different damage extents, number of sensors, and measurement error.

Element 1										
Remaining Stiffness Number of Sensors	$\varepsilon_{Me}= 0.05\text{m/s}^2$					$\varepsilon_{Me}= 0.15 \text{ m/s}^2$				
	99%	95%	90%	80%	50%	99%	95%	90%	80%	50%
1 sensor	0.994 (0.019)	0.982 (0.023)	0.977 (0.022)	0.969 (0.026)	0.503 (0.010)	0.989 (0.056)	0.986 (0.057)	0.985 (0.058)	0.982 (0.064)	0.615 (0.063)
3 sensors	0.993 (0.010)	0.984 (0.017)	0.962 (0.015)	0.821 (0.019)	0.500 (0.003)	0.995 (0.030)	0.985 (0.031)	0.976 (0.033)	0.912 (0.038)	0.519 (0.030)
6 sensors	0.993 (0.008)	0.973 (0.013)	0.901 (0.012)	0.803 (0.011)	0.500 (0.001)	0.997 (0.025)	0.986 (0.027)	0.969 (0.030)	0.848 (0.033)	0.499 (0.022)

As shown in table 2.7, the sensitivity of the algorithm decreases for small damage extents. However, for such damage, the sensitivity can usually be recovered by adding more sensors. For 10% and 20% damage, results were less exact when using 3 sensors (or less), thus, the additional 3 sensors (for the case of 6 sensors) improved these results. For moderate and severe damage, the mean of the damage extent distribution is very close to the actual one when using 3 sensors (or more). Implementing 1 sensor only lead to accurately quantifying severe damage (50% remaining stiffness). However, the accuracy of the results usually depends on the sensor location. Hence, 1 sensor implemented on another DOF may result in



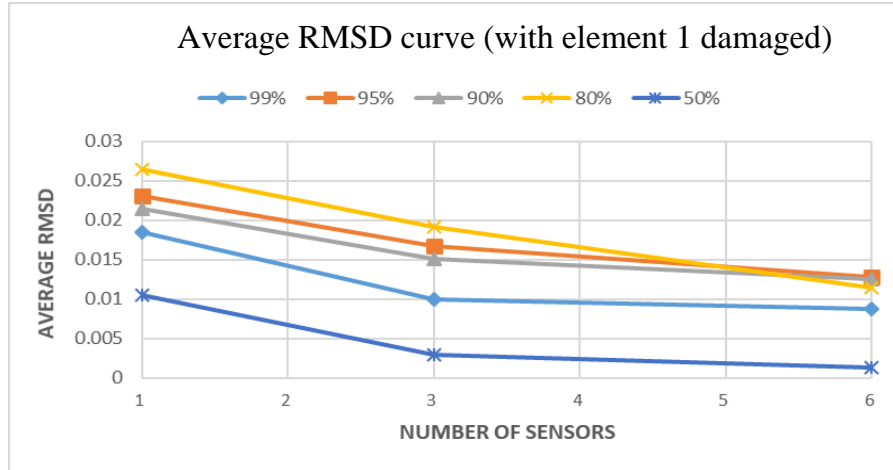
a more precise quantification. The obtained average RMSD values seem also to be low which reflects narrowed distributions and thus, accurate results. As for the case of a 5% damage extent, one could assume that a damage has occurred since the mean values differ from the ones assigned to the distributions of undamaged elements (Table 2.8). In such a case, an exact quantification of the damage might be harder. Yet, when implementing more sensors the mean becomes closer to the actual damage. And as it was the case for the previous example, a 1% damage is hardly detected in the presence of a noisy data.

Looking at the section where  $\varepsilon_{Me}=0.15 \text{ m/s}^2$ , it can be noticed that severe damage (50% deterioration) are detected and well quantified. Yet, when implementing 1 sensor, results are less certain. When the damage is less severe, with 5% to 20% damage extent, the difference between the results of undamaged and damaged elements indicates the presence of a damage (Table 2.8). In the case of 6 implemented sensors or more, the algorithm was able to quantify a 20% damage with a certain level of uncertainty (mean=0.848, average RMSD=0.033). Yet, the quantification of 5% and 10% damage was not accurately given. In such cases, the noise effect was higher than difference in mode shapes. The same case presents itself for a 1% damage.

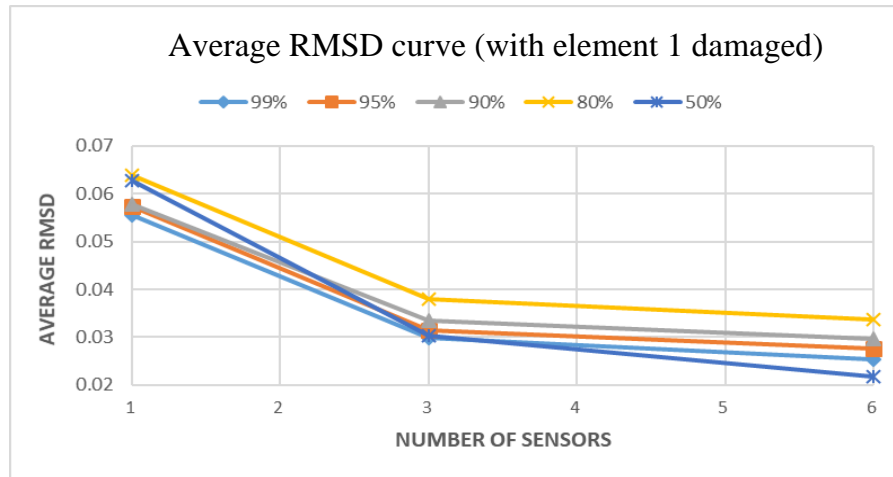
Table 2.8: Mean of the damage extent distributions of element 1 in its healthy state, for  $\varepsilon_{Me}=0.15\text{m/s}^2$ .

<b>Element 1</b>	
Number of Sensors	Mean ( $\alpha_e$ )
1 sensor	0.997
3 sensors	0.998
6 sensors	0.998

Similarly to the previous numerical application, one can notice the effect of the number of sensors on the accuracy of the results in figures 2.13 a-b.



(a)



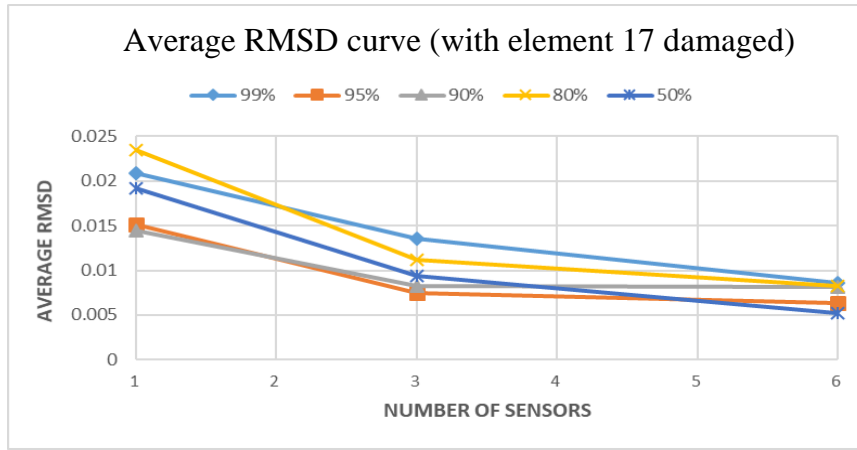
(b)

Figure 2.13: Average RMSD distribution for the different damage extents in element 1, different sensor numbers (1, 3 and 6) and for: (a)  $\epsilon_{Me}=0.05 \text{ m/s}^2$  and (b)  $\epsilon_{Me}=0.15 \text{ m/s}^2$ .

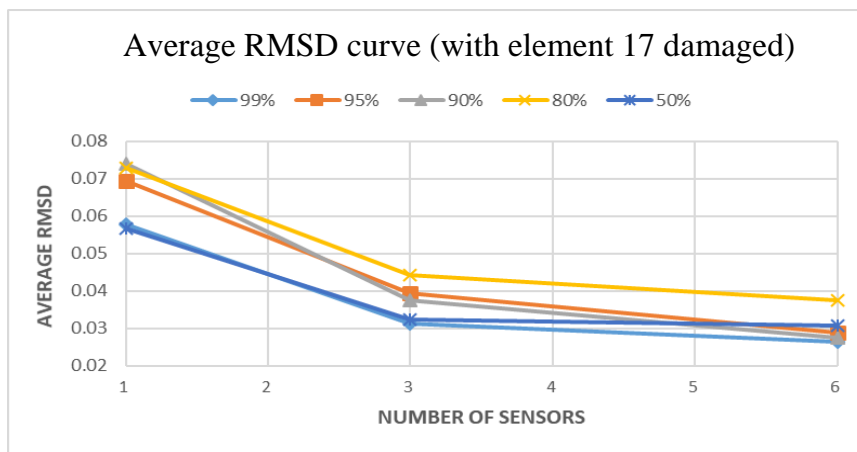
In the previous paragraphs, the sensitivity analysis is presented for element 1. Nevertheless, obtained results could differ depending on the damage location. Table 2.9 and figure 2.14 a-b show the results obtained for element 17. Comparing results for both elements, one can see that slight damage (i.e. 95% remaining stiffness) are better quantified in element 17. For both measurement errors,  $\epsilon_{Me}=0.05 \text{ m/s}^2$  and  $\epsilon_{Me}=0.15 \text{ m/s}^2$ , slight, moderate and severe damage are well quantified even with a small number of sensors. Yet, the difference in the average RMSD values between both cases shows that more exact results are given for  $\epsilon_{Me}=0.05 \text{ m/s}^2$ .

Table 2.9: Mean of the damage extent distributions of element 17 (and average RMSD) for different damage extents, number of sensors, and measurement error.

Element 17										
	$\varepsilon_{Me} = 0.05 \text{ m/s}^2$					$\varepsilon_{Me} = 0.15 \text{ m/s}^2$				
Remaining Stiffness Number of Sensors	99%	95%	90%	80%	50%	99%	95%	90%	80%	50%
1 sensor	0.997 (0.021)	0.935 (0.015)	0.920 (0.014)	0.810 (0.023)	0.503 (0.019)	0.994 (0.058)	0.962 (0.070)	0.932 (0.074)	0.845 (0.073)	0.650 (0.057)
3 sensors	0.998 (0.014)	0.942 (0.007)	0.890 (0.008)	0.802 (0.011)	0.498 (0.009)	0.994 (0.031)	0.923 (0.039)	0.902 (0.038)	0.805 (0.044)	0.552 (0.032)
6 sensors	0.997 (0.008)	0.950 (0.006)	0.892 (0.008)	0.806 (0.008)	0.500 (0.005)	0.994 (0.026)	0.921 (0.029)	0.917 (0.027)	0.781 (0.037)	0.550 (0.030)



(a)



(b)

Figure 2.14: Average RMSD distribution for the different damage extents in element 17, different sensor numbers (1, 3 and 6) and for: (a)  $\varepsilon_{Me} = 0.05 \text{ m/s}^2$  and (b)  $\varepsilon_{Me} = 0.15 \text{ m/s}^2$ .

The proposed methodology is therefore highly sensitive to moderate and severe damage. However, the degree of sensitivity highly depends on the measurement uncertainty and the sensor placement. As for slight damage (e.g. 95% remaining stiffness), results are less accurate depending on the damage location and sensor configuration, however they can be improved by increasing the number of sensors and optimizing their location. Hence, such degradations can be detected when their effect on the mode shapes outweighs the noisy data.

## 2.8 Conclusion

In this chapter, a hierarchical Approximate Bayesian Computation approach is presented for damage detection, localization and quantification using a global permanent SHM system. Starting with a prior distribution of the damage extent of the structural elements, this distribution is updated after observing the structural response.

The advantages of the proposed approach lie in the fact that: (i) it integrates, systematically, all kinds of uncertainties playing a major role in the accuracy of the results; (ii) it does not necessitate an explicit formulation of the likelihood function while applying the Bayesian updating to the structure.

The proposed methodology has been validated through two numerical applications: (i) steel truss and (ii) multistory concrete frame. These applications demonstrated that ABC is able to assess a damage. However, in some cases, slight damage might be hardly detected especially on elements that have low effects on the mode shapes of a structure. The source of this uncertainty stems from the measurement precision and the sensor placement. i.e. using more precise sensors, at their optimal location, will improve detection capability. Nevertheless, such sensors might not be always available or might be very costly. In subsequent chapters, we will develop methodologies to enhance the detection capability by: (i) borrowing strength Bayesian updating, (ii) decision analysis taking into consideration the results of the Bayesian updating and (iii) optimal sensor placement.

## **Chapter 3: Information amplifying by borrowing strength for Structural Health Monitoring**

### **3.1 Introduction**

Devising novel schemes for the optimization of SHM techniques and Inspection, Maintenance and Rehabilitation decision-making has been the focus of relentless research. Interest in these subjects does not appear to be waning despite the abundance of methodologies proposed and the substantial performance improvements. For instance, dependencies in the IM&R optimization of several structures subject to resource constraints is proposed in Faddoul et al. (2013). Lagrangian relaxation technique is used to cancel out the induced dependencies among different structures. Taking account of epistemic uncertainties in partially observable Markov decision process by considering probability distributions of transition matrix is proposed in Faddoul et al. (2015). Faddoul et al. (2013) propose an IM&R methodology integrating Bayesian Networks in partially observable Markov decision process. The aim of the approach is to be able to dynamically take into account information relevant to the deterioration process. Such information could originate from weather conditions, recorded solicitation on the structure and/or observed element condition states on a similar structure. Tran et al. (2016) suggest improved Bayesian Network configurations to identify parameters related to chloride ingress models when inspection data is limited. Their methodology also defines the optimal number of inspection points in depth that minimizes the identification errors and the inspection cost. The evolution of Inspection, Maintenance and Rehabilitation decision-making during the last decades hinged mainly on three main issues, namely: (i) increase the efficiency of the optimization algorithms; (ii) increase the availability of relevant data and (iii) development of new cost effective maintenance and inspection techniques. Hence, one could note that a significant and increasing portion of the specialized literature is devoted to methodologies aiming to improve the optimality of the decision-making process by exploiting as much as possible the available data. Aiming to maximize such an objective is easier said than done. As a matter of fact, increasing the amount and diversifying the types of data used can easily lead to intractable optimization problems. In addition, useful data sources might not be immediately obvious to researchers and decision makers. At one extreme, one could assume that the stochastic deterioration process is independent of any other variable and as such rely entirely on historical recordings of inspections; at the other extreme, every related observable data is taken into account, leading to intractable optimization problems.

In this chapter, a methodology is proposed to improve the information yielded by SHM sensors and/or inspection by applying the Bayesian concept of Borrowing Strength in hierarchical models. Using this approach, information about less monitored elements and/or structures can be extracted from other similar well monitored elements and/or structures. The elements benefiting from borrowing strength can belong to the same or to a different structure.

In the first part of the chapter, the classification scheme of the elements according to their similarity is defined. The methodology is then presented and illustrated by two numerical applications on different types of structures.

### 3.2 Classification Scheme for Elements

Applying the borrowing strength method on certain elements (or structures) requires a certain degree of similarity between these elements (or structures). By similar elements, we denote elements sharing one or several feature values, such as, same material, similar geometry, similar mechanical joints, loads of the same types and order of magnitude, similar environmental conditions, being built by the same contractor or belonging to the same structure, etc. In what follows, a classification scheme is proposed in order to classify elements based on their similarity with respect to a given deterioration mechanism.

The feature vector of an element is defined by  $\bar{f}^e = [f_1^e, \dots, f_i^e, \dots, f_F^e]$  (3.1)

where  $F$  is the total number of relevant features and  $f_i$  a measure of feature  $i$ .

$f_i$  can be taken as: (i) a continuous variable as for example the porosity of a material or the cement content of a reinforced concrete member; (ii) a binary Boolean variable which can for example designate the material from which the element is made or the structural location of the elements in similar structures; (iii) an ordinal integer variable which can for example denote the environmental exposure of the element. Thus, each element belongs essentially to an  $F$  dimensional feature space. Some of the dimensions of that space are not continuous.

A class of elements is considered as the Cartesian product of  $F$  features intervals (one on each dimension):

$$C = \prod_{i=1}^F [f_{i,L_i}, f_{i,U_i}] \quad (3.2)$$

where  $f_{i,L_i}$  and  $f_{i,U_i}$  are respectively the lower and upper endpoints of a subinterval of feature  $f_i$ .

In particular, we consider that for the discrete dimensions, the interval consists of only one point. Elements of the same class can belong to one or several structures. As for the number of hierarchy levels, at one extreme, one might assign a level for each additional relevant feature. In such a case, the ranking of the hierarchy depends on the feature importance. At the other extreme, one might opt for a two-level hierarchy only. In such a case, all features are assumed to have the same importance. The choice on the number of levels depends on the number of available elements to classify and computational complexity.

According to this definition of classes, the degree of similarity between the elements belonging to the same class will be: (i) a monotone decreasing function of the interval length of each dimension; and (ii) a monotone increasing function of the dimensionality  $F$  of the feature space. For each feature added, a smaller nested class is obtained. Hence, by specifying

a particular sequence of features, one defines a hierarchy of element classes. As such, there could be  $F!$  possible sequences. In the proposed methodology, the set of possible sequences are restricted to the ones that represent an increasingly finer classification in terms of similarity of the elements of the same class with respect to a given deterioration mechanism. That is, the classification scheme consists of classifying the elements starting by the most relevant feature (the highest class level), with respect to a given deterioration mechanism, to the least relevant one (the finest/lowest class level). For example, if one considers a section loss due to corrosion, the first feature would be the material type of the element (concrete, steel, timber, glass, etc.), the second one might be the element type (structural, non-structural), the third one the environmental exposure of the element, the fourth one the structure number (structure to which the elements belong), etc. (Figure 3.1). With respect to a section loss due to corrosion, the most relevant feature would be the material type. Concrete, glass and steel elements do not behave the same way with regard to corrosion. Hence, for an adequate sequencing, the highest level would consist of separating elements having different material types. As an example of inappropriate sequencing, consider the environmental exposure as the first feature, the material type as the second feature, etc. In such a case, the outermost class could contain glass as well as concrete elements which do not share similarities with respect to section loss due to corrosion. On the other hand, in our example, the least relevant feature is the structure number to which the elements belong. When dealing with corrosion, it would be more important to classify elements with respect to their environmental exposure. If all elements to be classified belong to the same structure, the environmental exposure class would be the finest class. The higher the class in the hierarchy, the larger it will be and the less specific will be the characterization of the elements belonging to that class.

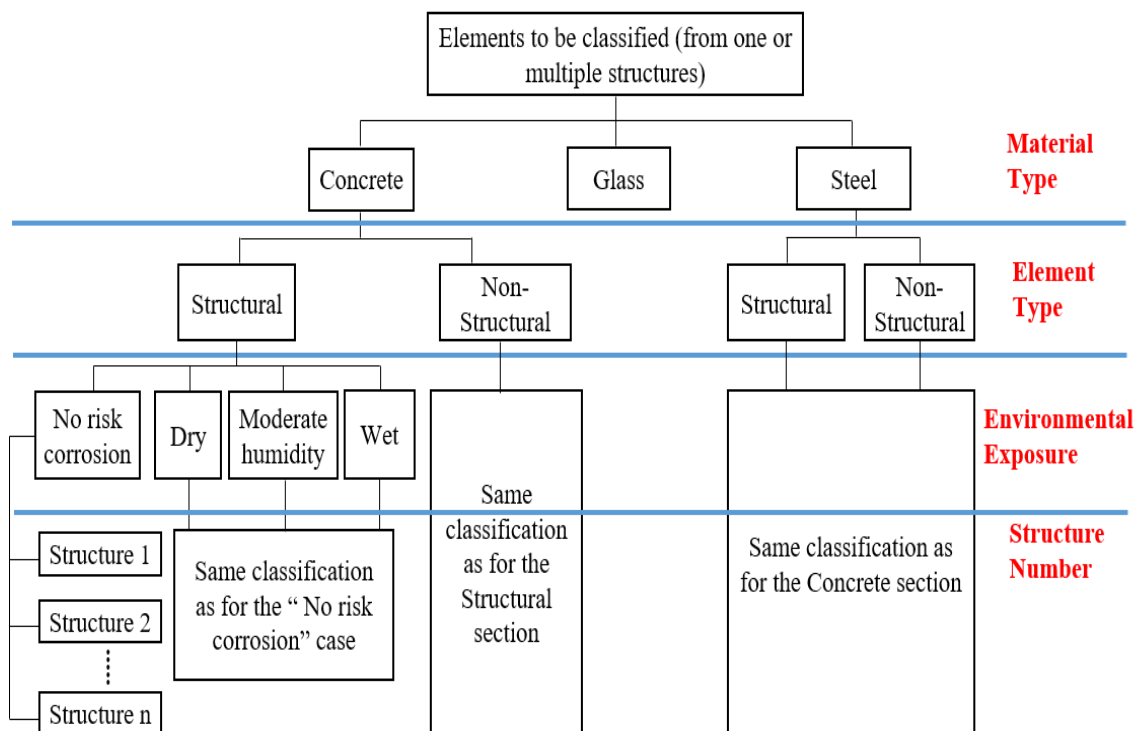


Figure 3.1: Classification scheme of elements with respect to a section loss due to corrosion.

### 3.3 Hierarchical Approximate Bayesian Computation for Borrowing Strength

The aim of the presented methodology is to allow elements and/or structures to be well monitored even if they are subject to a low monitoring effort. This can be done by updating the condition state of a specific element and/or structure using data generated from monitoring similar elements and/or structures belonging to the same class. Classifying similar elements and using a hierarchical Bayesian updating to update the posterior distribution probability of the class parameter and the element degradation rate will: (i) strengthen the degradation assessment of elements and (ii) help in reducing the cost required to monitor multiple elements and/or multiple structures at a time. Without borrowing strength, sensors should be implemented on each structure independently in the case of  $N$  multiple identical structures (e.g. in compounds or schools). In such a case, a highest number of sensors is needed.

We assume that the elements are subject to a deterioration process and that it is reasonable to postulate that the deterioration mechanism, i.e. the deterioration process of an element, is correlated with the element features, thus with that element class. The present chapter uses the ABC framework described in the previous chapter. Hence, we assume that the deterioration of an element is characterized by a change of the mechanical behavior of that element (Chapter 2 section 2.3). If we hypothetically assume that the deterioration process were deterministic and that the monitored structures were identical (including environment and loading conditions), then the estimated belief states of the parameters of such process from a single structure would be identical to those of all elements of the other structures. Hence, in a Structural Health Monitoring (SHM) setting, one would place the sensors of a SHM system on only one structure and be able to identify accurately the condition state of the elements of all the structures (needless to say that such a setting is not realistic). Conversely, if the deterioration process were totally uncertain or the considered structures dissimilar, then the deterioration of the elements of the different structures would be unrelated. In such case, the sensors would have to be distributed among various structures. Moreover, for the case where the structures are exactly similar, the symmetry of the problem implies that the optimal placement of the sensors will be identical for all the structures.

In real world, the deterioration process related to a class of elements is usually not deterministic due to (i) intrinsic uncertainties related to the effect of the material, environment, loading, manufacturing, construction processes, etc.; (ii) dissimilarities between the elements belonging to that class; (iii) statistical uncertainties due to the fact that the estimation of the deterioration process parameters is usually based on estimators calculated from finite size samples. These uncertainties, in addition to other types of uncertainties due to measurement errors and incomplete information are taken into consideration in our methodology as described in chapter 2 section 2.4.

In the classical hierarchical Bayesian modeling, presented in this section, element degradation rate depends on two parameters: one is related to the class (as such represents the



commonality among the elements of that class) and the other is related to the individual element (as such represents the variability of the elements of the same class).

One could reasonably assume that the higher up the class is in the hierarchy defined above, the more uncertain is the deterioration process related to that class. This increase of uncertainty is due to the fact that classes that are high in the hierarchy have fewer defining features, and hence they contain more dissimilar elements. However, as one goes up in the classification hierarchy more elements are included in the estimation process, and hence the statistical uncertainty decreases. Thus, while deciding for the number of features needed to define the classification, an optimal level must be sought. The optimal level corresponds to the minimum of the sum of the two abovementioned uncertainties. The variance of the obtained posterior PDF can be used as an estimate of uncertainties.

In this section, we assume that each of the elements of the structure is unique, in the sense that we do not consider class deterioration rates. The deterioration rate of an element is based on the difference between the posterior PDFs of the deterioration extent  $\alpha_e$  of an element evaluated at two consecutive time points. The deterioration rate  $\beta_e$  of each element is calculated as the increase of  $\alpha_e$  per time unit.

Using the ABC methodology to estimate the deterioration rate of a structural element in a single structure, the posterior PDF of the deterioration rate of an element  $\beta_e$  will be:

$$f(\beta_e | \bar{\lambda}^{Md}, \bar{\Phi}^{Md}) = \frac{f(\bar{\lambda}^{Md}, \bar{\Phi}^{Md} | \beta_e) \times f(\beta_e)}{f(\bar{\lambda}^{Md}, \bar{\Phi}^{Md})} \quad (3.3)$$

where  $f(\beta_e)$  is the prior distribution of the deterioration rate  $\beta_e$  of element  $e$ ,  $f(\beta_e | \bar{\lambda}^{Md}, \bar{\Phi}^{Md})$  is the posterior distribution given the observed data  $\bar{\lambda}^{Md}, \bar{\Phi}^{Md}$  and  $f(\bar{\lambda}^{Md}, \bar{\Phi}^{Md} | \beta_e)$  is the likelihood function.

One of the main advantages of Bayesian updating is the possibility of using knowledge about the parameter that is being inferred on to augment the information stemming from the observed data. This knowledge may originate from different sources and may have different formats. For example, useful information relevant to the deterioration rate of an element might be: (i) the condition of the elements during previous inspections/evaluations; (ii) the deterioration rate of similar elements; i.e. elements belonging to the same class; (iii) expert estimation of the impact of environmental conditions on the deterioration rate; etc. In the Bayesian paradigm, this variety of information is accounted for via two main mechanisms, namely, prior PDFs for the unknown parameters and hierarchical modeling. While prior PDF allows the use of available information about an uncertain parameter  $\beta_i$  besides the observed data, hierarchical modeling allows the use of information about related parameters  $\beta_{j \neq i}$  to infer on the posterior PDF of  $\beta_i$ . This flow of information from the parameters  $\beta_{j \neq i}$  to the parameter  $\beta_i$  is often denoted ‘‘Borrowing Strength’’ in the Bayesian literature. For example, suppose that while there are no observations available for the deterioration rate of a given structural element, some observations are available for a similar element. Using the fact that the deterioration rates of the two elements are linked hierarchically via the parent class

parameter, one can infer about the deterioration rate of the first element given observations related to the second element. This concept can be considered as a particular case of the Bayesian Network where each node can have at most one parent node (Imounga et al. 2020, Tran et al. 2018).

In this scheme, we use a hierarchical Bayesian modeling for the deterioration rate  $\beta_c^e$ . The stochastic information related to the deterioration rate is split into two levels, namely element level and class level.

The posterior probability distribution in a hierarchical scheme will be:

$$f(\beta_c^e, \beta_c | \bar{\lambda}^{Md}, \bar{\Phi}^{Md}) = \frac{f(\bar{\lambda}^{Md}, \bar{\Phi}^{Md} | \beta_c^e, \beta_c) \times f(\beta_c^e | \beta_c) \times f(\beta_c)}{f(\bar{\lambda}^{Md}, \bar{\Phi}^{Md})} \quad (3.4)$$

where  $(\bar{\lambda}^{Md}, \bar{\Phi}^{Md})$  is the measured structural response of the damaged structure,  $\beta_c^e$  is the deterioration rate of element  $e$ , and  $\beta_c$  is a class parameter upon which  $\beta_c^e$  is stochastically dependent. A frequently used hierarchical scheme would be to assume that the higher level parameter ( $\beta_c$  in our case) is the expected value of the PDF from which the lower level parameters (in our case, the deterioration rates  $\beta_c^e$ , related to each element), are sampled. In this scheme,  $\beta_c$  is a random variable having a PDF.

The proposed approach is a Hierarchical Bayesian Approximate Computing (HABC) method (Turner and Van Zandt 2014). HABC is the implementation of the ABC method in a hierarchical model where parameters are structured into different dependent levels. The relationship between the parameters in multiple levels is given by a conditional probability distribution. An example of such a relationship is given in Chapter 2, Equations (2.20 a-c). Hierarchical Bayesian modelling is a statistical method used for parameter estimation and which allows the combination of information coming from different sources. For instance, suppose we have  $(L_1, L_2, \dots, L_N)$  sets of observations  $y$  about a structure for the  $N$  different ambient conditions. In each ambient condition, the structure has a different PDF of the degradation rate  $\beta_i$ . However, it is assumed that all distributions, related to the  $N$  conditions, arise from a common distribution of their mean  $\mu(\beta)$ . One might be interested in the variability in the different degradation rates  $\beta_i$  and in the posterior distribution of the mean  $\mu$ . Hence, in this case, the hierarchical Bayesian modelling is structured as shown in figure 3.2, and the posterior distribution for the unknown parameters would be:

$$f(\mu(\beta), \beta | y) \propto f(y | \beta, \mu(\beta)) f(\beta | \mu(\beta)) f(\mu(\beta)) \quad (3.5)$$

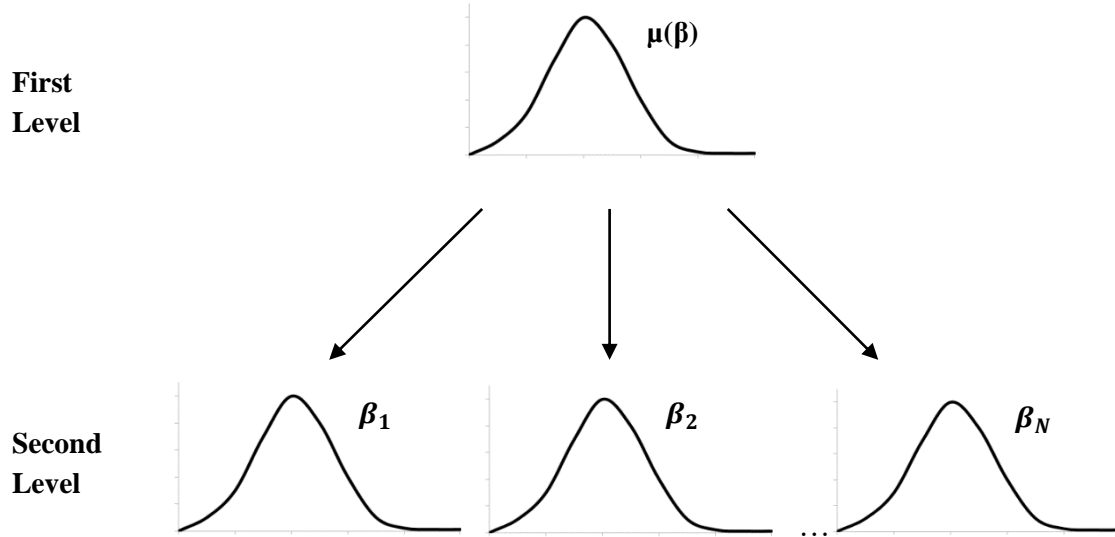


Figure 3.2: Example of a Hierarchical Bayesian Modelling representation.

In this chapter, we propose a HABC method to update the condition state of multiple similar elements simultaneously. These elements could belong to one or multiple structures. The steps of the proposed HABC are as follows (Figure 3.3):

- 1- Classify the elements of the structures according to a feature set as discussed in section 3.2;
- 2- For each class of elements, postulate a prior probability distribution for a parameter  $\beta_c$ ;
- 3- For each element in each of the structures, assume a parametrized prior PDF of the degradation rate  $\beta_c^e$  depending on  $\beta_c$  and based on prior inspections and/or SHM evaluations;
- 4- From each class of elements C:
  - a. Draw a random value for  $\beta_c$  from the prior distribution defined in step 2;
  - b. For each structure and for each element  $e$  belonging to class C, draw a random value for the degradation rate  $\beta_c^e$  from the probability distribution defined in step 3 and based on the value of  $\beta_c$  drawn in step a;
  - c. Using the values  $\beta_c^e$  generated in b, calculate, for each structure, the distance  $\rho_s$  between the observed structural response and the simulated one as defined in Eq. (2.22) (refer to Chapter 2).
- 5- Accept  $\beta_c$  and  $\beta_c^e$  ( $1 \leq e \leq N$ ) with probability equal to  $\psi(\rho_1, \dots, \rho_s, \dots, \rho_{NS})$ , where  $\psi$  is a monotonic decreasing kernel function of  $\rho_s$  and  $NS$  represents the number of structures.
- 6- Using the accepted values  $\beta_c$  and  $\beta_c^e$  ( $1 \leq e \leq N$ ), define the posterior distribution of the deterioration rates  $f(\beta_c, \beta_c^e (1 \leq e \leq N) | \bar{\lambda}^{Md}, \bar{\Phi}^{Md})$ .

As stated in chapter 2, the main power of ABC algorithms lies in the fact that no constraints are imposed on the form of the prior, likelihood function or posterior. Prior and

likelihood functions not even need to have an analytical mathematical expression. Priors can be simulated by some sampling mechanism and likelihood functions can be simulated by any model or algorithm simulating data based on sampled parameters from the prior. This modeling flexibility ensures that a wider range of problems can be solved by ABC, and most importantly, better optimal solutions are achieved by not imposing artificial modeling constraints just to ensure the computability of the Bayesian approach.

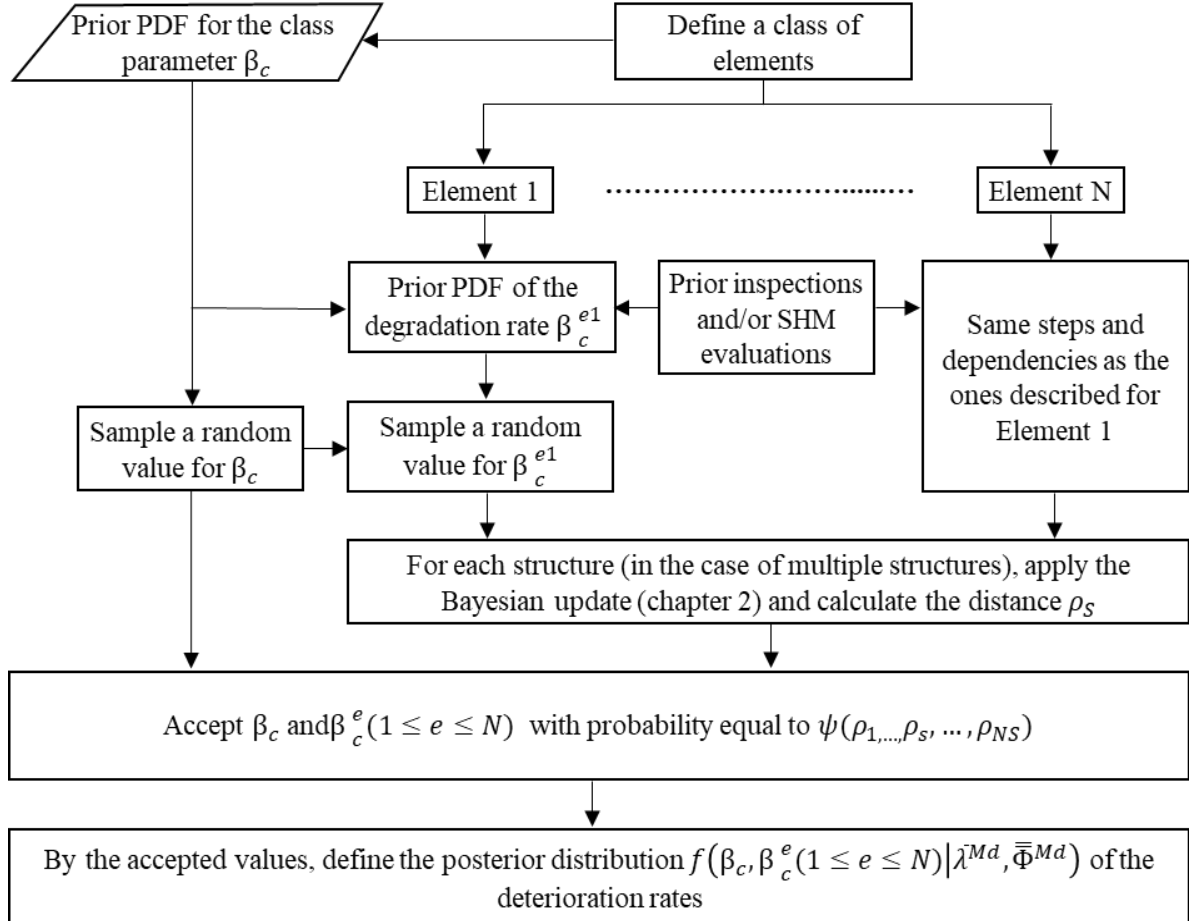


Figure 3.3: Flowchart of the HABC method for SHM problems.

### 3.4 Numerical Applications

Two numerical applications are considered hereafter to evaluate the performance of the proposed HABC methodology. The first example aims at detecting, simultaneously, damage in similar elements belonging to four similar steel truss structures. In the second example, the similar elements for which the deterioration rates are to be determined belong to the same concrete frame structure (in contrast to the first example where the class contains elements from different structures). The applications are chosen to have different types of structures and types of classes in order to show the applicability of the methodology in different situations.

As mentioned in Chapter 2, the continuous damage space  $[0, 1]$  of each element is discretized into four ordinal states  $\{1, 2, 3, 4\}$  (Table 2.1).

The measured and simulated structural responses are given by FEM algorithms so the real existing structure is modelled by a FEM, and a measurement error is added to the obtained structural response in order to simulate the reality.

In order to simplify the presentation, we assume (without loss of generality), in the following applications, that the initial state (at time  $t_0 = 0$ ) of the structure is free of defects. Consequently, the degradation rate of an element between  $t_0$  and  $t_1$  could be considered as the degradation extent of the element during this period of time. Hence, it is assumed that  $\beta_c^e = \alpha_c^e$ .

The degradation extent  $\alpha_c^e$  of elements belonging to a specific class  $C$  is defined using a multiplicative model as follows:

$$\alpha_c^e = \alpha_e \times \alpha_c \quad (3.6)$$

where  $\alpha_e$  and  $\alpha_c$  are respectively, the degradation extent of element  $e$  and a class dependent multiplicative factor. The prior of these variables is usually based on prior inspections and/or SHM evaluations.

We consider, without loss of generality, a non-informative prior probability distribution for the deterioration extent  $\alpha_e$  of the elements and the class parameter  $\alpha_c$  represented by a uniform distribution since no previous information about the structure is provided. The measurement error is assumed to be a uniform random variable with zero mean and a range equal to  $0.15 \text{ m/s}^2$  (Sharp and Yu, 2019).

### 3.4.1 Four Steel Truss Structures

Consider the case of four similar hinged steel truss structures, sharing the same geometry, element sections and material properties. Each one of them is modelled by a simply supported plane structure, the same as the one described in the numerical application in Chapter 2 (section 2.7.1). The structures are monitored by twelve accelerometers as follows:

- Structure A: two horizontal accelerometers on nodes N3 and N17 and three vertical accelerometers on nodes N4, N7 and N10 (Figure 3.4a);
- Structure B: three horizontal accelerometers on nodes N5, N11 and N19 (Figure 3.4b);
- Structure C: one horizontal accelerometer on node N17 and two vertical accelerometers on nodes N4 and N10 (Figure 3.4c);
- Structure D: three horizontal accelerometers on nodes N6, N12 and N17 (Figure 3.4d);

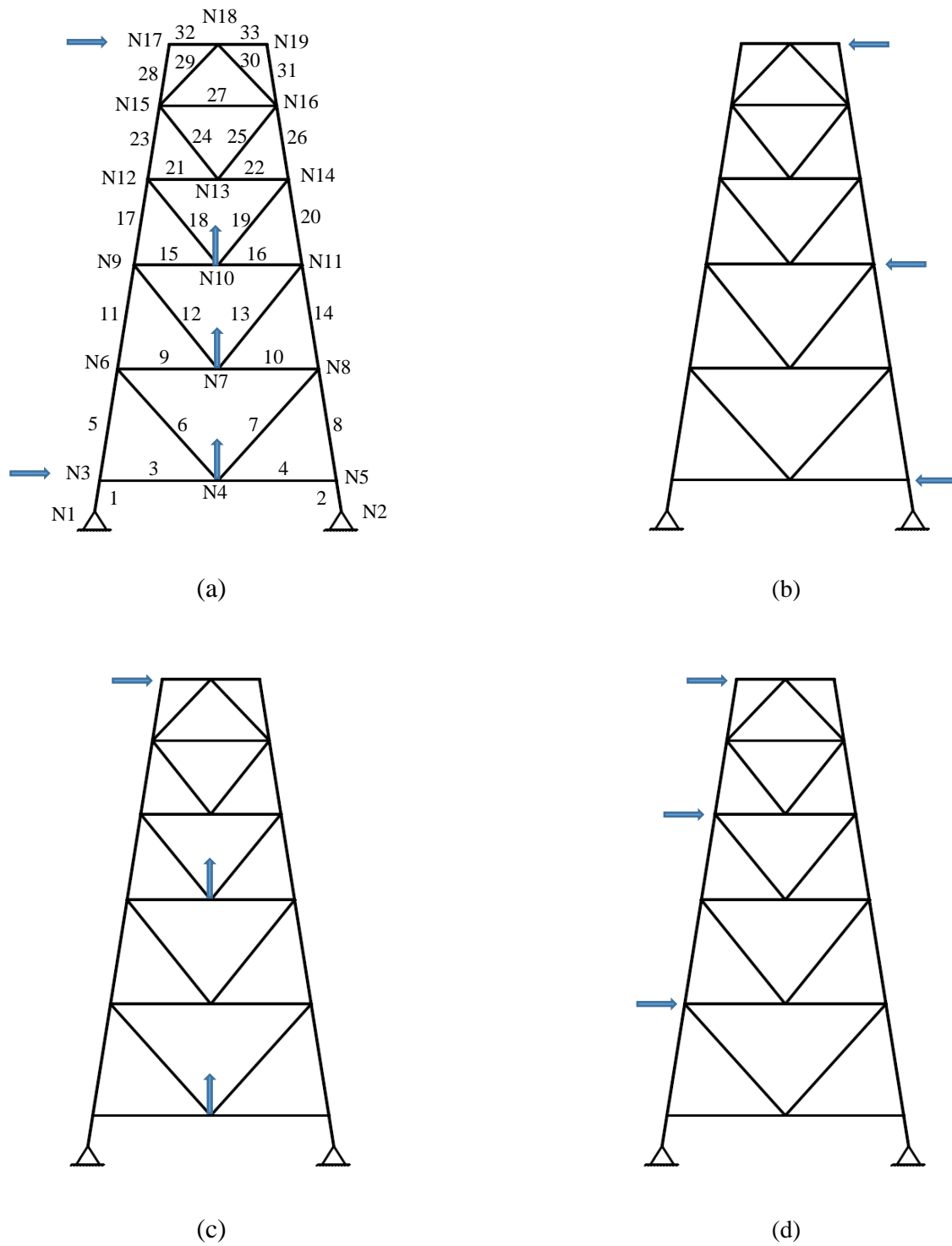


Figure 3.4 Simply supported steel truss structures: (a) structure A, (b) structure B, (c) structure C and (d) structure D.

For illustration purposes, the accelerometers have been implemented based on an engineering judgement. More accelerometers have been chosen for a structure in order to have more information about it and allow an information flow from a structure to less monitored ones. Different locations and measurement directions were chosen for the four structures except for the highest level where an accelerometer is implemented for all the structures. The reason behind is that, due to vibrations, the largest movements appear on the top of the structure. Hence, a sensor implemented on the top of the structure can more easily detect movements (due to a higher signal-to-noise ratio) which can be due to a defect in the structure.

The objective of this numerical application is to update the condition state of each of the elements in the structures by taking information from data yielded by all the accelerometers distributed on the four structures. Since the structures behave as truss systems, only the axial stiffness is considered in this study and therefore, a damage is defined by a loss of the axial stiffness. In this example, it is assumed that the four structures are subjected to the same loads and environmental conditions. If these conditions differed between the structures, results would be negatively affected to a certain extent.

It is assumed that, in the first three structures, element 8 is 50% deteriorated. In the fourth structure, element 8 has lost 80% of its initial rigidity due to accidental actions or fatigue loading, which means that its remaining axial stiffness represents 20% of its initial total stiffness. However, the damage have not been detected yet. In our case, and as a simplification, we neglect the overall buckling of compressed members. From the modal analysis, the first three mode shapes and their identified frequencies are presented in Appendix A for the intact and damaged structure.

The reference state of the structures, from which any future deviation is considered as an additional damage, is assumed to be an intact state (i.e. a newly constructed structure).

Since all the structures are similar with respect to the elements properties (material, section properties and deterioration mechanism), the geometry and the loading, all these features in addition to the element location are combined to define the class of elements. In this example, elements are classified according to their location in the structure. For instance, all elements located between nodes N5 and N8 in the four structures belong to the same class.

Even though the initial structure is an intact one, the modelled structural response of the initial structure does not exactly reflect the measured one so the results are affected by uncertainties such as model uncertainties, numerical approximations, geometric imperfections, parameter's uncertainties, incomplete data, etc. Hence, the HABC is first applied on the structures in their initial state as a model tuning. Data coming from newly implemented sensors, on the different structures, will be used simultaneously (as described in section 3.3) to update the prior distributions of  $\alpha_c$  and  $\alpha_e$  of the four similar elements. The resulting PDFs will be used then as prior distributions of  $\alpha_c$  and  $\alpha_e$ , when applying the HABC method, for future damage assessment.

Figures 3.5 illustrates the posterior distributions of the damage extents of element 8,  $\alpha_c^{e8}$ , in the four structures .

For illustration purposes, the degradation extent will be represented in the following graphs using the PDF of the remaining stiffness (relative to the initial stiffness). The most probable degradation extent value is represented by the shift of the curve's peak from the value 1 as degradation is defined by loss of stiffness. In these figures, a value equal to 1 means that the element has conserved the integrity of its initial rigidity while a value near 0 means that it has lost all its rigidity.

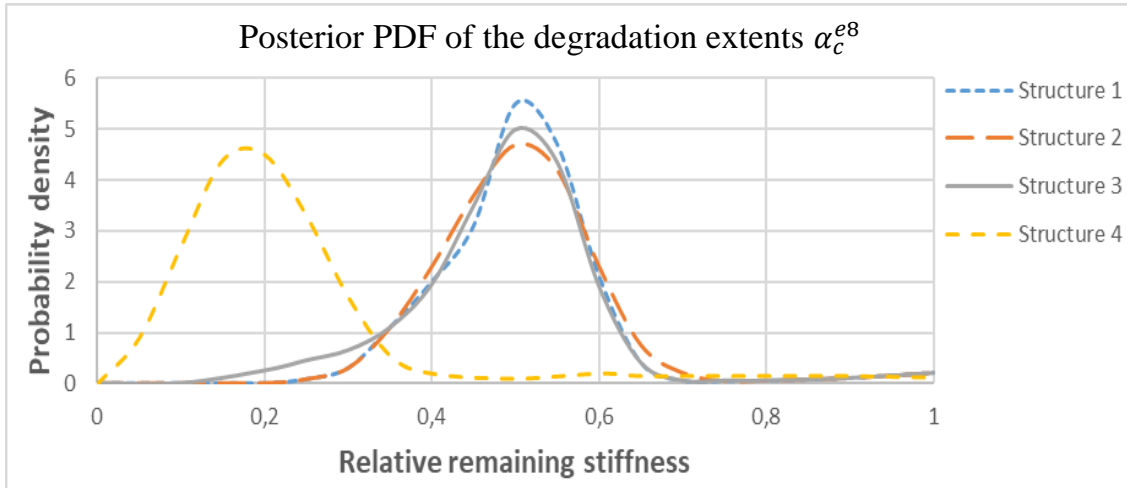


Figure 3.5: Posterior PDF of the degradation extents  $\alpha_c^{e8}$  of elements 8 for different damage states in four similar structures.

In reality, the damage is unknown and the posterior PDF should indicate the presence of a damage. It is herein assumed that, in order to obtain accurate results about the degradation extent of elements belonging to the same class, these elements should present similar deterioration process.

As one can see in figure 3.5, the PDF of the remaining stiffness of element 8 is significantly shifted from 1 for all structures. For structures 1 to 3, the peaks have shifted toward 0.5 while for structure 4 the peak is located around 0.18. This indicates that elements located between N5 and N8 have undergone almost the same deterioration extent (around 50% deterioration) in structures 1 to 3, while in structure 4, element 8 seems to be more seriously damaged having lost around 82% of its initial stiffness. These curves have accurately reflected the hypothesis taken which meets our expectations. However, in order to further explore the efficiency of the presented methodology, the obtained curves have been compared to the curves of the PDF of element 8 when updating each structure alone according to the sensors implemented on it exclusively.

These curves are represented in figures 3.6 to 3.9 which illustrate the degradation extent  $\alpha_c^{e8}$  of element 8, in structures 1 to 4 respectively, in two cases: (i) sensors implemented on each structure independently; (ii) sensors implemented according to HABC methodology for information amplifying.



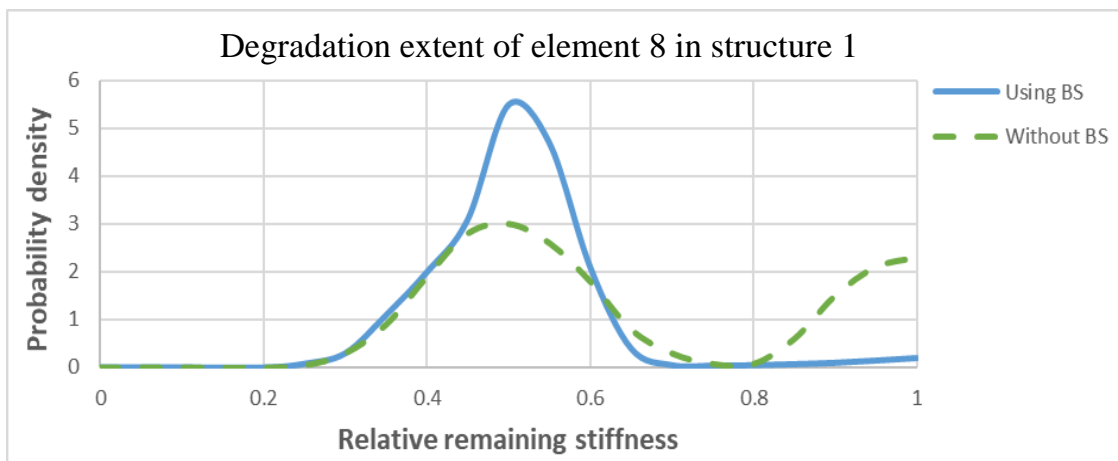


Figure 3.6: Degradation extent of element 8 in the first structure without and with HABC for borrowing strength (BS) method.

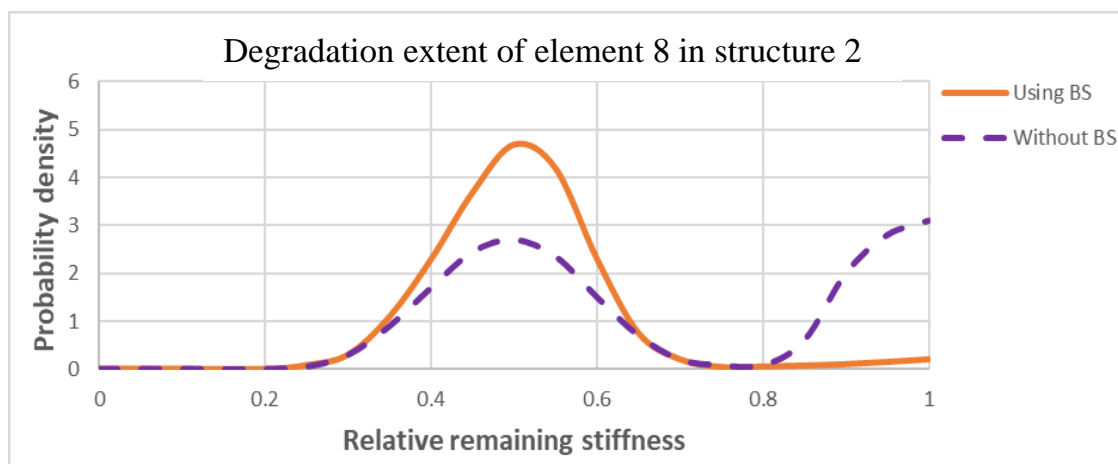


Figure 3.7: Degradation extent of element 8 in the second structure without and with HABC for borrowing strength (BS) method.

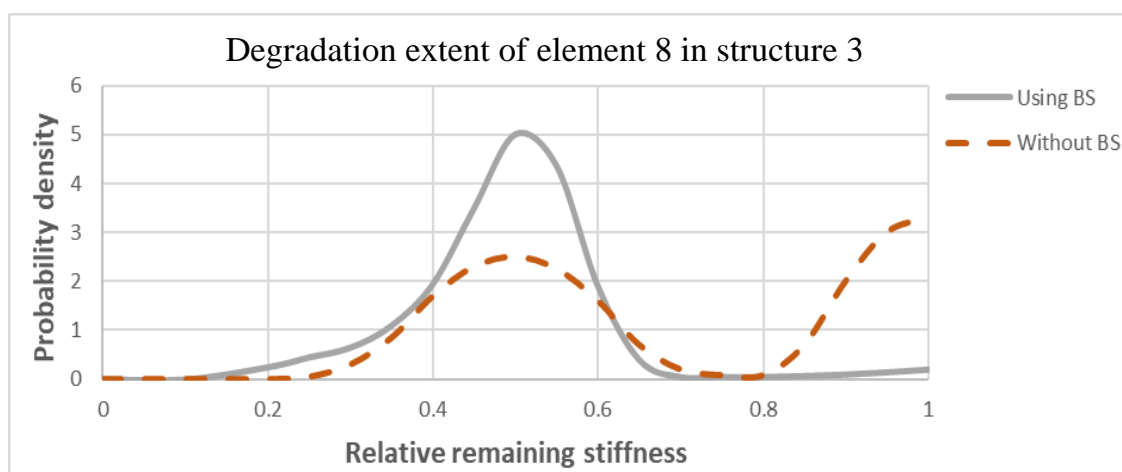


Figure 3.8: Degradation extent of element 8 in the third structure without and with HABC for borrowing strength (BS) method.

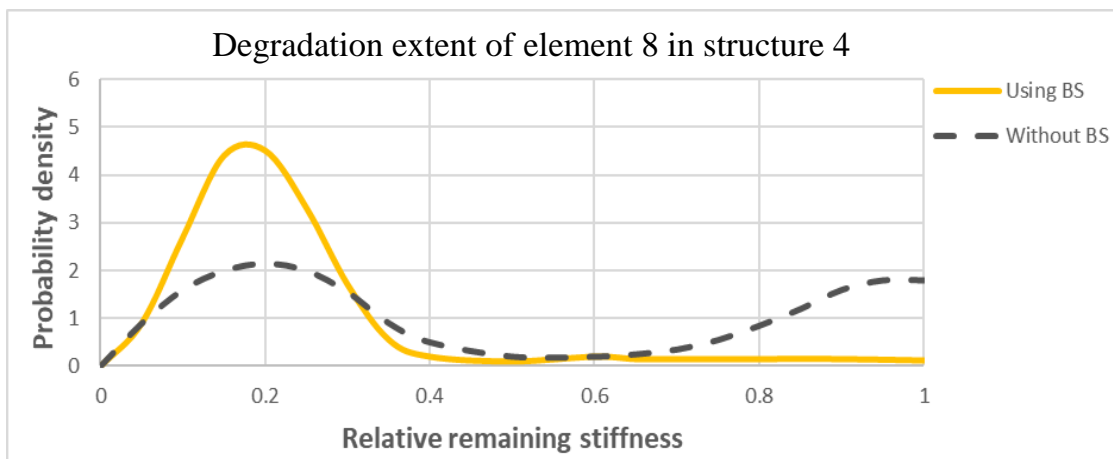
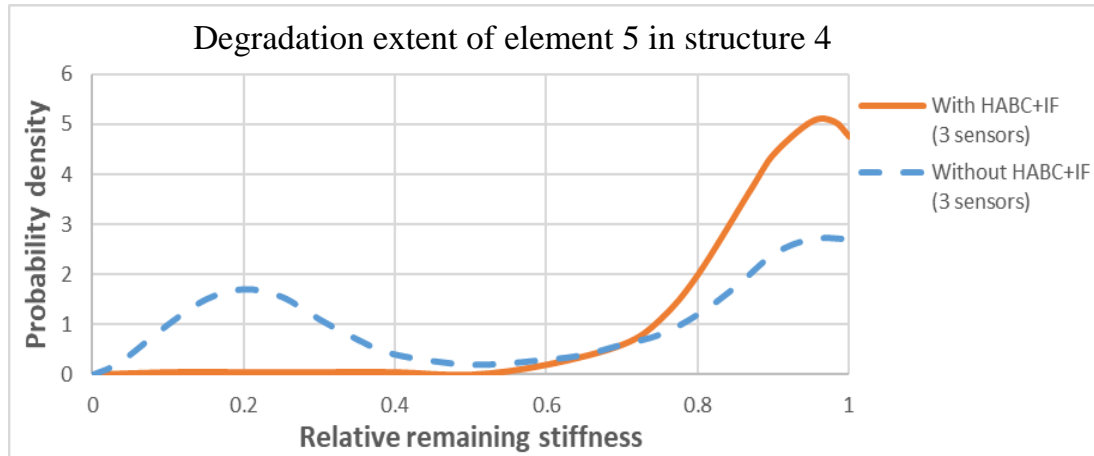


Figure 3.9: Degradation extent of element 8 in the fourth structure without and with HABC for borrowing strength (BS) method.

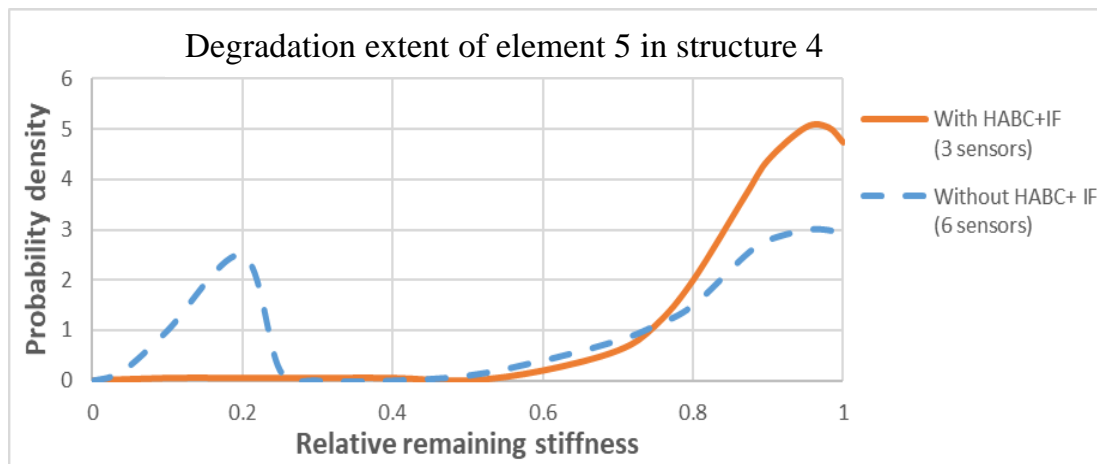
As it can be noticed, when each structure is updated independently, the condition state of element 8 cannot be precisely determined. In this case, the PDFs of element 8 present two peaks in each of the four structures. In the first three structures, the two peaks appear around 0.5 and 1, while in the fourth structure a peak appears around 0.2 and another one around 0.95. Even in the case where 5 sensors have been implemented on structure 1, one could not judge whether element 8 is in a good condition or not, even though a higher peak appears around 0.5. This is due to the symmetry between elements 5 and 8 which leads to a similar effect on some mode shapes and therefore, one can be lost concerning the states of elements 5 and 8. However, when the HABC method is applied, the classification of the elements according to which the elements have been updated has played a major role in giving more certain information about the condition state of element 8 in the four structures. Looking at the PDF curves resulting from the HABC, one can clearly see that element 8 is 50% damaged in the first three structures and 82% damaged in the fourth structure. Comparing these curves in both situations (without and with HABC), one can conclude that distributing the sensors in the case of similar structures and using the HABC by gathering information from multiple similar structures masked the symmetry effect which resulted in more specific distributions and in a better judgment concerning the states of the elements.

The interest of using the proposed methodology appears moreover in figure 3.10. After having obtained the degradation extent  $\alpha_c^{e8}$  of element 8 in each structure, one can take advantage of this information in order to update the condition state of other elements belonging to the same structure and obtain more precise information about it. The phenomenon of information flow from an element belonging to a certain class, to elements which do not belong to its class will be dealt in depth in the next chapter. Two examples of the HABC followed by the information flow are given in figures 3.10 a-b. Figure 3.10a illustrates the degradation extent of element 5 in structure 4, using 3 sensors, in two cases: (i) element updating according to sensors implemented on structure 4 only without taking into consideration the similarity; (ii) considering degradation extent  $\alpha_c^{e8}$  of element 8 and then updating the condition state of the other elements using the information flow concept. Figure

3.10b illustrates the degradation extent of element 5 in structure 4 using the same cases as figure 3.10a but with 6 sensors in case (i) and 3 sensors in case (ii). Comparing the PDF of element 5 in structure 4 in both cases and both situations (Figures 3.10a and 3.10b), it can be shown that using the borrowing strength HABC has led to more exact results. When updating structure 4 without taking into account the similarity between structures, doubts are raised concerning the deterioration of elements 5. This is due to the symmetry effect as it was explained in the previous paragraph. The probability of element 5 being in states  $\theta^e = 4$  is quite high. However, when using the similarity between multiple structures and information flow, the condition state of element 5 has been more precisely determined even when using less sensors on the structure (Figure 3.10b). Using 3 sensors on structure 4 with the HABC method has given more information than using 6 sensors and updating structure 4 independently of the other structures. As one can see in figure 3.10, the HABC method followed by information flow phenomenon has made it clear that element 5 is in a good condition (its curve presenting a peak around 0.95). Hence, the importance of the HABC method which affects, not only the elements belonging to the class, but also helps in reducing the uncertainty about other elements belonging to the structures.



(a)



(b)

Figure 3.10: Degradation extent of element 5 in structure 4 without and with HABC and information flow (IF): (a) using 3 sensors in both cases, (b) using 6 sensors without HABC+IF and 3 sensors with HABC+IF.

### 3.4.2 Multistory Concrete Frame

This application aims at assessing the degradation extent of the structural elements of a 4-story concrete frame structure using the HABC method (Figure 3.11). Unlike the previous numerical application where similar elements belong to different structures, this application considers the case of similar elements within the same structure. We consider the case of the same simply supported frame structure as the one described in Chapter 2, section 2.7.2. The structure is monitored by three horizontal accelerometers on nodes N4 in the first story, N9 in the second story and N13 in the top story.

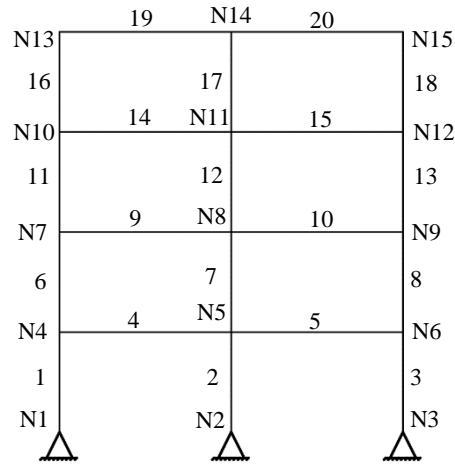


Figure 3.11: Simply supported concrete frame structure.

In this example, the deterioration of an element is represented by a loss of axial and flexural rigidities. In the damaged state of the structure, element 1 is assumed to have lost 40% of its initial stiffness (axial and flexural stiffness) and elements 4, 9 and 14 are assumed to have lost around 25% of their initial total stiffness each (axial and flexural stiffness).

The tuning of the model on the initial structure, and the HABC procedure applied on the damaged structure will be done as detailed in the previous numerical application. Any significant deviation of the initial values would indicate a possible future damage. From the modal analysis, the first three mode shapes and their identified frequencies are presented in Appendix A for the intact and damaged structure.

The class of elements considered in the current numerical application groups elements 4, 9 and 14 which share the same type (beam), the same material (concrete), the same geometry (40x70cm), the same loadings and the same environmental conditions. In our case, one class of three elements is taken into account. However, since we are dealing with a joint probability distribution for all the elements (Eq. 2.19), updating the condition state of elements belonging to that class will reduce the uncertainty related to the state of all the elements. This is due to the information flow which takes place: (i) between elements belonging to the same class and (ii) from elements belonging to a specific class to the other elements. Nevertheless, the methodology is not limited to one class of element. It can be applied to a case study with multiple classes where, for instance, all the elements in the structure can be grouped into different classes where their condition states will be updated simultaneously.

For illustration purposes, the degradation extent will be represented in the following graphs using the PDF of the remaining stiffness. A degradation is represented by the PDF shift in the range [1,0].

Figure 3.12 represents the posterior distributions of the degradation extents  $\alpha_c^e$  of elements 4, 9 and 14 obtained from the HABC method for borrowing strength.

Figures 3.13 to 3.15 represent the degradation extents of, respectively, elements 4, 9 and 14 in two cases: (i) elements updated independently; (ii) amplifying with three elements placed in the same class.

From the obtained results, the following observations can be drawn:

- Without taking into account the similarities between the elements, the update of their degradation extents has shown that element 4 is almost 25% damaged while elements 9 and 14 are most probably in a good condition. These results confirm the hypothesis for element 4, yet, they are far from what is expected for elements 9 and 14. The reason behind is that small damage in beams, especially those far from the supports, do not significantly affect the mode shapes of the structure. However, this is not the case for element 4 due to the fact that it is located close to the supports.
- After having applied the HABC method for information amplifying, the degradation extent's curve of element 4 has become a bit more precise, and the curves of element 9 and 14 imply that they are damaged having lost around 25% of their initial rigidity. Initially, there was not sufficient information about elements 9 and 14. The fact that they have been placed in the same class with element 4 and updated accordingly, has given them the opportunity to borrow strength from that specific element. The information obtained for element 4 has not only determined accurately its condition state, but helped in defining the condition state of other similar elements.
- The information flow direction is also shown in figure 3.12. As one can notice, the curve of element 4 is much more precise with a sharp peak while the curves of elements 9 and 14 look wider with a smaller peak. This could be also an indication that the information has been transmitted from element 4 to the other elements.

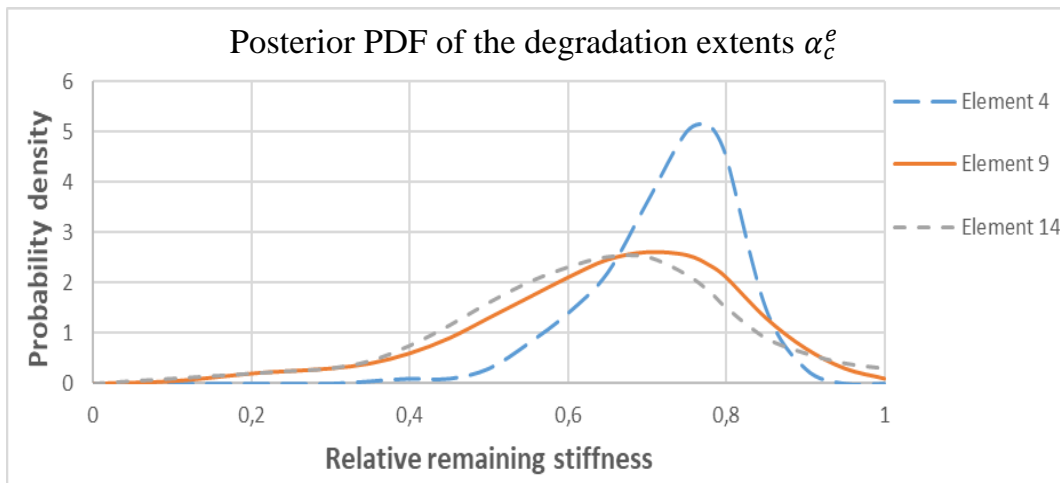


Figure 3.12: Posterior PDF of the degradation extents  $\alpha_c^e$  of elements 4, 9 and 14.

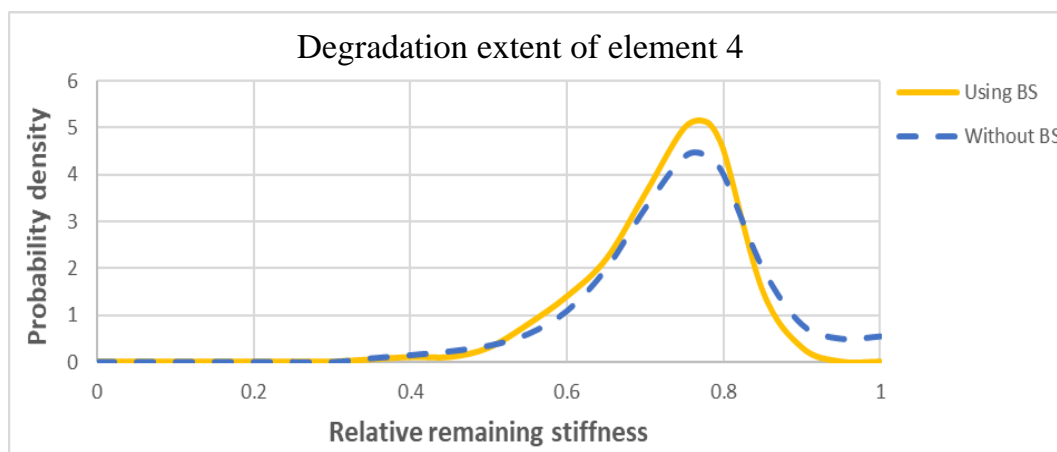


Figure 3.13: Degradation extent of element 4 without and with HABC for borrowing strength (BS) method.

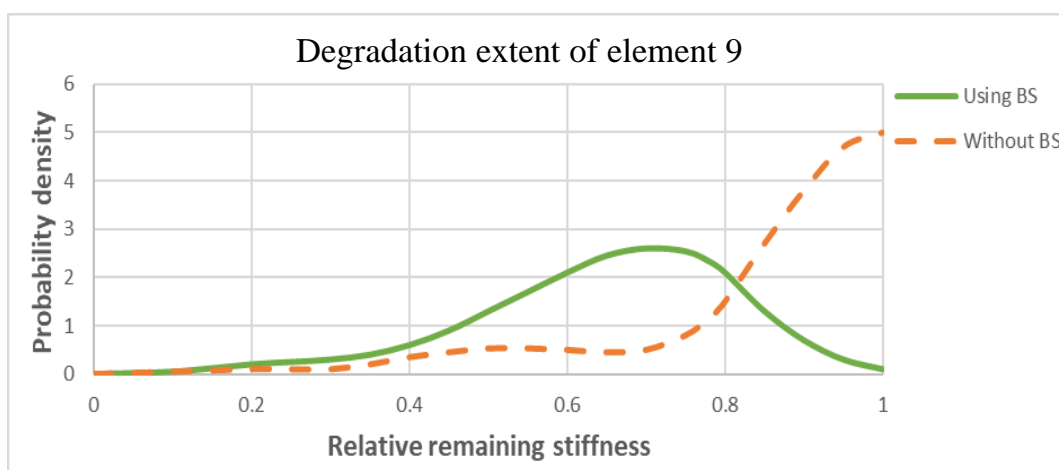


Figure 3.14: Degradation extent of element 9 without and with HABC for borrowing strength (BS) method.

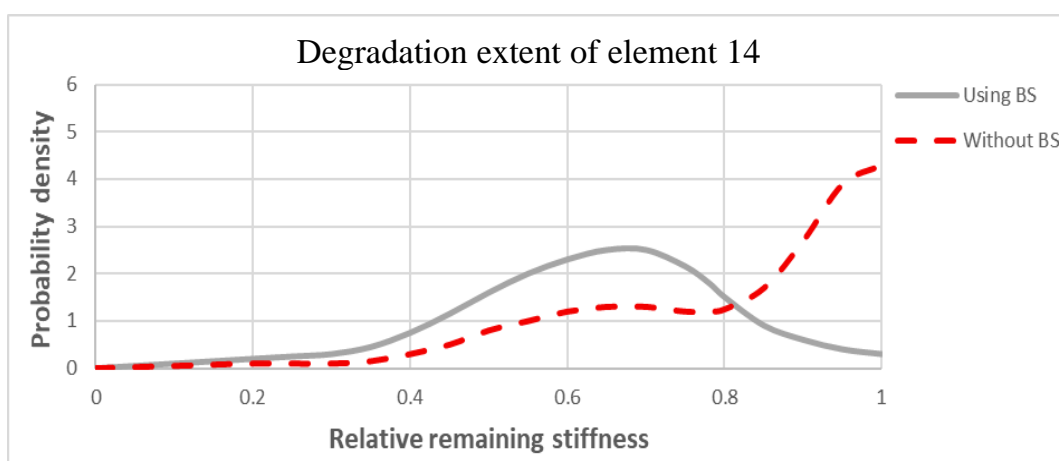


Figure 3.15: Degradation extent of element 14 without and with HABC for borrowing strength (BS) method.

### 3.4.3 Sensitivity analysis on damage detection

As done in Chapter 2 (Section 2.7.3), a sensitivity analysis is conducted for both applications, in order to evaluate the algorithm's performance with respect to parameter changes. Two parameters are considered in this chapter, namely: (i) the damage location and (ii) damage extent. For each combination, the mean of the damage extent distributions and the RMSD between the real and simulated results are calculated (refer to Chapter 2). The RMSD of each element is defined by:

$$RMSD = \sqrt{\frac{1}{N_{\alpha_e}} \sum_{i=1}^{N_{\alpha_e}} (\alpha_{ei} - \alpha_{e(Actual)})^2} \quad (3.7)$$

In this section, the measurement error is equal to  $\varepsilon_{Me}=0.15 \text{ m/s}^2$ . For both applications, four damage extents are studied (5% - 10% - 20% and 50%) and are represented by the following remaining stiffnesses: 95% - 90% - 80% - 50%.

#### 3.4.3.1 Four Steel Truss Structures

In the case of the four steel truss structures, the sensor configurations are the same as the ones described in the application in section 3.4.1. The same damage locations, as the one taken for the sensitivity analysis of Chapter 2, have been studied in the four structures simultaneously, namely elements 8, 15 and 25 (i.e. in each case, elements of the four structures located at the same place are subjected to similar damage extents).

Results for the three elements, in the different structures, are presented in tables 3.1 to 3.3 and figures 3.16 to 3.18 for the various damage extents. In table 3.1 to 3.3, the mean and RMSD values of the damage extent distributions of, respectively, element 8, 15 and 25 are stated. Figures 3.16 to 3.18 show the histograms of the calculated RMSD.

Table 3.1: Mean (and RMSD) of the damage extent distributions of element 8 for different damage extents, number of sensors and for  $\varepsilon_{Me}=0.15 \text{ m/s}^2$ .

Element 8				
Remaining Stiffness \ Number of Sensors	95%	90%	80%	50%
Structure 1	0.960 (0.039)	0.926 (0.071)	0.830 (0.131)	0.509 (0.037)
Structure 2	0.963 (0.087)	0.949 (0.085)	0.860 (0.147)	0.517 (0.061)
Structure 3	0.983 (0.049)	0.929 (0.088)	0.860 (0.145)	0.519 (0.046)
Structure 4	0.960 (0.055)	0.932 (0.087)	0.850 (0.146)	0.509 (0.063)



Table 3.2: Mean (and RMSD) of the damage extent distributions of element 15 for different damage extents, number of sensors and for  $\varepsilon_{Me}=0.15 \text{ m/s}^2$ .

<b>Element 15</b>				
Remaining Stiffness \ Number of Sensors	95%	90%	80%	50%
	Structure 1	0.956 (0.047)	0.904 (0.094)	0.811 (0.114)
Structure 2	0.966 (0.080)	0.919 (0.119)	0.796 (0.133)	0.540 (0.167)
Structure 3	0.957 (0.088)	0.922 (0.109)	0.816 (0.146)	0.550 (0.196)
Structure 4	0.959 (0.091)	0.925 (0.111)	0.829 (0.127)	0.527 (0.155)

Table 3.3: Mean (and RMSD) of the damage extent distributions of element 25 for different damage extents, number of sensors and for  $\varepsilon_{Me}=0.15 \text{ m/s}^2$ .

<b>Element 25</b>				
Remaining Stiffness \ Number of Sensors	95%	90%	80%	50%
	Structure 1	0.959 (0.039)	0.941 (0.079)	0.789 (0.121)
Structure 2	0.943 (0.050)	0.943 (0.096)	0.855 (0.140)	0.491 (0.058)
Structure 3	0.960 (0.064)	0.945 (0.093)	0.825 (0.142)	0.494 (0.052)
Structure 4	0.942 (0.080)	0.944 (0.090)	0.853 (0.129)	0.494 (0.069)

Tables 3.1 to 3.3 and figure 3.16 to 3.18 show that the proposed algorithm was able to detect slight, moderate and severe damage in most cases. Looking at the results obtained for elements 8, 15 and 25, it can be noticed that most of the mean values are close to the real damage. Even though the mean might shift a bit from the actual damage value, the distribution of the damage extent can still provide a decent amount of information. The obtained distributions are not always symmetrical, they might be skewed and in such cases the mode differs from the mean. It might coincide with the actual damage and in this case, the most probable damage extent does reflect the actual damage. However, the accuracy of the results depends on each structure's sensor configuration, on the damage location and its extent.

In table 3.1 and figure 3.16, it can be noticed that the most accurate results have been given for a 50% damage in element 8 while the less accurate were obtained for a 20% damage.

The same case present itself for element 25 yet, for element 15, a 5% damage is better assessed than a 50% damage. This might be due to two reasons: (i) the relationship between the measured dof and the results is not linear hence, depending on its location and severity, a specific damage could be well assessed or not; (ii) in most cases, the mean is seen to be shifted a bit toward the value 1; this shift would affect less the RMSD of elements with small damage severities (5% and 10% damage) since their remaining stiffness is close to the value 1. Yet, one might not be able to differentiate between a small shift resulting from a damage or from the presence of a noisy data. Nevertheless, in all cases, damage are well assessed since the mean values significantly shifted from the value 1. Even if for some cases the damage extent distribution is wider than for other cases, one could still assess the severity of the damage taking into account the peak of the PDF of the damaged element's extent.

Comparing results between the structures, results obtained for structure 1 are the most accurate ones in terms of mean and RMSD. For the three other structures, results can be better in a structure than in the others depending on the damage location and severity. The reason behind, is that structure 1 has 5 sensors while in each of the other structures only 3 sensors are implemented. Hence, the information in structures 2, 3 and 4 is amplified, basically, by the information coming from structure 1. Nevertheless, it does not imply that the accuracy is only coming from structure 1. All the structures borrow information from each other.

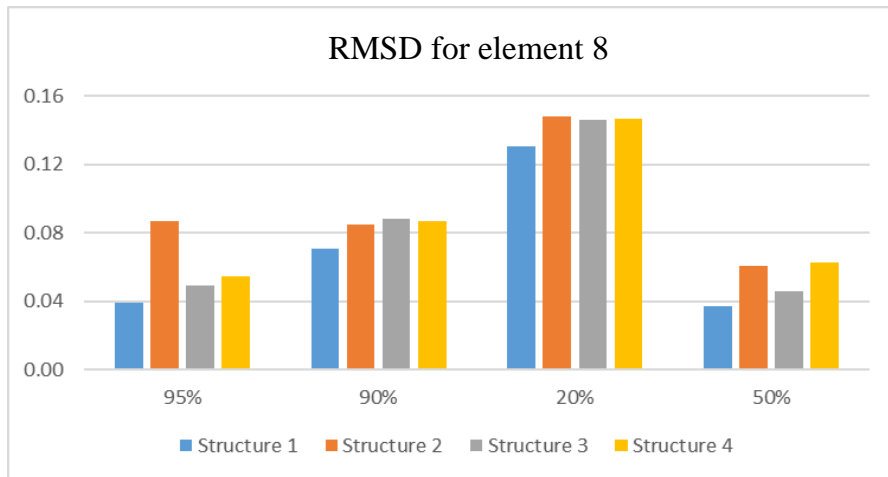


Figure 3.16: Histogram of RMSD values for element 8 ( $\epsilon_{Me}=0.15 \text{ m/s}^2$ ) for different damage extents (95%, 90%, 80% and 50% remaining stiffness).

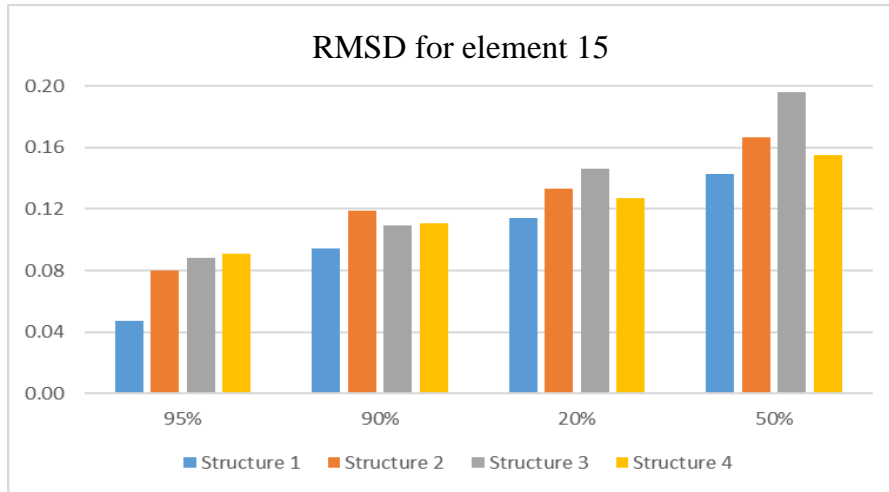


Figure 3.17: Histogram of RMSD values for element 15 ( $\varepsilon_{Me}=0.15 \text{ m/s}^2$ ) for different damage extents (95%, 90%, 80% and 50% remaining stiffness).

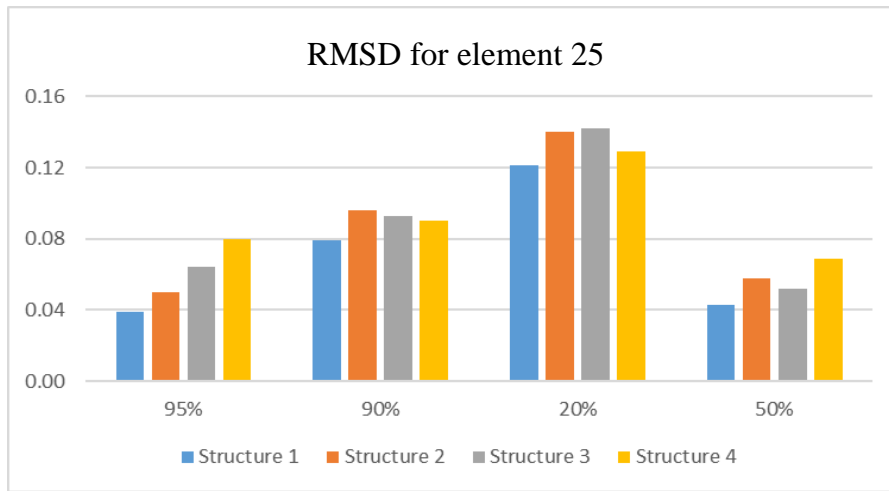


Figure 3.18: Histogram of RMSD values for element 25 ( $\varepsilon_{Me}=0.15 \text{ m/s}^2$ ) for different damage extents (95%, 90%, 80% and 50% remaining stiffness).

On the other hand, these results are obtained for a relatively high measurement error  $\varepsilon_{Me}=0.15 \text{ m/s}^2$ . Comparing them with the results obtained when updating each structure alone (Section 2.7.3, Chapter 2), one can notice the improvement in the accuracy. Even with 15 implemented sensors, updating the structures independently lead to accurately quantifying severe damage only (50% damage). Yet, when taking advantage of the similarity between the structures, the information has been amplified. Therefore, even a 5% damage could be quantified with 3 implemented sensors on a structure.

### 3.4.3.2 Multistory Concrete Frame

For the case of the concrete frame structure, the sensor configurations taken into consideration are the same as the ones considered in Chapter 2, section 2.7.3.2. The several damage locations have been taken as follows:

- Case 1: Element 1 – Element 2 – Element 3;
- Case 2: Element 5 – Element 10 – Element 15;
- Case 3: Element 7 – Element 12 – Element 17;

In each case, the similar elements are subjected to similar damage extents with  $\varepsilon_{Me}=0.15\text{m/s}^2$ .

Results obtained for elements 1, 5 and 7 are presented in table 3.4 to 3.6 and figures 3.19 to 3.21 for the different damage extents and sensor number. Tables 3.4 to 3.6 resumes the mean and RMSD values of the damage extent distributions of, respectively, elements 1, 5 and 7. Figures 3.19 to 3.21 represent the RMSD of their distributions. The results for the remaining elements are presented in Appendix B.

Table 3.4: Mean (and RMSD) of the damage extent distributions of element 1 for different damage extents, number of sensors and for  $\varepsilon_{Me}=0.15 \text{ m/s}^2$ .

<b>Element 1</b>				
Damage Extent \ Number of Sensors	95%	90%	80%	50%
1 sensor	0.957 (0.099)	0.953 (0.111)	0.791 (0.169)	0.403 (0.12)
3 sensors	0.954 (0.072)	0.936 (0.089)	0.829 (0.125)	0.520 (0.068)
6 sensors	0.953 (0.068)	0.914 (0.08)	0.800 (0.113)	0.467 (0.058)

Table 3.5: Mean (and RMSD) of the damage extent distributions of element 5 for different damage extents, number of sensors and for  $\varepsilon_{Me}=0.15 \text{ m/s}^2$ .

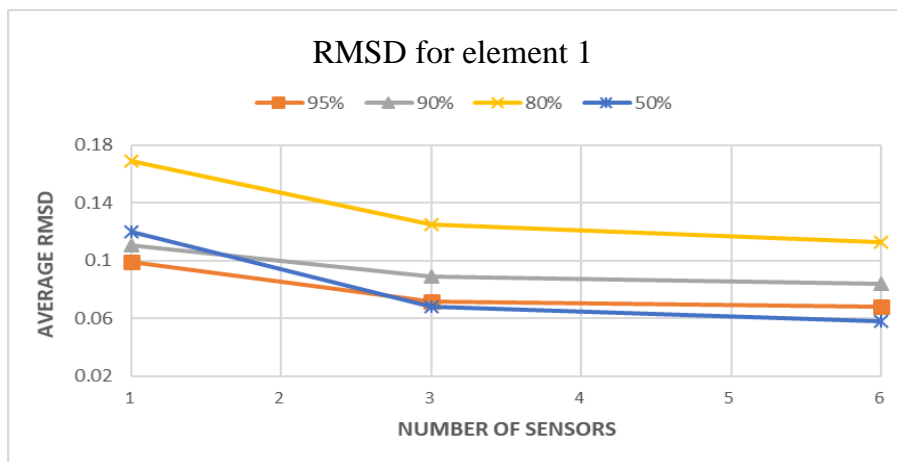
<b>Element 5</b>				
Damage Extent \ Number of Sensors	95%	90%	80%	50%
1 sensor	0.943 (0.110)	0.943 (0.118)	0.867 (0.146)	0.588 (0.133)
3 sensors	0.961 (0.068)	0.918 (0.100)	0.833 (0.127)	0.550 (0.107)
6 sensors	0.955 (0.059)	0.881 (0.089)	0.805 (0.112)	0.539 (0.094)

Table 3.6: Mean (and RMSD) of the damage extent distributions of element 7 for different damage extents, number of sensors and for  $\varepsilon_{Me}=0.15 \text{ m/s}^2$ .

Element 7				
Remaining Stiffness \ Number of Sensors	95%	90%	80%	50%
1 sensor	0.975 (0.109)	0.959 (0.125)	0.894 (0.112)	0.459 (0.093)
3 sensors	0.969 (0.052)	0.950 (0.099)	0.844 (0.079)	0.467 (0.062)
6 sensors	0.958 (0.047)	0.945 (0.093)	0.837 (0.067)	0.473 (0.052)

From tables 3.4 to 3.6 it can be seen that the mean values found for all damage extents are close to the actual damage, even for slight damage. For instance, 6 implemented sensors lead to obtaining mean values of 0.953, 0.955 and 0.958 for a 5% damage in, respectively, elements 1, 5 and 7. Their respective RMSD are also satisfactory being 0.068, 0.059 and 0.047. However, as it was concluded in the previous example, the degree of accuracy depends on the sensor configuration, damage location and severity. It should be noted that each table shows results obtained for one element by updating a class of elements to which it belongs. For example, element 1 belongs to the same class with elements 2 and 3. Hence, the 3 elements have been updated simultaneously.

Comparing results obtained for the different sensor configurations in figures 3.19 to 3.21, one can see that additional sensors are not always beneficial. For most cases, there are no significant changes when moving from 3 to 6 sensors. Depending on the effect of the damage on the mode shapes, some measurement points might be affected more than others. Especially when a good accuracy is reached with few sensors, using less sensors results in less noisy data.


 Figure 3.19: RMSD distribution for element 1 ( $\varepsilon_{Me}=0.15 \text{ m/s}^2$ ) for different damage extents (95%, 90%, 80% and 50% remaining stiffness).

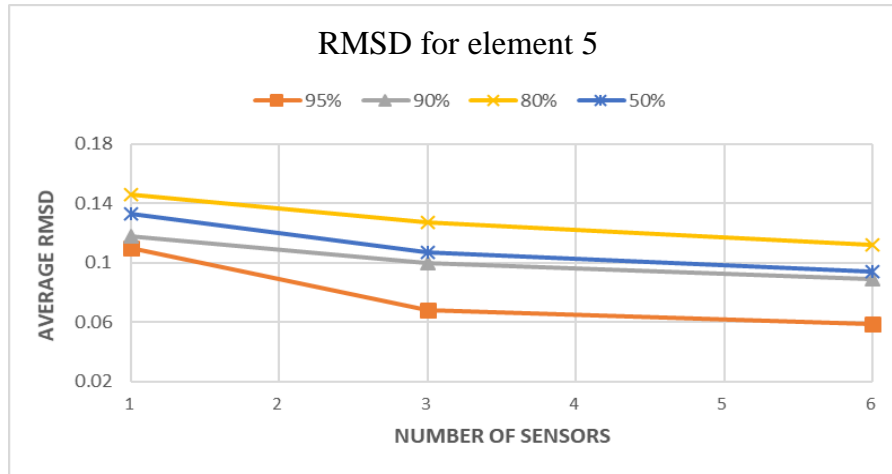


Figure 3.20: RMSD distribution for element 5 ( $\epsilon_{Me}=0.15 \text{ m/s}^2$ ) for different damage extents (95%, 90%, 80% and 50% remaining stiffness).

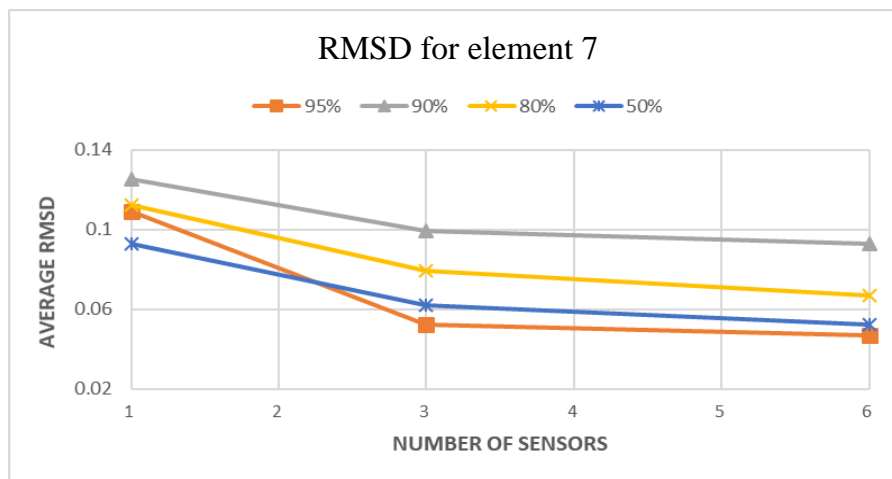


Figure 3.21: RMSD distribution for element 7 ( $\epsilon_{Me}=0.15 \text{ m/s}^2$ ) for different damage extents (95%, 90%, 80% and 50% remaining stiffness).

In order to evaluate the effectiveness of the proposed methodology, one should compare the obtained results to the ones in Chapter 2 where the similarity between elements is not considered. As observed, classifying the elements and updating them accordingly enhanced the results especially for slight to moderate damage (80% to 95% remaining stiffness). For instance, for  $\epsilon_{Me}=0.15 \text{ m/s}^2$  in table 2.6, a 5% damage in element 1 could be located however the mean values were around 0.986 (with 6 implemented sensors). Yet, taking into account the similarity between element 1, 2 and 3, results showed that the mean value of the damage extent distribution of element 1 is around 0.953 (with 6 implemented sensors). For the same number of sensors, results are more accurate using the HABC methodology for borrowing strength. Therefore, the information has been amplified in order to reflect more the actual damage even for a high measurement error.

### 3.5 Conclusion

In this chapter, a hierarchical Approximate Bayesian Computation (HABC) approach for borrowing strength is presented. It is an information amplifying methodology where information obtained from well monitored elements and/or structures is used to amplify the information available for elements and/or structures subjected to a lower monitoring effort and belonging to the same class of elements. Starting by classifying the elements according to a given features set, the PDFs of the class parameter and the deterioration rates of the elements belonging to the same class (which depend on the class parameter) are updated using a hierarchical approach. The proposed procedure would not only amplify the information about the deterioration rate of elements belonging to a specific class, but will also lead to more precise results concerning the deterioration rate of other elements of the structure(s). The proposed methodology has been applied to different types of structure in different situations: four steel truss structures and a concrete frame structure. The obtained results proved that:

- (i) It is possible to determine precisely the condition state of one or more elements in a specific structure using information obtained from other similar elements belonging to the same or to different structures;
- (ii) Using the proposed method lead to more accurate results concerning the deterioration extent of elements having low effects on the structural response;
- (iii) The proposed methodology is sensitive to slight, moderate and severe damage even with high measurement errors;
- (iv) Distributing the sensors on multiple structures sharing similar element features and assessing the damage using the presented methodology provides better results than implementing more sensors on each structure and assessing it individually.

The main benefits of this approach appear in its capability to: (i) take into consideration, systematically, any type of uncertainties; (ii) update the state of elements, not easily accessible for SHM and/or conventional inspections, using data from other similar elements which can belong to the same or different structures; (iii) reduce the number of implemented sensors (hence the cost of monitoring) while preserving the accuracy of the results. Nevertheless, for optimal results and less computational complexity, one should judiciously choose the number of hierarchy levels, the features and their intervals. The computation time is usually an increasing function of the number of hierarchy levels. Hence, it might be preferable to initially find the optimal number of hierarchy levels in order to reduce the computation time. Moreover, a wide feature interval results in less similarity between elements but also reduces the statistical error, while a narrow interval results in more similar elements with a high statistical error. Hence, a compromise must be made in order to define a relevant feature interval.

## **Chapter 4: Hybrid inspection-monitoring approach for optimal maintenance planning**

### **4.1 Overview**

Inspection, Maintenance and Rehabilitation (IM&R) of civil engineering structures has been the subject of extensive research during the last decades (Bastidas-Arteaga and Schoefs 2015; Stratt 2010; Atkins 2002). Many of the methodologies developed by the research community gained wide acceptance among asset owners and practicing engineers. The application of these methodologies by professional engineers was boosted by the increasing availability of substantial computational power, in addition to the development of increasingly reliable and efficient inspection technologies. However, the cost of an inspection technology is usually an increasing function of its accuracy. Hence, the optimal planning of inspections during the projected lifetime is central to IM&R approaches. A probabilistic framework using lifetime functions was proposed by Orcesi and Frangopol (2011) to determine optimal non destructive inspection strategies for a structure's components, taking into account its overall system safety. In their paper, the authors aimed at minimizing, simultaneously, the expected inspection/maintenance cost and the expected failure cost while considering different types of inspection. Algorithms for non-myopic planning of inspections over the lifetime of the structure were proposed by Corotis (2005) and Faddoul et al. (2011) among others. The possibility of merging information that might be available to the structure manager, in the future, with data obtained from planned inspections is addressed by Attoh-Okine and Bowers (2006) and Faddoul et al. (2012). Uncertainty related to imperfect inspection results received a considerable focus in the literature (Liu and Chen 2017; Alaswad and Xiang 2017). A recurrent leitmotif in the above-mentioned research effort is the ability to take into account, in the IM&R optimization problem, additional pertinent information stemming from multiple sources. Yet, classical approaches for IM&R, suffer from several shortcomings among which the fact that the condition state of the structure is only known at discrete points in time. Therefore, any defect that might appear in the time interval between two successive inspections and which may ideally require an immediate remedial action might remain undetected till the next inspection date. More recently, Structural Health Monitoring (SHM), using permanent sensors for measuring several features of the structure, started to be commonly applied to important structures. However, it is not practically possible to rely solely on sensors to measure every feature of a structure, in order to assess the condition state of all its elements. Thus, an optimal management planning of IM&R must be able to use different types of information arising from different data sources (e.g. sensors, visual inspection, destructive and/or non-destructive inspection techniques, etc.).

In this chapter, a methodology is proposed for defining an optimal IM&R planning by optimally combining conventional inspections and global SHM. The proposed methodology is an output-only modal identification method that integrates dynamic Bayesian update of the



belief state of the structure, based on the sensor readings, in a decision analysis framework. A key component of this approach consists of updating the sensor-based belief states of all the structural elements when additional information, resulting from imperfect inspections, is made available about the condition states of one or several elements. Uncertainties resulting from the model, the measurements, the imperfect inspections and the imperfect maintenance actions should be explicitly taken into account. First, the M&R and IM&R decision-making procedures are presented and the value of information is defined. The methodology is then broadly described by presenting the integration of the Bayesian update procedure in the decision analysis framework and highlighting its advantages. Two numerical applications illustrating the methodology are detailed in section 4.4.

## 4.2 Decision Making under Uncertainty

Maintenance planning problems usually involve decision-making under uncertainties which are categorized into: aleatory and epistemic (Der Kiureghian and Ditlevsen 2009). Aleatory uncertainty is defined as a non-reducible uncertainty resulting, for instance, from the intrinsic randomness of the variation of a physical property of a component. While epistemic uncertainty is related to a lack of accurate knowledge which may cause errors in parameter estimation and model formulation. Epistemic uncertainties can be reduced by collecting more data, and/or using models that are more elaborated. Thus, a decision maker has to weight between the benefits of decreasing epistemic uncertainty and the additional incurred costs related to increased data collection effort and decreased model tractability.

In the methodology presented in this chapter, an uncertain belief state about the condition state of the structure, based on sensor readings, is available to the decision maker. Additional information can be obtained by inspecting one or several elements of the structure.

### 4.2.1 M&R Decision-Making Without Inspection

An optimal M&R planning can be developed by continuously monitoring a structure and according to the results, decide whether maintenance action(s) should be done or not. This type of analysis takes place as following:

- 1- A set of possible element condition states :  $\theta \in \Theta$  is defined; i.e. Let  $\theta \in \Theta = \{1, 2, \dots, m\}$  be a discrete variable that describes the damage extent of an element i.e.  $\theta$  is a discretization mapping of  $\alpha_e$ . It is assumed that it takes its values from an ordinal and countable finite set. Each value in  $\Theta$  represents a particular subinterval from the domain of  $\alpha_e$ , i.e. a particular subinterval of  $[0, 1]$ .
- 2- A belief state for the condition state vector for each element is made available to the decision maker using SHM results analysis; i.e. The probability  $P(\theta = j)$  is calculated as the integral of the posterior distribution of  $\alpha_e$  over the corresponding subinterval. Let  $\bar{\theta}$  be a vector whose components are the condition state of each element. For example,  $\theta^e = j$  means that element  $e$  is in condition  $j$ .

- 3- A set of possible maintenance actions  $a \in A$  is compiled. Let  $\bar{a}$  be the vector whose components are the chosen action for each element. The maintenance actions  $a^e \in A = \{a_0, a_1, \dots, a_n\}$  are imperfect and are selected from a finite set of alternatives; where  $a_0$  means that no action is made. The uncertainty related to a maintenance action  $a^e$  is described by a square transition matrix  $\bar{A}^e$  where each element  $a_{ij}^e$  corresponds to the probability that the state  $\theta^e$  of element  $e$  changes from the value  $\theta^e = i$  to a new value  $\theta^e = j$  after the application of the action  $a^e$ .
- 4- A function  $c: A \times \Theta \rightarrow C$  associating a consequence for each couple  $(a, \theta)$  is determined. This consequence is uncertain since it depends on the uncertain state of nature  $\theta$  and on the action  $a$  which has uncertain outcomes.
- 5- A function  $u: C \rightarrow R$  is defined to associate a utility value for each possible consequence  $c$ .
- 6- The decision maker chooses the optimal maintenance action based on a predefined optimality criterion.
- 7- The costs taken into consideration are:
  - $ca(a^e)$  : cost of the action  $a^e$  applied on element  $e$ .
  - $cs(\theta^e)$ : user cost due to element  $e$  being in state  $\theta^e$ .
 The cost  $cs(\theta^e)$  is calculated as the expected cost of failure. i.e.:
 
$$cs(\theta^e) = \text{failure probability}|\theta^e \times \text{failure cost.} \quad (4.1)$$

Other costs due to the reduced performance of the structure can be included in  $cs(\theta^e)$ , such as increased vibration etc.

In order to illustrate several alternative solutions of a problem and the possible outcomes, a decision tree analysis is often used in a decision making problem (Luque and Straub 2019, Agusta et al. 2017, Florian and Sørensen, 2017). The graphic representation is a tree-shaped structure with two types of nodes: (i) square nodes representing a decision point (i.e. a node controlled by the decision maker) followed by (ii) a circle node representing a chance node which is an uncertain point where the outcome depends on the chance process. Once the various alternative decisions and the possible outcomes along with their probabilities are known, the best decisions are reached by folding back and then pruning the tree as follows:

- 1- Each chance node at the far right end of the tree is evaluated by calculating its expected value:  $EV = \sum_{\theta} P(\theta) \times C(a, \theta)$  where  $P(\theta)$  is the probability of a possible outcome or a condition state and  $C(a, \theta)$  is the consequence derived from an action  $a$  (or a decision).
- 2- After having calculated the expected values of all the far right chance nodes, at each decision node, the alternative with the maximum expected value is recorded in the square node and the expected value of the chosen alternative is written down under the node.
- 3- The process is done recursively starting from the terminal nodes of the tree (from right to left) by calculating the expected value at each chance node and maintaining

the most valuable decision at each decision node. The best path is then obtained when the far left decision node has been evaluated.

The decision tree differs from the canonical form by the fact that the Bayesian updating of the tree relies on the Bayesian updating procedure of the SHM system. The calculation is done recursively starting from the terminal nodes (leaves) of the tree up to the root. Every time a chance node is met, the expected utility is calculated and every time a decision node is met the cost is minimized. A chance node being a branch in the decision tree representing a family of possible outcomes characterized by a probability distribution.

In what follow, we use the word “cost” to denote a “decrease of the utility”. The most common optimality criteria are the “minimax cost” and the “minimum expected cost”. For the minimax criterion, the maximum cost over all the states of nature is found for each possible action. The optimal action would be the one that corresponds to the minimum of these maximum costs (Lee 2019, Min and Lim 2017, Esmail 2015, Matthias et al. 2014). An optimization using this criterion, is called a “robust optimization” and is usually chosen by an extremely risk-averse decision maker or when a decision should be made very prudently. In terms of utility, it is expressed by:

$$\min_a \max_{\theta} -u(c(a, \theta)) \quad (4.2)$$

An optimization procedure using the minimum expected cost criterion, uses the available probabilities associated with the states of nature to compute the expected cost over all the states for each possible action. The optimal action corresponds to the minimum expected cost. Such a decision procedure can be expressed, in terms of utility, by:

$$\min_{\theta} E[-u(c(a, \theta))] \quad (4.3)$$

Figure 4.1 represents the decision analysis framework without inspection where the decision maker has to choose the optimal maintenance action (repair, replace or nothing to do) for each element of the structure, depending on the SHM results and the condition state  $\theta$  of the element. We assume that each element has four possible condition states.

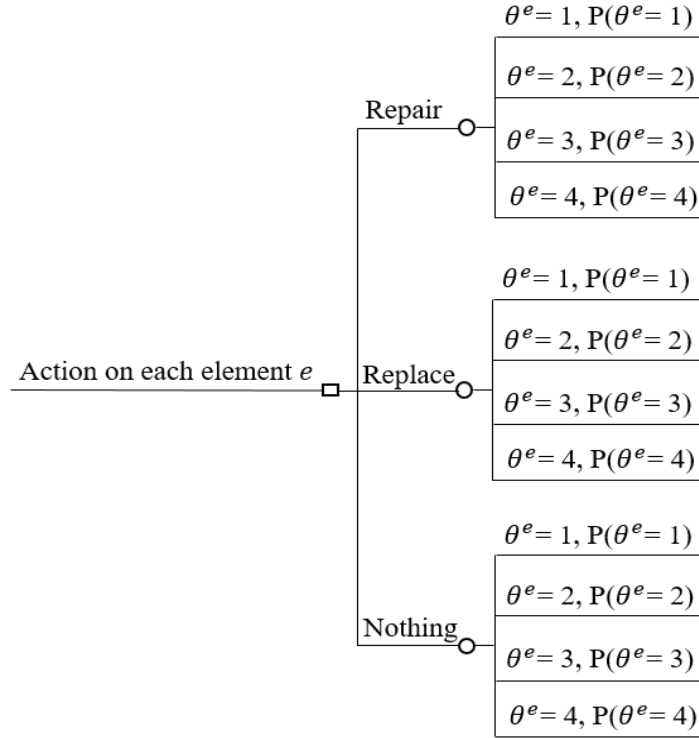


Figure 4.1: Representation of a decision making without inspection

#### 4.2.2 IM&R Decision Making With Inspection

In a decision analysis based on SHM only data, the prior belief state of a structural element is subjected to both types of uncertainties, the aleatory and epistemic. However, it is possible to decrease the epistemic uncertainty by acquiring more knowledge related to the structural degradation or the condition state of the element. Hence, including the possibility of an inspection in the data analysis, can lead to more informed decisions resulting in a lower total cost. The optimal decision will then depend on the outcome of the inspection when needed. It should be noted that the inspection techniques are also imperfect in the sense that their outcome are expressed in terms of probability distributions.

In addition to the steps outlined in the previous section, we assume that:

The available inspection techniques  $i \in I = \{i_0, i_1, \dots, i_p\}$  are imperfect and are selected from a finite set of alternatives; where  $i_0$  means that no inspection is made. The inspection results are described by discrete probability distributions. The uncertainty of inspection results is characterized by a conditional probability distribution  $(P[r_1|\theta^e, i^e], P[r_2|\theta^e, i^e], \dots, P[r_m|\theta^e, i^e])$ , where  $\theta^e$  is the true discretized condition state of the element  $e$ ,  $i^e$  is the type of the inspection technique applied to element  $e$ .

Let  $\bar{i}$  be the vector whose components are the chosen inspection for each element and  $ci(i^e)$  the cost due to the application of the inspection method  $i^e$  on element  $e$ .

Let:

- $N$  be the number of elements in the structure.
- $r_j \in R$  a possible result of an inspection.
- $P(\theta^e = i)$  the prior probability of element  $e$  being in condition state  $i$  ( $i = 1, \dots, m$ ).
- $P(\theta^e = i | R = r_j)$  the posterior probability of element  $e$  being in condition state  $i$  knowing that the inspection result is  $r_j$  ( $r_j = 1, \dots, m$ ).
- $P(R = r_j | \theta^e = i)$  the likelihood of the result being  $r_j$  knowing that the true condition state is  $i$ . This probability represents the uncertainty on the results of inspection.

If the prior probability  $P(\theta^e = i)$  and the likelihood  $P(R = r_j | \theta^e = i)$  are known for each combination  $(i, r_j)$ , the problem will consist in calculating the posterior belief states  $P(\theta^e = i | R = r_j)$  for each possible inspection result and the probability of getting each of these results  $P(R = r_j)$ . These probabilities are calculated using the following Bayes formula:

$$P(\theta^e = i | R = r_j) = \frac{P(R=r_j | \theta^e=i) \times P(\theta^e=i)}{\sum_{k=1}^m P(R=r_j | \theta^e=k) \times P(\theta^e=k)} \quad (4.4)$$

The solution to the problem will then have to answer, for each element, the below questions: Must an inspection be done and incur its cost before deciding on the optimal action? If yes, what type of inspection must be chosen?

Let  $\bar{a}$  and  $\bar{i}$  be the vectors whose components are respectively the chosen action and inspection for each element. For a given element  $e$ , the probability of obtaining the result  $r_l$  given the inspection type  $i^e$ , is:

$$P[r_l | i^e] = \sum_{k=1}^m P[r_l | \theta^e = k, i^e] \times P[\theta^e = k] \quad l = 1, \dots, m \quad (4.5)$$

Given the posterior probability distribution for the condition state of an element as obtained from the SHM system via the Bayesian updating previously described, given an inspection technique  $i^e$  and its result  $r_l$ , the posterior probability distribution of the condition state of a given element will be calculated from the following equation:

$$P[\theta^e | r_l, i^e] = \frac{P[r_l | \theta^e = j, i^e] \times P[\theta^e = j]}{\sum_{k=1}^m P[r_l | \theta^e = k, i^e] \times P[\theta^e = k]} \quad (4.6)$$

The total cost  $c | \bar{i}, \bar{r}, \bar{a}, \bar{\theta}$ , depends on the inspection vector  $\bar{i}$ , the inspection result vector  $\bar{r}$ , the action vector  $\bar{a}$  and the state of the system  $\bar{\theta}$ . Thus, the objective function of this dynamic problem will be:

$$c | \bar{i}, \bar{r}, \bar{a}, \bar{\theta} = ci(\bar{i}) + \sum_{e=1}^N (ca(a^e) + \sum_{k=1}^m cs(\theta^e = k) \times a_{jk}^e) \quad (4.7)$$

The optimization variables are (i)  $i^e$  which indicates the type of inspection for each element to inspect and (ii)  $\bar{a}$  which is the vector of actions to be applied on all the elements. The problem is constrained by the sets  $I$  and  $A$  of available inspection techniques and maintenance actions. Hence, the optimization problem takes the form:

$$\text{minimize } c|\bar{i}, \bar{r}, \bar{a}, \bar{\theta} = ci(\bar{i}) + \sum_{e=1}^N (ca(a^e) + \sum_k^m cs(\theta^e = k) \times a_{jk}^e) \quad (4.8)$$

$$\text{s.t.} \quad \bar{i} \in I$$

$$\bar{a} \in A$$

One could easily include, in the optimization formulation, other types of constraints such as budgetary constraints, minimum level of service constraints, etc.

The decision analysis calculation takes the form:

$$c|\bar{i}, \bar{r}, \bar{a} = ci(\bar{i}) + \sum_{e=1}^N (ca(a^e) + \sum_{j=1}^m [\sum_{k=1}^m cs(\theta^e = k) \times a_{jk}^e] \times P[\theta^e = j|\bar{r}, \bar{i}]) \quad (4.9a)$$

$$c|\bar{i}, \bar{r} = ci(\bar{i}) + \sum_{e=1}^N \min_{a^e \in A} (ca(a^e) + \sum_{j=1}^m [\sum_{k=1}^m cs(\theta^e = k) \times a_{jk}^e] \times P[\theta^e = j|\bar{r}, \bar{i}]) \quad (4.9b)$$

$${}^*c|\bar{i} = \sum_{l=1}^m {}^*c|\bar{i}, r_l \times P[r_l] \quad (4.9c)$$

$${}^*c = \min_{\bar{i} \in I} {}^*c|\bar{i} \quad (4.9d)$$

$${}^*\bar{i} = \text{arg min}_{\bar{i} \in I} {}^*c|\bar{i} \quad (4.9e)$$

### 4.2.3 Value of Information

Prior to making any decision, the decision maker must be aware of the added value that would be offered by a particular decision over another one. Sometimes, the information may not be worth the cost induced by the source of information. For instance, in our problem, the following questions can be addressed by the decision maker: What is the potential value of inspection? Is it worth the cost compared to using the SHM monitoring only? A perfect inspection reduces the uncertainty and gives more reliable results, but does it introduce much information compared to a less certain and less costly imperfect inspection?

The expected gain resulting from the reduction of uncertainty brought by the gathered information is assessed by the Value of Information (VI). The key measurements in VI are: the Expected Value of Perfect Information (EVPI) and the Expected Value of Imperfect Information (EVII). The difference between both measurements is the level of uncertainty which means that when the information is perfect, the outcome of each alternative is certain whereas the second case reflects the reality where decisions are made under uncertainty. They are calculated as follows:

$$EVPI = E[PI] - E[OI] = E_M[\max_A U(A, M)] - E_M[\bar{U}(A, M)] \quad (4.10)$$

$$EVII = E[II] - E[OI] = E_x[\max_A E_{M|x}[U(A, M)]] - E_M[\bar{U}(A, M)] \quad (4.11)$$

where  $E[OI]$  and  $\bar{U}(A, M)$  are respectively the expected value and the utility of the original information without inspection (experimentation),  $A$  is a set of actions,  $M$  is a model with prior weights on the alternative hypotheses,  $x$  represents the experimental information and  $U(A, M)$  is the utility of using additional information.

The optimal choice for an inspection technique as calculated by a decision tree, can be reduced to the comparison of the Value of Information (VI) brought by that particular

inspection technique (i.e. the reduction in maintenance expected costs obtained when applying this inspection) to its cost. The optimal inspection technique would be the one that yields the highest difference between the VI and the inspection cost.

### **4.3 Dynamic IM&R Optimal maintenance planning**

#### **4.3.1 Methodology**

The methodology developed herein, aims at prescribing an optimal IM&R policy for a structure having a permanent global SHM system, where information originating from conventional inspection techniques for a particular element is used to update the condition belief states for all the remaining elements in the structure. Using Bayesian updating techniques developed in Chapter 2, the inspection data for any element in the structure will not only reduce the uncertainty related to the condition state for that particular element but it will also reduce the uncertainty related to the state of all the remaining elements. In other terms, the posterior probability distribution of the condition state of any given element that results from sensor measurements might be updated and its uncertainty decreased when the condition states of one or several other elements are assessed by conventional inspection techniques.

Therefore, the questions to address sequentially will be:

- (i) What element to inspect (if any)?
- (ii) What type of inspection technique must be used for that particular element?
- (iii) Having obtained the inspection results for the selected element, and after having updated the belief states for all the elements of the structure accordingly, which element to choose next for the second inspection (if any)?
- (iv) When no more inspections can be optimally prescribed, what are the optimal maintenance actions to perform for each element of the structure?

Among the rationales fostering this approach, one can mention the facts that: (i) the inspection and/or accessibility of some elements might be costly or difficult. In such a case, the inspection of other more accessible and/or cheaper to inspect elements may yield the needed information for the non-accessible elements, more economically; (ii) the types of data generated by SHM systems and conventional inspection techniques are usually different and complementary. For example, the stiffness characterization given by the permanent SHM system, might be fruitfully combined with one or more conventional inspection techniques such as: visual corrosion assessment, non-destructive techniques, and/or destructive techniques; (iii) relying on information obtained solely from permanent SHM systems is not sufficient to characterize all the mechanical, physical and chemical states of a structural element; (iv) also, relying on intermittent time punctual classical inspections might be dangerous and suboptimal; (v) by using an appropriate utility mapping of the various involved costs (Hammond et al. 2015), the risk aversion attitude of the decision-maker can be taken into account.

The proposed methodology can be summarized by the following steps (Figure 4.2):

- 1- Obtain, from the SHM system, the damage PDF for all the elements in the structure;
- 2- Using the calculated PDF, calculate the Probability Mass Function (PMF) for the discretised damage state for each element;
- 3- For each element  $e$ , each inspection type  $i^e$  and each possible inspection result  $r_l$ :
  - a. Calculate the posterior PMF  $P[\theta^e | r_l, i^e]$  using equation (4.6);
  - b. Using the PMF calculated in step a, calculate a posterior PDF for all the elements of the structure. i.e We assume that the posterior belief state  $P[\theta^e | r_l, i^e]$  of a given element  $e$  has been obtained after an inspection has been applied on that element. This belief state is imposed for that particular element in the ABC framework of the SHM system presented in chapter 2. i.e. during the Monte-Carlo sampling, the  $\alpha_e$  sampling for the inspected element  $e$  is sampled from  $P[\theta^e | r_l, i^e]$  while the sampling of the  $\alpha_e$  of the remaining elements is done from their respective prior distributions;
  - c. Using the calculation of section 4.2.1 i.e. “M&R Decision Making Without Inspection” and the PDFs calculated in step b, calculate an optimal action to be applied for each element;
  - d. Calculate the total cost which includes: (i) the inspection cost, (ii) the maintenance action costs for all the elements, (iii) the user costs;
  - e. Calculate the expected cost of inspection  $i^e$
- 4- Choose the optimal element-inspection combination (i.e. choose the combination yielding the lowest cost).
- 5- Choose the optimal maintenance actions for all the elements in the structure using the calculation of section 4.2.1.
- 6- Choose the optimal decision using the decision tree: inspecting an element according to the combination chosen in step 4 or applying maintenance actions on the elements according to step 5. If no element is chosen for inspection and the best decision is applying maintenance actions on the elements then go to step 8;
- 7- Apply the prescribed inspection and, having obtained the inspection result of the element chosen in step 4, update the damage PDF for all the elements in the structure using the Bayesian update procedure (as described in steps 3.a and 3.b) and go to step 2;
- 8- Apply the optimal maintenance actions for all the elements.

The proposed methodology assumes that the prescribed inspections and maintenance actions are instantaneous and hence they do not affect the normal service of the structure. The optimization considers a myopic optimization of the maintenance of the structure at one point in time. As such, it does not take into account the effects of current decisions on the context of future decisions. However, the proposed methodology can be easily included in optimal IM&R planning over a time interval of the lifetime of the structure.



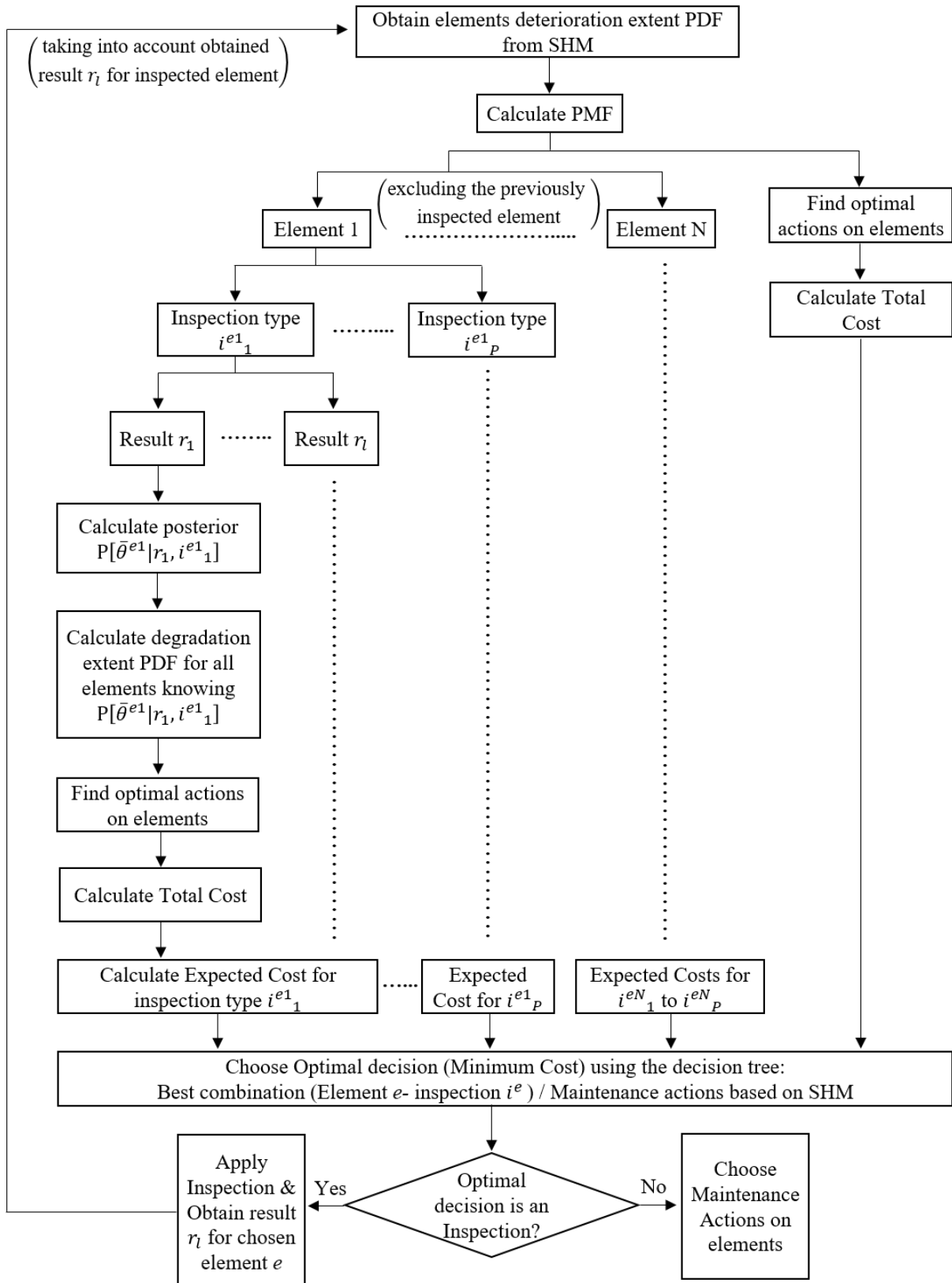


Figure 4.2: Flowchart of the proposed methodology.

The decision tree corresponding to the flowchart, for an inspection type, is synthesized in figure 4.3.

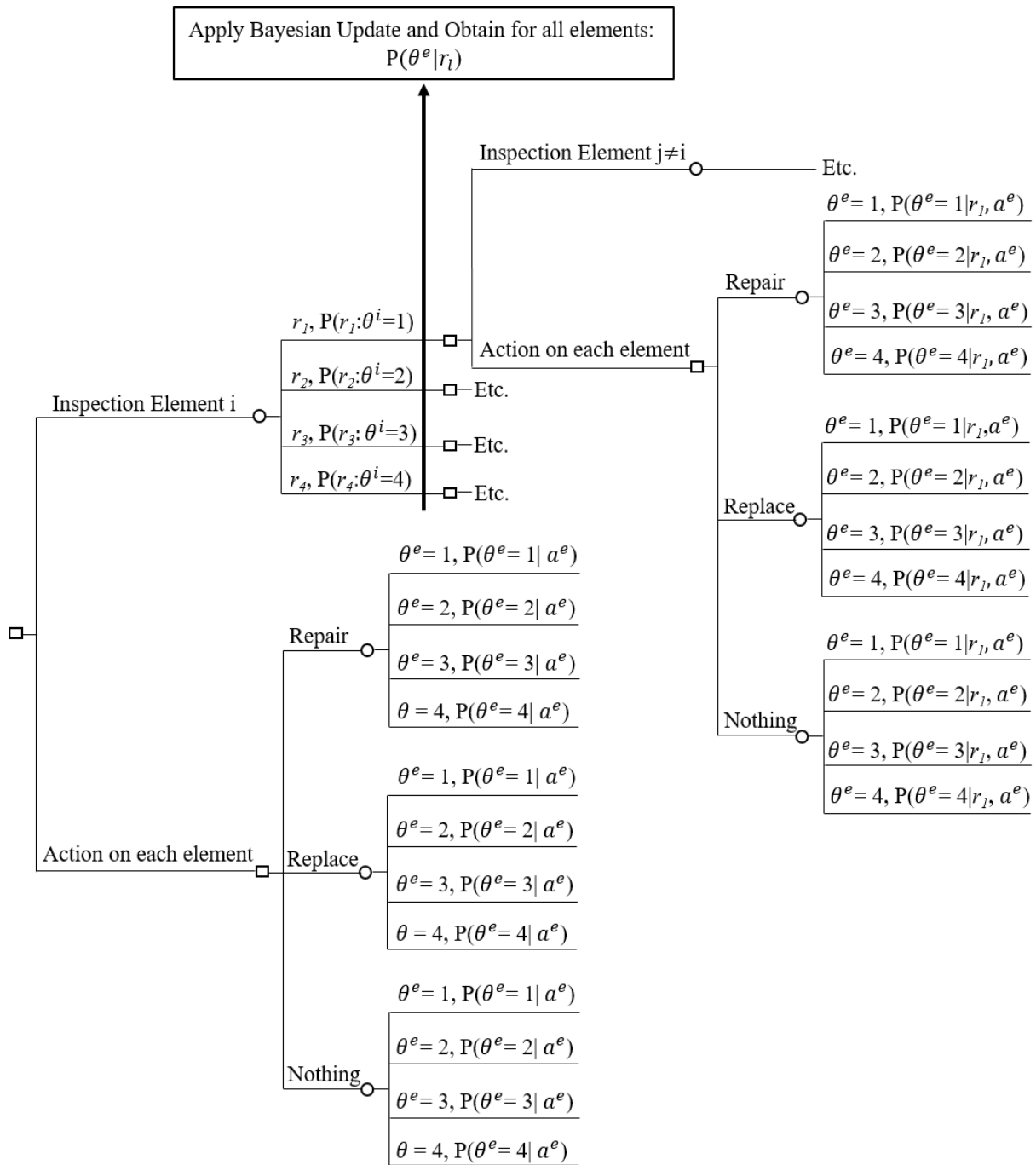


Figure 4.3: Layout of the decision tree.

### 4.3.2 False Positives and False Negatives

False positives and false negatives are two types of errors affecting an outcome, leading to wrong results since due to these errors, the outcome does not accurately reflect the reality. For an optimal maintenance planning for instance, it is mandatory to correctly detect a damage with the least possible errors. In this way, one should distinguish between four categories of results:

- True Positive (i.e. a damage is present and detected).
- True Negative (i.e. no indication of damage is given and damage is not present).
- False Positive (i.e. a damage is detected without being present).
- False Negative (i.e. a damage is present but not detected).

Usually, these false indications cannot be totally weeded and therefore researchers tend to minimize the risk of getting them and reduce their impacts. When searching for an optimal inspection technique, for example, a probability of detection function could be formulated for each alternative procedure (Chung et al. 2006). Another method often used is the ROC (Receiver Operator Characteristics) which compares the true positive rate and the false negative rate and assesses the balance between them. In our case, the belief states of a structural element is multinomial and the decision analysis itself takes into account the effect of the estimation error. This is done by considering all the possible states of the elements (Figure 4.3), each weighted by the probability of the element being in that state. Without any loss of generality, we illustrate our methodology by using the basic decision tree which minimizes the expected cost. Nevertheless, one could easily use instead robust optimization decision trees (e.g. minmax optimization) or minimize the expected utility of the decision maker which accounts for his attitude towards the risks. Depending on its shape, the utility function characterizes the decision maker behavior towards risk. Risk-averse, risk-neutral and risk-prone behaviors are characterized, respectively, by convex, linear and concave utility functions. For example, some may prefer low risk options while others are willing to take higher risks to earn more. In this thesis, without loss of generality, we assume that the utility curve of the decision maker is linear (i.e. risk neutral).

In our problem, quantifying a risk encountered by choosing an element inspection, for instance, might be done using the following formula in the decision tree:

$$RD = \sqrt{\sum_{l=1}^m (ci(r_l) - c)^2 P(r_l)} \quad (4.12)$$

where  $ci(r_l)$  is the cost of applying inspection  $i$  and obtaining the result  $r_l$ ,  $P(r_l)$  is the probability of obtaining the result  $r_l$ ,  $c = \sum_{l=1}^m ci(r_l) \times P(r_l)$  the expected cost and  $m$  the number of possible results.

## 4.4 Numerical Applications

For illustration purposes, the above proposed approach is applied on two types of structures: (i) a steel truss and (ii) a 4-story concrete frame.

### 4.4.1 Steel Truss

The case of a plane steel truss structure, representing one of the four faces of a hinged steel truss structure, is considered in this application (Figure 4.4). It is the same simply supported structure of the numerical application in Chapter 2, section 2.7.1.

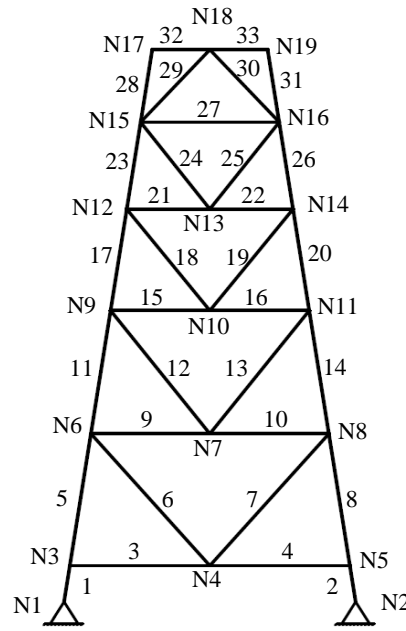


Figure 4.4: Simply supported steel truss structure.

The deterioration of the structural elements is assumed to be modelled by a Markov decision process having a yearly transition matrix  $\bar{D}$  as follows:

$$\bar{D} = \begin{bmatrix} 0.75 & 0.25 & 0 & 0 \\ 0 & 0.55 & 0.45 & 0 \\ 0 & 0 & 0.55 & 0.45 \\ 0 & 0 & 0 & 1 \end{bmatrix}$$

It is assumed that at the time  $t = 0$  all elements are defect free i.e. their discretized belief state is the probabilities vector  $[1 \ 0 \ 0 \ 0]$ . Using the SHM data, the proposed hybrid approach is automatically applied periodically (the time period is usually very short, its length depends on the structure type and use) to decide for the optimal inspection/action combination. In what follows, the proposed procedure is detailed for the structure at  $t=5$  years. The prior belief state, for each element, to be used as an input to the proposed decision analysis approach is then calculated as follows:

$$[1 \ 0 \ 0 \ 0] \times \begin{bmatrix} 0.75 & 0.25 & 0 & 0 \\ 0 & 0.55 & 0.45 & 0 \\ 0 & 0 & 0.55 & 0.45 \\ 0 & 0 & 0 & 1 \end{bmatrix}^5 = [0.237 \ 0.234 \ 0.269 \ 0.260]$$

In this example, element 8 is supposed to be damaged (with an axial rigidity decrease of 80%), but the structural manager is unaware of that damage. We assume that the element degradation may be due to corrosion and/or fatigue cracks causing a loss of the initial axial rigidity by a given percentage. The prior probability distribution of the degradation of all the elements is taken as a uniform distribution (i.e non informative). One horizontal accelerometer is placed on each level to monitor the structure (on nodes N5, N8, N11, N14, N16, N19). Measurement error is taken as a uniform random variable having a zero mean and a range equal to 0.15 m/s<sup>2</sup>.

The continuous damage space [0, 1] of each element is discretized into four ordinal states {1, 2, 3, 4} (refer Chapter 2, table 2.1).

It is assumed that three maintenance actions are available: (i) A0: ‘Do Nothing’ (*N*); (ii) A1 ‘Standard Repair’ (*SR*); (iii) A2: ‘Member Replacement’(*MR*). Their respective costs are 0, 2.6 and 9.5 monetary units (m.u = 1000 €). It is assumed, without any loss of generality, that the costs of the maintenance actions do not depend on the structural element. The transition matrices (T.M.) related to these maintenance actions are as following:

$$\bar{\bar{A}}_0 = \begin{array}{c|cccc} \theta^e & 1 & 2 & 3 & 4 \\ \hline 1 & 1 & 0 & 0 & 0 \\ 2 & 0 & 1 & 0 & 0 \\ 3 & 0 & 0 & 1 & 0 \\ 4 & 0 & 0 & 0 & 1 \end{array} \quad \bar{\bar{A}}_1 = \begin{array}{c|cccc} \theta^e & 1 & 2 & 3 & 4 \\ \hline 1 & 1 & 0 & 0 & 0 \\ 2 & 0.6 & 0.4 & 0 & 0 \\ 3 & 0.2 & 0.6 & 0.2 & 0 \\ 4 & 0.1 & 0.2 & 0.5 & 0.2 \end{array} \quad \bar{\bar{A}}_2 = \begin{array}{c|cccc} \theta^e & 1 & 2 & 3 & 4 \\ \hline 1 & 1 & 0 & 0 & 0 \\ 2 & 1 & 0 & 0 & 0 \\ 3 & 1 & 0 & 0 & 0 \\ 4 & 1 & 0 & 0 & 0 \end{array}$$

T.M. for ‘Do Nothing’

T.M. for ‘Standard Repair’

T.M. for ‘Member Replacement’

The costs of two inspection techniques are presented in table 4.1. The uncertainties associated with the results of the inspection techniques  $i_1$  and  $i_2$  are expressed by the probability distributions shown in Tables 4.2 and 4.3. User costs  $cs(\theta^e)$  due to the degraded performance of the structure are presented in Table 4.4. The user costs are assumed to be the same for all the elements. The optimization calculations were done using a specifically developed modal analysis library, based on finite element approach, that we integrated in our Bayesian update procedure.

Table 4.1: Inspection techniques costs.

Cost of inspection $i_1$ (m.u.)	Cost of inspection $i_2$ (m.u.)
7	3

Table 4.2: Uncertainties of inspection 1 results given the true state  $P(r_m|\theta^e, i_1)$ .

$\theta^e$	$r_1$	$r_2$	$r_3$	$r_3$
1	1	0	0	0
2	0	1	0	0
3	0	0	1	0
4	0	0	0	1

 Table 4.3: Uncertainties of inspection 2 results given the true state  $P(r_m|\theta^e, i_2)$ .

$\theta^e$	$r_1$	$r_2$	$r_3$	$r_4$
1	1	0	0	0
2	0.2	0.8	0	0
3	0	0.2	0.6	0.2
4	0	0	0.2	0.8

Table 4.4: User costs.

$\theta^e$	$cs(\theta^e)$ (in m.u.)
1	1
2	7
3	15
4	23

At any given point in time, the SHM system is providing the manager with Probability Density Functions (PDF) about the degradation state of each element. Based on these PDFs, the manager has to decide, using a decision tree, whether to do nothing, to perform an inspection on one or several elements or to make an optimal action on each one of the elements. If an inspection is performed, then, based on the updated PDF for each element, the manager has to run the decision tree again. This procedure is repeated until, based on the last updated PDFs, the optimal action would be to do nothing for all the elements.

Based on the modal parameters  $(\bar{\lambda}^{Md}, \bar{\Phi}^{Md})$  calculated from sensor readings for the intact and damaged structure, respectively, the Bayesian update procedure is applied for the two cases. Running this update, empirical posterior PDFs are obtained for each element in each case. Some of the resulting discretized PMFs are presented in table 4.5a for both cases. Figure 4.5 a-d represents, for the damaged structure, the probabilities of the elements being in each condition state according to SHM data only. One can notice that even for the intact structure, some uncertainty veils the true values. This is due to the measurement errors, the fact that only a subset of degree of freedoms are measured, etc. These PMF are considered as the initial belief state of the structure to be used as an input to the decision tree analysis. In table 4.5b, the updated discretized PMFs of the same elements of table 4.5a are presented, for the damaged structure, after having inspected element 8. Figure 4.6 a-d represents the

probabilities of all the elements being in each condition state taking into consideration the results of the inspection technique  $i_2$ .

Table 4.5a: Discretized belief states of elements 1-10 in the intact and damaged structures.

Element \ $P(\theta^e = i)$	Intact Structure				Damaged Structure			
	$i = 1$	$i = 2$	$i = 3$	$i = 4$	$i = 1$	$i = 2$	$i = 3$	$i = 4$
1	0.98	0.015	0.005	0	0.793	0.2	0	0.007
2	0.999	0.001	0	0	0.8	0.2	0	0
3	0.997	0.002	0.001	0	0.75	0.2	0	0.05
4	0.988	0.005	0.006	0.001	0.793	0.2	0	0.007
5	0.986	0.01	0.003	0.001	0.55	0.15	0	0.3
6	0.989	0.008	0.003	0	0.8	0.2	0	0
7	0.99	0.007	0.002	0.001	0.798	0.2	0.002	0
8	0.988	0.009	0.002	0.001	0.3	0.09	0.01	0.6
9	1	0	0	0	0.8	0.2	0	0
10	1	0	0	0	0.8	0.2	0	0

Table 4.5b: Discretized belief states of elements 1-10 in the damaged structure after having inspected element 8 using inspection technique  $i_2$ .

Element \ $P(\theta^e = i)$	Damaged Structure			
	$i = 1$	$i = 2$	$i = 3$	$i = 4$
1	0.993	0.005	0.002	0
2	0.999	0.0009	0.0001	0
3	0.997	0.002	0.001	0
4	0.993	0.005	0.0015	0.0005
5	0.997	0.002	0.001	0
6	0.994	0.004	0.002	0
7	0.999	0.0005	0.0005	0
8	0	0	0	1
9	1	0	0	0
10	1	0	0	0

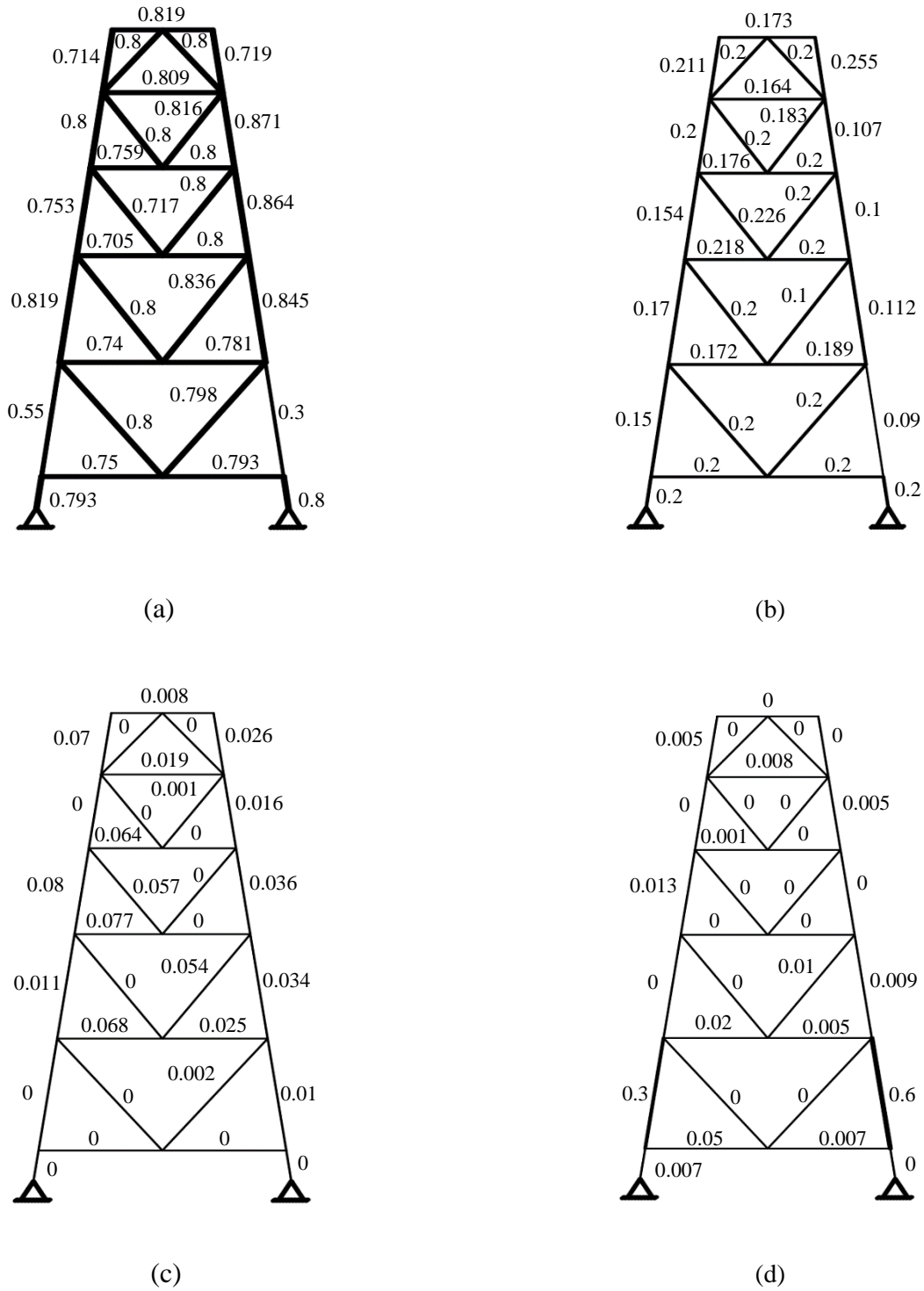


Figure 4.5: Probabilities of the elements being in: (a) condition state 1, (b) condition state 2, (c) condition state 3 and (d) condition state 4, according to SHM only data.



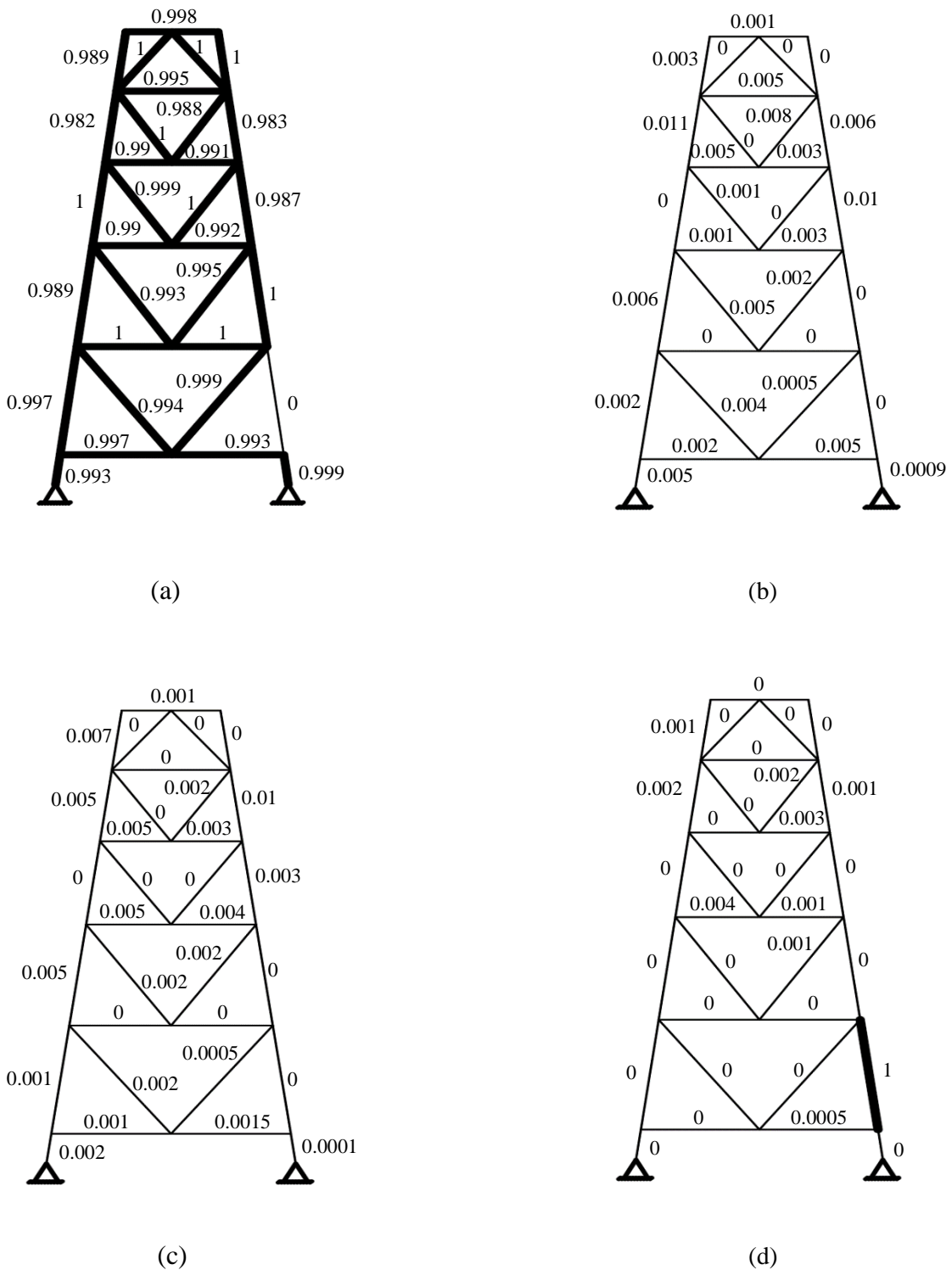


Figure 4.6: Probabilities of the elements being in: (a) condition state 1, (b) condition state 2, (c) condition state 3 and (d) condition state 4, according to SHM and inspection data (inspection  $i_2$ ).

In our case, the optimal decision consists of first inspecting element 8 (Figure 4.4) using inspection technique  $i_2$  (Figure 4.8). Even though inspection technique  $i_1$  is more precise than inspection technique  $i_2$ , its higher value of information does not compensate for the added cost. Hence, the total expected costs for inspection techniques 1 and 2, in the case of element 8, are respectively 47.46 m.u. and 43.32 m.u. Depending on the inspection results, the optimal maintenance actions prescribed for the elements are stated in table 4.6. Table 4.6 gives the probabilities of the inspection results of element 8 (each result corresponding to a possible condition state) and the corresponding optimal maintenance actions to be done on all the elements.

Table 4.6: The optimal actions to be done on each element after having inspected element 8 using inspection technique  $i_2$ .

$r_l$	$P(r_l)$	Total cost (m.u.)	Optimal actions on elements		
			1 to 7	8	9 to 33
$\theta^e=1$	0.318	35.78	<i>N</i>	<i>N</i>	<i>N</i>
$\theta^e=2$	0.074	40.73	<i>N</i>	<i>SR</i>	<i>N</i>
$\theta^e=3$	0.126	44.86	<i>N</i>	<i>MR</i>	<i>N</i>
$\theta^e=4$	0.482	42.06	<i>N</i>	<i>MR</i>	<i>N</i>

Table 4.7: The optimal actions to be done on each element without any inspection.

Total cost (m.u.)	Optimal actions on elements				
	1 to 4	5	6-7	8	9 to 33
51.81	<i>N</i>	<i>MR</i>	<i>N</i>	<i>MR</i>	<i>N</i>

In table 4.7, the optimal maintenance actions to be applied on elements and the corresponding total cost are given for the case where we rely solely on the SHM monitoring.

As can be noticed in tables 4.5a, element 8 is most probably in state 4 which meets our expectations, since element 8 is assumed to have lost 80% of its initial rigidity (which is unknown in a real problem). However, the probability of element 8 being in state 1 is relatively high (equal to 0.3). The same case presents itself for element 5 which is in a good condition but the probability of that element being in state 4 is also equal to 0.3. This is due to the fact that the influence of the stiffness of elements 5 and 8, on certain mode shapes, are approximately similar. Yet, after having inspected element 8, one can notice that the result probabilities of element 5 have been updated to more accurate values, and its probability of being in state 4 has decreased to zero (Table 4.5b & figure 4.7). These results are obtained by assuming that the inspection of element 8 revealed that it is in state 4 ( $\theta^e=4$ ). Therefore, it

can be concluded that substantial savings can be accomplished by updating the PDF of some of the non-inspected elements (i.e. some of the elements for which the belief states obtained by ABC only were significantly uncertain) based on the information acquired for a given element. Hence, the value of information gained by applying an inspection on a given element is far greater than the savings earned by optimizing the IM&R for that element alone.

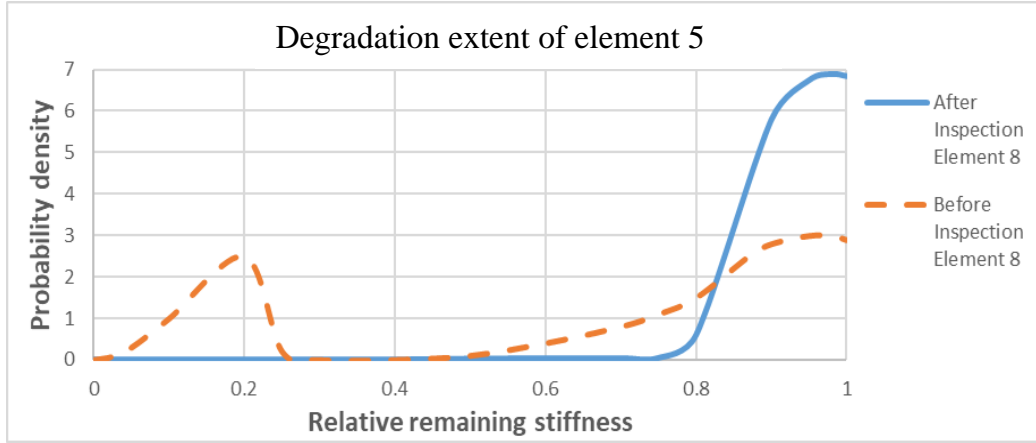


Figure 4.7: Degradation extent of element 5 before and after having inspected element 8 ( $r_l: \theta^e=4$ ).

Comparing results in tables 4.6 and 4.7, one can see the importance of applying a decision analysis taking into consideration element inspections. Allowing for an inspection reduces the expected cost by 8.49 m.u. (from 51.81 m.u. to 43.32 m.u.).

The accuracy of the proposed method is also shown in the optimal actions prescribed for element 8, depending on the inspection outcomes. When moving from one state to a better one, the actions are becoming less severe and less costly, which means that there is generally a good correlation between the state of the element and the actions to be done. Even though the prescribed actions are the same for the last two states, an inspection outcome stating that element 8 is in state  $\theta^e=4$  would cost less. This is due to the fact that, according to the hypothesis, element 8 is in state  $\theta^e=4$ . Hence, when the inspection outcome of element 8 describe the actual damage, the PDF curves of the other elements will become less uncertain after rerunning the ABC algorithm. This decrease in uncertainty will increase the probability of elements being in their actual state and therefore, decrease the total cost.

As for the optimal actions to be done on the elements after their PDFs have been updated based on the results of the inspection of element 8, the optimal decision for all the elements is to do nothing except for element 8 which should be repaired, replaced or kept as it is accordingly.

According to tables 4.5a, element 8 has a probability of 0.6 being in state 4 and a probability of 0.3 being in state 1. If one decides that element 8 is damaged, then there is a chance (probability of 0.3) of a false positive conclusion. A simulation of such a case is done by assuming that a perfect inspection is done on element 8 and revealed that its condition state is 1. As prescribed by the proposed methodology, the results of the inspection are imposed on the ABC algorithm which is subsequently rerun. The updated belief states indicate an increase

in the probability of element 5 being in state 4 from 0.3 to 0.61. In this case, a second inspection is prescribed for element 5.

If on the other hand a perfect inspection is initially done on element 5 (which has, according to table 4.5a, a probability of 0.3 being in state 4) and the result revealed that the element is not damaged, the updated belief states of the remaining elements indicate an increase in the probability of damage of element 8 from 0.6 to 0.72.

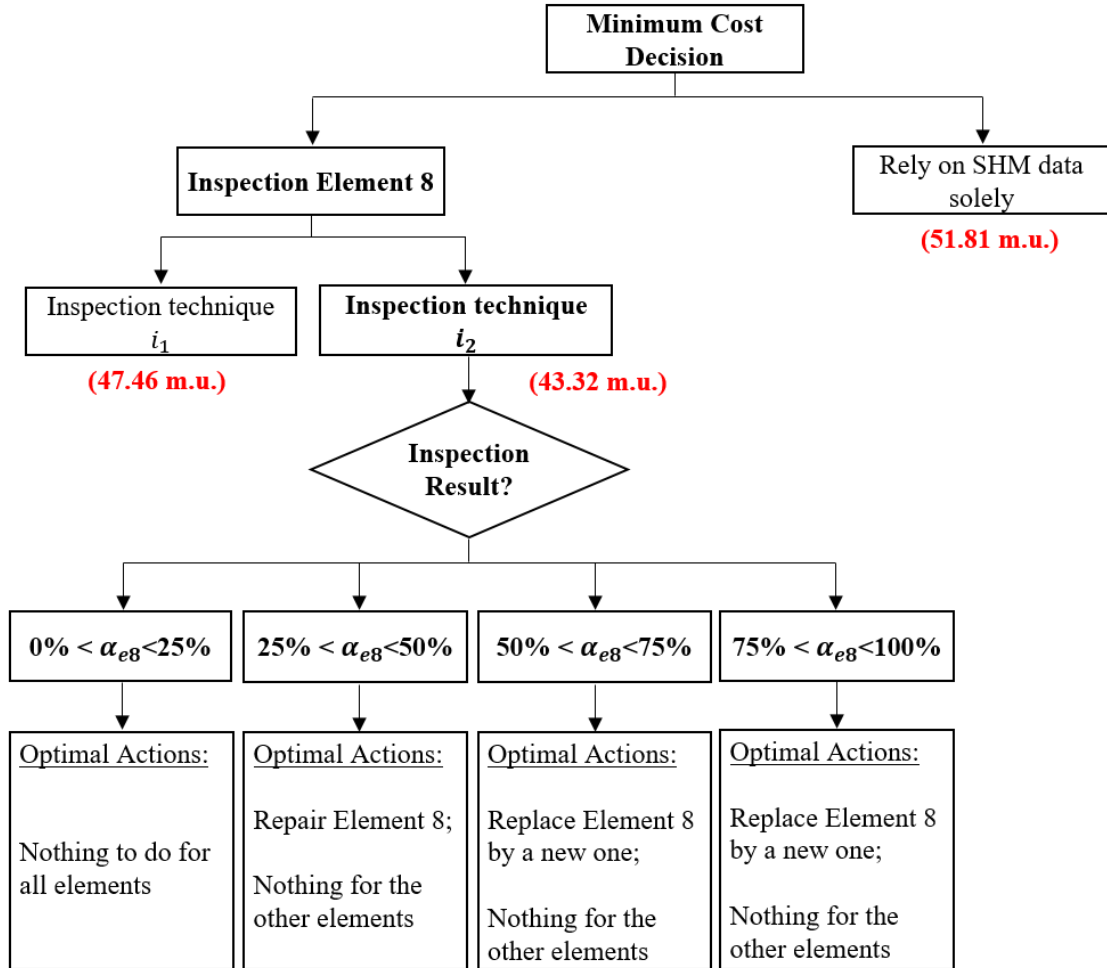


Figure 4.8: Flowchart of the minimum cost decision.

Finally, in order to show the capability of the proposed methodology in detecting small damage as well, a case is considered where the bracing element 13 has lost 20% of its initial stiffness. The degradation extent of element 13 based on SHM only data is shown in figure 4.9. For illustration purposes, the degradation extent is represented using the PDF of the remaining stiffness (relative to the initial stiffness). The most probable degradation extent value is represented by the shift of the curve's peak from the value 1 since a degradation is defined by a loss of stiffness. As can be noticed, the proposed approach is quite sensitive even for small damage extents. However, since the damage is not large, the resulting optimal

IM&R decision consists of doing nothing which means that no inspection nor actions are needed.

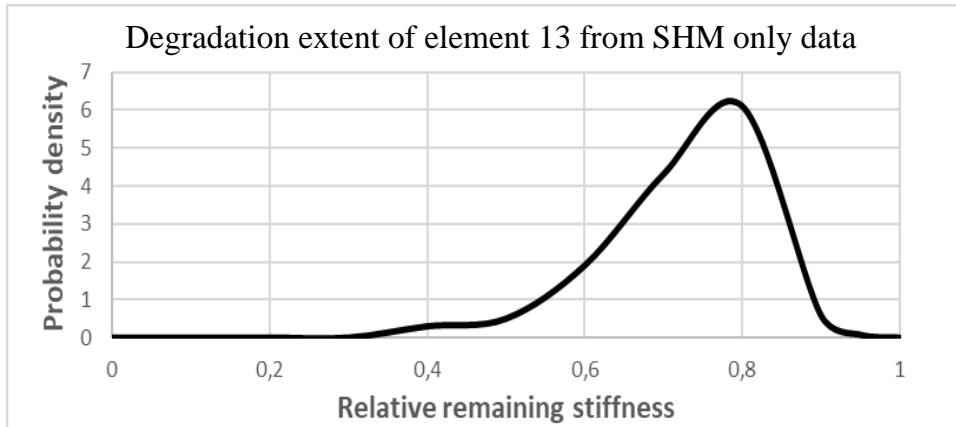


Figure 4.9: Degradation extent of element 13 according to SHM only data.

#### 4.4.2 Multistory Concrete Frame

A second application is presented herein for a different type of structure and material: The same 4-story simply supported concrete frame structure presented in Chapter 2, section 2.7.2 (Figure 4.10).

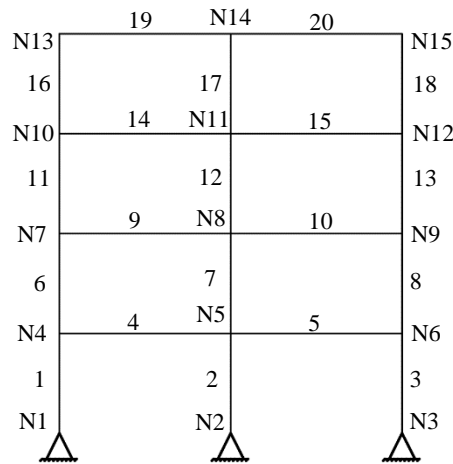


Figure 4.10: Simply supported concrete frame structure.

As described in the previous example, the deterioration of the structural elements is supposed to be modelled by a Markov decision process and the proposed procedure is detailed for the structure at  $t=5$  years.. In this numerical application, it is assumed that elements 1 and 10 are damaged with a rigidity decrease of 40% and 25%, respectively, but they have not been detected yet. For the manager, the prior distribution of the potential degradation of all the elements is taken as a uniform distribution (i.e non informative). Three horizontal accelerometers are used to monitor the structure on the nodes N4 in the first story, N9 in the

second story and N13 in the last story. Measurement error is taken as a uniform random variable having a zero mean and a range equal to  $0.15 \text{ m/s}^2$ .

A decision must be taken whether to perform an inspection on one or several elements of the structure or to make an action on each one of the elements. The obtained optimal policy will prescribe, after each element inspection, whether to inspect another element (and which one?) or whether to apply maintenance actions for all elements (i.e. which is the optimal maintenance action for each element) based on the updated PDF obtained by the SHM system. The decision tree is then run as many times as needed until the optimal action consists of doing nothing for all the elements.

Three maintenance actions can be performed on the elements: (i) A0: ‘Do Nothing’ ( $N$ ) which cost is 0; (ii) A1 ‘Standard Repair’ ( $SR$ ) with a cost of 1.8 monetary units (m.u.=100 €) and (iii) A2: ‘Member Replacement’( $MR$ ) which costs 6.2 m.u. The transition matrices (T.M.) related to these maintenance actions are as following:

$$\bar{A}_0 = \begin{array}{c|cccc} \theta^e & 1 & 2 & 3 & 4 \\ \hline 1 & 1 & 0 & 0 & 0 \\ 2 & 0 & 1 & 0 & 0 \\ 3 & 0 & 0 & 1 & 0 \\ 4 & 0 & 0 & 0 & 1 \end{array} \quad \bar{A}_1 = \begin{array}{c|cccc} \theta^e & 1 & 2 & 3 & 4 \\ \hline 1 & 1 & 0 & 0 & 0 \\ 2 & 0.6 & 0.4 & 0 & 0 \\ 3 & 0.1 & 0.6 & 0.3 & 0 \\ 4 & 0 & 0.1 & 0.6 & 0.3 \end{array} \quad \bar{A}_2 = \begin{array}{c|cccc} \theta^e & 1 & 2 & 3 & 4 \\ \hline 1 & 1 & 0 & 0 & 0 \\ 2 & 1 & 0 & 0 & 0 \\ 3 & 1 & 0 & 0 & 0 \\ 4 & 1 & 0 & 0 & 0 \end{array}$$

T.M. for ‘Do Nothing’

T.M. for ‘Standard Repair’

T.M. for ‘Member Replacement’

Two imperfect inspection techniques, presented in table 4.8, are compared and the one providing the highest value of information is chosen by the decision tree. The uncertainties associated with the results of the inspection techniques  $i_1$  and  $i_2$  are expressed by the probability distributions shown in Tables 4.9 and 4.10. And the user costs  $cs(\theta^e)$ , which are assumed to be the same for all the elements, are presented in Table 4.11.

Table 4.8: Inspection techniques costs.

Cost of inspection $i_1$ (m.u.)	Cost of inspection $i_2$ (m.u.)
2.5	1.6

Table 4.9: Uncertainties of inspection 1 results given the true state  $P(r_m|\theta^e, i_1)$ .

$\theta^e$	$r_1$	$r_2$	$r_3$	$r_4$
1	1	0	0	0
2	0.1	0.8	0.1	0
3	0	0.1	0.8	0.1
4	0	0	0.1	0.9

Table 4.10: Uncertainties of inspection 2 results given the true state  $P(r_m|\theta^e, i_2)$ .

$\theta^e$	$r_1$	$r_2$	$r_3$	$r_4$
1	0.9	0.1	0	0
2	0.2	0.7	0.1	0
3	0	0.2	0.6	0.2
4	0	0	0.3	0.7

Table 4.11: User costs.

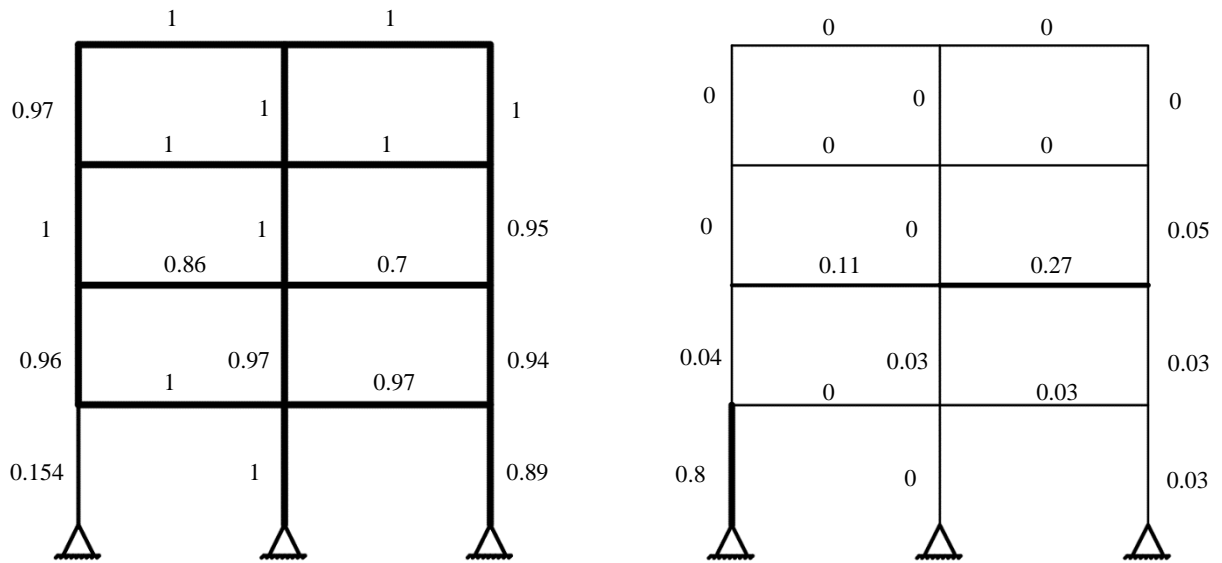
$\theta^e$	$cs(\theta^e)$ (m.u.)
1	1
2	5
3	11
4	18

The first two steps of the proposed method entail a Bayesian updating of the structure, which could be an intact or a damaged structure, and obtaining the posterior PDF for each element of the structure. These PDF can be discretized by calculating the PMF for each element, and will be considered as the initial belief state of the structure to be used as an input to the decision tree analysis. The updated discretized PMF for the intact and damaged structure before any inspection or maintenance action are presented in table 4.12. The outcome probabilities of the elements being in each condition state  $\theta^e$ , according to SHM only data are illustrated in figures 4.11 a-d.

Table 4.12: Discretized belief states of the elements in the intact and damaged structures.

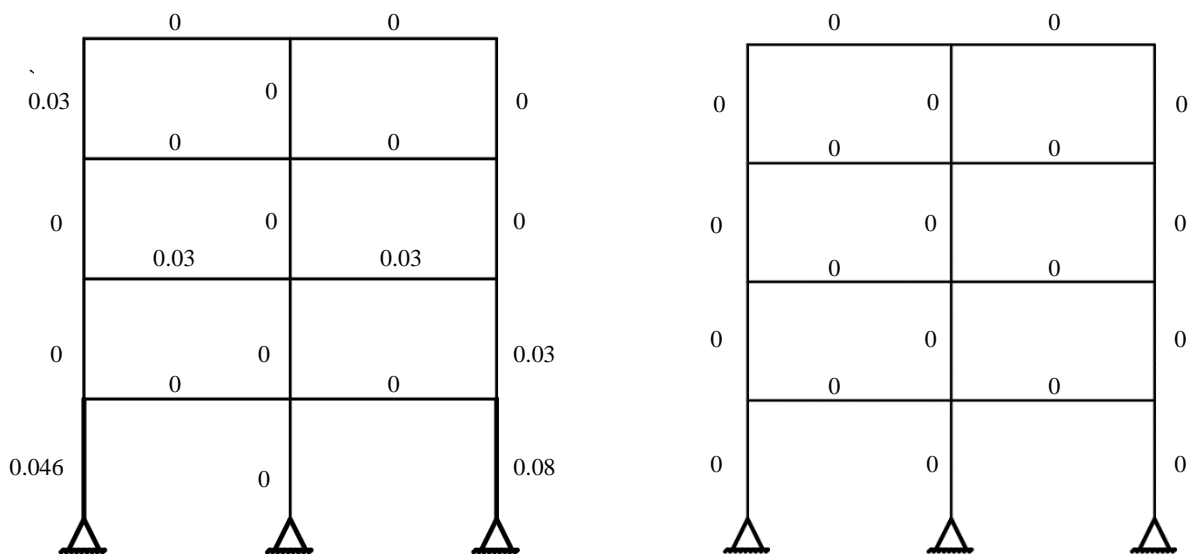
Element \ $P(\theta^e = i)$	Intact Structure				Damaged Structure			
	$i = 1$	$i = 2$	$i = 3$	$i = 4$	$i = 1$	$i = 2$	$i = 3$	$i = 4$
1	0.997	0.003	0	0	0.154	0.80	0.046	0
2	0.989	0.011	0	0	1	0	0	0
3	0.99	0.01	0	0	0.89	0.03	0.08	0
4	0.995	0.005	0	0	1	0	0	0
5	0.964	0.034	0.002	0	0.97	0.03	0	0
6	0.984	0.014	0.002	0	0.96	0.04	0	0
7	0.998	0.002	0	0	0.97	0.03	0	0
8	0.982	0.018	0	0	0.94	0.03	0.03	0
9	0.976	0.013	0.011	0	0.86	0.11	0.03	0
10	0.964	0.033	0.003	0	0.7	0.27	0.03	0
11	0.989	0.011	0	0	1	0	0	0
12	0.997	0.003	0	0	1	0	0	0
13	0.986	0.014	0	0	0.95	0.05	0	0
14	0.982	0.015	0.003	0	1	0	0	0
15	0.985	0.014	0.011	0	1	0	0	0
16	0.999	0.001	0	0	0.97	0	0.03	0
17	0.995	0.005	0	0	1	0	0	0
18	0.995	0.005	0	0	1	0	0	0
19	0.998	0.002	0	0	1	0	0	0
20	0.999	0.001	0	0	1	0	0	0





(a)

(b)



(c)

(d)

Figure 4.11: Probabilities of the concrete elements being in: (a) condition state 1, (b) condition state 2, (c) condition state 3 and (d) condition state 4, according to SHM only data.

In this example, the optimal decision consists of directly applying maintenance actions on the elements, depending on the SHM results only and without any inspection (Figure 4.13). As one can notice in table 4.13, the optimal maintenance actions to be done on the elements are: (i) repairing element 1 and (ii) doing nothing on the remaining elements. The corresponding total cost is 27.97 m.u. Looking at table 4.12, the state of element 1 belongs, most probably, to the category 2 where the damage affects 25% to 50% of the initial state of the element while the other elements are in a good condition. These probabilities justify the obtained optimal decision actions. They were also in line with our hypothesis except for the element 10 which is assumed to have lost 25% of its initial rigidity.

Table 4.13: The optimal actions to be done on each element without any inspection.

Total cost (m.u.)	Optimal actions on elements	
	1	2 to 20
27.97	<i>SR</i>	<i>N</i>

The state of element 10 is on the limit between the states 2 and 4. Its damage is also considered as a relatively small damage on a structural element (a beam) not affecting much the dynamic response of the structure. However, even though table 4.12 shows that this element is probably in state 1, its probability of being in state 2 is to be considered (equal to 0.27). The degradation extent of element 10 calculated according to the SHM only data, before and after having repaired element 1, is presented in figure 4.12. For illustration purposes, the degradation extent will be represented in the following graphs using the PDF of the remaining stiffness (relative to the initial stiffness). The most probable degradation extent value is represented by the shift of the curve's peak from the value 1 due to the fact that, in our case, a degradation is defined by a loss of stiffness. Comparing the PDFs of both elements before any maintenance action is applied, one can notice that the PDF of element 1 gives more precise information about its state (having a peak at around 0.6) than gives the PDF of element 10 about its condition state (the curve being more flattened). Yet, after the standard repair was applied to element 1 and the SHM has been updated accordingly, it is clearly shown that the PDF of element 10 has been highly improved presenting a peak at the value 0.8. Even if the peak does not coincide exactly with the value 0.75 due to uncertainties, it is still an indication that the corresponding element is somewhat damaged and has lost around 20% of its initial rigidity. Therefore, the chosen optimal maintenance action led to more accurate results concerning elements where no maintenance action has been applied.

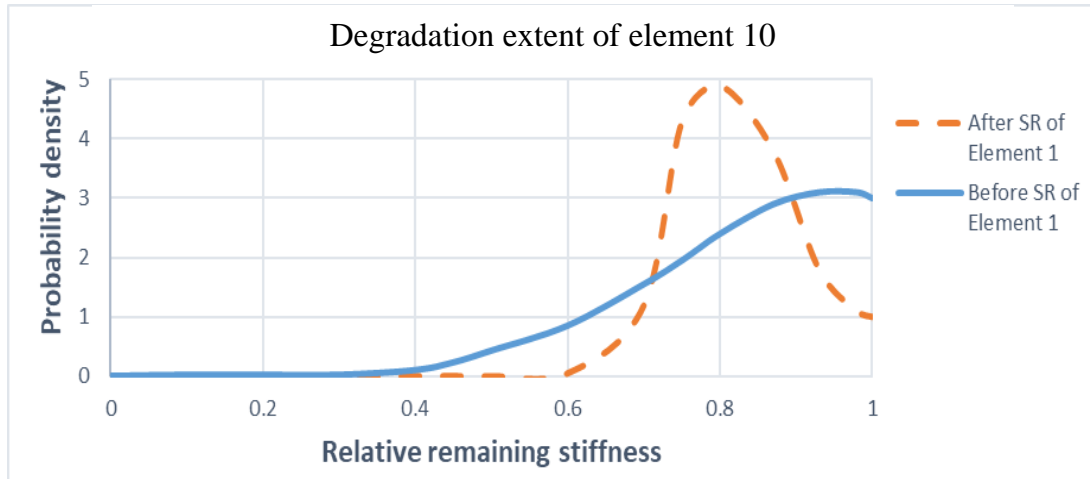


Figure 4.12: Degradation extent of element 10 according to SHM only data, before and after the repair of element 1.

On the other hand, in order to compare both choices of decisions (inspection or maintenance actions), table 4.14 presents the optimal actions to be done on all the elements if element 1 has been inspected, with the corresponding probabilities of inspection result. As it was concluded in the first example, the state of the element and the prescribed actions are well correlated since the severity of actions decreases when condition states are better. The prescribed maintenance actions when the results of the inspection revealed that element 1 is in state 2 (the most probable case) are the same as the ones prescribed by the SHM only data. Hence, in our case, there is no need for an inspection and one can rely solely on the SHM data. There is a slightly difference in the total costs of both decisions in favour of the SHM only, the costs being 27.97 m.u. for the SHM only and 28.8 m.u. when applying the inspection technique  $i_2$  to element 1.

The case of false positive conclusion can be observed in tables 4.12 and 4.14 for the category  $\theta^e=1$ . According to table 4.12, there is a probability of 0.22 for element 1 being in state 1 which could induce a false positive conclusion. Looking at the first row of table 4.14, the total cost incurred when element 1 is inspected and diagnosed as being in state 1 is relatively high compared to the remaining states even though no maintenance action is to be done on any element. This is because of the PDF curves of some elements becoming more flattened when rerunning the ABC algorithm and therefore, the relatively high cost is due to the increase of the probability of some elements being in more severe states which are affected by the user cost.

Table 4.14: The optimal actions to be done on each element after having inspected element 1 using inspection technique  $i_2$ .

$r_l$	$P(r_l)$	Total cost (m.u.)	Optimal actions on elements	
			1	2 to 20
$\theta^e=1$	0.298	29.87	$N$	$N$
$\theta^e=2$	0.585	25.58	$SR$	$N$
$\theta^e=3$	0.108	30.86	$MR$	$N$
$\theta^e=4$	0.009	N/A	$N/A$	$N/A$

Both inspection techniques have been also evaluated in this study for the inspection of element 1. The total expected costs for inspection techniques 1 and 2 are respectively 29.9 m.u. and 28.8 m.u. Thus, inspection technique  $i_2$  is more cost-effective than inspection technique  $i_1$  even though the latter is more accurate and gives more precise results. These results show, once again, that the extra cost paid for the accuracy of the technique are not worth the added value of information it provides.

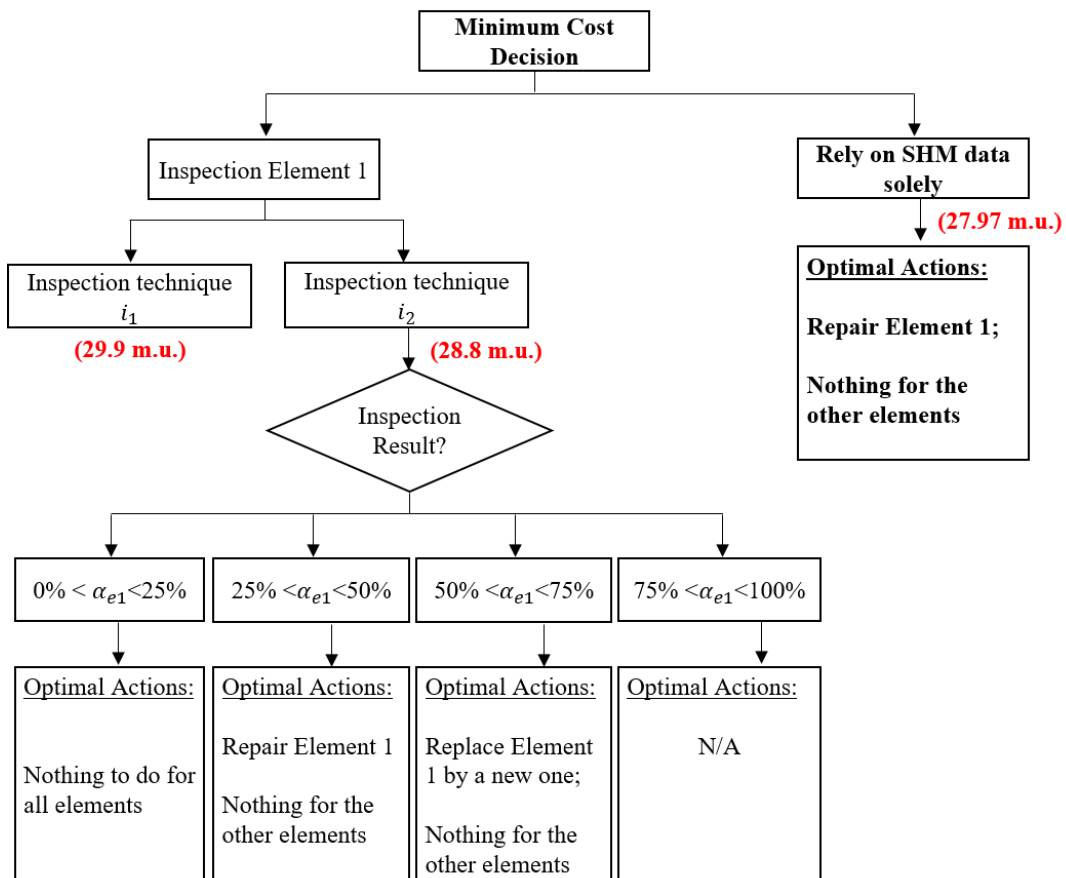


Figure 4.13: Flowchart of the minimum cost decision.

## 4.5 Conclusion

In this chapter, a hybrid inspection-monitoring approach is proposed for the optimal maintenance planning of civil engineering structures. A Bayesian procedure is applied for updating the probability density functions of the damage extent in structural elements based on data produced by a global permanent SHM system. This updating procedure is then integrated in a decision analysis framework, in order to decide whether further inspections are warranted on some elements of the structure. The methodology allows the decision maker to optimally choose the elements needing further inspections and to optimally decide for the appropriate inspection technique. The final step of the proposed methodology is the prescription of the optimal maintenance actions to be applied for each element of the structure. The applicability and advantages of the proposed methodology were demonstrated through two numerical applications for a steel truss structure and a 4-story concrete frame structure. Results showed that for some cases such structures with limited number of elements, one can rely on the data coming from the SHM only whereas for big and/or complex structures, it is often important to inspect one or more elements and combine results coming from both sources to achieve more precise results that reflects the real condition state of the structure.

The rationale behind this approach is that: (i) it allows the decision maker to combine different sources of information to reduce the uncertainty veiling the true damage extent; (ii) it takes into account the preference of the decision maker (i.e. attitude toward false alarms and false negatives); (iii) the shortcomings and the advantages of using classical inspection monitoring are generally different from those of SHM only approaches, therefore the integration of the two approaches is advantageous.

## Chapter 5: A predator-prey optimization for optimal sensor placement

### 5.1 Overview

Monitoring a structure to predict the condition states of its elements requires three main steps: (i) sensor implementation, (ii) data processing and (iii) structural health assessment. In general, it is believed that the accuracy of the results increases with the number of implemented sensors. This would involve a very large number of sensors in the SHM system of a structure which is not only constrained by the high cost of sensors and their maintenance, but also turns the data processing into a challenging task. This is the case of the TsingMa Bridge where a total of 786 sensors are permanently implemented and perform continuously (Dongsheng 2011; Ko et al. 2001). In most of the cases, the number of sensors to be installed is limited, mostly due to the cost constraint. In such cases, sensors used to be installed based on a past experience, past knowledge on the vibration of a structure and/or some empirical methods. However, for large and complex structures, determining the optimal locations of sensors can be hardly based solely on experience. Thus, it is important to develop methodologies for finding the optimal sensors configuration, i.e. optimal location and number, so that data acquired could lead to an accurate identification of the structural characteristics. Structural degradation would then be inferred based of the drift of the measured characteristics away from reference values calculated for undamaged structure.

Among the sources of uncertainty which result from the inverse problem of modal analysis, one can distinguish the measurement errors and the signal processing errors. Hence, the need to choose sensor configuration which maximizes the signal / noise ratio. While real civil engineering structures have infinitely many degrees of freedom, only a finite number of measurements could be practically available. Over the past two decades, the problem of optimizing sensor configuration for structural health monitoring has been the subject of many researchers (Tan and Zhang 2019; Sun and Büyüköztürk 2015; Papadimitriou 2004, 2012; Kammer 1991). Genetic optimization is receiving increased emphasis due to its capability to deal with high-dimensional complex problems. He et al. (2015) introduced a modified MAC function, created an adaptive adjustment process to the crossover and mutation function and integrated them in a GA procedure for optimal sensor placement. Zhou and Wu (2017) adopted the GA for the optimization of the location of strain gauges to evaluate the structural performance for large structures with high number of degrees of freedom. Su et al. (2019) proposed a “partitioned genetic algorithm” for high-piled wharf structures, to optimize initially partitioned measurement points in different areas of the structure (superstructure and piles) to increase the local search capability.

Genetic algorithms have therefore proved to be very efficient for solving complex problems with a rapid convergence, a great adaptability and without the need of calculating the derivative of an objective function to find a solution to the optimization problem.

However, GAs are sometimes subject to premature convergence on a local optimum. Several techniques might be used to avoid or minimize this shortcoming. A commonly used technique is to launch several runs and choose the best solution among the obtained suboptimal solutions. In addition, most of the researchers dealt with specific damage configurations or worked on maximizing the linear independence of the modal information in the initial structure. However, for real world civil engineering structures, optimal sensor configurations must be able to accurately identify most of the possible future damage scenarios.

Damage do not affect the mode shapes in the same way and at the same dof. Depending on the location and severity of a damage, its effect on mode shapes could differ (in terms of values and affected dofs). The accuracy of a damage assessment depends therefore on the sensor configuration. Hence, an optimal sensor configuration found for a specific damage configuration could not be optimal for other damage configurations. Some damage might even remain undetectable. For this reason, one should search for the sensor configuration that is able to detect as much damage configurations as possible for future assessment. Also, the optimal sensor configuration should be able to prioritize the detection of critical and costly damage.

This chapter, presents a novel methodology based on a genetic algorithm of type Predator-Prey with a Bayesian updating of the structural parameters. Starting with two initial populations representing the damage (prey) and the sensors (predator), both populations evolve through a genetic algorithm in order to find the optimal configuration of sensors, in terms of number and location. The main strength of this optimization is its capability to minimize the number of sensors and find their optimal location while maximizing the probability of detecting damage.

The present chapter is structured as follows. First, the concept of Predator-Prey relationship is presented. The Genetic Algorithm steps are then stated and described in section 5.3 starting from an initial population to the creation of a new population better than the previous one. This section is followed by the description of the methodology consisting of a predator-prey GA optimization which incorporates an imposed diversification scheme that will be discussed in section 5.5. The effectiveness of the algorithm is investigated, in the last section, through two numerical applications.

## **5.2 Predator-Prey Relationship**

The predator-prey relationship is a bilateral relationship corresponding to an antagonist interaction beneficial for the predator and detrimental for the prey. While predators evolve by improving their ability to chase the preys, the latter evolve by improving their ability to escape the predators. This type of interaction is found in several ecosystems and has been the subject of theoretical modeling (Abrams 2000; Kuno 1987).

Predation of one species by another can regulate the dynamics of the population consumed, and thus reduce the development and survival of the prey species. Preys also have an impact on the predator population. If abundance of preys is no longer sufficient to keep

predators alive, the rate of increase of predators will then decrease. Thus, the availability of preys strongly impacts the predation rate and the development of predators.

This type of interaction can be used not only in ecology but also in optimization. It helps in reaching the global optimal solution and not being trapped in a local solution (Higashitani et al. 2006). In the proposed methodology, we shall not consider the two above-mentioned characteristics of the predator-prey algorithm, i.e. population size dynamics will not be taken into account in the sense that the size of each of the co-evolving populations is constant. The fitness of sensor configurations (predators) is solely based on their ability to detect, locate and quantify damage modes (preys).

In what follows, the relationship between sensors and damage is modeled by a predator-prey behavior. Mimicking the natural evolution in the wild life, one could consider a sensor configuration as a predator and a damage configuration as a prey which co-evolve in a genetic optimization framework. The aim of the evolution of defect configurations (preys) is to evade sensor configurations (predators), while the aim of the predators' evolution is to increase their ability to detect the preys.

### 5.3 Genetic Algorithm steps

A genetic algorithm implements a schematic version of the mechanisms of biological evolution and is defined essentially by four basic elements: the individuals (chromosomes), population, environment and fitness function. The general idea and steps of a traditional genetic algorithm are described in Chapter 1, section 1.5.3. In the following sections, we detail the steps of the GA corresponding to the proposed methodology.

#### 5.3.1 Initialization

The first step in the genetic algorithm problem consists in mapping the possible states of the optimization variable to an adequate coding scheme. A population of coded solutions (chromosomes) is then randomly created. In our case, this step requires the creation of two populations which will co-evolve: a population “ $P_{sensors}$ ” representing a random set of sensor configurations and a population “ $P_{defects}$ ” representing a random set of defects configurations.

$P_{sensors}$  is made of chromosomes having a size equal to the number of degrees-of-freedom. These chromosomes are binary code so the value of the genes can be either 0 or 1. The value 1 means that a sensor is monitoring the correspondent degree-of-freedom (DOF) and therefore, the non-measured DOF is represented by the value 0. Here is an example of a chromosome of  $P_{sensors}$ :

$$Ch_{sensors}: \quad \boxed{0} \boxed{0} \boxed{1} \boxed{0} \boxed{1} \boxed{0} \boxed{0} \boxed{0}$$

This code, for instance, represents a structure with eight DOFs in total where the third and fifth ones are observed by sensors.



$P_{defects}$  is a population where each chromosome has a size equal to the number of elements in the structure. A real coded chromosome is used in this population where a gene takes a real value between 0 and 1, representing the extent of the defect for a particular element. Thus, a defect gene with the value of 1 means that the element has conserved the integrity of its initial rigidity while a value of 0 means that it has lost all its rigidity. The following coding is an example of a chromosome of  $P_{defects}$ :

$$Ch_{defects}: \quad \boxed{0.43} \quad \boxed{0.8} \quad \boxed{0.95}$$

This code means that we are in presence of a structure with three elements having lost 57%, 20% and 5% of their initial rigidity, respectively.

### 5.3.2 Evaluation (Fitness function calculation)

Each chromosome provides a potential solution to the problem. It is the fitness function that assesses the performance of each individual to allow the algorithm reaching the best solution. In the proposed predator-prey model, the GA seeks to optimize two fitness functions instead of using one fitness function (as in classical genetic optimization). It allows for a co-evolution of two types of populations: a population representing the configuration of sensors and acting like predators and another representing the configuration of defects and acting like preys. Both populations should therefore evolve antagonistically, each one according to a specific fitness function reflecting their “interests”. Nevertheless, the proposed methodology is not multi-objective. It has a unique objective aiming at improving the sensor configuration through the improvement of the damage configurations to increase the challenge on the sensor population. Hence, improving the damage configurations is a means to reach the best sensor configuration.

In what follows we adopt the mapping introduced in chapter 4 for the discretization of deterioration PDFs into belief state vectors  $\bar{v}$ . Sensor and defect fitness functions are defined using the following parameters:

- $n_c$ : number of installed sensors.
- $N_d$ : number of chromosomes in the defect population (i.e. possible configurations of defects).
- $c_c$ : sensor unit price.
- $\bar{v}$ : vector whose components are the belief states of the individual elements.
- ${}^*\bar{v}$ : vector whose components are the certain belief states of the individual elements.
- $C({}^*\bar{v})$ : cost induced by applying the optimal maintenance actions based on  ${}^*\bar{v}$ .
- $C_{IMP}({}^*\bar{v})$ : real cost induced by imposing the optimal actions obtained based on  $\bar{v}$  on the structure with certain belief states vector  ${}^*\bar{v}$ .

### 5.3.2.1 Sensor configuration fitness

The fitness of a sensor configuration  $s$  is defined as its ability to accurately identify, locate and evaluate as much damage configurations as possible. We define then the corresponding fitness  $f_s$  as the inverse of the following cost:

$$C_s = n_c \times c_c + \frac{\sum_{d=1}^{N_d} |C(*\bar{v}_d) - C_{s-IMP}(*\bar{v}_d)|}{N_d} \quad (5.1)$$

where  $*\bar{v}_d$  is the perfect information belief states vector calculated based on a defect configuration  $d$ . i.e. each component  $*v_d^e$  of  $*\bar{v}_d$  is a one-hot encoding vector whose components are all zeros except one representing the true condition state of element  $e$ .

Formally:

$$*v_{dj}^e = \begin{cases} 0 & \text{if } j \neq \text{true state of element } e \\ 1 & \text{otherwise} \end{cases} \quad (5.2)$$

The function  $C(*\bar{v})$  is a generic cost function resulting from a maintenance optimization methodology and taking as input the vector of certain belief states for each element of the structure. In the numerical application at the end of this chapter, we adopt as cost function, the decision tree approach presented in chapter 4. Hence,  $C(*\bar{v})$  is the cost incurred if we apply the optimal actions based on a perfect information.

$C_{IMP}(*\bar{v}_d)$  is the cost incurred if we apply the optimal maintenance actions, based on the imperfect information  $\bar{v}_d$ , on a structure with a true certain state  $*\bar{v}_d$ .

$\bar{v}_d$  is a vector whose components are the belief states, of the individual elements, calculated based on a defect configuration  $d$  and on the related measurements yielded by the sensors configuration using the ABC methodology described in chapter 2.

$$\text{i.e. each component of } \bar{v}_d \text{ is } v_d^e = [\text{Pr}(\theta^e = 1), \dots, \text{Pr}(\theta^e = m)] \quad (5.3)$$

where  $m$  is the number of possible condition states of element  $e$ .

If we assume the maintenance optimization methodology presented in chapter 4 where imperfect maintenance actions  $a^e \in A = \{a_0, a_1, \dots, a_a\}$  are described by square transition matrix  $\bar{A}^e$  where each element  $\bar{a}_{ij}^e$  corresponds to the probability that an element  $e$  moves from a state  $\theta^e$  to another after the application of  $a^e$ , and if we assume the following costs:

$ca(a^e)$ : cost of the action  $a^e$  applied on element  $e$ .

$cs(\theta^e)$ : cost suffered by the user of the structure due to element  $e$  being in state  $\theta^e$ .

Since this cost is included in the fitness functions of both populations, it can be used to take explicitly into account critical defects (i.e. severe defects) and critical elements (i.e. elements that are most likely to be deteriorated in the structure).

Then, the costs  $C(*\bar{v})$  and  $C_{IMP}(*\bar{v})$  will be:

$$C(*\bar{v}) = \sum_{e=1}^N \min_{a^e \in A} (c_a(a^e) + \sum_{j=1}^m (\sum_{k=1}^m c_s(\theta^e = k) \times a_{jk}^e) \times *v_j^e) \quad (5.4)$$

$$C_{IMP}(*\bar{v}) = \sum_{e=1}^N (c_a(a_{IMP}^e) + \sum_{j=1}^m (\sum_{k=1}^m c_s(\theta^e = k) \times a_{IMP-jk}^e) \times *v_j^e) \quad (5.5)$$

Equation (5.4) represents a decision tree without inspection (refer to chapter 4). i.e. we use a decision tree for the maintenance optimization for the uncertain case where the degradation PDFs represented by  $\bar{v}_d$  are obtained based on sensors measurements. These measurements are obtained by simulating the structural response (e.g. using FEM models). However, we stress the fact that the methodology introduced in this chapter, for sensor configuration optimization, is general and not constrained to using decision trees for cost calculation. One could, for example, include inspections in the decision tree calculations or use any other decision framework that can account for degradation uncertainty.

For the numerical application of this chapter, the used costs are defined by equations (5.4) and (5.5).

The costs  $C(*\bar{v})$  and  $C_{IMP}(*\bar{v})$  are then calculated following the below steps:

- 1- Define the vector of certain belief states  $*\bar{v}_d$  for each defect configuration  $d$  according to Eq. (5.2);
- 2- Using the M&R optimization described in Chapter 4 section 4.2.1, find the optimal actions based on  $*\bar{v}_d$  and calculate the cost  $C(*\bar{v}_d)$  according to Eq. (5.4). This is the cost of perfect information;
- 3- Apply a Bayesian updating to update the condition state of the structure based on each combination “*defect chromosome-sensor chromosome*”. Obtain for each combination the vector of belief states  $\bar{v}_d$ ;
- 4- Using the M&R methodology (as in step 2), find the optimal actions based on  $\bar{v}_d$  for each combination “*defect chromosome-sensor chromosome*”;
- 5- Suppose that the maintenance actions found in step 4 are applied on the structure with a certain belief state  $*\bar{v}_d$  and calculate  $C_{IMP}(*\bar{v}_d)$  according to Eq. (5.5). In this step we impose the maintenance actions optimized for imperfect information, on the structure with a perfect information and calculate the cost incurred.

The cost  $C_{IMP}(*\bar{v})$  is related to how much the obtained actions match the true state of the structure. i.e. when applying maintenance actions obtained by imperfect information on the true belief state,  $C_{IMP}(*\bar{v})$  tends to be higher if the imposed actions are not suitable to the states to which the elements belong. An example of such a case is prescribing a replacement, based on a sensor configuration, to an element which is in reality in good condition. Hence, the gap between the cost of perfect information  $C(*\bar{v})$  and the cost  $C_{IMP}(*\bar{v})$  quantifies the consequences of imperfect information. It is the cost of the lack of information. In terms of value of information (i.e.  $c_c=0$ ), the best sensor configuration is defined as the one minimizing

the most the gap between both costs. It is then the configuration that is able to identify the most possible defect configurations.

Hence, the cost of equation (5.1) is made up of two components: (i) the cost of the sensors; (ii) the added average cost due to a decision making process with imperfect information (the average is taken with respect to the defect population).

### 5.3.2.2 Defect configuration fitness

We define the fitness of a defect configuration as the added cost due to imperfect information yielded by the best sensor configuration for that particular defect configuration.

Formally, the fitness of a defect configuration  $f_d$  will be equal to:

$$C_d = |C(*\bar{v}_d) - C_{best\ sensor-IMP}(*\bar{v}_d)| \quad (5.6)$$

The aim of each defect chromosome is then to “escape” all configurations of sensors by simply “escaping” the best sensor configuration and make itself harder to be detected. That is, the best defect chromosome represents the least detectable damage configuration and hence, it is the chromosome that increases the most the added cost due to imperfect information. Conversely, each sensor chromosome seeks to decrease this added cost by decreasing the added average cost due to imperfect information with respect to the defect population. At the same time, it seeks to minimize the number of sensors to be implemented. In other words, each sensor chromosome, representing a sensor configuration, will try to accurately detect and quantify as many damage configurations as possible with the smallest possible number of sensors. The smaller the difference  $|C(*\bar{v}) - C_{IMP}(*\bar{v})|$ , the greater the capability of sensors in detecting damage.

### 5.3.3 Selection

This operator determines the capacity of each individual to persist in the population to reproduce, survive or disappear. In general, an individual's probability of survival will be directly related to their relative performance in the population. The individuals who are best adapted to their environment are more inclined to reproduce and transmit their genetic heritage to their offspring, while the less adapted tend to disappear before reproduction. Among the available selection methods, the principle of the roulette wheel selection and the elitism are adopted in our algorithm.

According to the roulette wheel selection scheme, the probability of a chromosome being selected is proportional to its fitness. First, a cumulative fitness is calculated for each chromosome by summing its fitness  $f_i$  and the fitness of the chromosome which is right before  $f_{i-1}$ . Then the cumulative probability of selection of a particular chromosome in the new population of size  $N_C$  is calculated as follows:

$$P_{cum_i} = \frac{f_{cum_i}}{\sum_{j=1}^{N_C} f_j} = \frac{f_i + f_{i-1}}{\sum_{j=1}^{N_C} f_j} \quad (5.7)$$

where  $f_{cum_i}$  is the cumulative fitness of the chromosome  $Ch_i$  and  $f_i$  is the fitness (not cumulative) of the chromosome  $Ch_i$ .

Individuals with high relative fitness are therefore more likely to be selected and reproduced. Each individual is expected to be selected a number of times defined by:

$$n_i = N_C \times P_i \quad (5.8)$$

where  $P_i$  is the non-cumulative probability of selection of a particular chromosome.

Based on the cumulative probability  $P_{cum_i}$ , the roulette wheel defines a range for each chromosome. And by randomly drawing a number between 0 and 1, a chromosome is selected if the random number falls within its range.

The elitism is also another very well-known and used selection method. It systematically keeps the best evaluated individual from one generation to the next. This type of selection prevents the best performing individual from disappearing during selection or when being affected by the crossing and mutation operators. Therefore, after having evaluated the population, the best chromosome is stored while other chromosomes will undergo crossing over and mutations depending on their respective rates. This elite individual is added again to the new population which will be evaluated in the next generation.

### 5.3.4 Crossover

The purpose of a crossover is to enrich and diversify the population by manipulating the structure of the chromosomes. It is considered to be the main operator for producing new individuals. By combining two parents (two chromosomes of the population) and exchanging information between them, the crossover generates two offspring having mixed genes. This combination is applied with a crossover probability  $p_c$ . The higher is  $p_c$ , the more the population undergoes significant changes. A crossover probability is generally between 0.5 and 0.9 (Rakotomahefa et al. 2019).

For each selected pair of chromosomes (obtain by the roulette wheel), a random number is generated according to a uniform distribution between 0 and 1. If this number is less than  $p_c$ , then the crossover takes place. Another number(s) is randomly generated (less than the number of genes of the chromosomes) in order to choose the crossover point(s). Depending on the chromosome length, one might choose to perform simple or multiple crossovers. For a simple crossover (with a single point), parent 1 (respectively parent 2) receives the genes from parent 2 (respectively from parent 1) that follow the crossover point allowing them to produce two offspring as shown in figure 5.1a. For multiple crossover, chromosomes are cut at several crossover points, and genes of both parents are inverted two by two, every two cut sections, to create two offspring (Figure 5.1b). In our methodology, we randomly choose one of the two offspring.

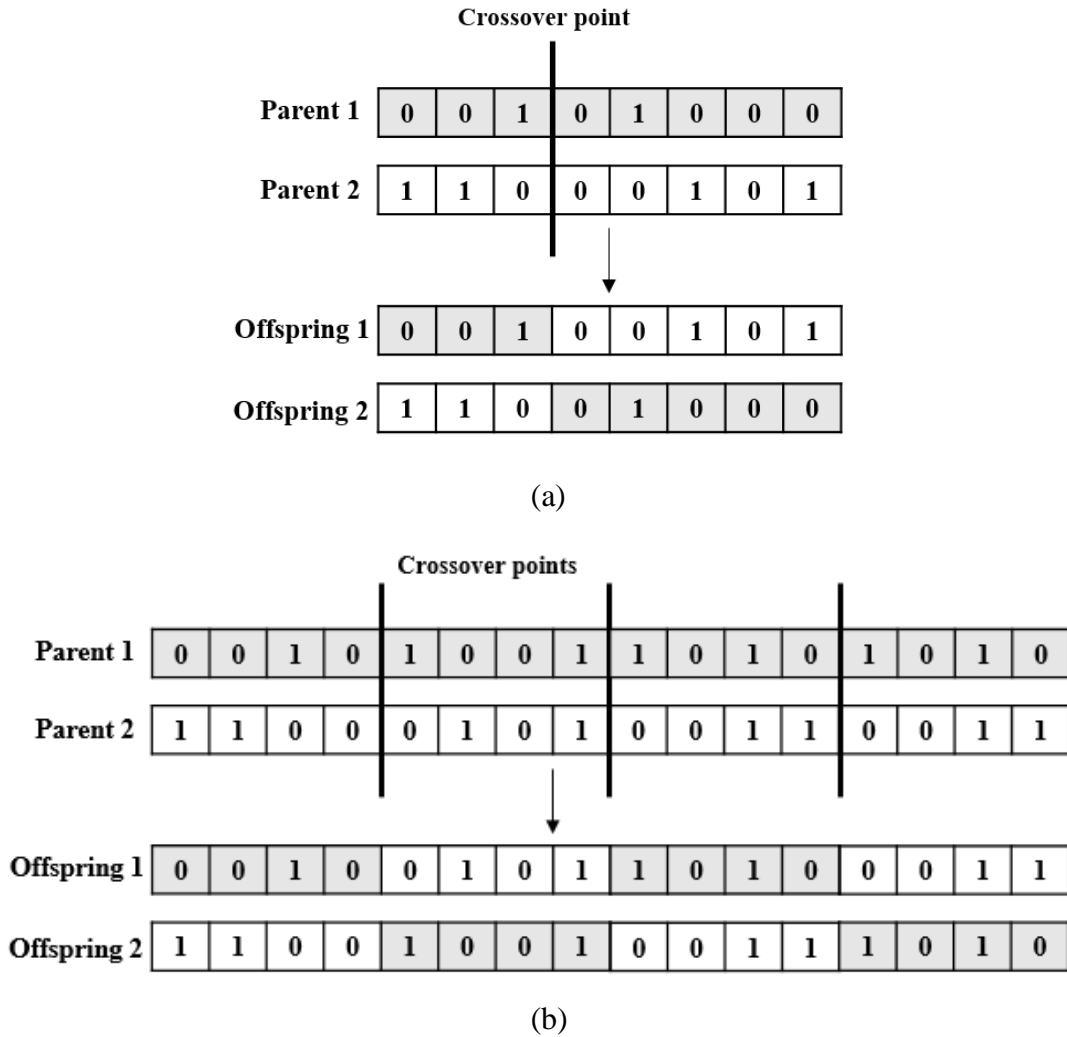


Figure 5.1: Crossover Scheme: (a) Single-Point Crossover, (b) Multiple-Points Crossover.

### 5.3.5 Mutation

The rationale for including this operator is to avoid premature convergence of the GA which would then be stuck in a local optimum. Most often, applying this operator reduce to randomly modify the value of a gene in a chromosome to form another one that will replace it. The convergence properties of genetic algorithms are not only dependent on the crossover operator, but also dependent on the mutation operator to avoid convergence to a local minimum. Each chromosome has a mutation probability  $p_m$ .  $p_m$  is generally chosen low to keep the natural evolution of the population and avoid transforming the genetic algorithm into a simple random search. Similarly to the crossover operator, a random number is generated for each chromosome according to a uniform distribution between 0 and 1. If this number is less than  $p_m$ , then the mutation takes place on a random gene of the chromosome as shown in figure 5.2.

In the case of a sensor chromosome, a gene  $g_i \in \{0,1\}$  is replaced by its complementary  $\bar{g}_i = 1 - g_i$ . However, in the case of a defect chromosome, a gene  $g_i \in ]0,1[$  is replaced by any number between 0 and 1 excluding its initial value.

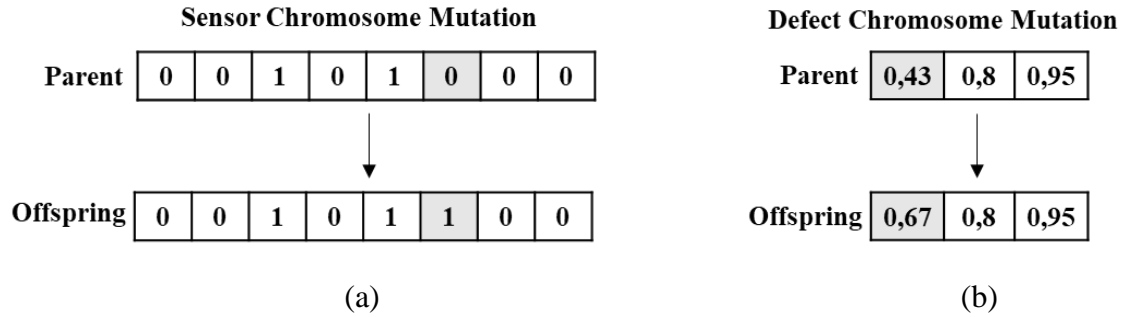


Figure 5.2: (a) Sensor Chromosome Mutation; (b) Defect Chromosome Mutation. (The grey gene is the modified gene)

### 5.3.6 Termination criterion

The stopping criterion is usually defined in genetic algorithms according to one of the following constraints:

- Fitness: The algorithm comes to its end when the fitness function converges to the desired fitness value.
- Number of generations: The algorithm ends when the preset number of generations is reached. This number depends on computational time and problem size.
- Time: For problems with high computational time, it is possible to put a time limit where the algorithm will end.

In our case, time is not a problem and the fitness limit is unknown. Therefore, the number of generations has been chosen as a termination criterion.

## 5.4 Predator-Prey optimization with Genetic Algorithm

The methodology developed herein seeks to obtain an optimal configuration of sensors able to identify most of structural damage configurations. By damage configuration we denote the location and severity of one or several damage on the structural elements.

Typically, if sensors are to be implemented on all the degrees-of-freedom, then any damage can be readily discovered. However, this tends to be very costly and sometimes hard to accomplish for some elements. Therefore, optimizing the configuration of sensors is needed to reduce the number of sensors and to maximize the probability of detection.

Assuming that the structural response is obtained by measuring modal parameters (i.e. eigenvalues & eigenvectors) and that a structural damage is defined by a loss in the stiffness of the elements, the methodology can be described as follows:

- 1- Create a population of  $N_d$  chromosomes representing the configurations of defects;
- 2- Create a population of  $N_s$  chromosomes representing the configurations of sensors;
- 3- For each configuration of sensors and configuration of defects, update the structural parameters (the stiffness in our case) according to the sensors' measurements through the Approximate Bayesian Computation detailed in chapter 2;
- 4- For each type of population (preys and predators):
  - a. Evaluate the chromosomes using the fitness appropriate to the type of population (refer to section 5.3.2);
  - b. Save the best chromosome by elitism (refer to section 5.3.3);
  - c. Select the best chromosomes from the  $N_d$  (or  $N_s$  in the case of sensors) chromosomes of the population according to their probabilities using the roulette wheel selection (refer to section 5.3.3);
  - d. Randomly choose two chromosomes from each population and combine the two selected chromosomes from each population using the crossover operator (refer to section 5.3.4);
  - e. Randomly choose one of the obtained offspring and apply a mutation on the chosen chromosome (refer to section 5.3.5);
  - f. Add the chosen offspring to the new population;
  - g. Repeat steps (d) to (f) until reaching  $N_d-1$  (or  $N_s-1$  in the case of sensors) offspring;
  - h. Add the elite individual to the  $N_d-1$  (or  $N_s-1$  in the case of sensors) offspring to obtain the new populations;
- 5- Repeat steps (3) and (4) using the new populations, until satisfying the termination criterion (refer to section 5.3.6) or until a predetermined maximum number of generations is reached;
- 6- Select the best chromosome of sensors representing the optimal sensor configuration.



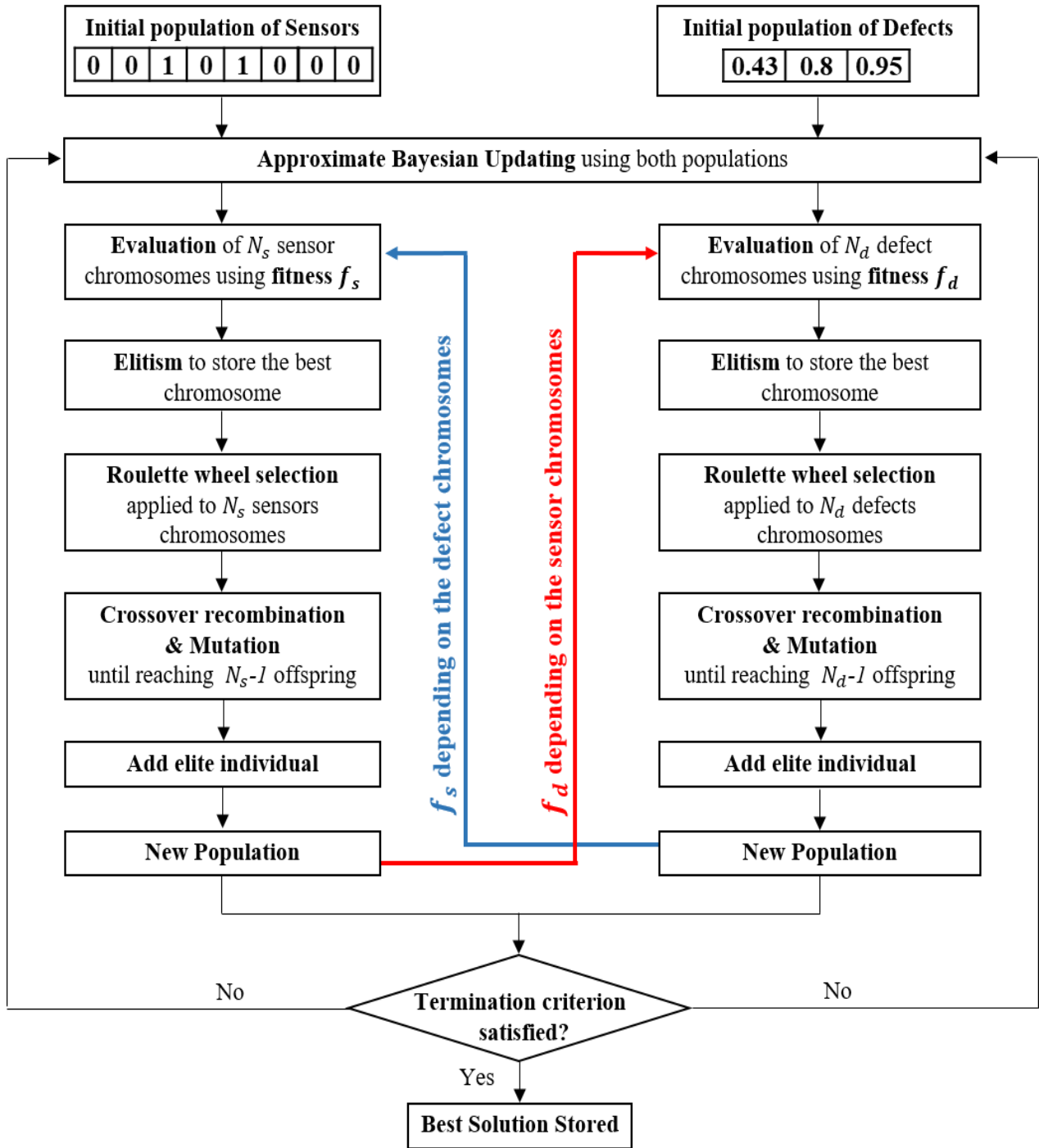


Figure 5.3: Predator-Prey Genetic Algorithm methodology.

## 5.5 Diversification

One of the common drawbacks of the genetic algorithm is the risk of premature convergence where the solution is trapped into a local optimum. This is basically caused by the rapid concentration of individuals in a small region of the search space due to incorrect selection pressure, very low mutation rate, small population, etc. Therefore, after some generations, individuals within the same population risk to be duplicated which limits the search space and decreases the chance of reaching the global solution. Thus, the importance of preserving the diversity of the population or at least minimizing its loss. This can be achieved by, among others: (i) using adaptive crossover and/or mutation rates, (ii) introducing diversity in the fitness function which affects the selection procedure, (iii) using the fitness sharing where individuals with uncommon fitness values are more likely to be selected, (iv) applying a restricted mating where similar individuals cannot be recombined (Byron and Iba 2016; Chen et al. 2014; Mc Ginley et al. 2011). In some cases, in addition to maintaining the diversity, one could also generate diversity when solutions are stuck in a search space by keeping  $n$  best individuals from the previous generation and completing the next generation by new individuals according to the initialization process (Ha et al. 2020).

In our case, the best configuration of sensors must be able to detect a wide range of possible damage (as much defect configurations as possible), not only the hardest ones to find. It is then important to keep the populations of defects diversified, with the least number of repetitive chromosomes in the same population. This would allow reaching the global optimum while optimizing the configuration of sensors according to a wide possibility of defect configurations.

Therefore, we introduce a diversification criterion to the optimization process when creating the new generation. After having selected the best chromosomes and applied the crossover and mutation operators, the offspring (or the selected parent if the recombination did not occur) is either accepted or not in the new population depending on how close it is to the chromosomes that have already been accepted. This closeness is represented by the Euclidean distance between the offspring and each chromosome  $Ch_i$  of the new population as follows:

$$d_{off-ch_i} = \sqrt{\sum_{j=1}^{N_G} (g_{j(Offspring)} - g_{j(Ch_i)})^2} \quad (5.9)$$

where  $g_{j(Offspring)}$  and  $g_{j(Ch_i)}$  are the gene number  $j$  of the offspring and the gene number  $j$  of a chromosome  $Ch_i$  of the new population, respectively, and  $N_G$  the number of genes in each chromosome.

The minimum between all distances  $d_{off-ch_i}$  is then compared to a random number:

$$offspring \text{ is } \begin{cases} \text{accepted} & \text{if } rnd \leq \min_{i \leq N_{C-acc}} d_{off-ch_i} \\ \text{not accepted} & \text{if } rnd > \min_{i \leq N_{C-acc}} d_{off-ch_i} \end{cases} \quad (5.10)$$

where  $rnd$  is a random number between 0 and 1, and  $N_{C-acc}$  is the number of chromosomes accepted in the new population before the evaluation of the current offspring.

## 5.6 Numerical Application

Two examples dealing with the problem of optimal sensor placement are presented in this section to test the performance of the predator-prey genetic algorithm.

The assumptions concerning the damage and the ABC are similar to the ones stated in the previous chapters for both examples:

- The degradation of an element is defined as a loss of a fraction of its initial rigidity.
- The prior degradations PDFs of all elements is taken as a uniform distribution between 0 and 1.
- The measurement error is a uniform random variable with zero mean and a range equal to  $0.15 \text{ m/s}^2$ .
- Each element of the structure is characterized by four damage states (Table 2.1).

### 5.6.1 Steel Truss

The first example considers the same steel truss structure as the one presented in Chapter 2, section 2.7.1 (Figure 5.4).

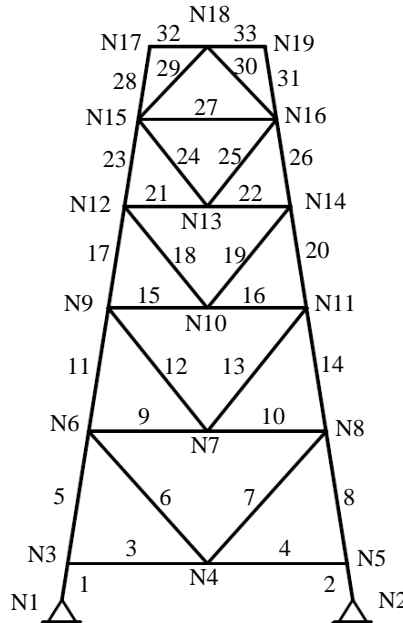


Figure 5.4: Simply supported offshore steel structure.

It is assumed that maintenance actions are divided into three groups: (i) A0: ‘Do Nothing’ ( $N$ ); (ii) A1: ‘Standard Repair’ ( $SR$ ); (iii) A2: ‘Member Replacement’ ( $MR$ ). Their respective costs are 0, 2.6 and 9.5 monetary units ( $m.u = 1000 \text{ €}$ ). These costs are supposed to be independent of the structural element properties (size, position, etc.). The transition matrices (T.M.) related to these maintenance actions are presented in Chapter 4, section 4.4.1.

User costs  $cs(\theta^e)$ , which assigns a cost for each state, is also supposed to be the same for all elements and are presented in Chapter 4, table 4.4.

For both types of populations, sensors and defects, the genetic algorithm hyperparameters are as follows:

- Number of generations: 100
- Population size: 400
- Crossover rate  $p_c$ : 0.9 (a value above 0.8 is usually recommended)
- Mutation rate  $p_m$ : 0.1 (recommended value)

The sensor chromosome size is equal to 34, number of horizontal and vertical translations. The defect chromosome size is 33 since the structure contains 33 elements.

Two cases have been considered in our study with two sensor prices  $c_c$ : (a)  $c_c = 0.1$  m.u.; (b)  $c_c = 0.5$  m.u.

The objective of this study is to find the best configuration of sensors (number and position) which are to be placed on the degrees-of-freedom of the structure.

In each generation, and for each combination of sensor configuration ( $Ch_{sensors}$ ) and defect configuration ( $Ch_{defects}$ ), a Bayesian update is run, followed by a decision analysis in order to decide which actions are to be applied on the elements. These actions are then applied on the structure taking into consideration the certain belief states as described in section 5.3.2.1. The obtained cost  $C_{IMP}(*\bar{v})$  is compared to  $C(*\bar{v})$  to evaluate the performance of  $Ch_{sensors}$  in accurately detecting damage in  $Ch_{defects}$ . The difference between both costs is introduced in the fitness of both types of chromosomes according to equations (5.1) and (5.6).

Both types of chromosomes evolve antagonistically. Hence, for a better visualization of this evolution, a fitness indicator is defined for each type of populations as:

$$FI_{Sensor} = \frac{1}{f_s} \quad (5.11)$$

$$FI_{Defect} = f_d \quad (5.12)$$

where  $f_s$  and  $f_d$  are the fitness of, respectively, a sensor and a defect configuration. This indicator is used in figure 5.5 representing the co-evolution of the best sensor and best defect configurations for the case where  $c_c = 0.1$  m.u. A similar figure has been obtained for the case where  $c_c = 0.5$  m.u. In addition, the diversity rate of the defects population has been shown on the graph of figure 5.5. In each generation, a diversity rate is defined as:

$$DR = \frac{\sum_{i=0}^{N_c} \sum_{j=i+1}^{N_c} d_{Ch_i - Ch_j}}{N_{comb}} \quad (5.13)$$

where  $d_{Ch_i - Ch_j}$  is the Euclidean distance between two chromosomes  $Ch_i$  and  $Ch_j$  defined in

Eq. (5.9),  $N_C$  is the number of chromosomes in the population, and  $N_{comb}$  is the number of combinations between the chromosomes defined by:

$$N_{comb} = \frac{N_C!}{2!(N_C-2)!} \quad (5.14)$$

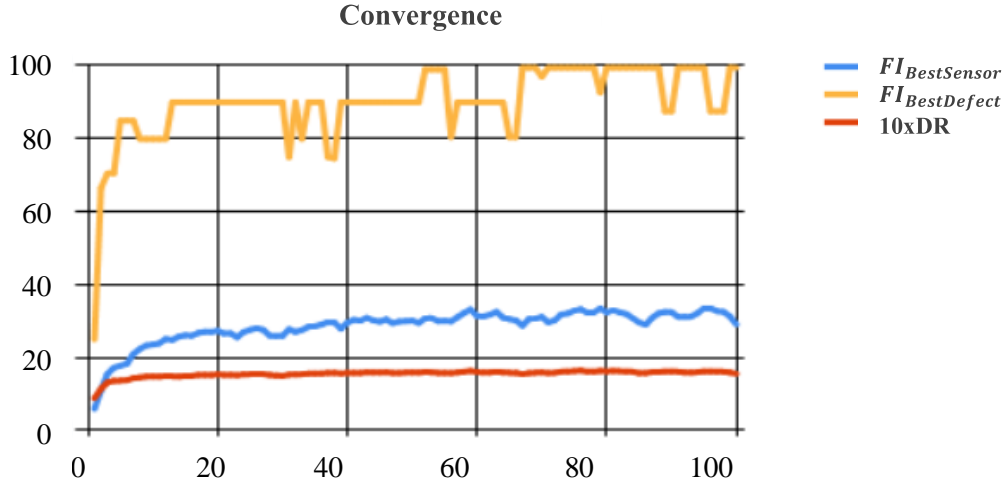


Figure 5.5: Co-evolution of two populations: defects and sensors in the steel structure

In figure 5.5, the fitness curve of the best defect configuration evolves on a wide scale across the 100 generations, its value ranging from 24 in the first generation to a 100 in the last generation. The drastic evolution is seen in the first 5 generations where the fitness curve increased rapidly from 24 to 85. In parallel with this large increase, it is observed that the curve of the inverse of the fitness of the best sensor configuration increases as well instead of decreasing as would be anticipated. This shows that the defects configurations in the first 5 generations evolved faster than the sensors configurations and were able to avoid being effectively detected. However, as the number of generations increases the fitness value of each configuration moves upwards and downwards along its respective curve depending on how well the other type of configuration is evolving. For instance, a decrease in the fitness value of the best defect configuration indicates that the evolution of the sensor configurations has led to an improved configuration which is able to better detect the defects. As one can notice, the changes in the sensor curve are very small compared to the changes in the defect curve. This difference is due to the fact that the best defect in the objective functions is evaluated according to one best sensor while the best sensor is evaluated according to the average fitness of all defects.

On the other hand, and due to the imposed diversification, the population of defects has kept a certain level of diversification which means that the chromosomes of the same population are quite different from one another. This avoids the convergence of the defects population towards one specific configuration and therefore being trapped in a local optimum. It also creates a selection pressure on the population to create new offspring so the sensors can be evaluated according to a wide number of defect configurations.

The best configurations of sensors obtained for each generation for the case a ( $c_c=0.1$  m.u.) are presented in table C.1 in Appendix C. As observed, across the generations, the obtained number of sensors did not significantly decrease. Looking back to Eq. (5.1), which is the inverse of the fitness function of the sensors, one can notice that the first part of the equation highly depends on the sensor price  $c_c$  while the second part depends on the amount of information gained. Therefore, when the sensor price is low as it is in our case, the fitness function depends less on the first part of the equation and for this reason, the number of sensors will not decrease a lot (contrary to the case b where  $c_c=0.5$  m.u.).

Furthermore, one can notice that the number of potential sensor configurations is relatively high. Throughout 100 generations, 73 potential sensor configurations have been obtained. This might be an indication of multiple suboptimal solutions depending on how close their fitness values are. Unlike classical GA, the proposed predator-prey GA technique tends to lose memory throughout the whole process. In each generation, each type of population is evolving according to the other type of population in the same generation. Therefore, when a best sensors configuration is chosen for a specific generation, it might not be the best one for the previous generations. However, the dynamic of the predator-prey model resides in the fact that the evolution of a population makes it harder for the other population to converge and find the best solution due to their simultaneous evolution. In order to make sure that we have reached the global solution, the first three steps of the methodology have been run again, but instead of creating two populations, the population of defects consisted of all the configurations of defects obtained throughout the generations and the population of sensors consisted of all the best configurations obtained from each generation. Hence all obtained best sensors configurations have been compared to each other's according to all the configurations of defects. In total, the sizes of the populations of defects and sensors are respectively 40000 and 100. Table C.2 in Appendix C summarizes the 73 potential sensor configurations, each assigned a value representing the cost induced by the configuration according to all configurations of defects obtained throughout all the generations. Five potential sensor configurations obtained for different generations are presented in figure 5.6. The best three potential sensor configurations are presented in figure 5.7.

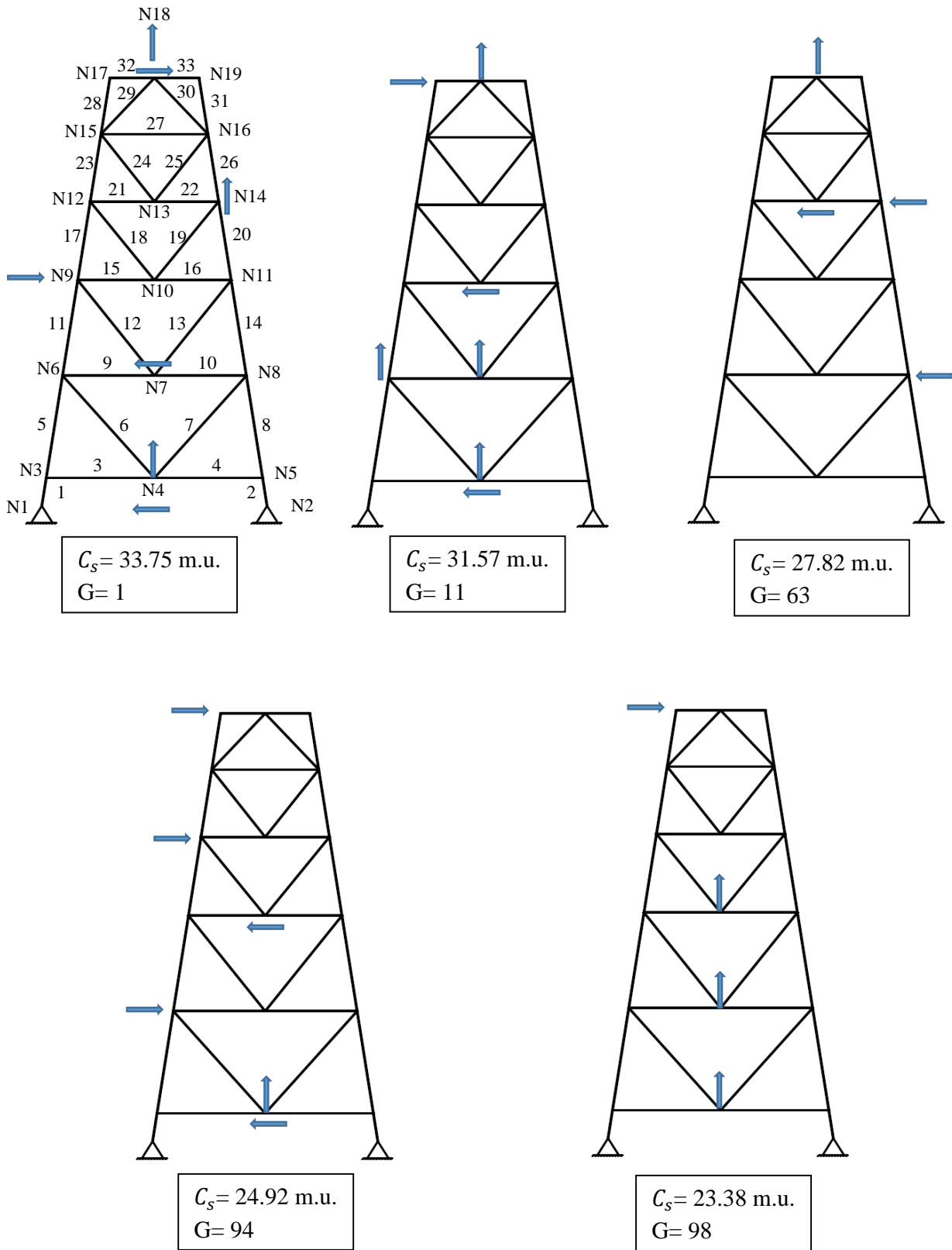


Figure 5.6: Five potential sensor configurations obtained for different generations in case a with their total cost  $C_s$  ( $G$ : generation).

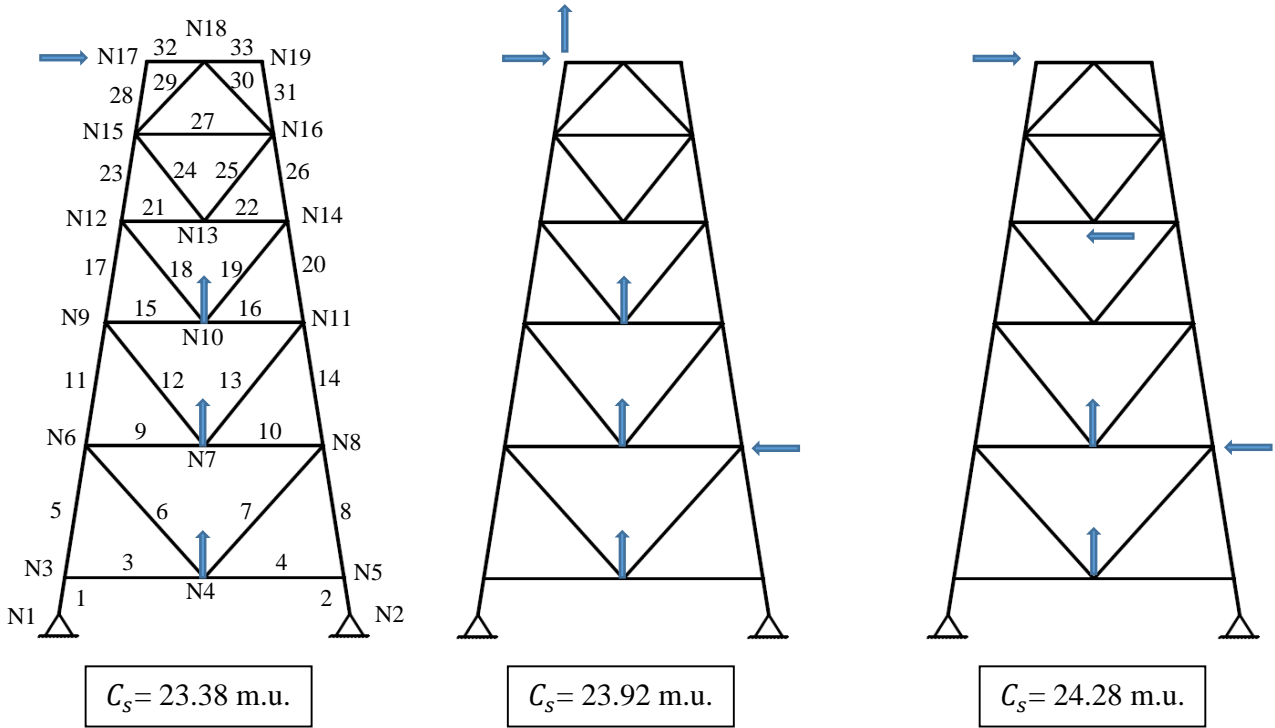


Figure 5.7: Best three sensors configurations obtained in case a with their total cost  $C_s$ .

Results proved that, indeed, a big part of the sensors configurations presents very close costs and therefore have very close fitness values. Still, one configuration can be considered as an optimal solution with the lowest cost where a horizontal sensor is implemented on node 17, and vertical sensors are implemented on nodes N4, N7 and N10 (Figure 5.7, first layout) with a total cost  $C_s = 23.38$  m.u. These results seem reasonable. For horizontal vibration modes, it is logical that node N17 presents the largest displacement (horizontal) especially for the fundamental mode (largest period), hence the presence of a sensor at this point can record the slightest movements in the structure which may be caused by defects. This makes it possible to compare the values before and after a damage has occurred and to deduce the most relevant conclusions. For vertical vibration modes, bar 1-2 has the longest length, followed by bar 9-10 and bar 15-16 respectively. Vertical movements are more amplified in bars with greater span which explains the presence of the vertical sensors on these 3 bars, in particular bar 1-2. This bar, despite the presence of node N4 (bolted connection) which partially blocks it, has a lower stiffness for vertical vibrations than the stiffness of the vertical members of the structure (i.e. bars 8, 14, 17) which are basically subjected to axial force. Hence, the vertical displacement, due to the vibration, is greater at nodes N4, N7 and N10 which supports the need for the presence of sensors on them.

The same study has been run for case b with a higher sensor cost ( $c_c = 0.5$  m.u.). Table C.3 in Appendix C shows the best sensor configurations in each generation. Unlike the previous case, one can see that the number of potential sensors locations suddenly decreases starting the second generation and is much lower compared to case a. This points out the



importance of the sensor price while evaluating sensor configurations. Because of the high price, the algorithm tends to reduce, as much as possible, the number of sensors while maintaining an adequate amount of information. In this case, the algorithm has been stopped at generation 70, after having noticed that configuration “N4-V; N17-H” (representing a vertical sensor on node N4 and a horizontal one on node N17) has been repeatedly chosen as the best sensors configuration by a significant number of generations. This might be an indication that this configuration is a global optimal solution.

In order to affirm our outcome, as done for the first case, the algorithm has been run again for all configurations of defects and the best configurations of sensors. Table C.4 in Appendix C presents the 20 potential sensors configurations with their total cost with their total cost  $C_s$  according to all configurations of defects previously obtained throughout the generations. Three potential sensor configurations obtained for different generations are presented in figure 5.8. The best three potential sensor configurations are presented in figure 5.9.

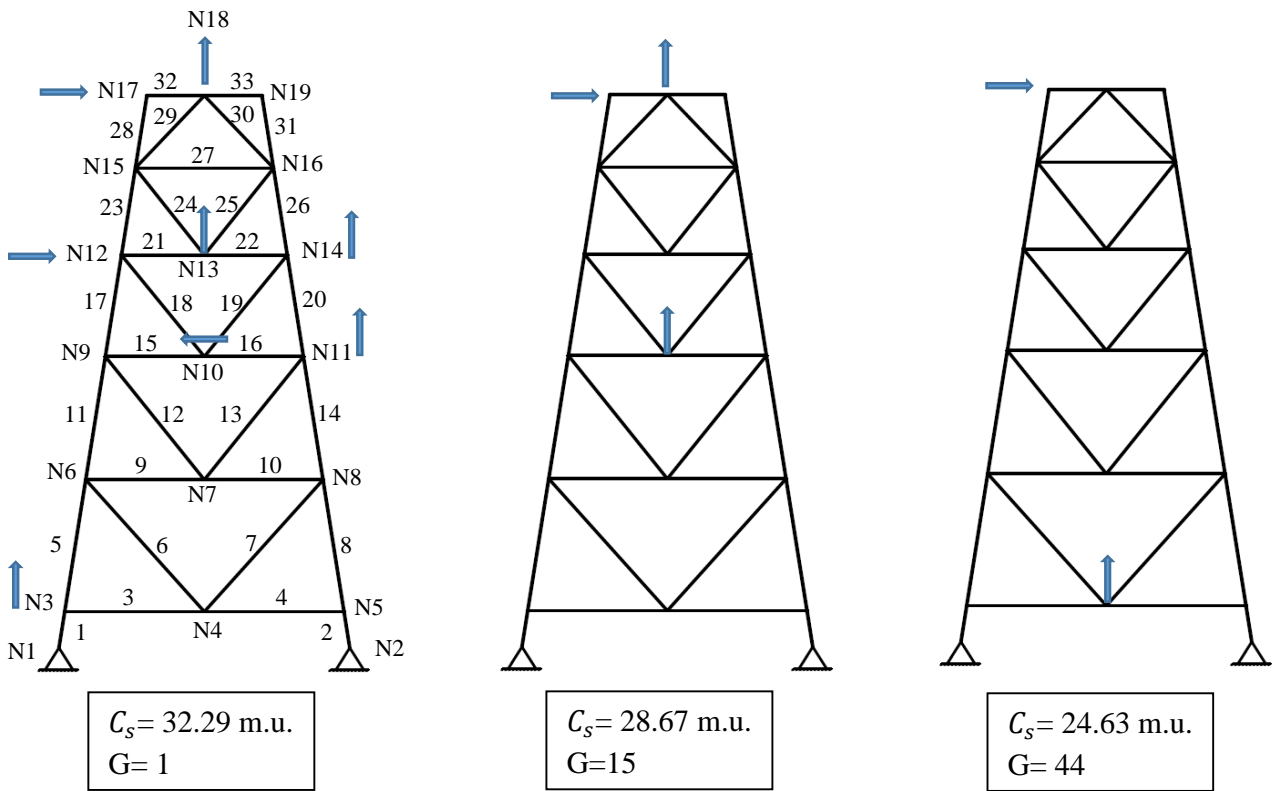


Figure 5.8: Three potential sensor configurations obtained for different generations in case b with their total cost  $C_s$  (G: generation).

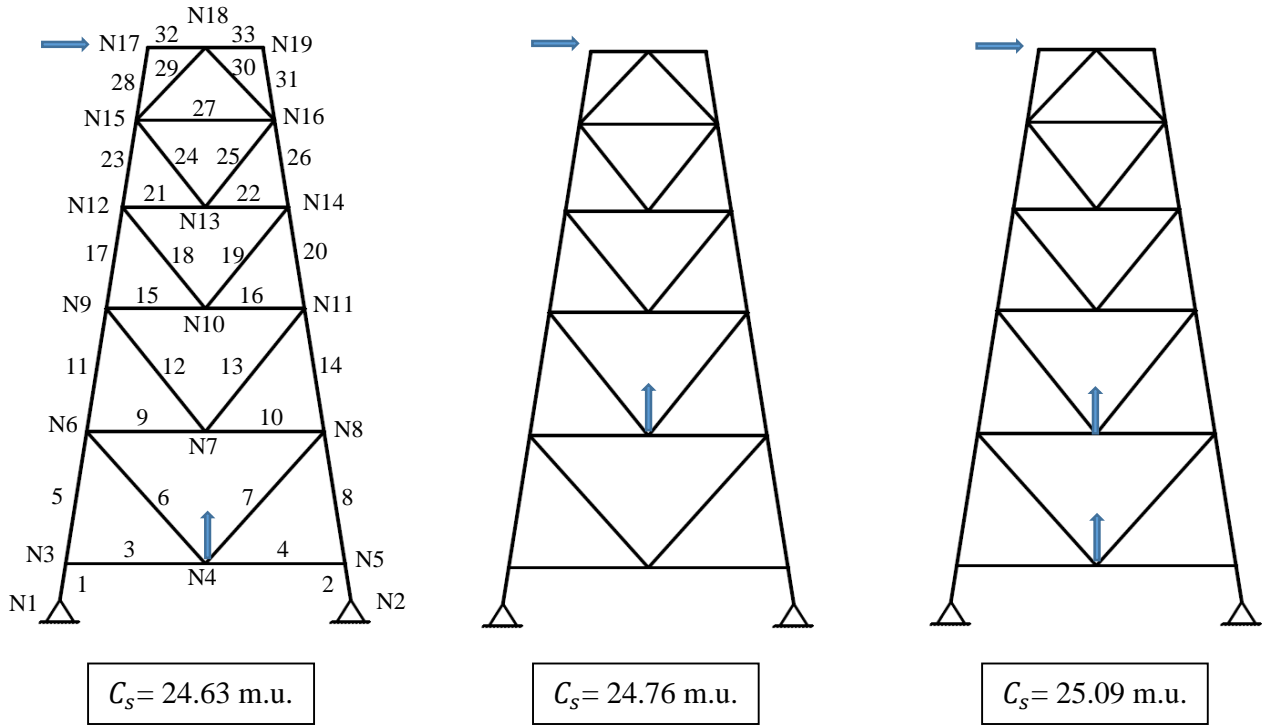


Figure 5.9: Best three sensors configurations obtained in case b with their total cost  $C_s$ .

As expected, and due to the high price, the lowest cost was assigned to a configuration involving only 2 sensors. The best solution consists of implementing a vertical sensor on node N4 on the first level, and a horizontal sensor on node N17 on the highest level which is most affected by any vibration in the structure. Since the biggest movements appear on the highest level, the difference between these movements in two different states of the structure is quite large and thus, at this level, results are less affected by the measurement uncertainty.

The best sensor configuration in case b includes 2 sensors, each costing 0.5 m.u. while in case a, 4 sensors locations have been chosen with a sensor unit price being equal to 0.1 m.u. In terms of sensor price defined by  $n_c \times c_c$  in Eq. (5.1), the best configuration in case a is less expensive with a difference of 0.6 m.u. However, when comparing the total costs  $C_s$  between both cases, the difference becomes greater with a value of 1.25 m.u. This is due to the fact that the second part of Eq. (5.1)  $\left(\frac{\sum_{d=1}^{N_d} |C_s(*\bar{v}_d) - C_{s-IMP}(*\bar{v}_d)|}{N_d}\right)$ , defining the added cost due to imperfect information provided by the sensors, had an important effect on the final result. The best sensor configuration in case a has given more information about the condition states of the elements in the structure. Consequently, in our problem, if one has to choose between optimally implementing sensors according to case a or b, the best decision would be choosing the case a which involves more sensors with a lower price. The compromise between the information acquired and the price of the sensors is the key element of our problem.

The accuracy of the obtained results is further supported by applying the ABC updating, presented in chapter 2, on the damaged steel truss structure (same example as in chapter 2)

using the best sensors configurations in both cases a and b. The damage is supposed to be on element 8 which is considered to have lost 80% of its initial rigidity. Tables 5.1 to 5.3 presents the discretized belief states of the first 10 elements using the configurations of sensors obtained in case a, case b and the configuration used in chapter 2 (with 6 horizontal accelerometers), respectively. Comparing results in the three cases (Figure 5.7), it is noticeable that the most accurate and precise results are given by the configuration obtained by case a. In table 5.1, it is clear that all elements are in a good condition except element 8 which seems to be in very bad condition having a probability of 0.803 being in state  $\theta^e = 4$  (which represents the state of elements having lost 75% to 100% of their initial rigidity). Yet, in tables 5.2 and 5.3 all elements seem to be in good condition except element 8 and 5. A probability of 0.55 or 0.65 being in a good state might be a bit concerning and an inspection might be needed to make sure that element 5 is not damaged. Moreover, in this numerical example, when using 2 sensors only (Table 5.2) even though at their best locations, results are not fully clear as element 8 has similar probabilities of being in state  $\theta^e = 1$  (0.41) and  $\theta^e = 4$  (0.49). One can make an assumption that element 8 is highly damaged but without making sure of it. However, when the sensor price is high we are forced to sacrifice part of the information. To sum up, between the three configurations, the one obtained in ‘case a’ is the most cost-effective one and the one used in chapter 2 gives a bit more information than the one obtained in ‘case b’. Comparing the last two configurations, with respect to the assumed damage configuration, the resulting costs of imperfect information are almost the same with a slight difference. Hence, the added value in information given by the sensors used in Chapter 2 is not worth the cost of the additional sensors. The comparison of the three configurations is shown more clearly in figure 5.10 representing the degradation extent of element 8 (damaged element) in the three previously mentioned cases. As observed, the curve that represents best the condition state of element 8 is given by the optimal sensor placement in ‘case a’ while less information is provided by the curves in the other two cases. These results prove the efficiency of the algorithm and shows how accurate are results obtained when implementing sensors in their optimal locations given by case a.

Table 5.1: Discretized belief states of elements 1-10 using the optimal configuration of sensors for case a.

Element \ $P(\theta^e = i)$	Damaged Structure			
	$i = 1$	$i = 2$	$i = 3$	$i = 4$
1	0.92	0	0.08	0
2	0.94	0.06	0	0
3	0.87	0.13	0	0
4	0.92	0	0.08	0
5	0.864	0.030	0.015	0.091
6	0.89	0.11	0	0
7	0.94	0.06	0	0
8	0.106	0.03	0.061	0.803
9	1	0	0	0
10	1	0	0	0

Table 5.2: Discretized belief states of elements 1-10 using the optimal configuration of sensors for case b.

Element \ $P(\theta^e = i)$	Damaged Structure			
	$i = 1$	$i = 2$	$i = 3$	$i = 4$
1	0.754	0.228	0.013	0.005
2	0.786	0.121	0.093	0
3	0.76	0.01	0.147	0.083
4	0.777	0.151	0.072	0
5	0.65	0.03	0.02	0.3
6	0.795	0.15	0.055	0
7	0.78	0.155	0.065	0
8	0.41	0.04	0.06	0.49
9	0.817	0.183	0	0
10	0.81	0.19	0	0

Table 5.3: Discretized belief states of elements 1-10 obtained in chapter 2 using six measured DOFs: N5, N8, N11, N14, N16, N19

Element \ $P(\theta^e = i)$	Damaged Structure			
	$i = 1$	$i = 2$	$i = 3$	$i = 4$
1	0.793	0.2	0	0.007
2	0.8	0.2	0	0
3	0.75	0.2	0	0.05
4	0.793	0.2	0	0.007
5	0.55	0.15	0	0.3
6	0.8	0.2	0	0
7	0.798	0.2	0.002	0
8	0.3	0.09	0.01	0.6
9	0.8	0.2	0	0
10	0.8	0.2	0	0

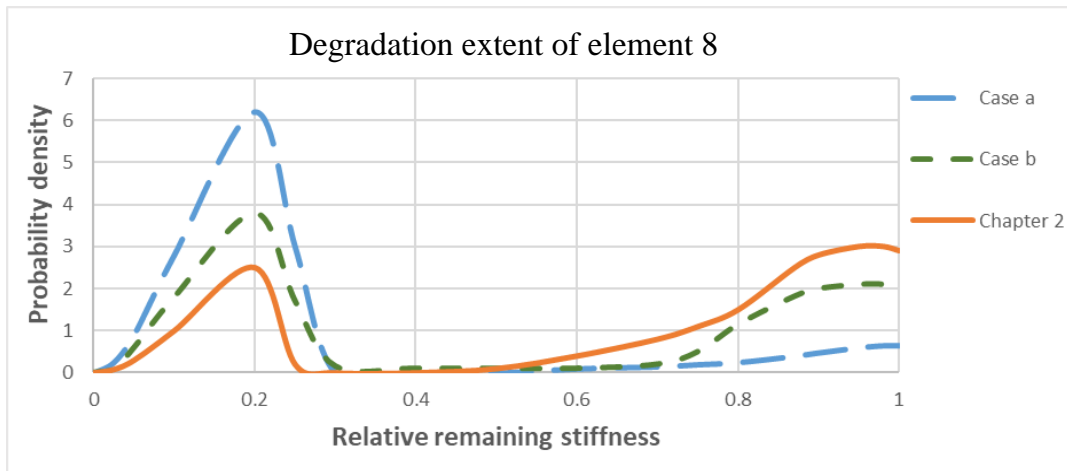


Figure 5.10: Degradation extent of element 8 obtained from: (i) Optimal Sensor Placement (OSP) in case a, (ii) OSP in case b, (iii) sensor placement used in Chapter 2 (six measured DOF).

### 5.6.2 Multistory Concrete Frame

In this numerical application we consider a 4-story simply supported concrete frame structure. It is the same structure presented in Chapter 2, section 2.7.2. composed of 20 elements and 15 nodes (Figure 5.11).

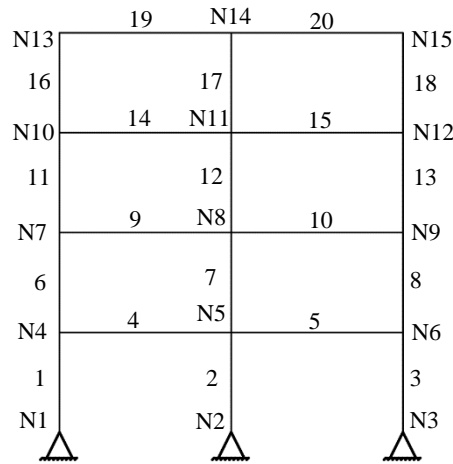


Figure 5.11: Simply supported concrete frame structure.

For the cost function, it is assumed that three type of maintenance actions are available: (i) A0: ‘Do Nothing’ ( $N$ ) with 0 cost; (ii) A1 ‘Standard Repair’ ( $SR$ ) with a cost of 1.8 monetary units (1 m.u.=100 €) and (iii) A2: ‘Member Replacement’( $MR$ ) with a cost of 6.2 m.u. To simplify the presentation, we assume that the costs are independent of the structural element. The transition matrices (T.M.) related to these maintenance actions are presented in Chapter 4, section 4.4.2.

User costs  $cs(\theta^e)$ , which are considered to have same  $\theta$  values for all the elements, are presented in Table 4.11.

For both types of populations (sensors and defects configuration populations), the genetic algorithm hyperparameters are as follows:

- Number of generations: 70
- Population size: 200
- Crossover rate  $p_c$ : 0.9 (a value above 0.8 is usually recommended)
- Mutation rate  $p_m$ : 0.1 (recommended value)

The sensor chromosome size is 24 (number of vertical and horizontal degrees-of-freedom) while the defect chromosome size is 20 (number of elements in the structure). The price of a sensor, supposed to be an accelerometer in our example, is 2.5 m.u.

The aim of this numerical application is to find the best configuration of sensors (number and position) in a frame type of structure different that the truss type structure described in section 5.6.1.

As it was stated in the previous example, for each combination of sensors and defects chromosomes, a Bayesian update is run to obtain the updated posterior PDF of each element of the structure. A decision analysis is then applied on the structure using the belief states obtained by the Bayesian update to find the corresponding optimal actions. The costs calculated for the updated belief states and the true certain belief states when applying the optimal actions, obtained based on the uncertain belief states, are compared with one another to evaluate both types of chromosomes (sensors and defects chromosomes).

The evolution of the fitness functions of both types of chromosomes is shown in figure 5.12. As can be seen, it is clear that the best defect configuration is moving forward and evolves across the generations since its fitness values increased from around 16 in the first generation to around 84 in the last generation. However, the curve of the inverse of the fitness of the best sensor, representing the cost induced by the configuration of sensors, did not decrease as it was expected, even though the best configuration of sensors is evolving. This is due to the averaging factor in the fitness function of sensors which slightly changes compared to the change in the fitness of the best defect configuration.

In figure 5.12, one can also notice that the fitness of the best defect does not always increase, sometimes it decreases or stays stable. The same case presents itself in the case of sensors but less clearly. Since the best defect fitness depends on how well the best sensor chromosome is capable of detecting the configuration of defects it represents, a decrease in this fitness gives credit to the best sensor and shows that, in the generation in question, the sensor's chromosome has evolved in a better way. On the other hand, the metastable state is justified by the presence of a local optimum which is followed, suddenly after a long period of equilibrium, by a more stable or less stable neighboring state. In order not to be stuck in these local optima, an imposed diversification has been added to the algorithm in addition to the effect of the mutation operator. This diversification, which helped in keeping the defect population diversified as it is illustrated in the graph (Figure 5.12), played a major role in reducing the period of equilibrium and broadened the search space for the population of sensors.

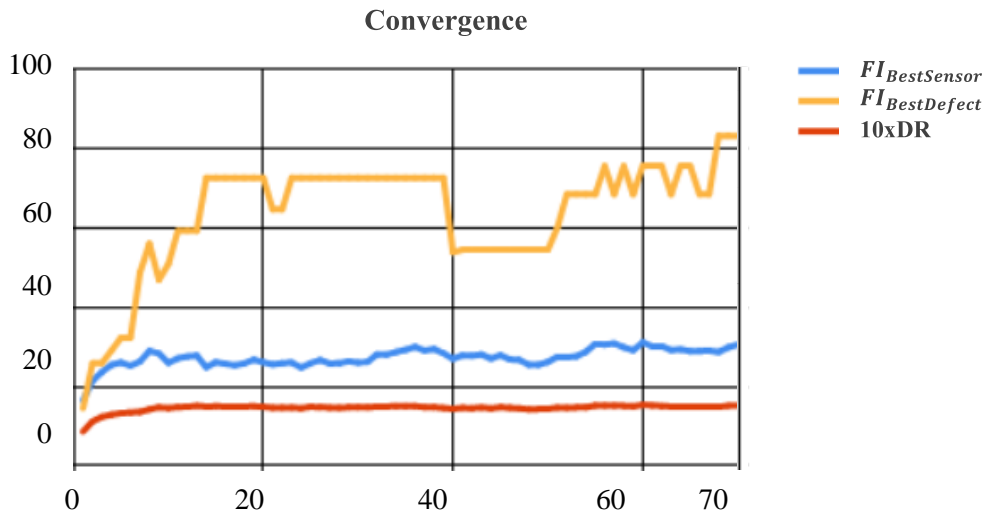


Figure 5.12: Co-evolution of two populations: defects and sensors in the concrete structure.

The importance of imposing a diversification to the population of defects has been shown in figures 5.13 and 5.14. Using a mutation operator is not enough and as one can notice, the natural diversification decreased rapidly for the first 10 generations, whereas these generations are responsible for the exploration. It is usually believed that, at the beginning of the search process, the algorithm should explore as much of the search space as possible to avoid premature convergence. After the exploration phase, comes the exploitation phase in order to choose the optimal solution between the previously found best solutions and ensure the convergence. Even though the mutation is responsible for diversifying the population, a high mutation rate is usually not recommended. The reason behind it is to keep a proper balance between the exploitation and the exploration. While the crossover leads to the good solutions in order to reach the global optimum, the mutation tries to slow down that convergence. Therefore, if this rate is high the crossover effect will be much reduced and in turn the chance of finding the best solution will decrease. In our case, we are interested in exploiting and exploring the defect population from the beginning till the end of the search process. The solution we are searching for, concerning the best sensor configuration, should be able to detect as much configurations of defects and at the same time the hardest and costliest configurations. Hence, when the diversification has been imposed in the selection of the offspring, the search space kept a certain diversity level (Figure 5.14) while keeping also the good defect chromosomes.



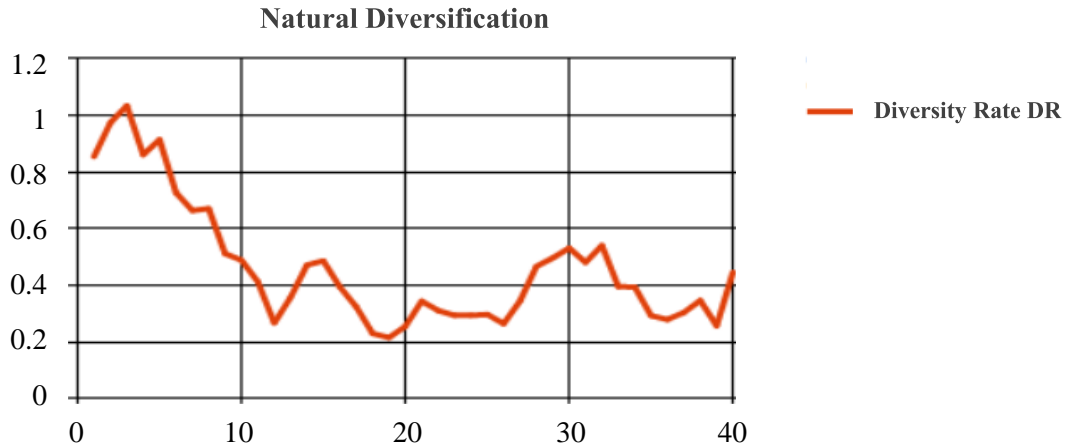


Figure 5.13: Natural diversification of the population of defects

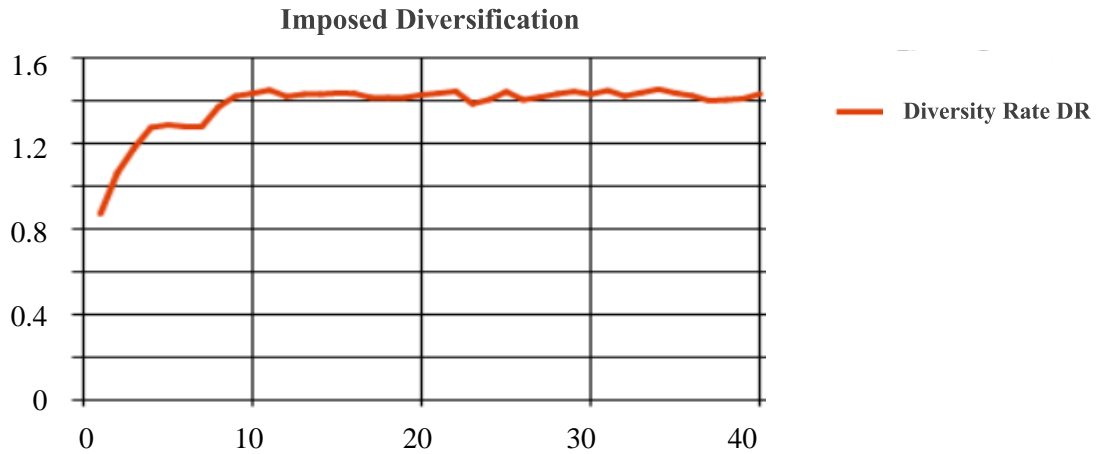


Figure 5.14: Imposed diversification on the population of defects

Tables C.5 and C.6 (Appendix C) displays, respectively, the evolution of the best sensors configuration through the generations and their total costs  $C_s$  according to all defect chromosomes. The first noticeable thing is the influence of the first term in Eq. (5.1) which encourages the algorithm to choose the least possible number of measured DOFs while simultaneously maintaining a good level of damage detection. For the first five generations, the algorithm has chosen five best sensor locations to accurately detect the possible damage configurations. This number decreased from one generation to another until ending up with 1 best sensor location which turns out to be on the last story. The effect of the sensor price on the fitness function is also shown in figure 2.15 where four potential sensor configurations obtained for different generations are presented. The best four potential sensor configurations are presented in figure 5.16.

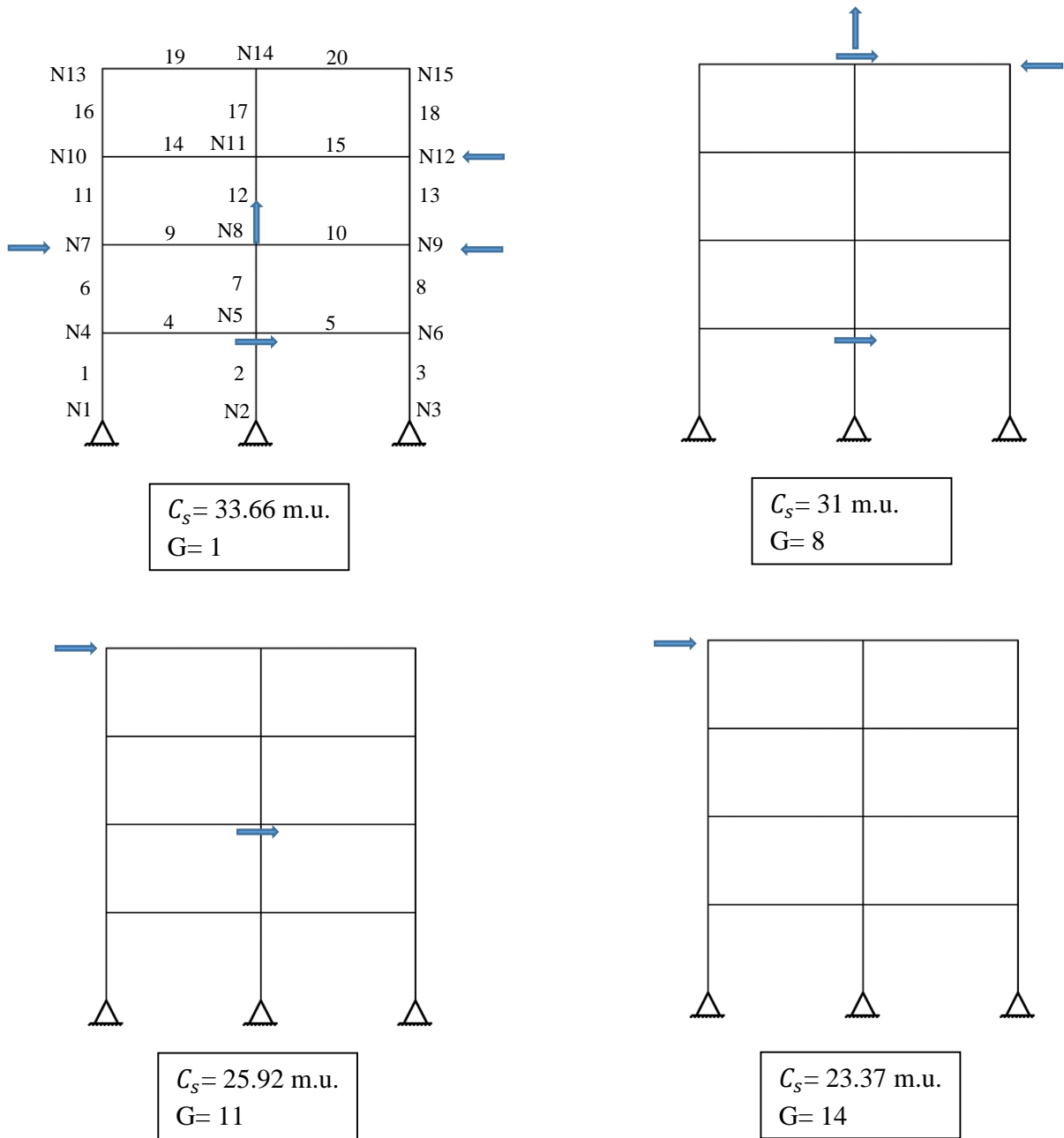


Figure 5.15: Four potential sensor configurations obtained for different generations with their total cost  $C_s$  ( $G$ : generation).

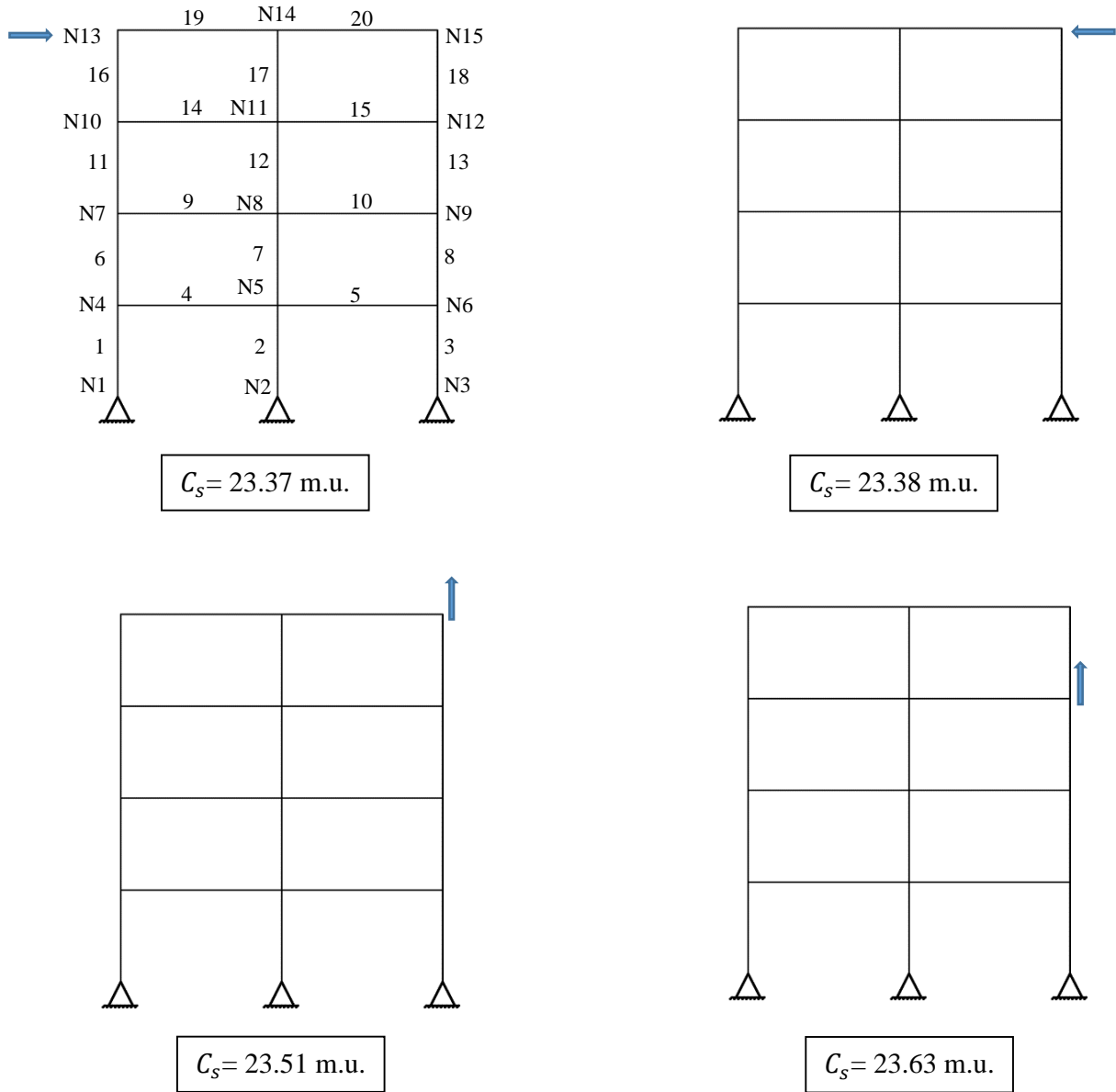


Figure 5.16: Best four sensor configurations with their total cost  $C_s$ .

To better study the influence of the sensor cost on the sensor placement, the algorithm has been run again without the intervention of this cost on the evaluation function. In this case, Eq. (5.1) becomes:

$$C_s = \frac{\sum_{d=1}^{N_d} |c_s(*\bar{v}_d) - c_{s-IMP}(*\bar{v}_d)|}{N_d} \quad (5.15)$$

As expected, results showed that when there are no cost constraints, the accuracy of the damage detection increases with the number of measured DOFs. When measuring more DOFs, one is getting more information about the structure. Hence, when  $c_c=0$ , the best

obtained solution to our problem consists of measuring all the DOFs, although after a certain number of sensors, the marginal benefit of sensors starts decreasing.

Looking at table C.5 (Appendix C), starting from generation 23 till the last generation, one can see that the algorithm is a bit confused between choosing a vertical or a horizontal accelerometer on the last story (Figure 5.16). This confusion is due to the assumption concerning the perturbation in the stiffness matrix. As it was stated in chapter 2, and for computational simplification, we assume that a damage in an element affects proportionally its stiffness matrix. Hence, the axial and flexural rigidity are equally affected by the damage and depending on the configurations of damage, it might be preferable at times to measure a vertical DOF and other times to measure a horizontal one. It should be noted that, since nodes N13 and N15 are symmetrical, implementing an accelerometer on one of them has the same overall effect as if a sensor was implemented on the other one. For that reason, as one can notice in figure 5.16, the first two layouts have almost the same total cost  $C_s$ .

Even though, for the last generation, the best configuration of sensors consisted of implementing one horizontal accelerometer on node N13, it is mandatory to check that this is the global solution. From one generation to another, our algorithm might lose some memory which means that a best sensor in a specific generation compared to a population of defects configurations in the same generation might not be the best for other populations of defects in other generations. Hence, at the end of the GA runs, it is important to rerun the first three steps of the methodology for 1 generation consisting of a population of all configurations of defects and a population of the best configurations of sensors previously obtained.  $C_s$  of the best configurations of sensors according to all configurations of defects are presented in table C.6 in Appendix C. Results proved that: (i) implementing a horizontal accelerometer on node N13 is the best solution (Figure 5.16, first layout) being the least costly configuration with  $C_s=23.37$  m.u.; (ii) there is a negligible difference between implementing a horizontal sensor on nodes N13 ( $C_s=23.37$  m.u.) or N15 ( $C_s=23.38$  m.u.). Because of the symmetry, implementing a horizontal sensor on one or the other has the same effect. These results seem to meet our expectation since the largest movements in a structure, due to a vibration, appear on the top of the structure. Hence, any defect in the structure would highly affect these movements which, in turn, will affect the sensor data. Consequently, when running the Bayesian update, the difference in the response amplitude at the top of the structure will be greater than the sensor noise and will therefore provide more information when assessing the structure.

Finally, the ABC updating procedure that was developed in chapter 2, has been applied on a damaged concrete frame structure to detect damage using the best sensor configuration. In this application, elements 1 and 10 are supposed to be damaged having lost respectively 40% and 25% of their initial stiffness. Results are presented in table 5.4 which reveals that indeed, element 1 is most probably in state  $\theta^e = 2$  (72% chance) which means that it has lost 25% to 50% of its initial stiffness while the other elements are in good condition. However, when comparing element 10 to the other elements, one can see that even though it seems to be in good condition, its probability of being in state  $\theta^e = 1$  is not as high as the others

indicating that this element's state might be on the limit between the first two states. Comparing these results to the ones obtained in chapter 2 (Table 5.5) using three horizontal accelerometers on nodes N4, N9 and N13, one can realize that the difference between them is very small. This comparison is illustrated in figures 5.17 and 5.18 representing the degradation extents of, respectively, elements 1 and 10 according to the optimal sensor placement and the sensor placement used in chapter 2. Looking at the curves in both cases, one can deduce that the information provided is almost the same for both cases (having very close curves). That is, the two additional accelerometers used in chapter 2 didn't provide significantly more information. Even though the belief states are slightly better for three sensors, the resulting optimal actions are the same. In terms of information, without taking into account the cost factor (Eq. 5.15), both cases resulted in the same cost. Hence, this slight difference is not beneficial and once again, it affirms that N13-H is the best solution to our problem.

Table 5.4: Discretized belief states of elements 1-10 using the optimal configuration of sensors.

Element \ $P(\theta^e = i)$	Damaged Structure			
	$i = 1$	$i = 2$	$i = 3$	$i = 4$
1	0.28	0.72	0	0
2	1	0	0	0
3	0.88	0.04	0.08	0
4	1	0	0	0
5	0.96	0.04	0	0
6	0.96	0	0	0.04
7	1	0	0	0
8	0.96	0.04	0	0
9	0.92	0.08	0	0
10	0.68	0.23	0.09	0

Table 5.5: Discretized belief states of elements 1-10 obtained in chapter 2 using three measured DOFs: N4H, N9H, N13H

Element \ $P(\theta^e = i)$	Damaged Structure			
	$i = 1$	$i = 2$	$i = 3$	$i = 4$
1	0.154	0.80	0.046	0
2	1	0	0	0
3	0.89	0.03	0.08	0
4	1	0	0	0
5	0.97	0.03	0	0
6	0.96	0.04	0	0
7	0.97	0.03	0	0
8	0.94	0.03	0.03	0
9	0.86	0.11	0.03	0
10	0.7	0.27	0.03	0

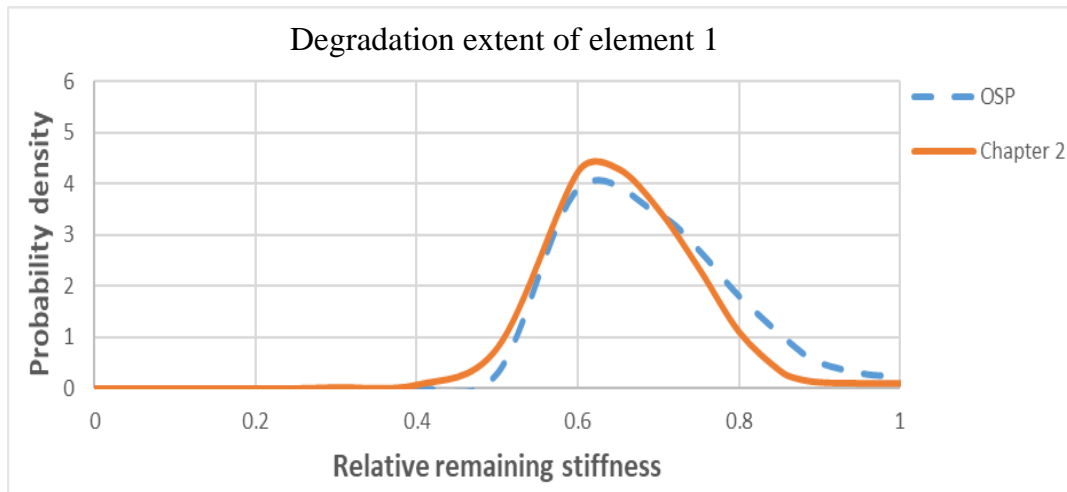


Figure 5.17: Degradation extent of element 1 obtained from: (i) Optimal Sensor Placement (OSP) in Chapter 5, (ii) sensor placement used in Chapter 2 (three measured DOF).

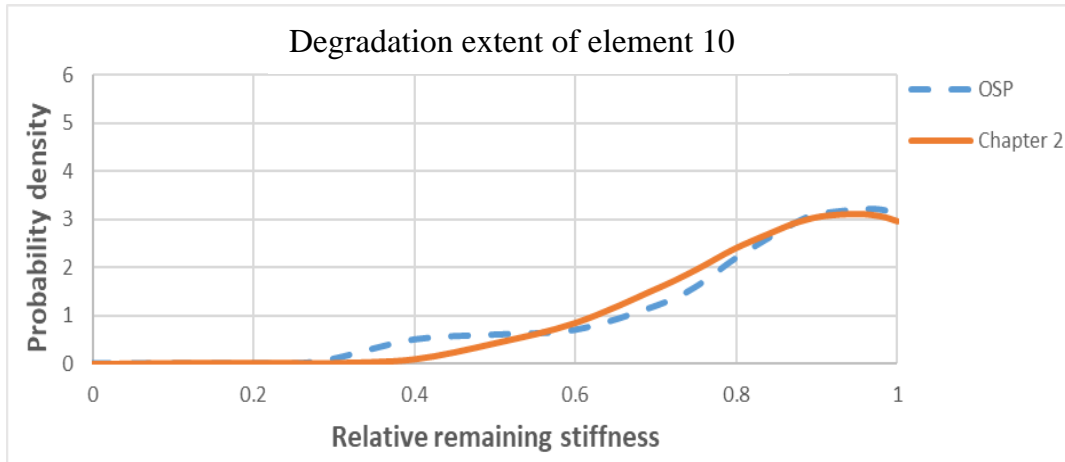


Figure 5.18: Degradation extent of element 10 obtained from: (i) Optimal Sensor Placement (OSP) in Chapter 5, (ii) sensor placement used in Chapter 2 (three measured DOF).

## 5.7 Conclusion

In this chapter, a predator-prey optimization based on a genetic algorithm is presented for an optimal sensor placement. Two populations are initially created, one defining defect configurations and the other defining sensor configurations. These two populations interact antagonistically; while defects evolve towards a configuration hard to be detected by the sensors, the latter evolve toward a configuration which is capable of efficiently detecting as many defects as possible. For each combination “*defect chromosome-sensor chromosome*”, a Bayesian update of the state of each structural element is calculated and integrated in a decision analysis, in order to calculate the costs (including the sensor price and the cost of the actions to be applied on an element depending on its condition state) and evaluate each chromosome by calculating its fitness. Based on the fitness, new populations are therefore evolved until the maximum generation number is reached. An important factor to be considered in our problem is the diversity of the defects population. To ensure that the best global solution has been obtained and that the sensor configurations have been evaluated against a wide set of defect configurations, an imposed diversity score has been added to their fitness function.

The proposed optimization methodology is validated through two numerical applications, namely a steel truss and a four-story concrete frame. These applications revealed that: (i) the populations are not always enough diversified, it is then important to impose an additional diversification on the defect population in order to broaden the search space for the sensor population and make sure that the best sensor configuration can detect as much defect configurations as possible; (ii) even though the accuracy of the information usually increases with the number of sensors, sometimes the added value in information is not worth the price of the additional sensors especially if they are not optimally located; (iii) on the other hand, when sensors are optimally positioned, the value of information could have a major effect so that the sensor price would lose a bit of its importance and in that case, the added value in

information brought by additional sensors would compensate their price to some extent. Thus, the importance of not only optimizing the location of sensors, but also searching for the optimal number of sensors to be placed. The main advantage of the proposed technique is then its contribution in improving the performance of the genetic algorithm to reach the global optimum and finding the best configuration of sensors to be placed on a structure able to detect as much damage configurations as possible.



## General Conclusion

The main objective of this thesis is to develop new SHM strategies for the monitoring of civil engineering structures. It focuses on three axes: (i) detection, localization and quantification of damage, (ii) Optimal IM&R planning and (iii) Sensor configuration optimization. Based on results provided by sensors, the developed strategies are categorized as output-only modal identification methods, belonging to the class of operational modal analysis.

The first part of this thesis is devoted to the presentation of several commonly used methods in the SHM domain concerning the three main axes of the thesis while highlighting the limits of these methods. This state of art lead in choosing the models to be based on for the development of the new strategies: (i) Approximate Bayesian Computation (ABC) for its ability to solve inverse problems without resorting to the calculation of the likelihood while taking explicitly into account the uncertainties veiling the true values, (ii) Hierarchical Approximate Bayesian Computation (HABC) for its capacity to model the flow of information between different nodes in a hierarchical settings, (iii) Decision Analysis for its ability in monetizing the value of information, (iv) Genetic Algorithm for its capability to efficiently search complex solution spaces with little or no prior knowledge about the problem to solve.

Four methodologies tackling SHM problems are presented in this work:

Using a global permanent SHM paradigm and the ABC method, the first developed methodology updates the damage extent PDFs of the structural elements according to a prior PDF and sensors measurements. This technique integrates, systematically, uncertainties affecting the accuracy of the results and do not need to pass by an explicit formulation of the likelihood function in the Bayesian process. Its application on two different types of structures, a steel truss structure and a concrete frame structure, proved its efficiency in accurately detecting most damage yet, it may be more difficult to detect small damage in elements that have no major effects on the mode shapes of the structure.

In the second methodology, an information amplifying technique is developed to improve the damage assessment of elements and/or structures that are weakly monitored using information available for strongly monitored elements and/or structures belonging to the same class. This approach is based on a hierarchical Approximate Bayesian Computation (HABC) for borrowing strength where a classification scheme is used to cluster elements according to specific features. It adopts the premise that elements belonging to the same class would exhibit similar deterioration behavior. The strength of this framework appears in its capability to obtain a good amount of information about a high number of elements (belonging to one or several structures), even the ones hardly accessible for SHM and/or conventional inspections, using a reduced number of sensors. The validation of this technique through two numerical applications revealed that even damaged elements which do not significantly affect the mode shapes can be accurately detected thanks to other well monitored elements belonging to the same class. Furthermore, in the case of multiple similar structures, it has been shown that distributing sensors on the structures and updating their condition states

accordingly, resulted in a more specific assessment than assessing each structure alone with a higher number of sensors. The improved accuracy of the updated condition states of elements belonging to a specific class is further used by our methodology for improving the assessment of the condition states of elements which do not belong to any class.

Based on the ABC procedure developed in the first methodology, a hybrid inspection-monitoring approach is developed for an optimal IM&R planning of civil engineering structures, integrating the Bayesian inference in a decision analysis framework. The aim of the methodology is to optimally decide whether: (i) an inspection is needed and on which element(s) or (ii) maintenance actions must be applied on the elements. The maintenance actions include a replacement, repair(s) or simply nothing to do if the element is in a good condition. Having applied the proposed technique on the same numerical applications as the one mentioned in the previous paragraph, results demonstrated that a permanent monitoring is fair enough for relatively small structures with limited number of elements while inspection(s) might be needed for bigger and/or more complex structures. Therefore, for such types of structures, it is important to combine data resulting from both sources, conventional inspections and permanent monitoring, to reduce the uncertainties and optimize the IM&R planning.

Taking advantage of this approach, a predator-prey optimization algorithm is proposed, based on a genetic algorithm, to optimally choose the number of sensors needed on a structure and their optimal locations. In our approach, unlike classical genetic algorithms, two populations interact and evolve antagonistically; while the population of defects evolves by trying to avoid being detected by the sensors, the population of sensors converges toward a configuration capable of detecting the largest number of defects. Hence, since our methodology is based on the coevolution of two populations, the evaluation of each type of chromosome depends on the number of chromosomes it can dominate from the other population and therefore it will encourage the population of sensors to better evolve toward a global solution. The application of this optimization algorithm on the steel structure and the concrete frame structure highlighted the importance of optimizing the number and location of sensors. Two factors are considered in our study: the diversification of the defects population and the sensors cost. Results demonstrated that imposing an additional diversification pressure on the defect population is vital to broaden the search space for the sensor population so the results are obtained taking into consideration as much defect configurations as possible. They have also shown that additional sensors do not always bring much information that is worth their price, especially if they are not optimally placed. In other situations, when sensors are optimally located, the added value in information brought by additional sensors could be more important than the increase in sensors price. It is therefore important not to only optimize the location of sensors, but also find the optimal number of sensors to be positioned.

## Perspectives

The strategies proposed in this study to overcome some limitations of structural health monitoring in civil engineering provided significant results. Nevertheless, the proposed methodologies could benefit from the implementation of several needed improvements.

One of the disadvantage of the Approximate Bayesian Computation presented in chapters 2 and 3 is its computational complexity which becomes quickly very high, even for a relatively small number of elements. The Metropolis-Hastings algorithm could have been used however, we choose to implement the original ABC formulation to avoid any potential biases that could arise from the Metropolis-Hastings algorithm (e.g. rare events are hardly taken and samples are correlated). Future works assessing the sensitivity of Metropolis-Hastings ABC & HABC in a SHM setting to such biases is needed.

One of the factors that could be taken into consideration while updating the condition states of the structural elements would be the presence of elements other than columns and beams, such as slabs, partition walls, bearing walls, etc. The contribution of the rigidity of these structural elements could affect the vibrational results and hence, contribute in improving the detection accuracy of the damage in the structure.

It would be also interesting to determine the sensitivity of the proposed methodologies in assessing damage according to various parameters such as: environmental factors (in particular the difference of temperature between day and night, and between the seasons), the variable loading, etc.

In addition to the sensitivity towards these parameters, one could add to the study other factors such as the lifetime of sensors and their probability of being damaged in a specific period of time. Such factors would help the decision maker in choosing the right type of sensors depending on the situation (i.e. the monitoring could be used for a short-term or could be needed for a long-term study).

Another factor that was not taken into account is the structure–soil interaction. In our numerical applications, structures are supposed to be simply supported. However, it would be also interesting to study the influence of the soil material to reflect the reality and understand in a more realistic way the behaviour of structures in relation to the soil which supports them.

## References

- Aasim, B. A., Karimi, A. K., & Tomiyama, J. (2021). "Assessment of a Real-life Concrete Bridge Structure using Vibration-based Damage Detection Method." In *IOP Conference Series: Materials Science and Engineering* (Vol. 1054, No. 1, p. 012011). IOP Publishing.
- Abdmouleh, Z., Gastli, A., Ben-Brahim, L., Haouari, M., & Al-Emadi, N. A. (2017). "Review of optimization techniques applied for the integration of distributed generation from renewable energy sources." *Renewable Energy*, 113, 266-280.
- Abdo, M. (2014). *Structural health monitoring history applications and future*. Open Science, New York.
- Abrams, P. A. (2000). "The evolution of predator-prey interactions: theory and evidence." *Annual Review of Ecology and Systematics*, 31(1), 79-105.
- Adams, R. D., Cawley, P., Pye, C. J., & Stone, B. J. (1978). "A vibration technique for non-destructively assessing the integrity of structures." *Journal of Mechanical Engineering Science*, 20(2), 93-100.
- Agusta, A., Thöns, S., & Leira, B. J. (2017). "Value of information-based inspection planning for offshore structures." In *ASME 2017 36th International Conference on Ocean, Offshore and Arctic Engineering*. American Society of Mechanical Engineers Digital Collection.
- Akhlaghi, M. M., Bose, S., Mohammadi, M. E., Moaveni, B., Stavridis, A., & Wood, R. L. (2021). "Post-earthquake damage identification of an RC school building in Nepal using ambient vibration and point cloud data." *Engineering Structures*, 227, 111413.
- Alaswad, S., & Xiang, Y. (2017). "A review on condition-based maintenance optimization models for stochastically deteriorating system." *Reliability Engineering & System Safety*, 157, 54-63.
- Allemang, R.J. (2003). "The Modal Assurance Criterion (MAC): Twenty Years of Use and Abuse." *Sound and Vibration*, 37.
- Altunışık, A. C., Okur, F. Y., & Kahya, V. (2017). "Modal parameter identification and vibration based damage detection of a multiple cracked cantilever beam." *Engineering Failure Analysis*, 79, 154–170.
- Atkins (2002). *CSS bridge condition indicators, Volume 3: Evaluation of condition indicators*. Lincoln: County Surveyors Society.
- Attoh-Okine, N.O., & Bowers, S. (2006). "A Bayesian belief network model of bridge deterioration." *Bridge Engineering*, 159(2), 69-76.
- Avcı, O., Abdeljaber, O., Kiranyaz, S., Hussein, M., Gabbouj, M., & Inman, D. J. (2021). "A review of vibration-based damage detection in civil structures: From traditional methods to

Machine Learning and Deep Learning applications.” *Mechanical Systems and Signal Processing*, 147, 107077.

Azim, M. R., & Gül, M. (2020). “Data-driven damage identification technique for steel truss railroad bridges utilizing principal component analysis of strain response.” *Structure and Infrastructure Engineering*, 1-17.

Bachmann, H., & Dieterle, R. (1981). “Experiments and models for the damping behavior of vibrating reinforced concrete beams in the uncracked and cracked conditions.” *Bericht Nr, 119*.

Balageas, D. (2006). *Introduction to structural health monitoring*. ISTE, London.

Barroso, L.R., & Rodriguez, R. (2004). “Damage detection utilizing the damage index method to a benchmark structure.” *Journal of Engineering Mechanics*, 130 (2), 142–151.

Bastidas-Arteaga E., & Schoefs F., (2015). “Sustainable Maintenance and Repair of RC Coastal Structures.” *Proceedings of the Institution of Civil Engineers: Maritime Engineering*.

Beck, J. L., & Katafygiotis, L. S. (1998). “Updating models and their uncertainties. I: Bayesian statistical framework.” *Journal of Engineering Mechanics*, 124(4), 455-461.

Behmanesh, I., & Moaveni, B. (2014). “Probabilistic identification of simulated damage on the Dowling Hall footbridge through Bayesian finite element model updating.” *Structural Control and Health Monitoring*, 22(3), 463–483.

Behmanesh, I., Moaveni, B., Lombaert, G., & Papadimitriou, C. (2015). “Hierarchical Bayesian model updating for structural identification.” *Mechanical Systems and Signal Processing*, 64-65, 360–376.

Behtani, A., & Bouazzouni, A. (2011). Localisation de défauts dans les structures poutres stratifiées basée sur des données modales. In *Congrès français de mécanique*. AFM, Maison de la Mécanique, 39/41 rue Louis Blanc, 92400 Courbevoie, France (FR).

Bergmeister K. (2003). *Monitoring and safety evaluation of existing concrete structures: State-of-art Report*. International Federation for Structural Concrete, Lausanne.

Bikhiet, M. M., El-Shafey, N. F., & El-Hashimy, H. M. (2014). “Behavior of reinforced concrete short columns exposed to fire.” *Alexandria Engineering Journal*, 53(3), 643-653.

Borah, S., Al-Habaibeh, A., & Kromanis, R. (2021). The effect of temperature variation on bridges-a literature review.

Brincker, R., & Ventura, C. (2015). *Introduction to operational modal analysis*. John Wiley & Sons, Chichester.

- Byron, J., & Iba, W. (2016). "Population Diversity as a Selection Factor: Improving Fitness by Increasing Diversity." *Proceedings of the 2016 on Genetic and Evolutionary Computation Conference Companion*, 953-959.
- Cao, M. S., Sha, G. G., Gao, Y. F., & Ostachowicz, W. (2017). "Structural damage identification using damping: a compendium of uses and features." *Smart Materials and Structures*, 26(4), 043001.
- Cao, M., Xu, W., Ostachowicz, W., & Su, Z. (2014). "Damage identification for beams in noisy conditions based on Teager energy operator-wavelet transform modal curvature." *Journal of Sound and Vibration*, 333(6), 1543-1553.
- Catbas, F. N., Moon, F. L., & Aktan, A. E. (2008). "Structural Identification of Constructed Systems: An Integrated Approach by the ASCE Committee." *Structures Congress 2008: Crossing Borders*.
- Cawley, P., & Adams, R. D. (1979). "The location of defects in structures from measurements of natural frequencies." *The Journal of Strain Analysis for Engineering Design*, 14(2), 49-57.
- Chang, P. C., Flatau, A., & Liu, S. C. (2003). "Review Paper: Health Monitoring of Civil Infrastructure." *Structural Health Monitoring*, 2(3), 257-267.
- Chapoulade, E. (2019). *Optimisation de l'instrumentation pour le suivi et l'évaluation de l'état des alvéoles de stockage de déchets radioactifs* (Doctoral dissertation, Université Clermont Auvergne).
- Chapoulade, A., Talon, A., Chateauneuf, A., Breul, P., Hermand, G., & Leconte, M. (2020). "Sensors position optimization for monitoring the convergence of radioactive waste storage tunnel." *Nuclear Engineering and Design*, 367, 110778.
- Chen, C., Yang, Z., Tan, Y., & He, R. (2014). "Diversity controlling genetic algorithm for order acceptance and scheduling problem." *Mathematical Problems in Engineering*, 1-11.
- Chen, G. S., Bruno, R. J., & Salama, M. (1991). "Optimal placement of active/passive members in truss structures using simulated annealing." *AIAA journal*, 29(8), 1327-1334.
- Chiachio, M., Beck, J. L., Chiachio, J., & Rus, G. (2014). "Approximate Bayesian Computation by Subset Simulation." *SIAM Journal on Scientific Computing*, 36(3), A1339-A1358.
- Ching, J., & Beck, J. L. (2004). "New Bayesian model updating algorithm applied to a structural health monitoring benchmark." *Structural Health Monitoring*, 3(4), 313-332.
- Chiu, P. L., & Lin, F. Y. (2004). "A simulated annealing algorithm to support the sensor placement for target location." In *Canadian Conference on Electrical and Computer Engineering 2004 (IEEE Cat. No. 04CH37513)*, 2, 867-870.

- Chung, H. Y., Manuel, L., & Frank, K. H. (2006). "Optimal inspection scheduling of steel bridges using nondestructive testing techniques." *Journal of Bridge Engineering*, 11(3), 305-319.
- Congdon, P. D. (2010). *Applied Bayesian hierarchical methods*. Chapman and Hall/CRC, Boca Raton.
- Corotis, R.B., Ellis, J.H., & Jiang, M. (2005). "Modeling of risk-based inspection, maintenance and life-cycle cost with partially observable Markov decision process." *Structure and Infrastructure Engineering*, 1, 75-84.
- Curadelli, R. O., Riera, J. D., Ambrosini, D., & Amani, M. G. (2008). "Damage detection by means of structural damping identification." *Engineering Structures*, 30(12), 3497-3504.
- Das, A.J., & Haldar, A. (2010). "Structural integrity assessment under uncertainty for three dimensional offshore structures." *International Journal of Terraspace Science and Engineering*, 2 (2), 101–111.
- Das, S., Saha, P., & Patro, S. K. (2016). "Vibration-based damage detection techniques used for health monitoring of structures: a review." *Journal of Civil Structural Health Monitoring*, 6(3), 477-507.
- Del Moral, P., Doucet, A., & Jasra, A. (2012). "An adaptive sequential Monte Carlo method for approximate Bayesian computation." *Statistics and Computing*, 22(5), 1009-1020.
- Der Kiureghian, A., & Ditlevsen, O. (2009). "Aleatory or epistemic? Does it matter?" *Structural safety*, 31(2), 105-112.
- Diamantidis, D. (Ed.). (2001). *Report 32: Probabilistic Assessment of Existing Structures-A publication for the Joint Committee on Structural Safety (JCSS)* (Vol. 32). RILEM publications.
- Dongsheng L. (2011). *Sensor placement methods and evaluation criteria in structural health monitoring*. PhD Dissertation, Université de Siegen.
- Eberhart, R., & Kennedy, J. (1995, November). "Particle swarm optimization." *Proceedings of the IEEE international conference on neural networks*, 4, 1942-1948.
- Enckell, M. (2006). *Structural health monitoring using modern sensor technology: long-term monitoring of the New Årsta Railway Bridge* (Doctoral dissertation, KTH).
- Faddoul, R., Raphael, W., & Chateauneuf, A. (2011). "A generalised partially observable Markov decision process updated by decision trees for maintenance optimisation." *Structure and Infrastructure Engineering*, 7(10), 783-796.
- Faddoul, R., Raphael, W., Soubra, A. H., & Chateauneuf, A. (2012). "Incorporating Bayesian networks in Markov Decision Processes." *Journal of Infrastructure Systems*, 19(4), 415-424.

- Fan, X., Li, J., & Hao, H. (2021). “Review of piezoelectric impedance based structural health monitoring: Physics-based and data-driven methods.” *Advances in Structural Engineering*, 13694332211038444.
- Fang, S.-E., Chen, S., Lin, Y.-Q., & Dong, Z.-L. (2019). “Probabilistic damage identification incorporating approximate Bayesian computation with stochastic response surface.” *Mechanical Systems and Signal Processing*, 128, 229–243.
- Farrar, C. R., & Doebling, S. W. (1997). *An overview of modal-based damage identification methods* (No. LA-UR-97-2468; CONF-9706153-). Los Alamos National Laboratory, United States.
- Figueiredo E. (2010). *Damage identification in civil engineering infrastructure under operational and environmental conditions*. PhD dissertation, University of Porto.
- Florian, Mihai; Sørensen, John Dalsgaard (2017). “Risk-based planning of operation and maintenance for offshore wind farms.” *Energy Procedia*, 137(), 261–272.
- Frigui, F., Faye, J. P., Martin, C., Dalverny, O., Pérès, F., & Judenherc, S. (2018). “Global methodology for damage detection and localization in civil engineering structures.” *Engineering Structures*, 171, 686-695.
- Gentile, C., & Saisi, A. (2007). “Ambient vibration testing of historic masonry towers for structural identification and damage assessment”. *Construction and Building Materials*, 21(6), 1311–1321.
- Gholizadeh, S. (2016). “A review of non-destructive testing methods of composite materials.” *Procedia Structural Integrity*, 1, 50-57.
- Giurgiutiu, V. (2007). *Structural Health Monitoring with Piezoelectric Wafer Active Sensors: with Piezoelectric Wafer Active Sensors*. Elsevier, New York.
- Gonzalez, I., & Karoumi, R. (2015). “BWIM aided damage detection in bridges using machine learning.” *Journal of Civil Structural Health Monitoring*, 5(5), 715-725.
- González, A., OBrien, E. J., & McGetrick, P. J. (2012). “Identification of damping in a bridge using a moving instrumented vehicle.” *Journal of Sound and Vibration*, 331(18), 4115-4131.
- Görl, E., & Link, M. (2003). “Damage identification using changes of eigenfrequencies and mode shapes.” *Mechanical systems and signal processing*, 17(1), 103-110.
- Guzman-Acevedo, G. M., Vazquez-Becerra, G. E., Millan-Almaraz, J. R., Rodriguez-Lozoya, H. E., Reyes-Salazar, A., Gaxiola-Camacho, J. R., & Martinez-Felix, C. A. (2019). “GPS, accelerometer, and smartphone fused smart sensor for SHM on real-scale bridges.” *Advances in Civil Engineering*, 2019.
- Ha, Q. M., Deville, Y., Pham, Q. D., & Hà, M. H. (2020). A hybrid genetic algorithm for the traveling salesman problem with drone. *Journal of Heuristics*, 26(2), 219-247.



- Hammond, J. S., Keeney, R. L., & Raiffa, H. (2015). *Smart choices: A practical guide to making better decisions*. Harvard Business Review Press, Massachusetts.
- He, L., Lian, J., Ma, B., & Wang, H. (2014). "Optimal multi-axial sensor placement for modal identification of large structures." *Structural Control and Health Monitoring*, 21(1), 61-79.
- He, C., Xing, J., Li, J., Yang, Q., Wang, R., & Zhang, X. (2015). "A new optimal sensor placement strategy based on modified modal assurance criterion and improved adaptive genetic algorithm for structural health monitoring." *Mathematical problems in engineering*, 1-10.
- Helal, J., Sofi, M., & Mendis, P. (2015). "Non-destructive testing of concrete: A review of methods." *Electronic Journal of Structural Engineering*, 14(1), 97-105.
- Heo, G., Kim, C., Lee, C., Hur, J., & Seo, S. (2017). "A damage assessment technique based on a revised Statistical Pattern-recognition Technique (SPRT)." *KSCE Journal of Civil Engineering*, 21(3), 882-888.
- Hu, C., & Afzal, M. T. (2006). "A statistical algorithm for comparing mode shapes of vibration testing before and after damage in timbers." *Journal of Wood Science*, 52(4), 348-352.
- John, H. (1975). Holland. 1975. "Adaptation in natural and artificial systems." *Ann Arbor: University of Michigan Press*.
- Hou, R., Xia, Y., Xia, Q., & Zhou, X. (2019). "Genetic algorithm based optimal sensor placement for L1-regularized damage detection." *Structural Control and Health Monitoring*, 26(1), e2274.
- Hu, C., & Afzal, M. T. (2006). "A statistical algorithm for comparing mode shapes of vibration testing before and after damage in timbers." *Journal of Wood Science*, 52(4), 348-352.
- IFSTTAR & CEREMA (2015). "Auscultation des ouvrages d'art" [Online website]. *Cahiers Interactifs, CIII*. (<http://www.ifsttar.fr/collections/CahiersInteractifs/CIII>)
- Imounga, H. M., Bastidas-Arteaga, E., Moutou Pitti, R., Ekomy Ango, S., & Wang, X. H. (2020). "Bayesian assessment of the effects of cyclic loads on the chloride ingress process into reinforced concrete." *Applied Sciences*, 10(6), 2040.
- ITSEOA, Fascicule 03 (2010). "Auscultation, surveillance renforcée, haute surveillance, mesures de sécurité immédiate ou de sauvegarde", *SETRA*. (<https://www.cerema.fr/fr/centre-ressources/boutique/instruction-technique-surveillance-entretien-ouvrages-art-2>)
- Jiang, X., & Mahadevan, S. (2009). "Bayesian hierarchical uncertainty quantification by structural equation modeling." *International journal for numerical methods in engineering*, 80(6-7), 717-737.

- Jin, H., Xia, J., & Wang, Y. Q. (2015). “Optimal sensor placement for space modal identification of crane structures based on an improved harmony search algorithm 基于改进和声搜索算法识别门式起重机结构空间模态的传感器优化布置方法研究.” *Journal of Zhejiang University-SCIENCE A*, 16(6), 464-477.
- Jung, B. K., Cho, J. R., & Jeong, W. B. (2015). “Sensor placement optimization for structural modal identification of flexible structures using genetic algorithm.” *Journal of Mechanical Science and Technology*, 29(7), 2775-2783.
- Kammer, D.C. (1991) “Sensor placement for on-orbit modal identification and correlation of large space structures.” *Journal of Guidance, Control and Dynamics*, 14, 251–259.
- Kato, M., & Shimada, S. (1986). “Vibration of PC bridge during failure process.” *Journal of Structural Engineering*, 112(7), 1692-1703.
- Kazemi, S., Rahai, A. R., Daneshmand, F., & Fooladi, A. (2011). “Implementation of modal flexibility variation method and genetically trained ANNs in fault identification.” *Ocean Engineering*, 38(5-6), 774-781.
- Keenahan, J., OBrien, E. J., McGetrick, P. J., & Gonzalez, A. (2014). “The use of a dynamic truck–trailer drive-by system to monitor bridge damping.” *Structural Health Monitoring*, 13(2), 143-157.
- Ko J. M., Ni Y. Q., Sun Z. G. Chan, H. T. (2003). “Remote visualized health monitoring of cablesupported bridges.” *Proceedings of SPIE: Smart Structures and Materials and Nondestructive Evaluation for Health Monitoring and Diagnostics*, 4337, 368-378.
- Kral, Z., Horn, W., & Steck, J. (2013). “Crack propagation analysis using acoustic emission sensors for structural health monitoring systems.” *The Scientific World Journal*, 2013.
- Kuno, E. (1987). “Principles of Predator–Prey Interaction in Theoretical, Experimental, and Natural Population Systems.” *Advances in Ecological Research*, 16, 249–337.
- Lestari, W., & Qiao, P. (2005). “Damage detection of fiber-reinforced polymer honeycomb sandwich beams.” *Composite Structures*, 67(3), 365-373.
- Lerman, I. C., & Ngouenet, R. (1995). Algorithmes génétiques séquentiels et parallèles pour une représentation affine des proximités. [Rapport de recherche] RR-2570, INRIA.
- Li, J., Zhang, X., Xing, J., Wang, P., Yang, Q., & He, C. (2015). “Optimal sensor placement for long-span cable-stayed bridge using a novel particle swarm optimization algorithm.” *Journal of Civil Structural Health Monitoring*, 5(5), 677-685.
- Liang, C., Sun, F. P., & Rogers, C. A. (1994). “An impedance method for dynamic analysis of active material systems.” *Journal of Vibration and Acoustics*, 116(1), 120-128.

- Liu, G. R., & Chen, S. C. (2002). "A novel technique for inverse identification of distributed stiffness factor in structures." *Journal of Sound and Vibration*, 254(5), 823-836.
- Liu, W., Gao, W. C., Sun, Y., & Xu, M. J. (2008). "Optimal sensor placement for spatial lattice structure based on genetic algorithms." *Journal of Sound and Vibration*, 317(1-2), 175-189.
- Liu, Y., & Chen, C. J. (2017). "Dynamic reliability assessment for non-repairable multistate systems by aggregating multilevel imperfect inspection data." *IEEE Transactions on Reliability*, 66(2), 281-297.
- Luque, Jesus; Straub, Daniel (2019). "Risk-based optimal inspection strategies for structural systems using dynamic Bayesian networks." *Structural Safety*, 76(), 68–80.
- Lynch, J. P., Farrar, C. R., & Michaels, J. E. (2016). "Structural health monitoring: technological advances to practical implementations [scanning the issue]." *Proceedings of the IEEE*, 104(8), 1508-1512.
- Mahdavi, M., Fesanghary, M., & Damangir, E. (2007). "An improved harmony search algorithm for solving optimization problems." *Applied mathematics and computation*, 188(2), 1567-1579.
- Manjarres, D., Landa-Torres, I., Gil-Lopez, S., Del Ser, J., Bilbao, M. N., Salcedo-Sanz, S., & Geem, Z. W. (2013). "A survey on applications of the harmony search algorithm." *Engineering Applications of Artificial Intelligence*, 26(8), 1818-1831.
- Marin, J.-M., Pudlo, P., Robert, C. P., & Ryder, R. J. (2011). *Approximate Bayesian computational methods. Statistics and Computing*, 22(6), 1167–1180.
- Marjoram, P., Molitor, J., Plagnol, V., & Tavaré, S. (2003). "Markov chain Monte Carlo without likelihoods." *Proceedings of the National Academy of Sciences*, 100(26), 15324–15328.
- Mc Ginley, B., Maher, J., O'Riordan, C., & Morgan, F. (2011). "Maintaining healthy population diversity using adaptive crossover, mutation, and selection." *IEEE Transactions on Evolutionary Computation*, 15(5), 692-714.
- Messina, A., Williams, E. J., & Contursi, T. (1998). "Structural damage detection by a sensitivity and statistical-based method." *Journal of sound and vibration*, 216(5), 791–808.
- Moughty, J. J., & Casas, J. R. (2017). "A state of the art review of modal-based damage detection in bridges: Development, challenges, and solutions." *Applied Sciences*, 7(5), 510.
- Mohan, V., Parivallal, S., Kesavan, K., Arunsundaram, B., Ahmed, A. F., & Ravisankar, K. (2014). "Studies on damage detection using frequency change correlation approach for health assessment." *Procedia Engineering*, 86, 503-510.

- Nair, K. K., & Kiremidjian, A. S. (2007). "Time series based structural damage detection algorithm using Gaussian mixtures modeling." *Journal of dynamic systems, measurement, and control*, 129(3), 285-293.
- Nasrollahi, A., Deng, W., Ma, Z., & Rizzo, P. (2018). "Multimodal structural health monitoring based on active and passive sensing." *Structural Health Monitoring*, 17(2), 395-409.
- Ngatchou, P. N., Fox, W. L., & El-Sharkawi, M. A. (2005). "Distributed sensor placement with sequential particle swarm optimization." *Swarm Intelligence Symposium, Proceedings 2005 IEEE*, 385-388.
- Nozari, A., Bose, S., Moaveni, B., & Stavridis, A. (2017). "Finite element model updating and damage identification of a school building in Sankhu, Nepal." In *16th World Conference on Earthquake Engineering*, Santiago Chile.
- Ntotsios, E., Papadimitriou, C., Panetsos, P., Karaiskos, G., Perros, K., & Perdikaris, P. C. (2009). "Bridge health monitoring system based on vibration measurements." *Bulletin of Earthquake Engineering*, 7(2), 469.
- O'Brien, E. J., & Malekjafarian, A. (2016). "A mode shape-based damage detection approach using laser measurement from a vehicle crossing a simply supported bridge." *Structural Control and Health Monitoring*, 23(10), 1273-1286.
- O'Brien, E. J., Sevillano, E., & Martinez, D. (2016). "Monitoring the condition of a bridge using a traffic speed deflectometer vehicle travelling at highway speed." *BCCCE 3rd International Balkans Conference on Challenges of Civil Engineering*, Epoka University, Tirana.
- Ohtsu, M. (2015). *Acoustic emission and related non-destructive evaluation techniques in the fracture mechanics of concrete: fundamentals and applications*. Woodhead Publishing, Cambridge.
- Okasha, N. M., Frangopol, D. M., & Orcesi, A. D. (2012). "Automated finite element updating using strain data for the lifetime reliability assessment of bridges". *Reliability Engineering & System Safety*, 99, 139-150.
- Orcesi, A. D., & Frangopol, D. M. (2011). "Use of lifetime functions in the optimization of nondestructive inspection strategies for bridges." *Journal of Structural Engineering*, 137(4), 531-539.
- Orcesi, A. D., & Frangopol, D. M. (2011). "Optimization of bridge maintenance strategies based on structural health monitoring information." *Structural Safety*, 33(1), 26-41.
- Oshima, Y., Yamamoto, K., & Sugiura, K. (2014). "Damage assessment of a bridge based on mode shapes estimated by responses of passing vehicles." *Smart Structures and Systems*, 13(5), 731-753.

- Oyarzo-Vera, C., & Chouw, N. (2017). "Damage identification of unreinforced masonry panels using vibration-based techniques." *Shock and Vibration*, 2017.
- Pandey, A. K., & Biswas, M. (1994). "Damage detection in structures using changes in flexibility." *Journal of sound and vibration*, 169(1), 3-17.
- Pandey, A. K., Biswas, M., & Samman, M. M. (1991). "Damage detection from changes in curvature mode shapes." *Journal of sound and vibration*, 145(2), 321-332.
- Papadimitriou, C. (2004). "Optimal sensor placement methodology for parametric identification of structural systems." *Journal of sound and vibration*, 278(4-5), 923-947.
- Papadimitriou, C., & Lombaert, G. (2012) "The effect of prediction error correlation on optimal sensor placement in structural dynamics." *Mechanical System and Signal Processing*, 28, 105–127.
- Park, S., Kim, Y. B., & Stubbs, N. (2002). "Nondestructive damage detection in large structures via vibration monitoring." *Electronic Journal of Structural Engineering*, 2, 59-75.
- Parloo, E., Guillaume, P., & Van Overmeire, M. (2003). "Damage assessment using mode shape sensitivities." *Mechanical systems and signal Processing*, 17(3), 499-518.
- Pastor, M., Binda, M., Harčarik, T. (2012) "Modal Assurance Criterion." *Procedia Engineering*, 48, 543-548.
- Posenato, D., Kripakaran, P., Inaudi, D., & Smith, I. F. C. (2010). "Methodologies for model-free data interpretation of civil engineering structures." *Computers & Structures*, 88(7-8), 467–482.
- Prado, D. M., Araujo, I. D. G., Haach, V. G., & Carrazedo, R. (2016). "Assessment of shear damaged and NSM CFRP retrofitted reinforced concrete beams based on modal analysis." *Engineering Structures*, 129, 54–66.
- Préaux J-P. 2018. *Méthode du recuit simulé*, Presentation, Université Aix Marseille.
- Rabiei, M., & Modarres, M. (2013). "A recursive Bayesian framework for structural health management using online monitoring and periodic inspections." *Reliability Engineering & System Safety*, 112, 154–164.
- Rakotomahefa A., Randimbindrainibe F., & Robinson M. (2019). "Application des algorithmes génétiques sur un planning sous contraintes." *Mada-Eti*, 2.
- Rainieri, C., & Fabbrocino, G. (2014). *Operational modal analysis of civil engineering structures*. Springer, 142, 143.
- Razak, H. A., & Choi, F.C. (2001). "The effect of corrosion on the natural frequency and modal damping of reinforced concrete beams." *Engineering Structures*, 23(9), 1126–1133.

- Reynders, E., Teughels, A., & De Roeck, G. (2010). "Finite element model updating and structural damage identification using OMAX data." *Mechanical Systems and Signal Processing*, 24(5), 1306-1323.
- Robert, C. (2006). *Le choix bayésien : Principes et pratique*. Springer Science & Business Media, Paris.
- Rodrigues, C., Félix, C., Lage, A., & Figueiras, J. (2010). "Development of a long-term monitoring system based on FBG sensors applied to concrete bridges." *Engineering Structures*, 32(8), 1993–2002.
- Rucevskis, S., Janeliukstis, R., Akishin, P., & Chate, A. (2016). "Mode shape-based damage detection in plate structure without baseline data." *Structural Control and Health Monitoring*, 23(9), 1180–1193.
- Ruffels, A., Gonzalez, I., & Karoumi, R. (2020). "Model-free damage detection of a laboratory bridge using artificial neural networks." *Journal of Civil Structural Health Monitoring*, 1-13.
- Rytter, A. (1993). *Vibration based inspection of civil engineering structures*. PhD dissertation, University of Aalborg.
- Salawu, O. S. (1997). "Detection of structural damage through changes in frequency: a review." *Engineering structures*, 19(9), 718-723.
- Santa, U., Bergmeister, K., & Strauss, A. (2002). "Guaranteeing structural service life through monitoring." *1st fib congress in Osaka*, 13-19.
- Santos, J. P., Cremona, C., Orcesi, A. D., & Silveira, P. (2017). "Early damage detection based on pattern recognition and data fusion." *Journal of Structural Engineering*, 143(2), 04016162.
- Sen, D., & Nagarajaiah, S. (2018). "Data-driven approach to structural health monitoring using statistical learning algorithms." In *Mechatronics for cultural heritage and civil engineering* (pp. 295-305). Springer, Cham.
- Sha, G., Radziński, M., Cao, M., & Ostachowicz, W. (2019). "A novel method for single and multiple damage detection in beams using relative natural frequency changes." *Mechanical Systems and Signal Processing*, 132, 335-352.
- Sharp I., Yu K. (2019). *Use of Sensors for Position Determination. In: Wireless Positioning: Principles and Practice*. Navigation: Science and Technology. Springer, Singapore.
- Shi, Z. Y., Law, S.S., & Zhang, L. M. (2000a). "Damage localization by directly using incomplete mode shapes." *Journal of engineering mechanics*, 126(6), 656-660.
- Shi, Z.Y., Law, S.S., & Zhang, L.M. (2000b). "Structural damage detection from modal strain energy change." *Journal of Engineering Mechanics*, 126 (12), 1216–1223.

- Sisson, S., Fan, Y., & Tanaka, M. M. (2008). *A note on backward kernel choice for sequential Monte Carlo without likelihoods*. Technical report, University of New South Wales.
- Srinivasan, M. G., & Kot, C. A. (1992). *Effect of damage on the modal parameters of a cylindrical shell*. Argonne National Lab., IL (United States).
- Stratt, R.W. (2010). "Bridge management a system approach for decision making." *School of Doctoral Studies European Union Journal*, 2, 67–108.
- Strauss, A., Frangopol, D. M., & Kim, S. (2008). "Use of monitoring extreme data for the performance prediction of structures: Bayesian updating." *Engineering structures*, 30(12), 3654-3666.
- Stubbs, N. (2011). "A literature review of recent methods for structural health monitoring systems to evaluate structural capacity and remaining service life of bridges." Final Report, Iowa State University Bridge Engineering Center.
- Stubb, N., & Kim, J. T. (1996). "Damage Localization in Structures without Baseline Modal Parameter." *AIAA Journal*, 34, 1644-1649.
- Su, J. B., Luan, S. L., Zhang, L. M., Zhu, R. H., & Qin, W. G. (2019). "Partitioned genetic algorithm strategy for optimal sensor placement based on structure features of a high-piled wharf." *Structural Control and Health Monitoring*, 26(1), e2289.
- Sun, H., & Büyüköztürk, O. (2015) "Optimal sensor placement in structural health monitoring using discrete optimization." *Smart Materials and Structures*, 24, 125034.
- Sung, S. H., Koo, K. Y., & Jung, H. J. (2014). "Modal flexibility-based damage detection of cantilever beam-type structures using baseline modification." *Journal of Sound and Vibration*, 333(18), 4123-4138.
- Sunnåker, M., Busetto, A. G., Numminen, E., Corander, J., Foll, M., & Dessimoz, C. (2013). "Approximate Bayesian Computation." *PLoS Computational Biology*, 9(1), e1002803.
- Sørensen, J. D. (2009). "Framework for risk-based planning of operation and maintenance for offshore wind turbines." *Wind Energy*, 12(5), 493–506.
- Tan, Y., & Zhang, L. (2019). "Computational methodologies for optimal sensor placement in structural health monitoring: A review." *Structural Health Monitoring*, 1-22.
- Tatar, A., Niousha, A., & Rofooei, F. R. (2017). "Damage detection in existing reinforced concrete building using forced vibration test based on mode shape data." *Journal of Civil Structural Health Monitoring*, 7(1), 123-135.
- Toni, T., Welch, D., Strelkowa, N., Ipsen, A., & Stumpf, M. P. (2008). "Approximate Bayesian computation scheme for parameter inference and model selection in dynamical systems." *Journal of the Royal Society Interface*, 6(31), 187-202.

- Tseng, K. K., & Wang, L. (2004). "Smart piezoelectric transducers for in situ health monitoring of concrete." *Smart Materials and Structures*, 13(5), 1017.
- Tran, T. B., Bastidas-Arteaga, E., Aoues, Y., Pambou Nziengui, C. F., Hamdi, S. E., Moutou Pitti, R., Fournely, E., Schoefs, F., & Chateauneuf, A. (2018). "Reliability assessment and updating of notched timber components subjected to environmental and mechanical loading." *Engineering Structures*, 166, 107-116.
- Tran, T. B., Bastidas-Arteaga, E., & Schoefs, F. (2016). "Improved Bayesian network configurations for random variable identification of concrete chlorination models." *Materials and Structures*, 49(11), 4705-4718.
- Turner, B. M., & Van Zandt, T. (2014). "Hierarchical approximate Bayesian computation." *Psychometrika*, 79(2), 185-209.
- Vakilzadeh, M. K., Huang, Y., Beck, J. L., & Abrahamsson, T. (2017). "Approximate Bayesian Computation by Subset Simulation using hierarchical state-space models." *Mechanical Systems and Signal Processing*, 84, 2–20.
- Vanik, M. W., Beck, J. L., & Au, S. (2000). "Bayesian probabilistic approach to structural health monitoring." *Journal of Engineering Mechanics*, 126(7), 738-745.
- Wahab, M. A., & De Roeck, G. (1999). "Damage detection in bridges using modal curvatures: application to a real damage scenario." *Journal of Sound and vibration*, 226(2), 217-235.
- Wang, D., He, J., Dong, B., Liu, X., & Zhang, W. (2016). "Novel damage detection techniques for structural health monitoring using a hybrid sensor." *Mathematical Problems in Engineering*, 2016.
- Wang, D., Song, H., & Zhu, H. (2013). "Numerical and experimental studies on damage detection of a concrete beam based on PZT admittances and correlation coefficient." *Construction and Building Materials*, 49, 564-574.
- Wang, J., & Zabarar, N. (2004). "Hierarchical Bayesian models for inverse problems in heat conduction." *Inverse Problems*, 21(1), 183–206.
- Wegmann, D., Leuenberger, C., & Excoffier, L. (2009). Efficient approximate Bayesian computation coupled with Markov chain Monte Carlo without likelihood. *Genetics*, 182(4), 1207-1218.
- Wilkinson, R. D. (2013). "Approximate Bayesian computation (ABC) gives exact results under the assumption of model error." *Statistical applications in genetics and molecular biology*, 12, 129– 141.
- Wongprasert, N., & Symans, M. D. (2004). "Application of a genetic algorithm for optimal damper distribution within the nonlinear seismic benchmark building." *Journal of Engineering Mechanics*, 130(4), 401-406.



- Worden, K., Manson, G., & Fieller, N. R. (2000). "Damage detection using outlier analysis." *Journal of Sound and Vibration*, 229(3), 647-667.
- Yadav, P., Kumar, R., Panda, S. K., & Chang, C. S. (2012). "An intelligent tuned harmony search algorithm for optimisation." *Information Sciences*, 196, 47-72.
- Yan, W. J., Ren, W. X., & Huang, T. L. (2012). "Statistic structural damage detection based on the closed-form of element modal strain energy sensitivity." *Mechanical Systems and Signal Processing*, 28, 183-194.
- Yan, W. J., & Ren, W. X. (2011). "A direct algebraic method to calculate the sensitivity of element modal strain energy." *International Journal for Numerical Methods in Biomedical Engineering*, 27(5), 694-710.
- Yang, Y., & Divsholi, B. S. (2010). "Sub-frequency interval approach in electromechanical impedance technique for concrete structure health monitoring." *Sensors*, 10(12), 11644-11661.
- Yao, L., Sethares, W. A., & Kammer, D. C. (1993). "Sensor placement for on-orbit modal identification via a genetic algorithm." *AIAA journal*, 31(10), 1922-1928.
- Yi, T. H., Li, H. N., & Gu, M. (2011a). "Optimal sensor placement for health monitoring of high-rise structure based on genetic algorithm." *Mathematical Problems in Engineering*, 2011.
- Yi, T. H., Li, H. N., & Gu, M. (2011b). "Optimal sensor placement for structural health monitoring based on multiple optimization strategies." *The Structural Design of Tall and Special Buildings*, 20(7), 881-900.
- Yu, L., Giurgiutiu, V., Yu, J., Ziehl, P., & Zhao, L. (2012). "Comparative study of active and passive sensing with AE and PWAS transducers." *Nondestructive Characterization for Composite Materials, Aerospace Engineering, Civil Infrastructure, and Homeland Security 2012*, 8347, 834720.
- Zdunek A.D., Prine D. (1995). "Early Detection of Steel Rebars Corrosion by Acoustic Emission Monitoring." Infrastructure Technology Institute, Illinois.
- Zhang, C., Ji, H., Qiu, J., Wu, Y., & Hu, N. (2014). "Impact identification using a passive imaging method." *International Journal of Applied Electromagnetics and Mechanics*, 46(4), 835-844.
- Zhang, H., Lennox, B., Zhang, H., Goulding, P. R., & Leung, A. Y. T. (2000). "A float-encoded genetic algorithm technique for integrated optimization of piezoelectric actuator and sensor placement and feedback gains." *Smart Materials and Structures*, 9(4), 552-557.

Zhang, J., Maes, K., De Roeck, G., Reynders, E., Papadimitriou, C., & Lombaert, G. (2017). "Optimal sensor placement for multi-setup modal analysis of structures." *Journal of Sound and Vibration*, 401, 214-232.

Zhang, Q. W. (2007). "Statistical damage identification for bridges using ambient vibration data." *Computers & structures*, 85(7-8), 476-485.

Zhang, Y., Wang, L., & Xiang, Z. (2012). "Damage detection by mode shape squares extracted from a passing vehicle." *Journal of Sound and Vibration*, 331(2), 291-307.

Zhao, J., & Zhang, L. (2012). "Structural damage identification based on the modal data change." *International Journal of Engineering and Manufacturing*, 4, 59-66.

Zhou, K., & Wu, Z. Y. (2017). "Strain gauge placement optimization for structural performance assessment." *Engineering Structures*, 141, 184-197

## Appendix A: Modal analysis results

This appendix presents the frequencies and the mode shapes of the first modes in the undamaged and damaged structures treated in Chapters 2 and 3.

- **Steel Truss**

Table A.1: Frequencies of the first three modes in the damaged and undamaged steel truss structure.

	Undamaged (Hz)	Damaged (50% element 8) (Hz)	Damaged (80% element 8) (Hz)
1 <sup>st</sup> mode	3.23	3.08	2.73
2 <sup>nd</sup> mode	7.19	7.12	6.95
3 <sup>rd</sup> mode	13.47	12.98	11.12

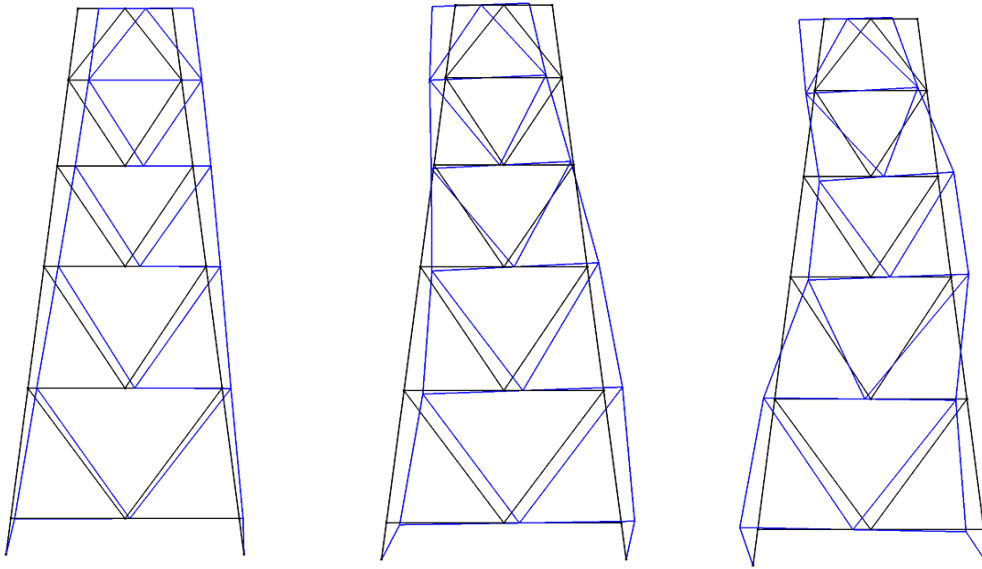


Figure A.1: Mode shapes of the first three modes in the undamaged steel truss structure.

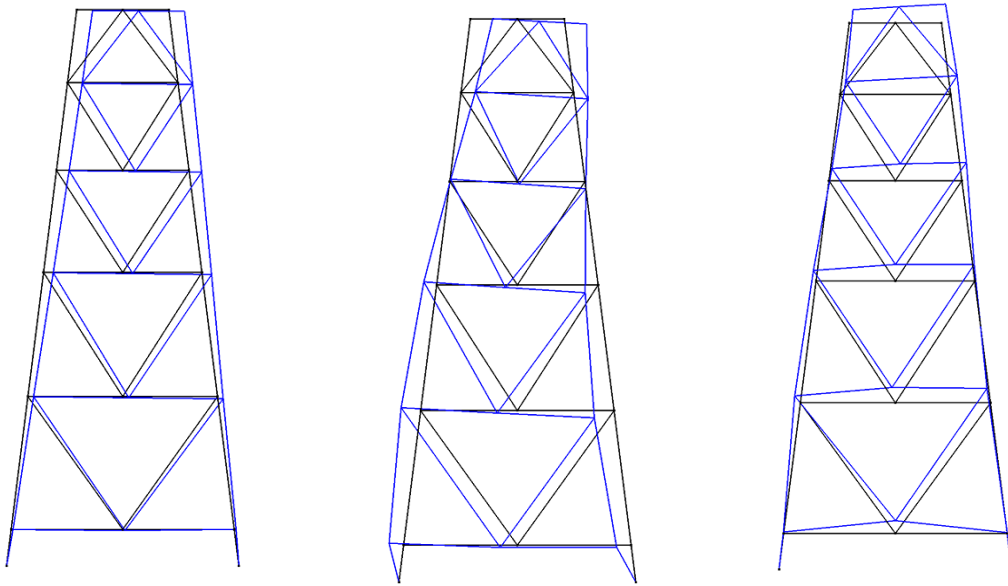


Figure A.2: Mode shapes of the first three modes in the damaged steel truss structure (80% damage in element 8).

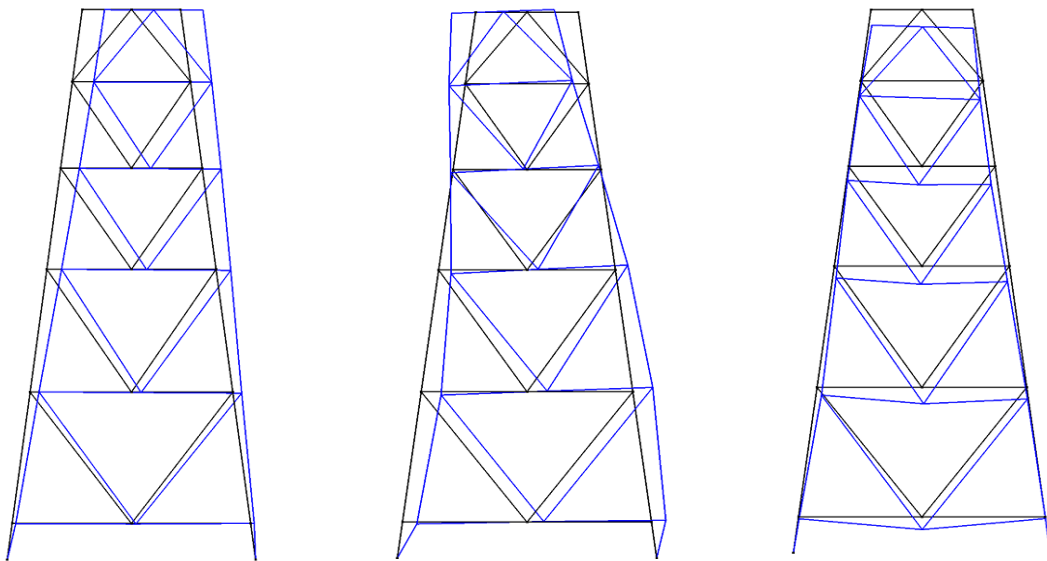


Figure A.3: Mode shapes of the first three modes in the damaged steel truss structure (50% damage in element 8).

- **Multistory Concrete Frame**

Table A.2: Frequencies of the first three modes in the undamaged and damaged multistory concrete frame structure (Case 1: 40% in element 1 – 25% in element 10; Case 2: 40% in element 1 – 25% elements 4, 9 and 14).

	Undamaged (Hz)	Damaged (Case 1) (Hz)	Damaged (Case 2) (Hz)
1 <sup>st</sup> mode	5.08	4.9	4.80
2 <sup>nd</sup> mode	19.43	18.87	18.63
3 <sup>rd</sup> mode	40.45	39.76	39.17

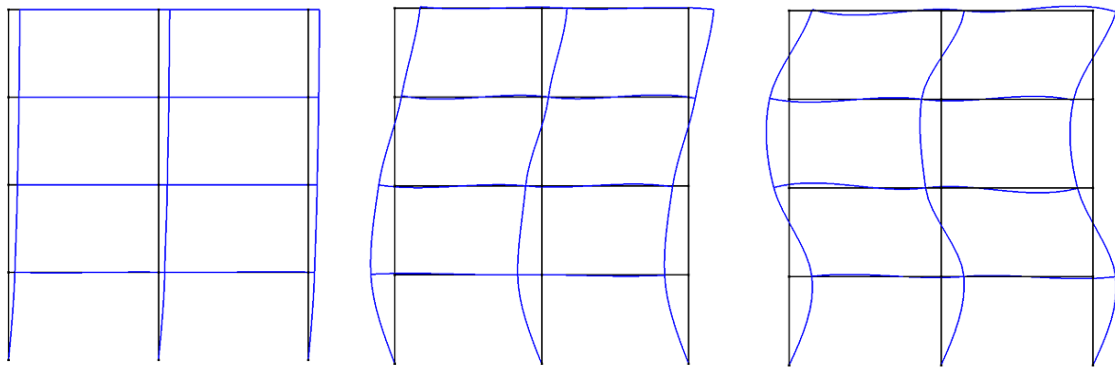


Figure A.4: Mode shapes of the first three modes in the undamaged concrete frame structure.

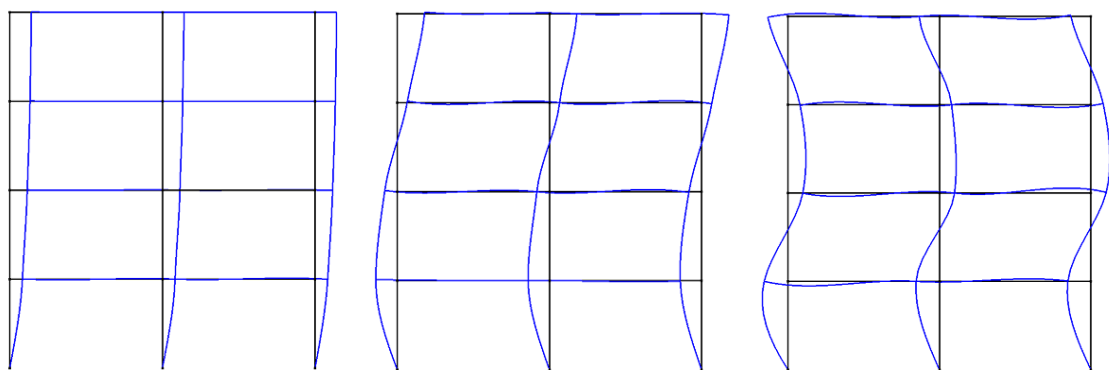


Figure A.5: Mode shapes of the first three modes in the damaged concrete frame structure (40% damage in element 1 – 25% damage in element 10).

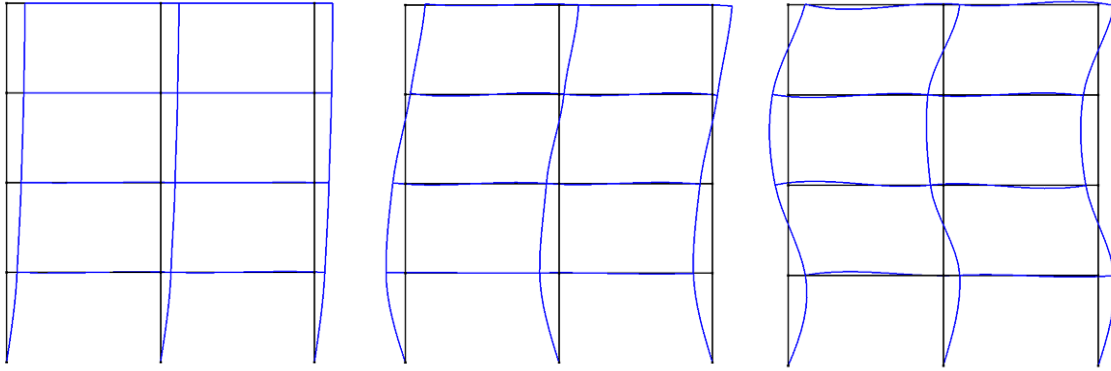


Figure A.6: Mode shapes of the first three modes in the damaged concrete frame structure (40% damage in element 1 – 25% damage in elements 4, 9 and 14).

## Appendix B: Sensitivity Analysis results

This appendix presents the means of the damage extent and the calculated RMSD for the sensitivity analysis treated in Chapters 2 and 3.

- **Steel Truss**

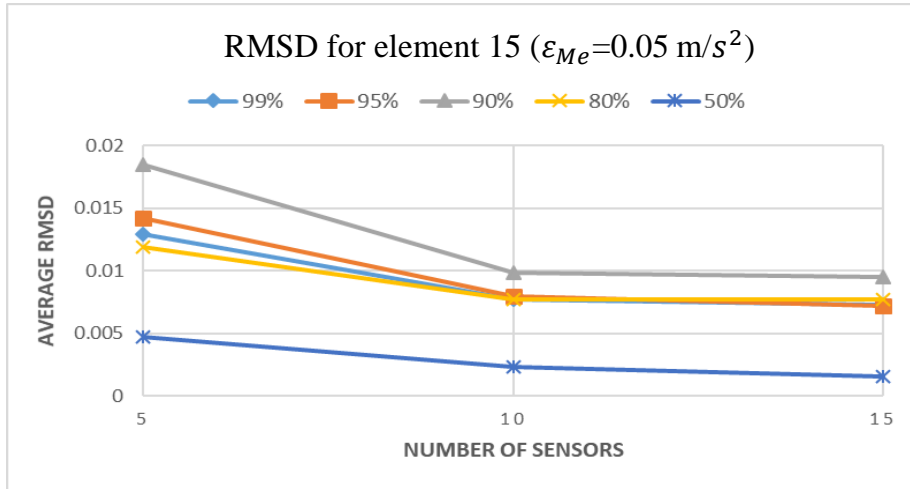
**Single structure (Chapter 2)**

Table B.1: Mean of the damage extent distributions of element 15 (and average RMSD) for different damage extents, number of sensors, and measurement error.

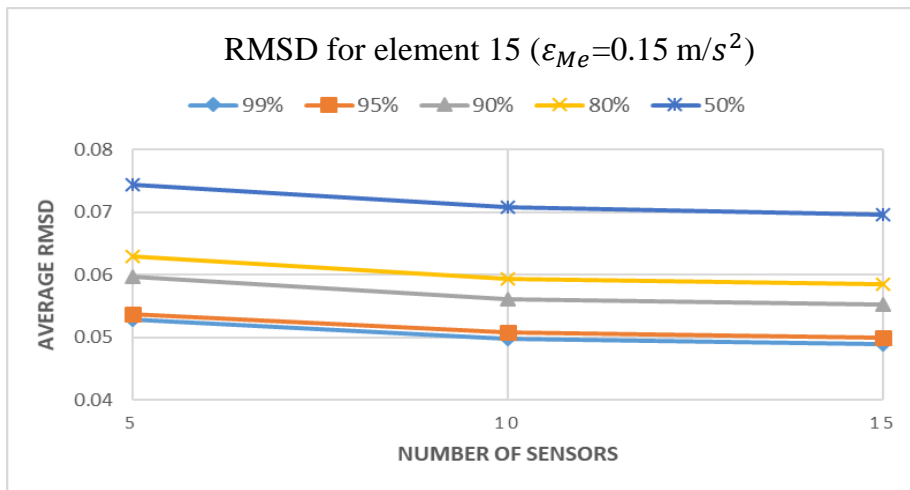
Element 15										
Remaining Stiffness Number of Sensors	$\varepsilon_{Me} = 0.05 \text{ m/s}^2$					$\varepsilon_{Me} = 0.15 \text{ m/s}^2$				
	99%	95%	90%	80%	50%	99%	95%	90%	80%	50%
5 sensors	0.999	0.983	0.947	0.800	0.491	0.991	0.979	0.961	0.928	0.811
10 sensors	0.999	0.983	0.943	0.792	0.494	0.992	0.980	0.962	0.920	0.692
15 sensors	0.999	0.980	0.943	0.782	0.494	0.992	0.981	0.961	0.923	0.704

Table B.2: Mean of the damage extent distributions of element 25 (and average RMSD) for different damage extents, number of sensors, and measurement error.

Element 25										
Remaining Stiffness Number of Sensors	$\varepsilon_{Me} = 0.05 \text{ m/s}^2$					$\varepsilon_{Me} = 0.15 \text{ m/s}^2$				
	99%	95%	90%	80%	50%	99%	95%	90%	80%	50%
5 sensors	0.990	0.977	0.950	0.875	0.487	0.994	0.982	0.973	0.942	0.655
10 sensors	0.982	0.972	0.945	0.786	0.487	0.992	0.981	0.972	0.917	0.606
15 sensors	0.982	0.974	0.945	0.786	0.487	0.992	0.981	0.971	0.914	0.517



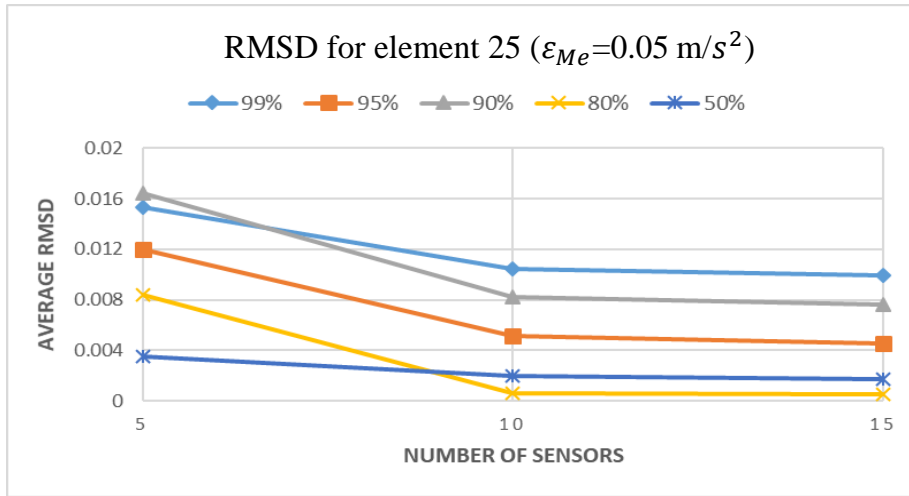
(a)



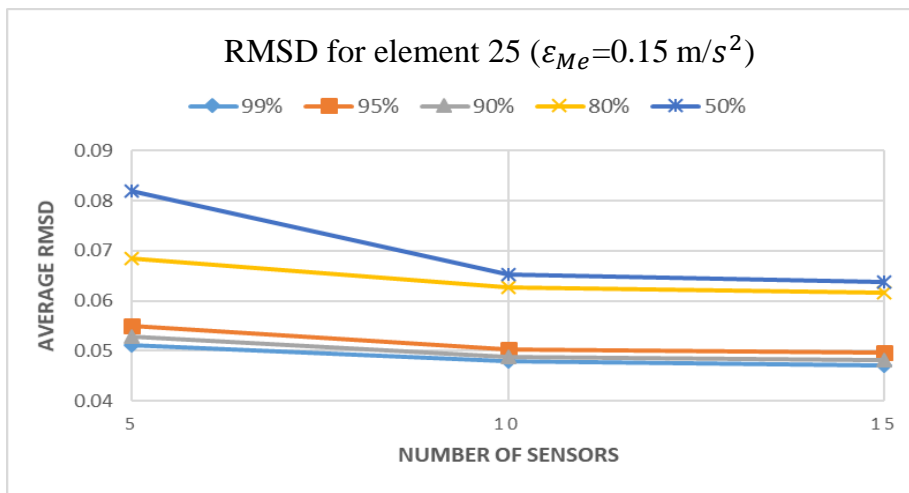
(b)

Figure B.1: Average RMSD distribution for the different damage extents (99%, 95%, 90%, 80% and 50% remaining stiffness) in element 15, different sensor numbers (5, 10, 15) and for:  
 (a)  $\epsilon_{Me}=0.05 \text{ m/s}^2$  and (b)  $\epsilon_{Me}=0.15 \text{ m/s}^2$ .





(a)



(b)

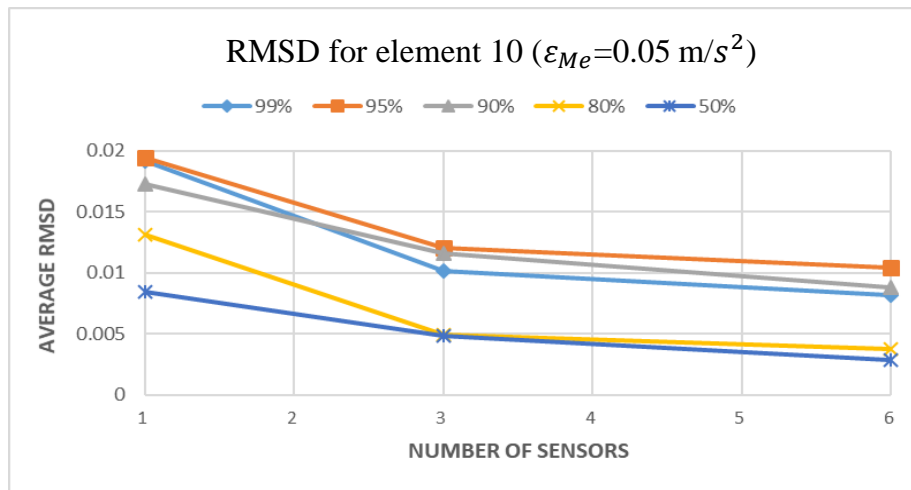
Figure B.2: Average RMSD distribution for the different damage extents in element 25, different sensor numbers (5, 10, 15) and for: (a)  $\epsilon_{Me}=0.05 \text{ m/s}^2$  and (b)  $\epsilon_{Me}=0.15 \text{ m/s}^2$ .

• **Multistory Concrete Frame**

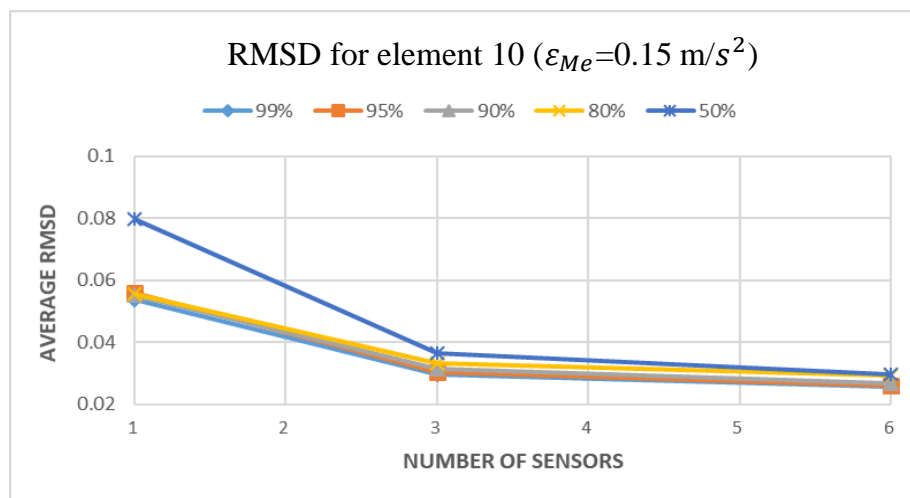
**Single structure (Chapter 2)**

Table B.3: Mean of the damage extent distributions of element 10 (and average RMSD) for different damage extents, number of sensors, and measurement error.

Element 10										
Remaining Stiffness Number of Sensors	$\epsilon_{Me} = 0.05 \text{ m/s}^2$					$\epsilon_{Me} = 0.15 \text{ m/s}^2$				
	99%	95%	90%	80%	50%	99%	95%	90%	80%	50%
1 sensor	0.994	0.992	0.979	0.827	0.497	0.997	0.914	0.923	0.781	0.499
3 sensors	0.996	0.985	0.963	0.796	0.49	0.976	0.974	0.975	0.963	0.652
6 sensors	0.998	0.982	0.900	0.791	0.49	0.981	0.980	0.978	0.962	0.644



(a)



(b)

Figure B.3: Average RMSD distribution for the different damage extents in element 10, different sensor numbers (5, 10, 15) and for: (a)  $\epsilon_{Me} = 0.05 \text{ m/s}^2$  and (b)  $\epsilon_{Me} = 0.15 \text{ m/s}^2$ .

**Single structure with borrowing strength (Chapter 3)**

Table B.4: Mean of the damage extent distributions of element 2 and 3 for different damage extents, number of sensors, and  $\epsilon_{Me}=0.15 \text{ m/s}^2$ .

Damage Extent Number of Sensors	Element 2				Element 3			
	95%	90%	80%	50%	95%	90%	80%	50%
1 sensor	0.939	0.937	0.832	0.451	0.979	0.951	0.779	0.448
3 sensors	0.966	0.926	0.797	0.548	0.968	0.936	0.787	0.469
6 sensors	0.953	0.934	0.813	0.544	0.955	0.935	0.785	0.532

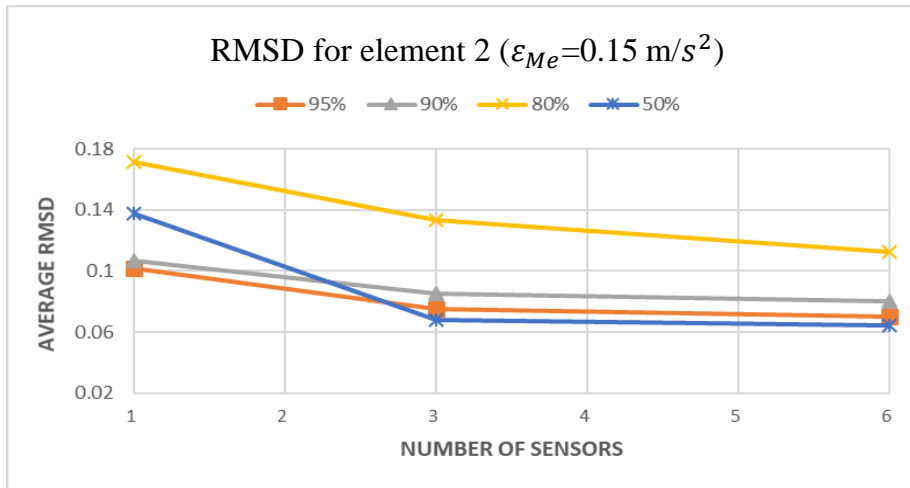


Figure B.4: RMSD distribution for element 2 ( $\epsilon_{Me}=0.15 \text{ m/s}^2$ ) for the different damage extents.

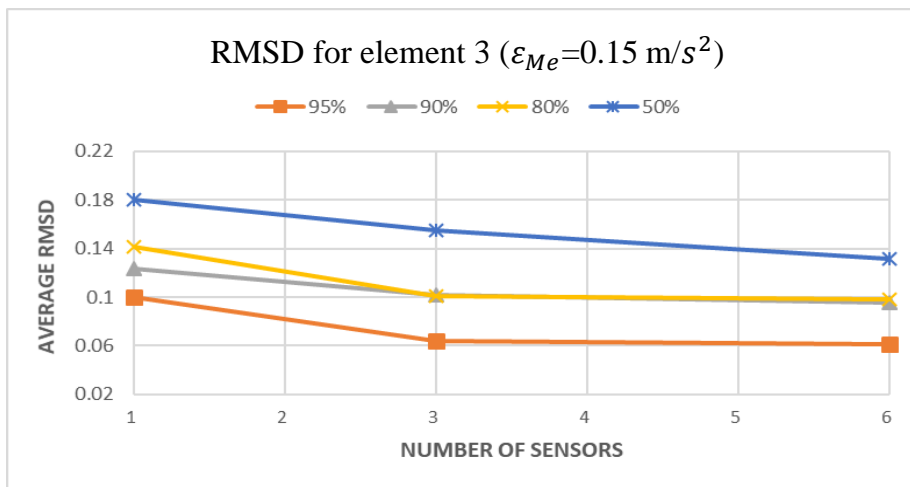


Figure B.5: RMSD distribution for element 3 ( $\epsilon_{Me}=0.15 \text{ m/s}^2$ ) for the different damage extents.

Table B.5: Mean of the damage extent distributions of element 10 and 15 for different damage extents, number of sensors, and  $\varepsilon_{Me}=0.15 \text{ m/s}^2$ .

Damage Extent Number of Sensors	Element 10				Element 15			
	95%	90%	80%	50%	95%	90%	80%	50%
1 sensor	0.938	0.936	0.903	0.558	0.980	0.865	0.740	0.534
3 sensors	0.945	0.935	0.864	0.514	0.976	0.882	0.757	0.475
6 sensors	0.951	0.925	0.860	0.497	0.965	0.873	0.768	0.499

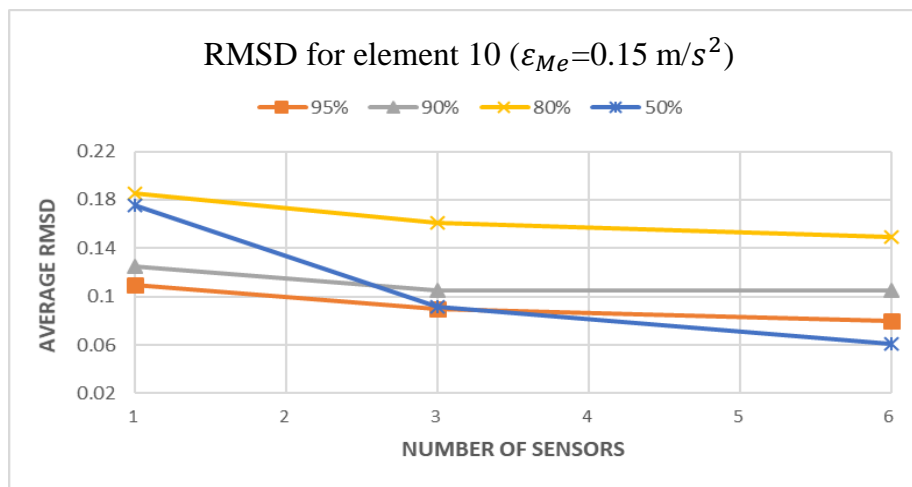


Figure B.6: RMSD distribution for element 10 ( $\varepsilon_{Me}=0.15 \text{ m/s}^2$ ) for the different damage extents.

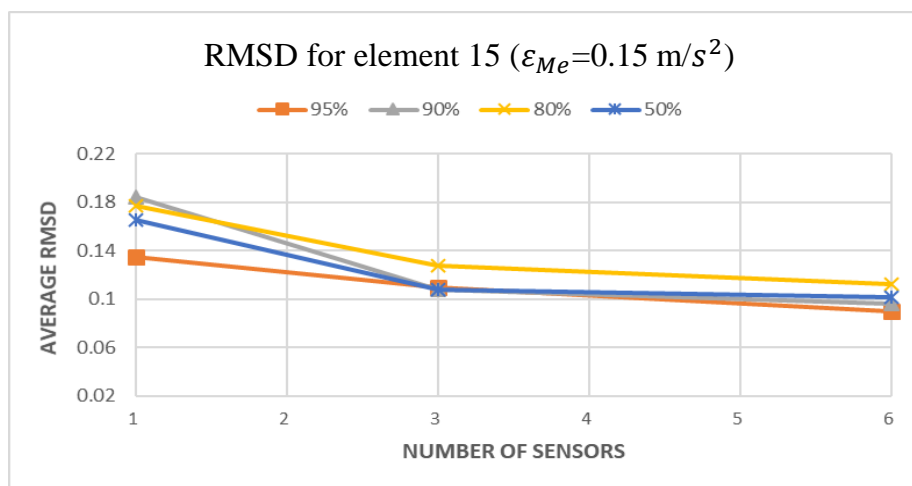


Figure B.7: RMSD distribution for element 15 ( $\varepsilon_{Me}=0.15 \text{ m/s}^2$ ) for the different damage extents.

Table B.6: Mean of the damage extent distributions of element 12 and 17 for different damage extents, number of sensors, and  $\varepsilon_{Me}=0.15 \text{ m/s}^2$ .

Damage Extent Number of Sensors	Element 12				Element 17			
	95%	90%	80%	50%	95%	90%	80%	50%
1 sensor	0.921	0.939	0.863	0.563	0.964	0.957	0.863	0.490
3 sensors	0.959	0.916	0.848	0.541	0.944	0.943	0.818	0.494
6 sensors	0.955	0.900	0.818	0.542	0.950	0.924	0.818	0.493

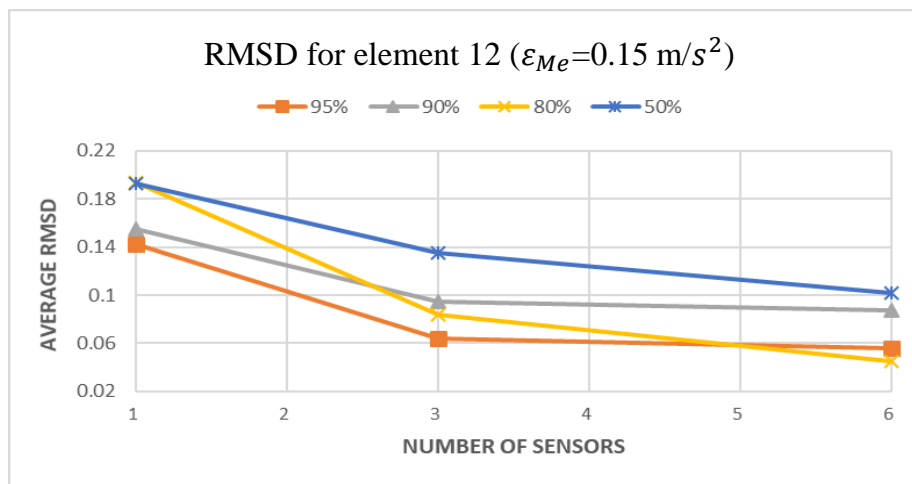


Figure B.8: RMSD distribution for element 12 ( $\varepsilon_{Me}=0.15 \text{ m/s}^2$ ) for the different damage extents.

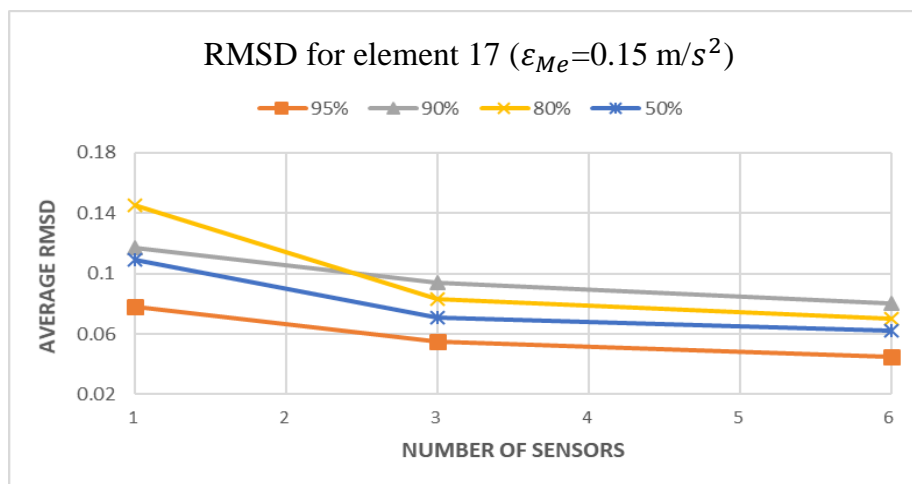


Figure B.9: RMSD distribution for element 17 ( $\varepsilon_{Me}=0.15 \text{ m/s}^2$ ) for the different damage extents.

## Appendix C: Best configurations of sensors obtained by the numerical applications

The following tables show the evolution of the best sensor configuration (and the respective cost) along the generations for the sensor placement examples treated in Chapter 5.

- **Steel Truss**

Table C.1: Best sensor configurations for the steel truss structure with  $c_c=0.1$  m.u.

Generation Number (s)	Best Nodes Numbers and Directions (Horizontal “H” / Vertical “V”)
1	N4-H ; N4-V ; N7-H ; N9-H ; N14-V ; N18-H ; N18-V
2	N3-H ; N4-V ; N6-H ; N10-H ; N14-H ; N17-V ; N18-V ; N19-H
3	N7-V ; N8-V ; N18-H ; N18-V ; N19-V
4	N3-H ; N4-V ; N7-H ; N8-H ; N13-H ; N13-V ; N14-H ; N18-V ; N19-H
5	N3-H ; N4-H ; N6-H ; N7-V ; N10-V ; N14-V ; N17-H ; N18-V
6	N4-V ; N5-H ; N6-V ; N12-H ; N17-H ; N17-V ; N18-V
7	N4-H ; N4-V ; N5-H ; N8-H ; N9-H ; N10-V ; N14-V ; N15-H ; N17-H
8	N3-H ; N4-H ; N7-V ; N8-H ; N8-V ; N10-H ; N18-V ; N19-H
9	N4-H ; N5-H ; N10-H ; N10-V ; N13-H ; N18-H ; N18-V
10	N3-H ; N4-V ; N6-H ; N7-V ; N10-H ; N12-H ; N15-H ; N18-H ; N18-V
11	N4-H ; N4-V ; N6-V ; N7-V ; N10-H ; N17-H ; N18-V
12	N3-H ; N4-H ; N10-V ; N12-V ; N13-H ; N18-V
13	N4-V ; N6-H ; N10-H ; N12-H ; N13-H ; N18-H ; N19-H ; N19-V
14, 15	N8-H ; N10-H ; N12-H ; N16-H ; N18-H ; N18-V
16	N4-H ; N6-H ; N7-V ; N13-H ; N15-V ; N18-H ; N18-V
17, 18	N3-V ; N4-V ; N6-V ; N7-V ; N12-V ; N13-H ; N13-V ; N15-V ; N18-H ; N19- H

19, 20	N4-H ; N4-V ; N5-H ; N8-H ; N7-V ; N9-H ; N10-V ; N12-H ; N12-V ; N17-H ; N18-H
21	N8-H ; N13-H ; N14-H ; N15-V ; N18-V
22	N4-V ; N5-H ; N6-H ; N6-V ; N14-V ; N18-H ; N18-V
23	N4-V ; N6-H ; N7-V ; N8-V ; N10-V ; N14-V ; N17-H ; N18-H
24	N8-H ; N9-H ; N12-V ; N18-H ; N18-V
25	N3-H ; N6-V ; N7-V ; N14-V ; N18-H ; N18-V
26	N3-H ; N4-H ; N4-V ; N7-H ; N7-V ; N8-H ; N13-V ; N14-V ; N15-V ; N17-H ; N18-H
27	N4-H ; N5-H ; N9-H ; N12-H ; N18-H
28	N3-H ; N7-V ; N10-V ; N13-H ; N18-V
29	N4-H ; N4-V ; N6-H ; N11-H ; N14-H ; N14-V ; N17-H ; N19-V
30, 31	N3-V ; N4-H ; N4-V ; N6-H ; N10-V ; N1-H ; N19-H ; N19-V
32	N5-V ; N7-V ; N8-H ; N13-V ; N18-H
33	N3-V ; N4-H ; N7-H ; N10-H ; N12-H ; N16-H ; N18-H ; N18-V
34, 35	N3-V ; N7-V ; N10-V ; N13-H ; N18-V
36, 37, 38, 39	N3-H ; N4-V ; N6-H ; N7-H ; N7-V ; N10-V ; N16-V ; N18-H ; N19-H
40	N7-V ; N13-H ; N16-V ; N17-V ; N18-H
41	N4-H ; N8-H ; N9-V ; N13-H ; N17-H ; N18-V
42	N4-H ; N5-H ; N8-H ; N15-H ; N17-H ; N17-V ; N18-H
43, 44, 45, 46	N4-V ; N7-H ; N10-H ; N10-V ; N11-H ; N14-H ; N16-H ; N18-H ; N18-V
47	N7-V ; N13-H
48, 49	N5-H ; N6-H ; N10-V ; N13-H ; N15-V ; N17-H ; N18-V
50	N4-V ; N6-V ; N10-V ; N11-V ; N12-H ; N13-H ; N15-H ; N18-H ; N18-V
51, 52, 53, 54	N4-H ; N6-H ; N7-V ; N8-V ; N10-V ; N14-V ; N17-H
55	N8-H ; N7-V ; N18-H
56, 57, 58	N4-V ; N7-V ; N11-H ; N13-H ; N15-H ; N16-V ; N17-H ; N18-H

59	N4-V ; N5-H ; N8-H ; N10-V ; N13-H ; N16-H ; N18-H ; N17-H
60, 61, 62	N3-H ; N6-H ; N7-V ; N10-H ; N12-H ; N17-H ; N18-H
63, 64	N8-H ; N13-H ; N14-H ; N18-V
65	N4-V ; N6-H ; N7-H ; N9-H ; N9-V ; N10-H ; N12-H ; N17-H ; N18-V
66	N3-H ; N12-H ; N13-H ; N15-V ; N18-V
67	N7-V ; N8-H ; N10-H ; N10-V ; N12-H ; N17-H
68, 69	N4-H ; N6-V ; N11-H ; N16-V ; N17-V ; N18-H ; N18-V
70	N4-H ; N4-V ; N8-V ; N10-V ; N16-H ; N17-H ; N17-V ; N18-H
71, 72	N3-H ; N7-H ; N8-H ; N10-V ; N12-V ; N16-H ; N19-H
73	N4-V ; N6-H ; N7-H ; N7-V ; N10-V ; N13-H ; N13-V ; N18-H ; N19-H
74	N4-V ; N5-H ; N6-V ; N13-H ; N16-H ; N19-H ; N18-H
75-76	N5-H ; N6-H ; N10-H ; N10-V ; N13-H ; N15-V ; N17-H
77	N3-H ; N4-H ; N4-V ; N8-H ; N13-H ; N16-H ; N19-H ; N18-H
78, 79	N5-H ; N4-H ; N4-V ; N6-H ; N8-V ; N7- V ; N10-V ; N12-V ; N17-H ; N18-H
80	N4-H ; N4-V ; N6-H ; N10-V ; N12-V ; N18-H ; N17-H
81	N4-V ; N7-V ; N10-V ; N13-H ; N15-H ; N16-V ; N17-H
82	N4-H ; N4-V ; N7-V ; N9-H ; N9-V ; N10-H ; N12-H ; N17-H
83	N4-H ; N7-H ; N8-H ; N13-H ; N14-H ; N19-H
84	N6-H ; N10-H ; N12-H ; N13-H ; N14-V ; N17-H ; N18-V
85	N6-H ; N10-V ; N13-H ; N13-V ; N17-H ; N18-H
86	N4-H ; N4-V ; N7-V ; N12-H ; N13-V ; N17-H ; N18-H
87	N4-V ; N6-H ; N10-H ; N14-H ; N17-H
88	N6-H ; N6-V ; N7-V ; N13-V ; N18-H ; N19-H
89	N4-V ; N7-V ; N8-V ; N10-H ; N12-V ; N17-H ; N18-H
90	N4-V ; N7-V ; N8-H ; N10-V ; N17-H ; N17-V



91, 92	N4-V ; N7-V ; N8-H ; N13-H ; N17-H
93	N4-V ; N6-H ; N7-V ; N13-V ; N14-V ; N17-H
94	N4-H ; N4-V ; N6-H ; N10-H ; N12-H ; N17-H
95	N4-V ; N7-V ; N10-H ; N10-V ; N12-V ; N17-H ; N18-H
96	N4-V ; N5-H ; N8-H ; N10-H ; N10-V ; N12-V ; N19-H
97	N7-V ; N8-H ; N13-V ; N12-V ; N15-H ; N17-H
98, 99, 100	N4-V ; N7-V ; N10-V ; N17-H

Table C.2: Total costs  $C_s$  of the best sensor configurations according to all defect chromosomes (in all generations) for the steel truss structure with  $c_c=0.1$  m.u.

Best Nodes Numbers and Directions	$C_s$ according to all configurations of defects
N4-H ; N4-V ; N7-H ; N9-H ; N14-V ; N18-H ; N18-V	33.75
N3-H ; N4-V ; N6-H ; N10-H ; N14-H ; N17-V ; N18-V ; N19-H	32.76
N7-V ; N8-V ; N18-H ; N18-V ; N19-V	33.29
N3-H ; N4-V ; N7-H ; N8-H ; N13-H ; N13-V ; N14-H ; N18-V ; N19-H	33.57
N3-H ; N4-H ; N6-H ; N7-V ; N10-V ; N14-V ; N17-H ; N18-V	33.12
N4-V ; N5-H ; N6-V ; N12-H ; N17-H ; N17-V ; N18-V	31.84
N4-H ; N4-V ; N5-H ; N8-H ; N9-H ; N10-V ; N14-V ; N15-H ; N17-H	33.12
N3-H ; N4-H ; N7-V ; N8-H ; N8-V ; N10-H ; N18-V ; N19-H	32.25
N4-H ; N5-H ; N10-H ; N10-V ; N13-H ; N18-H ; N18-V	32.07
N3-H ; N4-V ; N6-H ; N7-V ; N10-H ; N12-H ; N15-H ; N18-H ; N18-V	30.98
N4-H ; N4-V ; N6-V ; N7-V ; N10-H ; N17-H ; N18-V	31.57
N3-H ; N4-H ; N10-V ; N12-V ; N13-H ; N18-V	30.06
N4-V ; N6-H ; N10-H ; N12-H ; N13-H ; N18-H ; N19-H ; N19-V	30.77
N8-H ; N10-H ; N12-H ; N16-H ; N18-H ; N18-V	31.12

N4-H ; N6-H ; N7-V ; N13-H ; N15-V ; N18-H ; N18-V	29.54
N3-V ; N4-V ; N6-V ; N7-V ; N12-V ; N13-H ; N13-V ; N15-V ; N18-H ; N19-H	28.88
N4-H ; N4-V ; N5-H ; N8-H ; N7-V ; N9-H ; N10-V ; N12-H ; N12-V ; N17-H ; N18-H	29.4
N8-H ; N13-H ; N14-H ; N15-V ; N18-V	29.14
N4-V ; N5-H ; N6-H ; N6-V ; N14-V ; N18-H ; N18-V	28.61
N4-V ; N6-H ; N7-V ; N8-V ; N10-V ; N14-V ; N17-H ; N18-H	27.95
N8-H ; N9-H ; N12-V ; N18-H ; N18-V	29.27
N3-H ; N6-V ; N7-V ; N14-V ; N18-H ; N18-V	28.22
N3-H ; N4-H ; N4-V ; N7-H ; N7-V ; N8-H ; N13-V ; N14-V ; N15-V ; N17-H ; N18-H	29.54
N4-H ; N5-H ; N9-H ; N12-H ; N18-H	29.27
N3-H ; N7-V ; N10-V ; N13-H ; N18-V	28.74
N4-H ; N4-V ; N6-H ; N11-H ; N14-H ; N14-V ; N17-H ; N19-V	29.4
N3-V ; N4-H ; N4-V ; N6-H ; N10-V ; N1-H ; N19-H ; N19-V	28.08
N5-V ; N7-V ; N8-H ; N13-V ; N18-H	30.2
N3-V ; N4-H ; N7-H ; N10-H ; N12-H ; N16-H ; N18-H ; N18-V	30.33
N3-V ; N7-V ; N10-V ; N13-H ; N18-V	29.14
N3-H ; N4-V ; N6-H ; N7-H ; N7-V ; N10-V ; N16-V ; N18-H ; N19-H	26.9
N7-V ; N13-H ; N16-V ; N17-V ; N18-H	29.4
N4-H ; N8-H ; N9-V ; N13-H ; N17-H ; N18-V	27.16
N4-H ; N5-H ; N8-H ; N15-H ; N17-H ; N17-V ; N18-H	26.9
N4-V ; N7-H ; N10-H ; N10-V ; N11-H ; N14-H ; N16-H ; N18-H ; N18-V	26.76
N7-V ; N13-H	26.24
N5-H ; N6-H ; N10-V ; N13-H ; N15-V ; N17-H ; N18-V	28.61
N4-V ; N6-V ; N10-V ; N11-V ; N12-H ; N13-H ; N15-H ; N18-H ; N18-V	26.37
N4-H ; N6-H ; N7-V ; N8-V ; N10-V ; N14-V ; N17-H	25.97

N8-H ; N7-V ; N18-H	26.63
N4-V ; N7-V ; N11-H ; N13-H ; N15-H ; N16-V ; N17-H ; N18-H	26.5
N4-V ; N5-H ; N8-H ; N10-V ; N13-H ; N16-H ; N18-H ; N17- H	25.97
N3-H ; N6-H ; N7-V ; N10-H ; N12-H ; N17-H ; N18-H	25.44
N8-H ; N13-H ; N14-H ; N18-V	27.82
N4-V ; N6-H ; N7-H ; N9-H ; N9-V ; N10-H ; N12-H ; N17-H ; N18-V	26.59
N3-H ; N12-H ; N13-H ; N15-V ; N18-V	28.88
N7-V ; N8-H ; N10-H ; N10-V ; N12-H ; N17-H	25.31
N4-H ; N6-V ; N11-H ; N16-V ; N17-V ; N18-H ; N18-V	26.63
N4-H ; N4-V ; N8-V ; N10-V ; N16-H ; N17-H ; N17-V ; N18- H	27.42
N3-H ; N7-H ; N8-H ; N10-V ; N12-V ; N16-H ; N19-H	25.97
N4-V ; N6-H ; N7-H ; N7-V ; N10-V ; N13-H ; N13-V ; N18-H ; N19-H	27.03
N4-V ; N5-H ; N6-V ; N13-H ; N16-H ; N19-H ; N18-H	25.18
N5-H ; N6-H ; N10-H ; N10-V ; N13-H ; N15-V ; N17-H	26.27
N3-H ; N4-H ; N4-V ; N8-H ; N13-H ; N16-H ; N19-H ; N18-H	26.37
N5-H ; N4-H ; N4-V ; N6-H ; N8-V ; N7-V ; N10-V ; N12-V ; N17-H ; N18-H	26.63
N4-H ; N4-V ; N6-H ; N10-V ; N12-V ; N18-H ; N17-H	24.92
N4-V ; N7-V ; N10-V ; N13-H ; N15-H ; N16-V ; N17-H	25.44
N4-H ; N4-V ; N7-V ; N9-H ; N9-V ; N10-H ; N12-H ; N17-H	26.24
N4-H ; N7-H ; N8-H ; N13-H ; N14-H ; N19-H	25.59
N6-H ; N10-H ; N12-H ; N13-H ; N14-V ; N17-H ; N18-V	25.58
N6-H ; N10-V ; N13-H ; N13-V ; N17-H ; N18-H	25.05
N4-H ; N4-V ; N7-V ; N12-H ; N13-V ; N17-H ; N18-H	25.58
N4-V ; N6-H ; N10-H ; N14-H ; N17-H	24.46
N6-H ; N6-V ; N7-V ; N13-V ; N18-H ; N19-H	25.31
N4-V ; N7-V ; N8-V ; N10-H ; N12-V ; N17-H ; N18-H	25.71

N4-V ; N7-V ; N8-H ; N10-V ; N17-H; N17-V	23.92
N4-V ; N7-V ; N8-H ; N13-H ; N17-H	24.28
N4-V ; N6-H ; N7-V ; N13-V ; N14-V ; N17-H	24.51
N4-H ; N4-V ; N6-H ; N10-H ; N12-H ; N17-H	24.92
N4-V ; N7-V ; N10-H ; N10-V ; N12-V ; N17-H ; N18-H	24.62
N4-V ; N5-H ; N8-H ; N10-H ; N10-V ; N12-V ; N19-H	24.78
N7-V ; N8-H ; N13-V ; N12-V ; N15-H ; N17-H	24.57
<b>N4-V ; N7-V ; N10-V ; N17-H</b>	<b>23.38</b>

 Table C.3: Best sensor configurations for the steel truss structure with  $c_c=0.5$  m.u.

Generation Number (s)	Best Nodes Numbers and Directions (Horizontal “H” / Vertical “V”)
1	N3-V; N10-H; N11-V; N12-H; N13-V; N14-V; N17-H; N18-V
2,3,4	N7-V; N15-V; N18-V; N19-H
5	N7-V; N15-H; N18-V
6	N17-H; N18-V
7,8	N7-H; N16-V; N19-H
9,10	N5-H; N10-V; N15-H; N17-H
11,12,13,14	N7-V; N13-V; N19-H
15	N10-V; N17-H; N18-V
16,17,18,19	N7-V; N10-V; N13-V; N17-H
20,21	N7-V; N10-V; N13-H; N17-H
22	N13-H; N19-H
23	N7-V; N10-V; N17-H
24,25,26	N7-V; N10-V; N13-V; N17-H
27	N7-V; N10-V; N13-H; N17-H
28	N7-V; N10-V; N13-V; N17-H
29	N13-V; N17-H
30	N9-H; N17-H
31	N7-V; N15-V; N19-H

32, 33	N12-H; N17-H
34 TO 41	N10-H; N10-V; N17-H
42,43	N12-H; N17-H
44 TO 51	N4-V; N17-H
52,53	N13-V; N17-H
54	N4-V; N17-H
55,56,57	N7-V; N10-V; N17-H
58	N10-H; N10-V; N17-H
59	N4-V; N7-V; N17-H
60 TO 68	N4-V; N17-H
69	N7-V; N17-H
70	N4-V; N17-H

Table C.4: Total costs  $C_s$  of the best sensor configurations according to all defect chromosomes (in all generations) for the steel truss structure with  $c_c=0.5$  m.u.

Best Nodes Numbers and Directions	$C_s$ according to all configurations of defects
N3-V; N10-H; N11-V; N12-H; N13-V; N14-V; N17-H; N18-V	32.29
N7-V; N15-V; N18-V; N19-H	29.35
N7-V; N15-H; N18-V	27.41
N17-H; N18-V	27.26
N7-H; N16-V; N19-H	26.81
N5-H; N10-V; N15-H; N17-H	28.1
N7-V; N13-V; N19-H	26.54
N10-V; N17-H; N18-V	28.67
N7-V; N10-V; N13-V; N17-H	28.04
N7-V; N10-V; N13-H; N17-H	28.1
N13-H; N19-H	25.31
N7-V; N10-V; N17-H	26.6
N13-V; N17-H	25.22
N9-H; N17-H	25.31
N7-V; N15-V; N19-H	26.72

N12-H; N17-H	25.25
<b>N4-V; N17-H</b>	<b>24.63</b>
N10-H; N10-V; N17-H	26.72
N4-V; N7-V; N17-H	25.09
N7-V; N17-H	24.76

- **Multistory Concrete Frame**

Table C.5: Evolution of the sensor configuration across the generations for the concrete frame structure.

Generation Number (s)	Best Nodes Numbers and Directions (Horizontal “H” / Vertical “V”)
1	N5-H; N7-H; N8-V; N9-H; N12-H
2,3,4	N4-H; N5-H; N11-V; N12-V; N13-H
5	N7-H; N8-H; N11-V; N12-V; N13-H
6,7	N7-H; N9-H; N10-V; N14-H
8	N5-H; N14-H; N14-V; N15-H
9	N5-H; N10-V; N14-H
10	N12-V; N14-H
11,12,13	N8-H; N13-H
14 TO 20	N13-H
21,22	N12-V
23 TO 39	N13-H
40,41,42,43	N15-H
44 TO 50	N13-H
51,52,53,54,55	N15-V
56	N13-H
57	N15-V
58	N13-H
59	N15-V
60,61,62	N13-H
63	N15-V
64,65	N13-H

66,67	N15-V
68,69,70	N13-H

Table C.6: Total costs  $C_s$  of the best configurations of sensors according to all defect chromosomes (in all generations).

Best Nodes Numbers and Directions	$C_s$ according to all configurations of defects
N5H; N7-H; N8-V; N9-H; N12-H	33.66
N4-H; N5-H; N11-V; N12-V; N13-H	33.32
N7-H; N8-H; N11-V; N12-V; N13-H	33.35
N7-H; N9-H; N10-V; N14-H	30.99
N5-H; N14-H; N14-V; N15-H	31
N5-H; N10-V; N14-H	28.5
N12-V; N14-H	25.98
N8-H; N13-H	25.92
N12-V	23.63
<b>N13-H</b>	<b>23.37</b>
N15-H	23.38
N15-V	23.51